THE UNIVERSITY of ADELAIDE

Development of Advanced Graphene-based Composites for Water Purification

Pei Lay Yap

A thesis submitted in fulfillment of the
requirements for the degree of
Doctor of Philosophy

School of Chemical Engineering and Advanced Materials
The University of Adelaide

October 2020

BLANK PAGE

TABLE OF CONTENTS

ABSTRACT

Presence of a broad range of co-existing water pollutants including heavy metals, organic dyes, organic solvents and oils remains an unresolved environmental challenge. Majority of the existing water purification technologies are expensive, energy-intensive and ineffective, particularly for the removal of ultra- low concentration of heavy metals. This calls for the development of novel sorbent materials and new effective water purification technologies.

This thesis consolidates the development of multifunctional graphene-based composites to achieve highly efficient removal of a broad range of water pollutants. Three key aspects are addressed in this thesis: First, mastery of tailoring the multifunctional surface chemistry properties of graphene-based composites is underpinned through the simultaneous binary-heteroatom doping and reduction of graphene oxide (GO), followed by a thiol-ene click reaction using amino-terminated thiol molecules to create multifunctional graphene-based materials with tunable surface chemistry.

Second, based on four functionalization strategies (hydrothermal, chemical reduction, thermal and photoinitiated thiol-ene click), multifunctional groups are covalently attached to the GO to address the limitations of commercial adsorbent, activated carbon (AC). Precursors enriched with oxygen- (alginate), nitrogen- (hydrazine and mixed polyamine blend), sulfur- (pentaerythritol tetrakis-mercaptopropionate) as well as combined nitrogen- and sulfur- groups (cysteamine) are used to demonstrate these chemical functionalization concepts for higher

mechanical strength, stability, better dispersion in water and enhanced sorption of diverse classes of water pollutants. Magnetic iron oxide nanoparticles are also incorporated to the graphene-based composites for easy separation after the sorption process besides improving the sorption capacity of water pollutants. The developed modification strategies are versatile, low cost, scalable, energy-efficient and eco-friendly compared to highly-energy-intensive activation process of AC.

Third, sorption performance of the developed graphene-based composites is studied in terms of the sorption isotherms, kinetics, selectivity, regenerability and real sample analysis. Both hydrothermally- and chemically- reduced polyamine-modified rGO composites follow the Freundlich isotherm models with a maximum sorption capacity of 63.80 mg/g and 59.90 mg/g, respectively, achieved towards Hg^{2+} ions. Langmuir isotherm model is used to describe the interaction of graphene-based composites with their respective contaminants studied and maximum sorption capacity attained as the following: cysteamine-modified partially rGO (169.00 mg/g for Hg^{2+} ions), multithiol functionalized graphene bio-sponge (101.01 mg/g for Pb^{2+} ions and 102.99 mg/g for Cd^{2+} ions) and multifunctional graphene biopolymer foam (789.70 mg/g for methylene blue, 107.00 mg/g for Hg^{2+} ions and 73.50 mg/g for Cu^{2+} ions). Meanwhile, all the graphene-based composites developed are well-fitted using the pseudo-second order kinetic models. Positive evaluation outcomes suggest that all the developed graphene-based composites outperformed AC and some sorbents reported in the literature in single and simultaneous pollutant removal studies using milli-Q, river and sea water. Different innovative functionalization approaches are demonstrated herein to engineer graphene-based composites with unique

multifunctional properties, which promise realistic water purification technology solutions for efficient uptake of diverse classes of water pollutants.

Research studies completed in this thesis integrate the fundamental understanding and application of knowledge on the surface, structural, chemical and thermal characteristics of functionalized graphene-based composites to address the most concerning water pollution challenges using cutting-edge and scalable water purification technologies.

PREFACE

This thesis is submitted as a "*thesis by publication*" in accordance to the "*Specifications for Thesis 2020*" of The University of Adelaide. This thesis contains the following list of publications over a span of 3 years of my PhD candidature. The outcomes generated during my PhD candidature include 14 published, accepted for publication or under reviewed journal articles (6 first-authored; 8 co-authored), a protocol (confidential, unpublished), 11 manuscripts under final preparation, 10 conference presentations and 6 awards.

LIST OF JOURNAL ARTICLES (Published/ Under Review)

1. **Yap, P. L.**, Md J. N., Hassan, K., Tung, T. T., Tran, D. N., & Losic, D. (2020). Graphene-based sorbents for multi-pollutants removal in water: A review of recent progress. *Advanced Functional Materials,* accepted for publication. **(IF: 16.836)**

2. **Yap, P. L.**, Auyoong, Y. L., Hassan, K., Farivar, F., Tran, D. N. H., Ma, J., & Losic, D. (2020). Multithiol functionalized graphene bio-sponge via photoinitiated thiol-ene click chemistry for efficient heavy metal ions adsorption. *Chemical Engineering Journal, 395*, 124965. doi:10.1016/j.cej.2020.124965 **(IF: 10.652)**

3. **Yap, P. L.**, Tung, T. T., Kabiri, S., Matulick, N., Tran, D. N. H., & Losic, D. (2020). Polyamine-modified reduced graphene oxide: A new and cost-effective adsorbent for efficient removal of mercury in waters. *Separation and Purification Technology, 238*, 116441. doi:10.1016/j.seppur.2019.116441 **(IF: 5.774)**

4. **Yap, P. L.**, Hassan, K., Auyoong, Y. L., Mansouri, N., Farivar, F., Tran, D. N., & Losic, D. (2020). All-in-one bioinspired multifunctional graphene biopolymer foam for simultaneous removal of multiple water pollutants. *Advanced Materials Interfaces*, 2000664. doi:10.1002/admi.202000664 **(IF: 4.948)-** featured in journal cover and news article

5. **Yap, P. L.**, Kabiri, S., Tran, D. N. H., & Losic, D. (2019). Multifunctional binding chemistry on modified graphene composite for selective and highly efficient adsorption of mercury. *Applied Materials & Interfaces, 11*(6), 6350-6362. doi: 10.1021/acsami.8b17131 **(IF: 8.758)**

6. **Yap, P. L.**, Kabiri, S., Auyoong, Y. L., Tran, D. N. H., & Losic, D. (2019). Tuning the multifunctional surface chemistry of reduced graphene oxide via combined elemental doping and chemical modifications. *ACS Omega, 4*(22), 19787-19798**.** doi: 10.1021/acsomega.9b02642 **(IF: 2.87)**

7. Hassan, K., Md J. N., Tung, T. T.,Stanley, N. J., **Yap, P. L.**, Rastin, H., Yu, L., Losic, D. (2020). Functional inks and extrusion-based 3D printing of 2D materials: a review of current research and applications. *Nanoscale*, 12 (37), 19007-19042. doi:10.1039/D0NR04933F **(IF: 6.895)**

8. Hassan, K., Tung, T. T., **Yap, P. L.**, Md J. N., Kim. H.C., Losic, D. (2020). Fast response hydrogen gas sensor based on Pd/Cr nanogaps fabricated by a single-step bending deformation. *Analytica Chimica Acta*, 1138, 49-58. doi:10.1016/j.aca.2020.09.012 **(IF 5.977)**

9. Wang, H., Tran, D., Moussa, M., Stanley, N., Tung, T. T., Yu, L., **Yap, P.L.**, Ding, F., Qian, J. & Losic, D. (2020). Improved preparation of MoS_2/graphene composites and their inks for supercapacitors applications. *Materials Science and Engineering: B, 262*, 114700. doi:10.1016/j.mseb.2020.114700 **(IF: 4.706)**

10. Hassan, K., Hossain, R., **Yap, P. L.**, Yu, L., Mansouri, N., Tung, T. T., Losic, D., Sahajwalla, V. (2020). Microrecycled ZnO nanoparticles decorated macroporous 3D hybrid structure for efficient detection of NO_2. *Sensors and Actuators B: Chemical*, accepted for publication. **(IF 7.100)**

11. Farivar, F., **Yap, P. L.**, Hassan, K., Tung, T. T., Tran, D. N. H., Losic, D. *Materials Horizon*, Unlocking the thermogravimetric analysis (TGA) in the fight against 'Fake Graphene' materials, under review. **(IF: 13.870)**

12. Yu, L., **Yap, P. L.**, Tran, D. N. H., Santos, A., Losic, D. Scalable and high-yield preparation of few-layers of hexagonal boron nitride (hBN) by direct wet chemical exfoliation route. *Applied Surface Science*, under review. **(IF: 6.182)**

13. Hassan, K., Tung, T. T., Stanley, N. J., **Yap, P. L.**,Farivar, F., Rastin, H., Md J. N., Losic, D. Graphene ink for 3D extrusion micro printing of chemo-resistive sensing devices for VOC detection. *Nanoscale*, under review. **(IF: 6.895)**

14. Zhu, Z., Zhang, Q., **Yap, P. L.**, Ni, Y and Losic, D., Magnetic Graphene Oxide as a Nano-Vehicle for Loading and Delivery of Curcumin, Spectrochimica Acta Part A: Molecular and Biomolecular Spectroscopy, under review. **(IF: 3.232)**

LIST OF JOURNAL ARTICLES (in final preparation)

15. **Yap, P. L.**, Yu, L., Hassan, K., Tung, T. T, and Losic, D., Sustainable and Green Synthesis of Biomagnetic Nanoparticles Decorated Aminoclay-Functionalized Graphene Composites as Silver Ions Scavenger in Mine Tailings, under preparation.

16. Rastin, H.,.,…. **Yap, P. L.**, Yu, L., Tung, T. T, Vreugde S, Losic, D, Converging 2D Nanomaterials and 3D Bioprinting Technology: State-of the-Art, Challenges and Potential Outlook in Biomedical Applications, under preparation.

17. Farivar, F., **Yap, P. L.**, Losic, D., Explosive Thermal Decomposition of Graphene Oxide: Effect of Physical Form, Mass Heating rate and Heating Environment, under preparation.

18. Farivar, F., **Yap, P. L.**, Karunagaran, R., Losic, D., Explosive Thermogravimetry of Graphene Materials: Effect of Flake Size and Thickness, under preparation.

19. Hassan, K., Tung, T. T., **Yap, P. L.**, Stanley, N. J., Md J. N., Losic, D. A Bio-inspired Fractal Designed VOC Sensors Fabricated by Graphene Inks using Extrusion 3D Printing Technology, *Applied Materials Today*, under preparation. **(IF: 7.970)**

20. Hassan, K., Tung, T. T., **Yap, P. L.**, Stanley, N. J., Md J. N., Losic, D. Direct ink writes 3D CNT/Graphene-based NO_X Sensors with an embedded heater, *Small*, under preparation. **(IF: 11.459)**

21. Hassan, K., Makar, S., **Yap, P. L.**, Tung, T. T., Stanley, N. J., Md J. N., Losic, D. A Hydrogen Sensor based on Highly Oriented TiO_2 Nanotubes, *International Journal of Hydrogen Energy*, under preparation. **(IF: 4.939)**

22. Hassan, K., **Yap, P. L.**, Tung, T. T., Stanley, N. J., Md J. N., Losic, D. High-Performance MXene based Flexible Heater for Sensing Applications, *Materials Letters*, under preparation. **(IF: 3.204)**

23. Yu, L., **Yap, P. L.**, Tran, D. N. H.,Santos, A., Losic, D., Bismuth oxide-titania composites (BTO) for X-ray radiation shielding, *ACS Applied Materials and Interfaces*, under preparation. **(IF: 8.758)**

24. Yu, L., **Yap, P. L.**, Tran, D. N. H.,Santos, A., Losic, D., Effect of graphene and hBN in X-ray radiation shielding, under preparation.

25. Yu, L., **Yap, P. L.**, Tran, D. N. H.,Santos, A., Losic, D., Bio-Magnetic-Beads for virus detection, under preparation.

LIST OF CONFERENCE/WORKSHOP PRESENTATIONS

1. **Yap, P. L.**, **Magic Bio-Carpet for Clean Water, BLiSS Adelaide 2020 Virtual Conference**, 20-23 October 2020, BLiSS Science & Innovation Inc., Adelaide, Australia (Oral Presentation)-**People's Choice Award**.

2. **Yap, P. L.**, Hassan, K., Farivar, F., Tran, D. N., and Losic, D., Multithiol Functionalized Graphene Bio-Sponge through Photoinitiated Thiol-ene Click Chemistry for Heavy Metal Ions Adsorption**, ACS Fall 2020 Virtual Meeting and Expo**, 17-20 Aug 2020, San Francisco, USA (Virtual Platform: On-demand Oral Presentation)

3. **Yap, P. L., Magic Bio-carpet for Clean Water,** ECMS 3MT Challenge 2020, 27 July 2020, The University of Adelaide, Adelaide, Australia (Oral Presentation)- **Faculty Finalist Prize 2020**.

4. **Yap, P. L.**, Hassan, K., Farivar, F., Tran, D. N., and Losic, D., Multithiol Functionalized Graphene Bio-Sponge for Efficient Removal of Heavy Metal Ions in Water, **Graphene and 2D Materials Industrial Forum Online Conference**, 27 May 2020, Madrid, Spain (Virtual Platform: e-Poster Presentation)

5. **Yap, P. L.**, Tung, T., Kabiri, S., Tran, D. N. H., & Losic, D., **Low Cost Polyamine-Modified Graphene Composites for Effective Mercury Remediation in Water,** ACS Spring 2020 National Meeting and Expo, Macromolecular Chemistry: The Second Century, 22-26 Mac 2020, Philadelphia, USA (Virtual Platform: Oral Presentation) doi:10.1021/scimeetings.0c02603

6. **Yap, P. L.**, Tung, T., Kabiri, S., Tran, D. N. H., & Losic, D., **Polyamine-Functionalized Graphene Composites for Effective Water Remediation,** Second Annual ARC Graphene Research Hub Workshop, 12-13 Mac 2020, Monash University, Clayton, Victoria, Australia (Poster Presentation)

7. **Yap, P. L.**, Tung, T., Kabiri, S., Tran, D. N. H., & Losic, D., **Polyamine-Functionalized Graphene Composites for Effective Water Remediation,** ICONN 2020, 9-13 Feb 2020, Brisbane, Australia (Poster Presentation)**- Best Poster Award**

8. **Yap, P. L.**, Kabiri, S., Tran, D. N. H., & Losic, D., **Thiol-ene Clicked Partially Reduced Graphene Oxide as an Effective Mercury (II) Adsorbent,** Graphene Week 2019, Graphene Flagship, 23-27 Sept 2019, Helsinki, Finland (Poster Presentation)

9. **Yap, P. L.**, Kabiri, S., Tran, D. N. H., & Losic, D., **Highly Selective Mercury Removal using Graphene Hybrid Modified with Thiol(Cysteamine)-ene Click Chemistry,** 2019 First ARC Graphene Research Hub Workshop, 28-

29 Mac 2019, Adelaide, Australia (Poster and Oral Presentation)- **Certificate of Excellent Oral Presentation**

10. **Yap, P. L.**, Kabiri, S., Tran, D. N. H., & Losic, D., **Functionalized Graphene Hybrid with Thiol-(Cysteamine)-ene Click Chemistry for Efficient Hg (II) Ions Removal,** 2018 First Australian-EU Graphene Workshop, 17-19 Oct 2018, Adelaide and Sydney, Australia (Poster Presentation)

OTHER CONTRIBUTIONS

1. **Protocol (confidential, unpublished): Yap, P.L.**, Farivar, F., Losic D. In *Thermogravimetric Analysis (TGA) Protocol for Versailles Project on Advanced Materials and Standards (VAMAS) Technical Working Area (TWA) 41 "Graphene and Related 2D Materials"*: Adelaide, Australia: ARC Graphene Research Hub, The University of Adelaide; 2020:20. http://www.vamas.org/twa41/index.html

2. **ISO Standard (under development)**: International Organization for Standardization (2021). *Chemical characterisation for graphene flakes by Thermogravimetric analysis (TGA) (*ISO/PWI 23359).

3. **Team Leader** for Versailles Project on Advanced Materials and Standards (VAMAS) Technical Working Area (TWA) 41 "Graphene and Related 2D Materials" for *Thermogravimetric Analysis (TGA).* http://www.vamas.org/twa41/index.html

4. **Leading researcher** for completion of Versailles Project on Advanced Materials and Standards (VAMAS) Technical Working Area (TWA) 41 "Graphene and Related 2D Materials" for Structural Characterisation of CVD-grown Graphene using Raman Spectroscopy, National Physical Laboratory (NPL), UK, March 2019. http://www.vamas.org/twa41/index.html

LIST OF AWARDS

1. **Science Bites People's Choice Award (Healthy Futures)**, BLiSS Adelaide 2020 Virtual Conference, 20-23 October 2020, BLiSS Science & Innovation Inc., Adelaide, Australia.

2. **3-Minute-Thesis (3MT) Faculty Finalist Prize** 2020, ECMS, 20 August 2020, The University of Adelaide, SA, Australia.

3. **Best Poster Award**, **RSC Nanoscale Horizons Poster Prize**, Nano Energy and Environment symposium, at International Conference on Nanoscience and Nanotechnology (ICONN 2020), 9-13 Feb 2020, Brisbane, Australia.

4. **Merdeka Award 2019** by the Australia Malaysia Business Council (South Australia) Inc., 31 Aug 2019, Adelaide Convention Centre, SA, Australia.

5. **Certificate of Excellent Oral Presentation** at 2019 First ARC Graphene Hub Workshop, 28-29 Mac 2019, Adelaide, Australia.

6. **Chemical Engineering Active & Productive HDR Student 2018**, by School of Chemical Engineering, The University of Adelaide, 28 Nov 2018.

7. Faculty of Engineering, Computer & Mathematical Sciences (ECMS) Divisional Scholarship, 2017

8. ARC Grant Funded Supplementary Scholarship, 2017

9. Full fee Scholarship, University of Adelaide, 2017

Featured cover article: Vol. 7, No. 18, 2020, 2000664, Advanced Materials Interfaces: The cover picture, featuring article number 2000664 by Dusan Losic, Pei Lay Yap and co-workers, unlocks the bio-inspired material design concept based on the unique wettability micro-topology of a darkling beetle to develop a novel all-in-one water pollutant adsorbent using multifunctional graphene biopolymer (Alg-Fe_3O_4-rGO-4S) foam, constructed with a combined hydrophilic-hydrophobic wettability synthesised by a photoinitiated thiol-ene functionalization approach. Excellent performance for simultaneous uptake of multiple pollutants from waters including heavy metal ions, cationic dyes, oils and organic solvents are demonstrated.

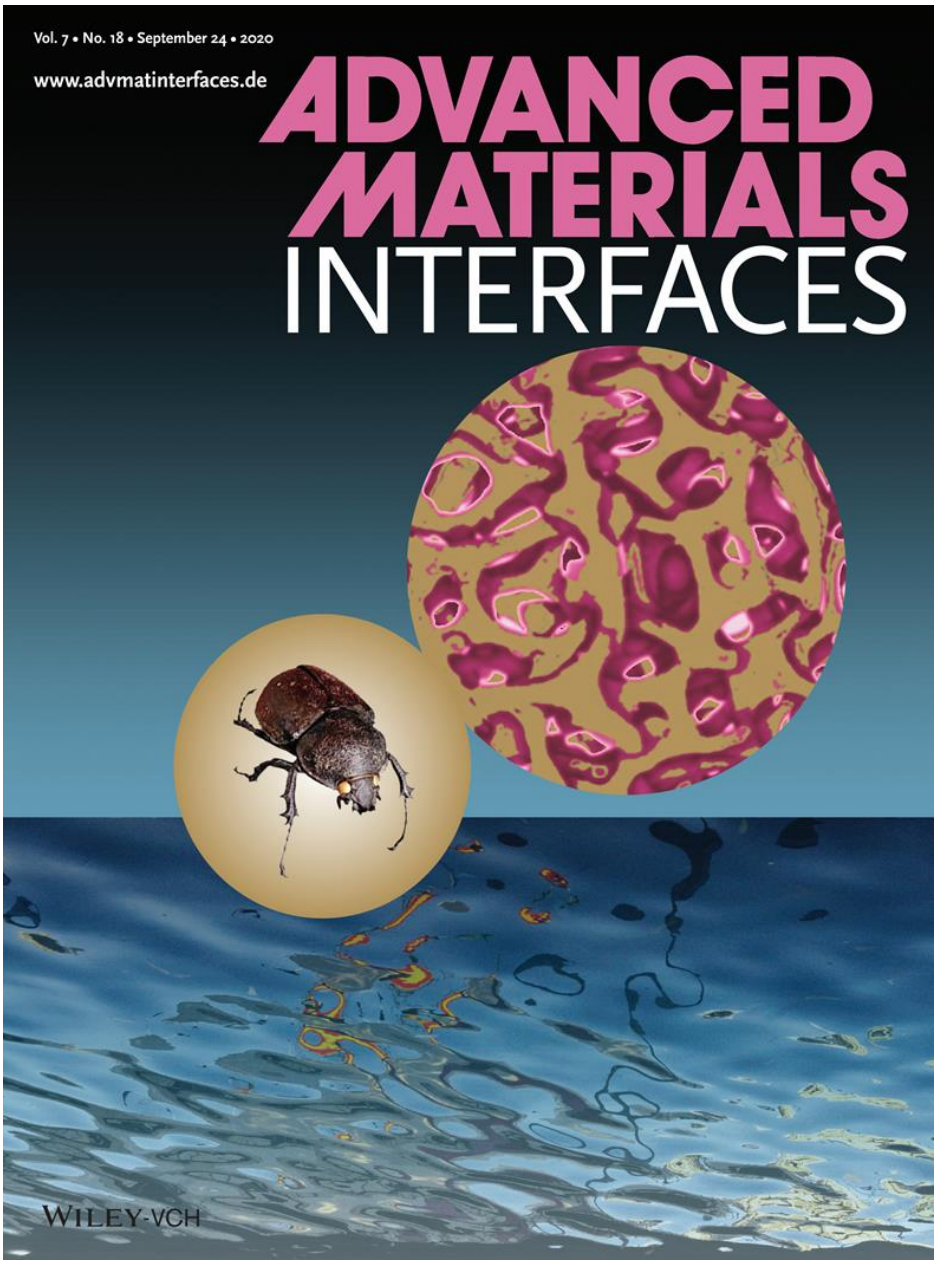

HDR THESIS DECLARATION

I certify that this work contains no material which has been accepted for the award of any other degree or diploma in my name, in any university or other tertiary institution and, to the best of my knowledge and belief, contains no material previously published or written by another person, except where due reference has been made in the text. In addition, I certify that no part of this work will, in the future, be used in a submission in my name, for any other degree or diploma in any university or other tertiary institution without the prior approval of the University of Adelaide and where applicable, any partner institution responsible for the joint-award of this degree.

I acknowledge that copyright of published works contained within this thesis besides with the copyright holder(s) of those works.

I also give permission for the digital version of my thesis to be made available on the web, via the University's digital research repository, the Library Search and also through web search engines, unless permission has been granted by the University to restrict access for a period of time.

I acknowledge the support I have received for my research through the provision of an Australian Government Research Training Program Scholarship.

Pei Lay Yap Date: 15.10.2020

ACKNOWLEDGEMENTS

Thank You. It is my great pleasure to thank everyone who has walked me through my incredible PhD journey to seek light at The University of Adelaide. My heartfelt gratitude undoubtedly goes to my supervisor, **Prof. Dusan Losic**, for his enthusiasm, tremendous guidance and inspiration to enlighten me and push me beyond my limits. I could not have sailed this far without his endless support. No words can express my gratitude for his unfading commitment and dedication.

I would like to convey my deepest appreciation to Dr. Diana Tran (co-supervisor), Dr. Shervin Kabiri, Dr. Tran Tung, Dr. Farzaneh Farivar, Kamrul Hassan, Dr. Grant Matthieson, Dr. Nathan Stanley, Dr. Julker Nine and Dr. Jacqui McRae for sharing their scientific insights and knowledge to help shaping a better version of myself each day. My sincere gratitude also goes to School of Chemical Engineering and Advanced Materials supporting staff, ECMS technical staff as well as the experts from Adelaide Microscopy and Biogeochemistry and Stable Isotope Facility for their technical support.

This research voyage could not have been smoothly sailed without the encouragement and strong support from my beloved family and my caring friends. In particular, Dr. John Au Yoong, for his unconditional love, patience, and everlasting support to have brought me this far.

Last but not least, I would also like to acknowledge the financial support from ECMS Divisional Scholarship, ARC Graphene Research Hub (IH 150100003) Grant Funded Supplementary Scholarship and Full Fee Scholarship. ***'Terima Kasih'***

Pei Lay Yap **15.10.2020.**

BLANK PAGE

CHAPTER 1

INTRODUCTION

1. INTRODUCTION

1.1. Background

"*You never miss the water, till the well runs dry*". Recent water shortages have reminded us that water is an indispensable fundamental component for life, including food and energy supplies.[1] The demand for this precious, yet finite natural resource continues to rise as a result of deteriorating water supply due to immense industrialization and urbanization. About 70 % of our planet is water-covered, yet one out of three people worldwide is still struggling to have access to safe drinking water. This is because 96.5 % of water on the earth is made up of ocean that is oversaturated with salt, thus undrinkable. Only about 1 % of the accessible surface fresh water that exists as atmospheric water, lakes, rivers, ice and snow (**Figure 1**) is currently thriving to make up for the global water demand, as a result of over-growing population, global climate change and water pollution.[2-3] Ocean desalination seems to be promising to help curbing water shortages worldwide, however, this technology comes with many pitfalls including large amount of energy consumption, high carbon footprint, high cost, disruption of the marine ecosystem, and the creation of water pollution apart from releasing harmful chemicals into the drinking water supply.[4] Hence, the focus of the worsening water crisis has to be adjusted to recovery of freshwaters from pollution rather than ocean desalination to maintain a sustainable, clean and safe water supply globally.

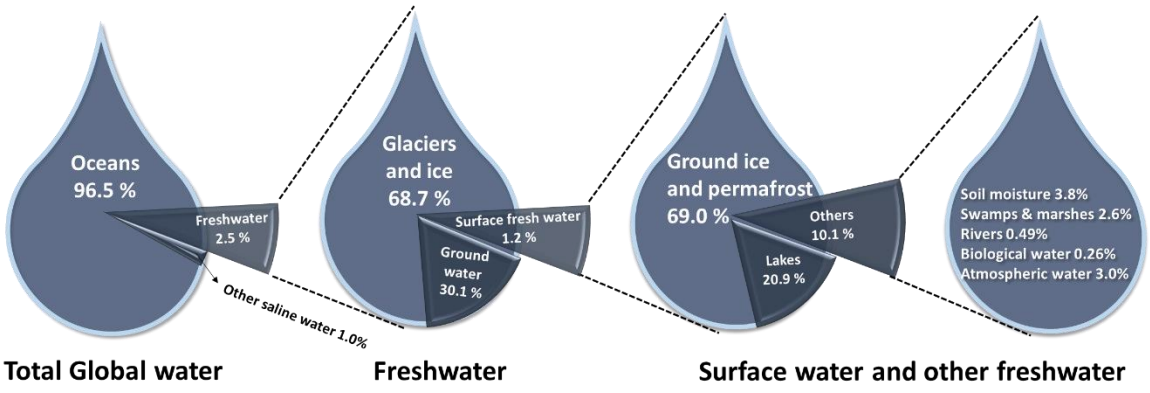

Figure 1. Distribution of Earth's water including total global water, fresh water, surface and other fresh water.[2-3]

Water pollutants vary in terms of their concentrations and types ranging from biological pollutants and organic contaminants to inorganic pollutants, which co-exist in waterways worldwide. Biological pollutants (*e.g.* bacteria, viruses, molds and mildew) found in wastewaters often originate from faecal contamination and soil pollution.[5] Nearly 30 % of water pollutants in sewage water are inorganic pollutants including heavy metals and polyatomic compounds, which are often discharged from electronic, pulp and steel manufacturing, mining, petroleum and agricultural industries. Although heavy metals are not the main constituent that make up the pollution in water, they are one of most concerning pollutants due to their high toxicity even at low concentration, bioaccumulation and biomagnification in the food chain, leaving long-term negative impact to the environment and human health.[5-6] While, organic pollutants such as dyes, spilled oil, volatile organic compounds, pesticides, pharmaceuticals and personal care products make up about 70 % in sewage waters, they are introduced mainly from textile, printing, pharmaceutical and agricultural industries.[5] Despite that majority of the organic pollutants are organic compounds, which are biodegradable, with no serious health risks linked to their exposure at low concentrations, their removal is still crucial to prevent implications associated with our endocrine hormones and mutagenocity.[5] Effluents from manufacturing factories, agricultural farms and sewage water treatment plants containing these water pollutants, not only dwindles the clean water supply in terms of quantity, but also its quality that trigger alarming public health issues and deaths.[5, 7-8]

It is vital to highlight that water pollutants do not present as a single entity, rather these multi-pollutants co-exist in the water bodies, which makes the water purification process a more complex and challenging task in reality. Critical challenges as summarized in **Figure 2** have been identified in water purification including simultaneous removal of co-existing pollutants from different classes using a single sorbent material and ineffective removal of heavy metals using existing water purification technology. It should be highlighted that heavy metals are usually present in trace levels (ppb range to less than 10 ppm) in various natural water matrices.[9] Apparently, more stringent permissible limits especially for heavy metals (**Table 1**) have been imposed by international organizations to regulate the standard

of drinking water since exposure to these pollutants even at trace levels can adversely jeopardize our health.[10-12]

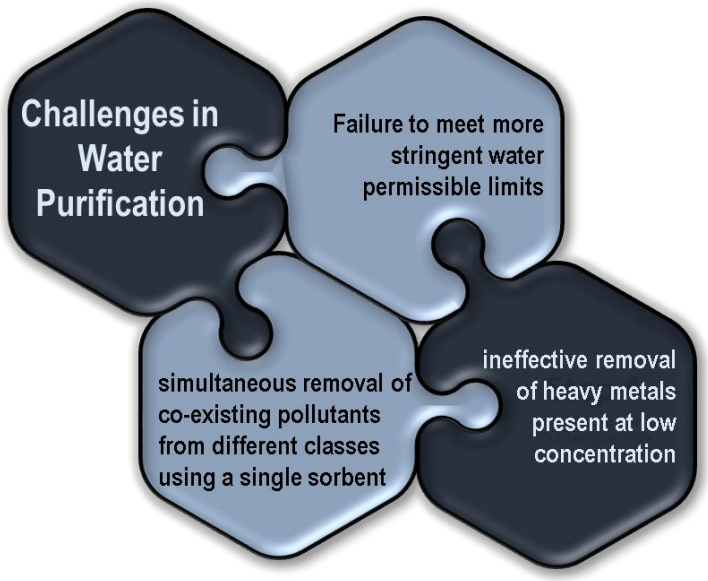

Figure 2. Current challenges identified in water purification.

Table 1. Permissible limits of selected heavy metals in drinking water.[10, 12]

Heavy Metals	Permissible Limit (mg/L)			
	US EPA*	WHO*	EC*	Australia
Lead	0.015	0.01	0.5	0.05
Mercury	0.002	0.001	0.001	0.001
Arsenic	0.01	0.01	0.01	0.007
Cadmium	0.005	0.003	0.005	0.002
Copper	1.3	2.0	2.0	2.0

**US EPA: United States Environment Protection Agency, WHO: World Health Organization; EC: European Community.*

Current water purification technologies such as oxidation, precipitation, ion exchange, photocatalysis, electrochemical treatment, capacitive deionization and membrane filtration are only able to meet more than 99 % efficiency under ideal operating parameters (pH, temperature and concentration of pollutants). Majority of

these technologies are high cost, energy-intensive, low removal efficiency and often generate secondary pollution.[13] Among them, adsorption still appears as a highly-desirable water purification technology owing to myriads advantages including cost-effectiveness, versatility in field operation, less energy- and labor-demanding.[13-14]

To date, a wide array of adsorbents such as metal oxides, metal sulfides, metal organic framework (MOF), clay minerals, silica, biopolymers, synthetic polymers, activated carbon (AC), carbon nanotubes (CNTs), graphene and its derivatives have been studied with some of them demonstrating promising water purification capability.[14-15] Among the adsorbents, AC has long been established as a commercial adsorbent owing to its low cost, large specific surface area and high porosity. However, it still suffers from some setbacks including energy-intensive activation process, inconsistent quality due to the use of a broad range of raw sources, high tendency to pore blockage and inefficient removal of water pollutants at low concentrations.[16-17] Although nanomaterials such as metal oxides have demonstrated their superior adsorption performance to remove water pollutants, drawbacks including poor recovery after the adsorption process and potential risk to induce water security issues due to the remaining nanomaterials in treated waters still present.[15, 18-19] These limitations (**Figure 3**) have compelled researchers to develop new-generation adsorbents using a sustainable raw source to tackle the technical issues encountered in the engineering of adsorbents.

Figure 3. Current challenges identified in existing adsorbents.

Extracted from graphite, graphene is an atom-thick planar sheet 2D material consisting of sp^2 hybridized carbon atoms arranged in a honeycomb lattice. It has recently emerged as a new-generation adsorbent for removing noxious pollutants from contaminated water bodies. Benefited from its cheap raw source (graphite), graphene with its high specific surface area, remarkable mechanical strength and tailorble surface chemistry appears as a promising candidate for new-generation water purification technology. Nevertheless, graphene is bounded by several limitations including its poor dispersion in water due to π-π stacking, which inhibits the exposure of conjugated π region of graphene that can potentially attract aromatic pollutants in water.[20] The lack of functional groups on the graphene surface also restricts its interaction with charged pollutants such as heavy metals and dyes in the water.[20] Meanwhile, graphene oxide (GO) and reduced graphene oxide (rGO) are well-known derivatives of graphene, appear to have ovecome the water dispersion issue faced by graphene. Depending on the degree of oxidation, GO and rGO are grafted with certain levels of oxygen-containing groups (epoxides, carboxyl and

hydroxyl groups) that can enhance their dispersion in water apart from attracting pollutants in water.[20] However, GO nanosheets may not be ideal to be practically applied in water treatment owing to its high dispersion in water that leads to strong colloidal stability in aqueous systems, which poses difficulty in separation after the sorption process. This results in poor material recovery and potential risk with remaining nanomaterial in treated water that may trigger water security issue.[21] Furthermore, oxygen functionalities found on the surface of GO are inadequate to selectively and effectively remove heavy metals that are often present at low concentration in water matrices.

Hence, to address these limitations, in this work, a comprehensive scope of research gaps and strategies are delivered as illustrated in **Figure 4.** Key research gaps are identified to address several critical challenges in water purification and existing adsorbents, as well as the limitations in pristine graphene and its derivative (GO) towards the formation of ultra-active, selective and high performing graphene-based adsorbents. Rational material design approaches are strategized to focus on the critical challenges as described in the following:

1. **Dispersion:** grafting of ionizable groups onto the graphene structure to resolve the agglomeration issue of graphene in water
2. **Activity:** tailoring the surface and interface of graphene with functional groups that can enhance the binding activity of modified adsorbents with the water pollutants
3. **Water security:** engineering of 2D nanomaterials (graphene and GO nanosheets) to 3D microstructure foam to minimize the water security risk due to potential leaching of nanosheets in the treated water after the sorption process
4. **Recovery:** tuning the hydrophilicity and hydrophobicity of a sorbent material to reduce the colloidal stability of GO in water for greater separation after the sorption process. Magnetic nanoparticles were also introduced into the graphene composites for magnetic separation apart from its heavy metal ions uptake capability.

5. **Selectivity:** tailoring the surface and interface of graphene with functional groups that can improve the selectivity towards specific classes of water pollutants

To attain the desired surface, interfacial and structural properties of adsorbents, functionalizing agents such as cysteamine, pentaerythritol tetrakis-mercaptopropionate and polyamine blend (main constituents: multi-type of amino groups including polyethylenepolyamine, triethyelenpolyamine and tetraethylenepentamine) were introduced to functionalize GO with multifunctional binding chemistry for trapping different classes of water pollutants. Ultimately, the devised material design strategies pave a promising pathway with plethora of benefits including scalable production, economical-feasibility, environmentally sustainability, time- and energy-efficiency to prepare new-generation multifunctional graphene adsorbents with high activity, selectivity and improved recovery that outperform the commercial adsorbent (AC).

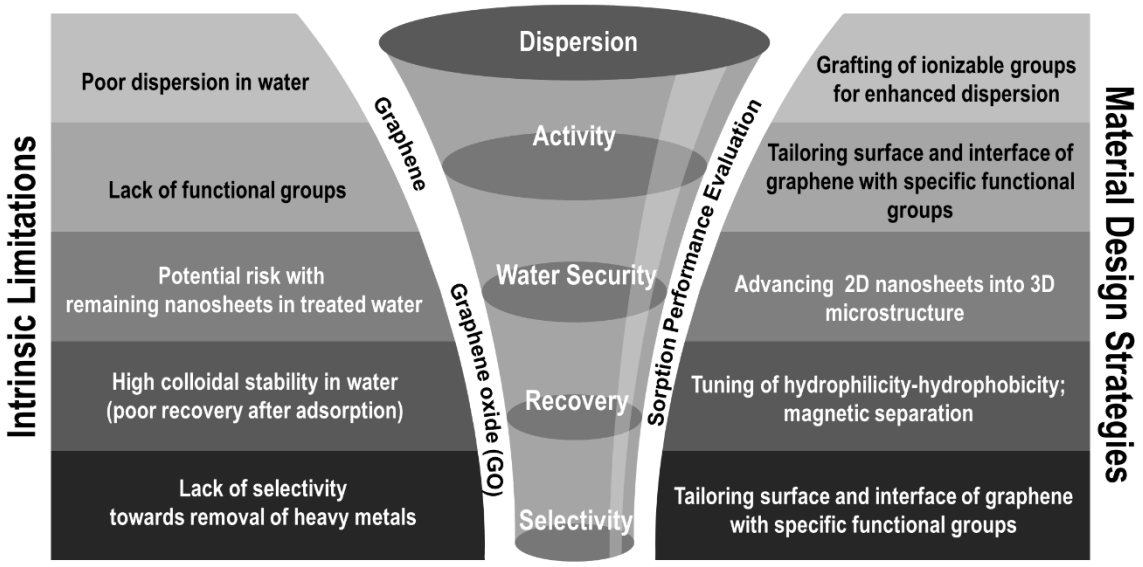

Figure 4. Schematic diagram to address intrinsic limitations of graphene and GO through material design strategies to tackle global water pollution challenges.

1.2. Aim and Objectives

The aim of this PhD work is to explore new directions for the preparation, chemical modifications and applications of advanced graphene-based composites with goals of demonstrating their capability, for the development of ultra-active adsorbents to remove water pollutants in providing sustainable clean water worldwide.

The detailed objectives are as the following:

- **Objective 1:** To identify limitations and research gaps of graphene-based adsorbents with the commercial adsorbent for water purification
- **Objective 2:** To establish fundamental understanding on the surface engineering and structural design of functionalized graphene-based materials
- **Objective 3:** To devise new, environmentally friendly, cost- and energy-efficient methodologies for the preparation of advanced graphene-based composites
- **Objective 4:** To evaluate the sorption performance of advanced graphene-based composites towards the removal of water pollutants

1.3. Thesis Outline

This thesis compiles the comprehensive outcomes of my PhD research structured in the form of journal publications and summarized in the following chapters:

Chapter 1 presents a general overview of the challenges encountered in current water pollution and existing adsorbents as well as strategies for water purification through the engineering of graphene and GO. Key aim and objectives involved in

this research work are also elaborated with detailed contents of each chapter summarized in accordance with the listed objectives.

Chapter 2 reviews the recent progress of advanced graphene-based composites as emerging sorbents for removing myriad classes of pollutants from water. This chapter addresses Objective 1 with its corresponding outcomes as a review article accepted for publication: **Yap, P. L.**, Md J. N., Hassan, K., Tung, T. T., Tran, D. N., & Losic, D. (2020). Graphene-based sorbents for multipollutants removal in water: a review of recent progress. *Advanced Functional Materials*.

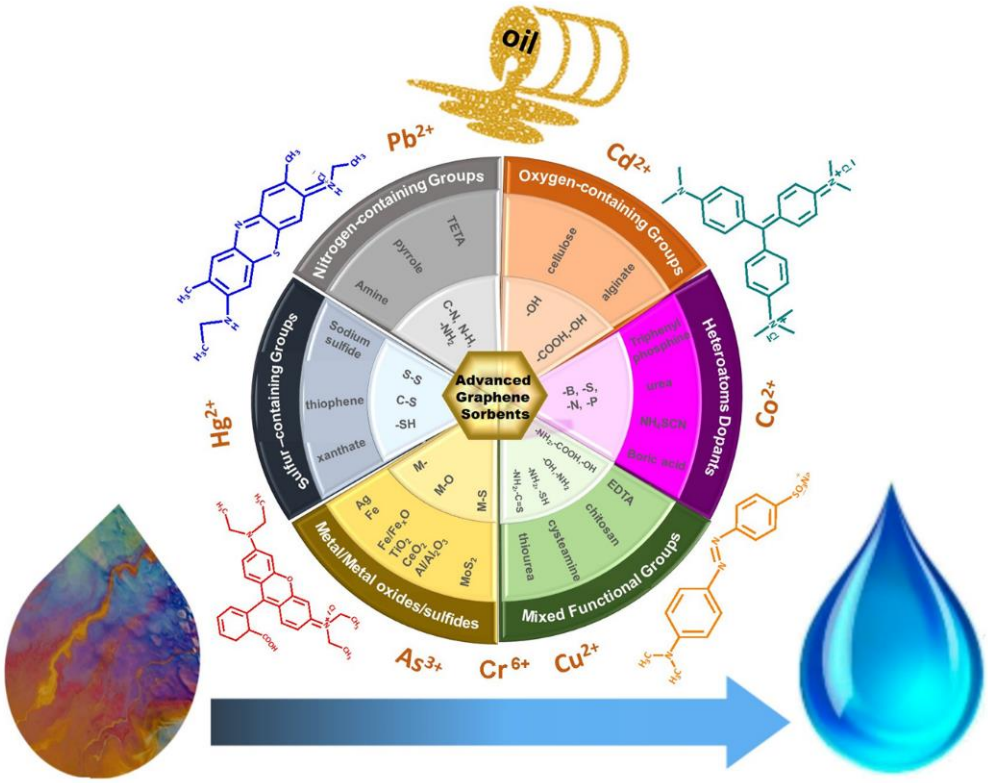

Figure 5. Graphical abstract of *"Graphene-based Sorbents for Multipollutants Removal in Water: A Review of Recent Progress". Reproduced with permission.*[25] *Copyright (2020) Wiley-VCH.*

Chapter 3 underpins the fundamental understanding on surface engineering and structural design of functionalized graphene materials through combined modifications of chemical doping, reduction and thiol-ene click reaction. Findings from this chapter fulfil Objective 2 and are consolidated in a published peer-reviewed research article: **Yap, P. L.**, Kabiri, S., Auyoong, Y. L., Tran, D. N. H., & Losic, D. (2019). *Tuning the multifunctional surface chemistry of reduced graphene oxide via combined elemental doping and chemical modifications*. *ACS Omega*, 4(22), 19787-19798. doi: 10.1021/acsomega.9b02642

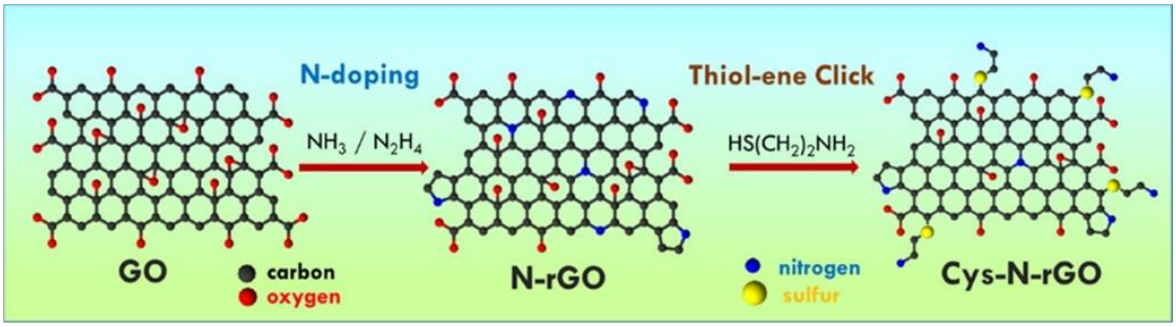

Figure 6. Graphical abstract of *"Tuning the multifunctional surface chemistry of reduced graphene oxide via combined elemental doping and chemical modifications". Reproduced with permission.*[22] *Copyright (2019) American Chemical Society.*

Chapter 4 reports the development of advanced graphene composites (polyamine-rGO) through hydrothermal and chemical modification approaches with high adsorption rate, remarkable working pH range and good selectivity towards mercury (II) ions. This work achieves Objectives 3 and 4 with the related results combined in a published peer-reviewed research article: **Yap, P. L.**, Tung, T. T., Kabiri, S., Matulick, N., Tran, D. N. H., & Losic, D. (2020). *Polyamine-modified reduced*

graphene oxide: a new and cost-effective adsorbent for efficient removal of mercury in waters. Separation and Purification Technology, 238, 116441. doi: https://doi.org/10.1016/j.seppur.2019.116441

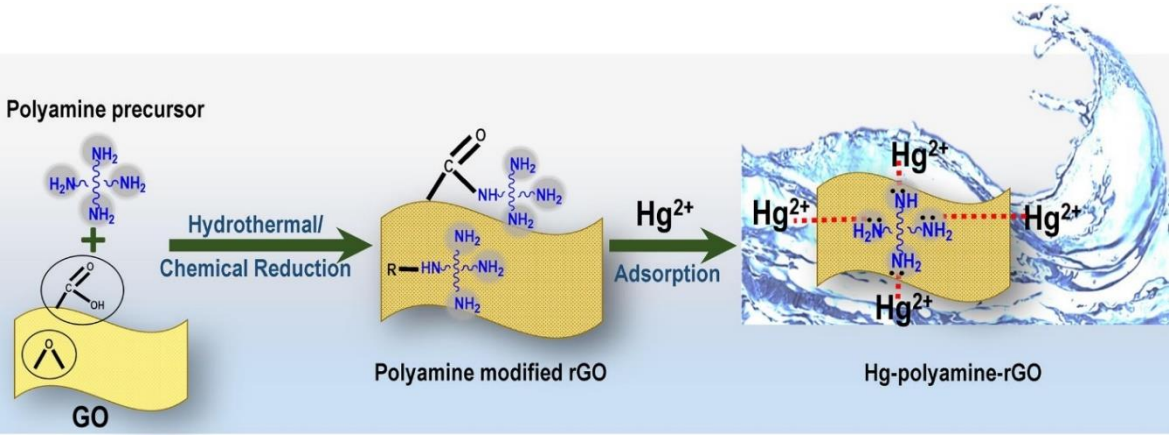

Figure 7. Graphical abstract of *"Polyamine-modified reduced graphene oxide: a new and cost-effective adsorbent for efficient removal of mercury in waters". Reproduced with permission.[23] Copyright (2019) Elsevier.*

Chapter 5 describes the rational design of advanced graphene composites (cysteamine-clicked partially rGO) with multiple binding fuctionalities through an optimized thermal thiol-ene click modification approach to achieve outstanding adsorption capacity, good selectivity, high adsorption rate and regeneration ability towards mercury (II) ions. The investigations in this chapter meet Objectives 3 and 4 with the corresponding discoveries summarized in a published peer-reviewed research article: **Yap, P. L.**, Kabiri, S., Tran, D. N. H., & Losic, D. (2019). *Multifunctional binding chemistry on modified graphene composite for selective and highly efficient adsorption of mercury.* ACS Applied Materials & Interfaces, 11(6), 6350-6362. doi: 10.1021/acsami.8b17131.

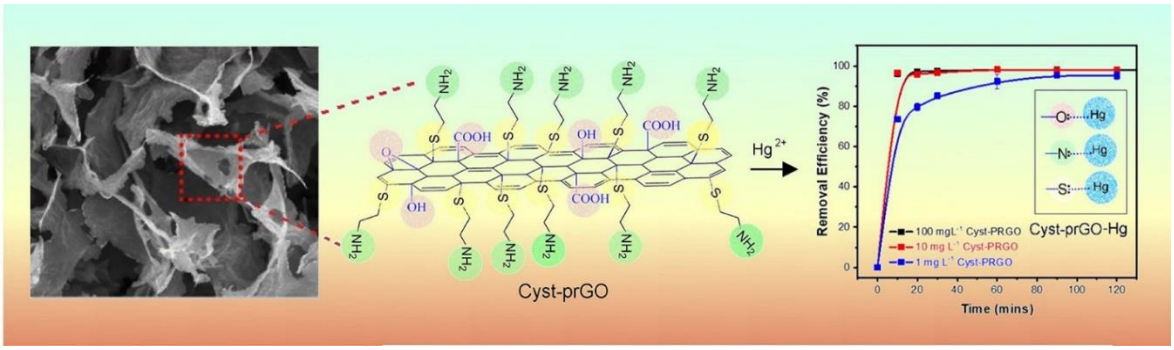

Figure 8. Graphical abstract of "*Multifunctional binding chemistry on modified graphene composite for selective and highly efficient adsorption of mercury*". *Reproduced with permission.[14] Copyright (2019) American Chemical Society.*

Chapter 6 explores the assembly of advanced graphene composites by combining GO, alginate, tetrathiol precursor and magnetic nanoparticles through a photoinitiated thiol-ene click modification approach for efficient trapping of multi-pollutants in water, including heavy metal ions, spilled oils and organic dyes. Scientific discoveries from this chapter address Objectives 3 and 4 that generated two published peer-reviewed articles as the following.

Yap, P. L., Auyoong, Y. L., Hassan, K., Farivar, F., Tran, D. N. H., Ma, J., & Losic, D. (2020). *Multithiol functionalized graphene bio-sponge via photoinitiated thiol-ene click chemistry for efficient heavy metal ions adsorption*. Chemical Engineering Journal, 395, 124965. doi: 10.1016/j.cej.2020.124965

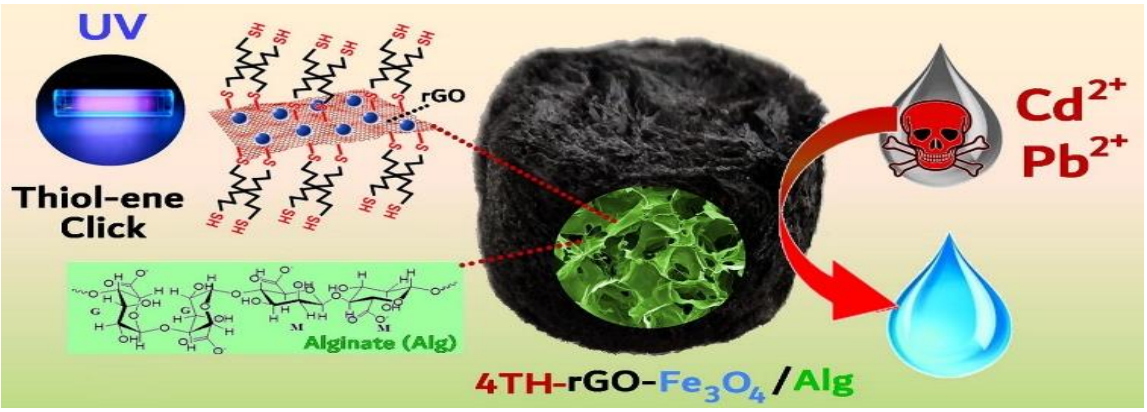

Figure 9. Graphical abstract of "*Multithiol functionalized graphene bio-sponge via photoinitiated thiol-ene click chemistry for efficient heavy metal ions adsorption*". *Reproduced with permission.*[19] *Copyright (2020) Elsevier.*

Yap, P. L., Hassan, K., Auyoong, Y. L., Mansouri, N., Farivar, F., Tran, D. N., & Losic, D. (2020). *All-in-one bioinspired multifunctional graphene biopolymer foam for simultaneous removal of multiple water pollutants.* Advanced Materials Interfaces, 2000664. doi: 10.1002/admi.202000664

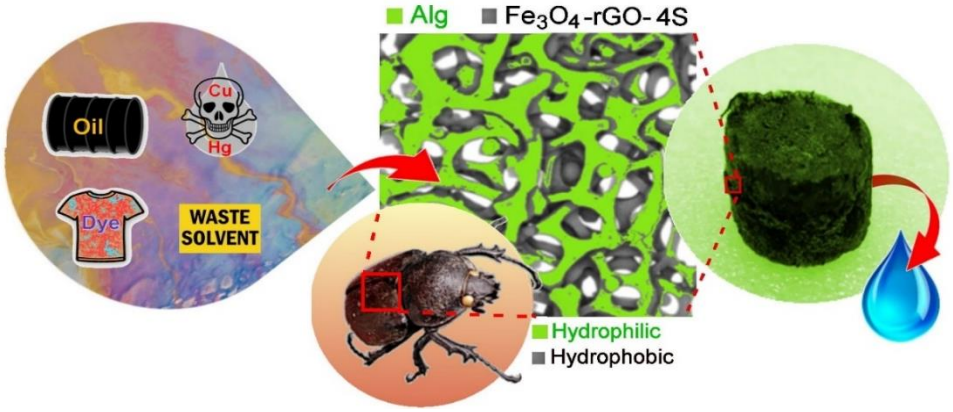

Figure 10. Graphical abstract of "*All-in-one bioinspired multifunctional graphene-biopolymer foam for simultaneous removal of multiple water pollutants*". *Reproduced with permission.*[24] *Copyright (2020) Wiley-VCH.*

Chapter 7 summarizes the development of advanced graphene composites in this thesis and provides the futuristic direction of advanced graphene-based composites as an emerging water purification technology.

CHAPTER 2

LITERATURE REVIEW

2. LITERATURE REVIEW

2.1. Overview and Significance of Work

In line with Objective 1, this chapter focuses on the recent progress of advanced graphene composites as emerging sorbents for removing myriad classes of pollutants from water. The rational design of advanced graphene sorbents is first discussed based on different functionalization approaches, followed by a strategic roadmap to unleash the underlying interaction mechanism between advanced graphene sorbents with different classes of water pollutants. A structure-function-performance relationship between the advanced graphene sorbents with the multi-pollutants in the water is also established to understand the fundamental relation between the adsorption properties (surface area, pore size, type of functional groups, C/O, C/N and C/S atomic ratio) of advanced graphene sorbents with the sorption performance of diverse pollutants in water. Finally, the reality, challenges and opportunities of advanced graphene materials as emerging sorbents for sustainable water purification technology are also discussed.

2.2. Statement of Authorship

Statement of Authorship

Title of Paper	Graphene-based Sorbents for Multi-Pollutants removal in Water: A Review of Recent Progress
Publication Status	☐ Published ☒ Accepted for Publication ☐ Submitted for Publication ☐ Unpublished and Unsubmitted work written in manuscript style
Publication Details	Pei Lay Yap, Md. J. Nine, Kamrul Hassan, Tung Tran, Diana N. H. Tran and Dusan Losic, Graphene-based Sorbents for Multi-Pollutants removal in Water: A Review of Recent Progress, Advanced Functional Materials, 2020.

Principal Author

Name of Principal Author (Candidate)	Pei Lay Yap		
Contribution to the Paper	Prepared, edited and revised the review manuscript.		
Overall percentage (%)	85%		
Certification:	This paper reports on original research I conducted during the period of my Higher Degree by Research candidature and is not subject to any obligations or contractual agreements with a third party that would constrain its inclusion in this thesis. I am the primary author of this paper.		
Signature		Date	30/11/20

Co-Author Contributions

By signing the Statement of Authorship, each author certifies that:

i. the candidate's stated contribution to the publication is accurate (as detailed above);

ii. permission is granted for the candidate in include the publication in the thesis; and

iii. the sum of all co-author contributions is equal to 100% less the candidate's stated contribution.

Name of Co-Author	Md. Julker Nine		
Contribution to the Paper	Edited and revised the manuscript.		
Signature		Date	01.12.2020

Name of Co-Author	Kamrul Hassan		
Contribution to the Paper	Edited and revised the manuscript		
Signature		Date	01.12.2020

Please cut and paste additional co-author panels here as required.

Statement of Authorship

Title of Paper	Graphene-based Sorbents for Multi-Pollutants removal in Water: A Review of Recent Progress
Publication Status	☐ Published ☒ Accepted for Publication ☐ Submitted for Publication ☐ Unpublished and Unsubmitted work written in manuscript style
Publication Details	Pei Lay Yap, Md. J. Nine, Kamrul Hassan, Tung Tran, Diana N. H. Tran and Dusan Losic, Graphene-based Sorbents for Multi-Pollutants removal in Water: A Review of Recent Progress, Advanced Functional Materials, 2020.

Principal Author

Name of Principal Author (Candidate)	Pei Lay Yap		
Contribution to the Paper	Prepared, edited and revised the review manuscript.		
Overall percentage (%)	85%		
Certification:	This paper reports on original research I conducted during the period of my Higher Degree by Research candidature and is not subject to any obligations or contractual agreements with a third party that would constrain its inclusion in this thesis. I am the primary author of this paper.		
Signature		Date	30/11/20

Co-Author Contributions

By signing the Statement of Authorship, each author certifies that:

i. the candidate's stated contribution to the publication is accurate (as detailed above);

ii. permission is granted for the candidate in include the publication in the thesis; and

iii. the sum of all co-author contributions is equal to 100% less the candidate's stated contribution.

Name of Co-Author	Tran Thanh Tung		
Contribution to the Paper	Edited and revised the manuscript.		
Signature		Date	1/12/2020

Name of Co-Author	Diana N.H. Tran		
Contribution to the Paper	Co-supervised and revised manuscript.		
Signature		Date	01/12/2020

Please cut and paste additional co-author panels here as required.

Statement of Authorship

Title of Paper	Graphene-based Sorbents for Multi-Pollutants removal in Water: A Review of Recent Progress
Publication Status	☐ Published ☒ Accepted for Publication ☐ Submitted for Publication ☐ Unpublished and Unsubmitted work written in manuscript style
Publication Details	Pei Lay Yap, Md. J. Nine, Kamrul Hassan, Tung Tran, Diana N. H. Tran and Dusan Losic, Graphene-based Sorbents for Multi-Pollutants removal in Water: A Review of Recent Progress, Advanced Functional Materials, 2020.

Principal Author

Name of Principal Author (Candidate)	Pei Lay Yap		
Contribution to the Paper	Prepared, edited and revised the review manuscript.		
Overall percentage (%)	85%		
Certification:	This paper reports on original research I conducted during the period of my Higher Degree by Research candidature and is not subject to any obligations or contractual agreements with a third party that would constrain its inclusion in this thesis. I am the primary author of this paper.		
Signature		Date	30/11/20

Co-Author Contributions

By signing the Statement of Authorship, each author certifies that:

i. the candidate's stated contribution to the publication is accurate (as detailed above);

ii. permission is granted for the candidate in include the publication in the thesis; and

iii. the sum of all co-author contributions is equal to 100% less the candidate's stated contribution.

Name of Co-Author	Dusan Losic		
Contribution to the Paper	Supervised the development of work, edited, revised the manuscript and acted as the corresponding author.		
Signature		Date	1/12/2020

Name of Co-Author			
Contribution to the Paper			
Signature		Date	

Please cut and paste additional co-author panels here as required.

2.3. Accepted Work for Publication

This section is presented as a review article as **Pei Lay Yap**, Md. J. Nine, Kamrul Hassan, Tung Tran, Diana N. H. Tran and Dusan Losic, *Graphene-based sorbents for multipollutants removal in water: a review of recent progress* in Advanced Functional Materials, 2020. Reproduced with permission.[25] Copyright (2020) Wiley-VCH.

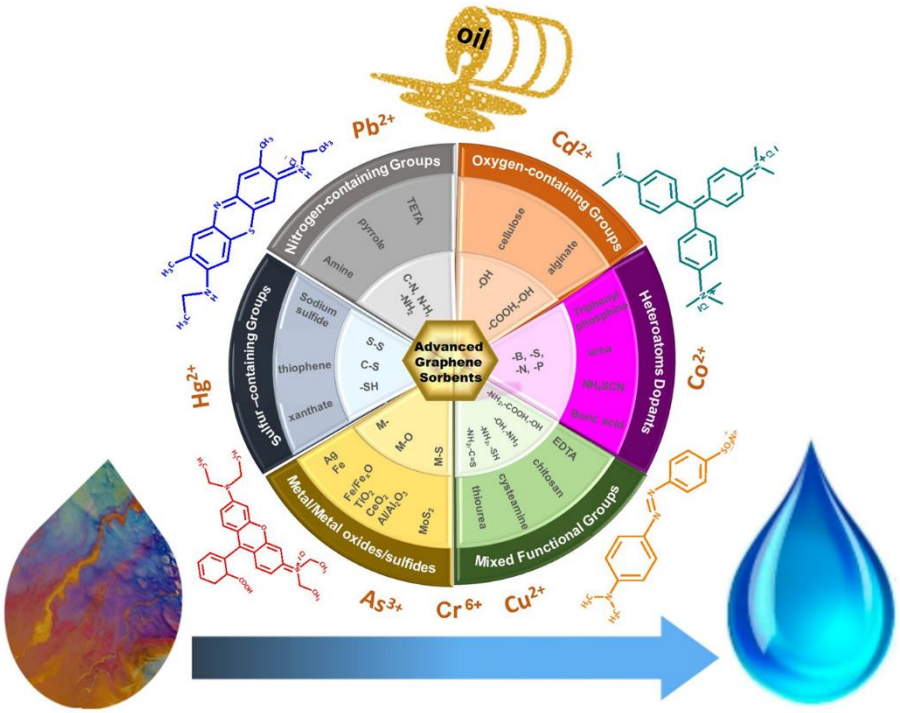

Figure 11. Graphical abstract of *"Graphene-based sorbents for multipollutants removal in water: a review of recent progress". Reproduced with permission.[25] Copyright (2020) Wiley-VCH.*

REVIEW

ADVANCED FUNCTIONAL MATERIALS
www.afm-journal.de

Graphene-Based Sorbents for Multipollutants Removal in Water: A Review of Recent Progress

*Pei Lay Yap, Md Julker Nine, Kamrul Hassan, Tran Thanh Tung, Diana N. H. Tran, and Dusan Losic**

The coexistence of multiple toxic water pollutants (heavy metals, organic dyes, oils, and organic solvents) limits the sustainable supply of clean water worldwide and urges the development of advanced water purification technology that can remove these contaminants simultaneously. Since its discovery, graphene-based materials have gained substantial attention toward development of new-generation sorbents for water purification. Despite several recently published reviews on water purification technology using graphene and its derivatives, there is still a gap in the review considering multiple water-pollutant remediation using advanced graphene materials. In this review, in the first instance, a comparative structure–function–performance relationship between graphene-based sorbents and the multipollutants in water is established. A fundamental correlation is made between the sorption performance for diverse pollutants in water with the more specific adsorption properties (surface area, pore size, type of functional groups, C/O, C/N, and C/S atomic ratio) of advanced graphene sorbents. Second, the underlying interaction mechanisms are uncovered between different classes of water pollutants using single graphene-based sorbents. Third, the rational design of advanced multipollutant sorbents based on graphene is elaborated. The reality, challenges, and opportunities of advanced graphene materials as emerging sorbents for sustainable water purification technology are finally presented in the last section.

1. Introduction

Majority of water resources such as rivers, lakes, groundwater, and even oceans are drowning in pollutants, including broad range of coexisting contaminants (dyes, spilled oils, organic solvents, and heavy metals) generated from the discharge of wastewater from industries, agriculture, and sewage that jeopardize our health, and environmental sustainability.[1] It is essential to realize that water pollution is complex in reality, given that it is not dealing merely with a single type of contaminant, but the co-occurrence of more than a single pollutant in the water systems.[2] Remediation of multicontaminants is also further hampered by incomplete water quality assessments and inadequate data compilation on purification technologies used for tackling multipollutants in water. Therefore, a paradigm shift from single pollutant to multipollutant control is crucial to tackle this water purification challenge,[2,3] which calls for a comprehensive water quality assessment and development of effective water purification technologies to remove these multipollutants.[2]

Conventional water purification treatments combine physical (adsorption, filtration, distillation, sedimentation, and skimming), chemical (chlorination, oxidation, precipitation, electrochemical, hydrolysis, neutralization, ozonation, and ultraviolet irradiation), as well as biological (anaerobic and aerobic treatment conversions) operations at different treatment levels (preliminary, primary, secondary, and tertiary) that are necessary to recover clean water from wastewater effluents containing different classes of multipollutants.[4] However, setbacks like high operation cost, large energy consumption, poor removal efficiency, generation of secondary pollutants and toxic side-products, have been identified with limited considerations in many water purification strategies.[4a,5] As presented in **Figure 1**a, achieving higher quality of treated water requires refining step to remove nitrogen, phosphorus, suspended solids, refractory organics, heavy metals, and dissolved solids that remain from primary and secondary treatments.[3b,6]

Under more stringent regulatory limits for water contaminants in controlling waterborne diseases, it has become more challenging for the water industry to remove emerging pollutants that are not easily detectable by our senses.[3b] Majority of the decontamination strategies are also particularly inefficient to cope with the removal of heavy metals (classical example of water pollutant), which are often present at very low concentration in the water bodies, but adequately to cause chronic diseases such as disorder of the kidney and nervous system, cancer, lung, and liver damage when exposed to these noxious pollutants at trace concentrations.[4a,7] Among the advanced water purification technologies, adsorption, membrane

P. L. Yap, Dr. Md J. Nine, K. Hassan, Dr. T. T. Tung, Dr. D. N. H. Tran, Prof. D. Losic
School of Chemical Engineering and Advanced Materials
The University of Adelaide
Adelaide, SA 5005, Australia
E-mail: dusan.losic@adelaide.edu.au
P. L. Yap, Dr. Md J. Nine, K. Hassan, Dr. T. T. Tung, Dr. D. N. H. Tran, Prof. D. Losic
ARC Hub for Graphene Enabled Industry Transformation
The University of Adelaide
Adelaide, SA 5005, Australia
The ORCID identification number(s) for the author(s) of this article can be found under https://doi.org/10.1002/adfm.202007356.

DOI: 10.1002/adfm.202007356

ADVANCED SCIENCE NEWS
www.advancedsciencenews.com

ADVANCED FUNCTIONAL MATERIALS
www.afm-journal.de

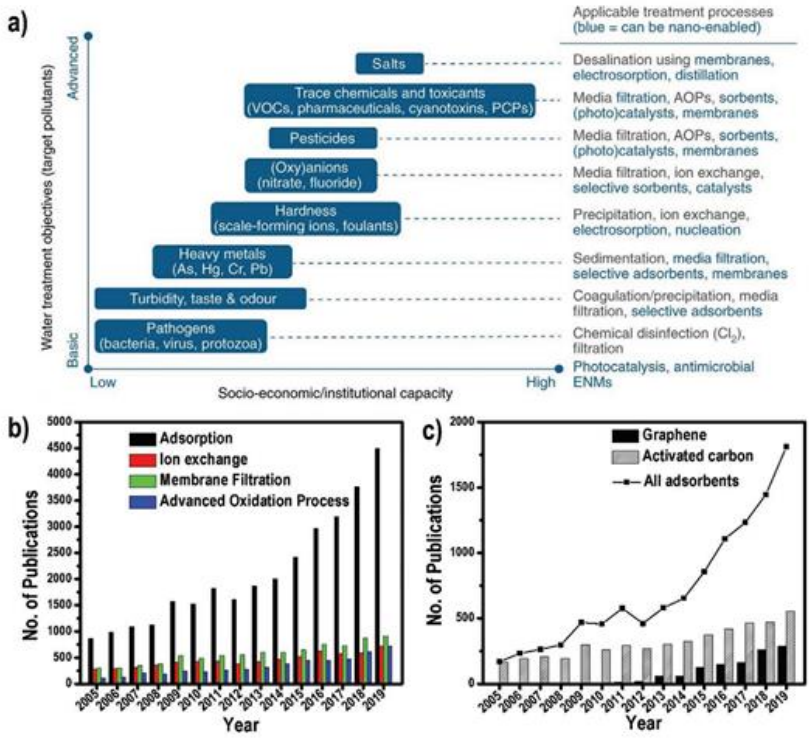

Figure 1. a) Water treatment priorities and processes that can be enhanced by nanotechnology. Reproduced with permission.[3b] Copyright 2018, Nature Publishing Group. Number of publications devoted to key water purification technologies. Data extracted from Scopus by applying title-abstract-keywords search function from 2005 to 2019 for comparison of b) different water treatment technologies based on search function (adsorption and water treatment), (ion exchange and water treatment), (membrane filtration and water treatment), (advanced oxidation and water treatment) c) adsorption in water treatment using different adsorbents based on search function (adsorption and water treatment and adsorbent), (adsorption and water treatment and graphene), (adsorption and water treatment and activated carbon).

filtration, ion exchange, and advanced oxidation process have captivated a great deal of interest recently due to their promising purification performances. Nevertheless, these technologies are associated with some drawbacks. For instance, although the ion exchange process is efficient in water treatment with no sludge generated, its process is very specific to certain pollutants with a high cost required for the replacement of the ion exchange resin in the long run. Despite that water decontamination using membrane filtration can achieve high removal efficiency by a simple separation process without generation of secondary pollution, its application is still limited by high manufacturing costs, severe fouling, and high energy consumption. Advanced oxidation process, on the other hand, emphasizes the use of strong oxidants or ultra–violet (UV) irradiation on a catalyst that often involves high operating cost with inefficient utilization of generated reactive oxygen species. This process is also limited to be applied for high concentration of dark colored wastewater containing organic pollutants due to low light transmissions apart from its complex operating procedures.[3b,5,8] A steady rise in the number of publications within these recent 1.5 decades (Figure 1b) clearly showed that adsorption still remains as the most desirable tertiary water purification technologies. This could be attributed to its low cost, energy efficient, high removal efficiency with promising quality treated effluent, flexibility in field operations, reversible nature that permits regeneration of adsorbents and feasibility to tackle multiple pollutant classes.[5,8] For adsorption, many sorbent materials such as metal oxides, metal chalcogenides, zeolites, metal organic frameworks (MOF), clays, polymers as well as carbon materials including fullerenes, nanodiamonds, activated carbon, carbon nanotubes (CNTs), graphene and its derivatives have been extensively explored to mitigate water pollution issues.[9]

Activated carbon (AC) holds the longest track record among the carbon-based materials in purification with its first use to decolorize sugar, to remove foul odor and taste dated back to 1500 BC. It is available in several forms including granule, powder, pellet and block that is able to eliminate pollutants ranging from industrial to municipal wastewaters owing to its low cost, large surface area (500–2500 $m^2 g^{-1}$) and highly porous structure.[10] Textural properties of AC including pore size, surface area, and pore volume are highly dependent on the activation process as well as the raw sources (coals, nutshells, wood, and bamboo) used to generate it.[10] Due to the varied quality

and inconsistency on the grade of AC that can be generated from a wide range of raw sources, their adsorption performance in water treatment can be greatly affected. Another disadvantage of AC can be related to its highly energy-intensive activation process with large amount of heat energy required and its high tendency to experience pore blockage by larger pollutants within its pore structure, which could limit the diffusion of subsequent smaller contaminants.[10a] Meanwhile, graphene and its derivatives appear to be rising stars in water purification owing to their remarkable adsorption properties such as high theoretical specific surface area (2600 $m^2 g^{-1}$), superior mechanical strength, tailorable surface chemistry and flexibility to be used in various forms (powder, film, suspension, hydrogel, or sponge).[9] Based on the published record since 2005 to 2019 (Figure 1c), graphene has gradually been showered with attention in water treatment despite that its emergence in water purification is still at its infancy compared to other existing adsorbents.

Recent reviews show that the full potential of graphene as the supersorbent of the century is yet to unlock with myriads of promising developments toward improving the global water quality issues.[11] The use of advanced graphene sorbents is expected to reduce the alarming water pollution and deliver clean water globally, particularly in dealing with the removal of multipollutants in water.[2,3] Although a great deal of reviews on environmental applications of graphene related materials have been recently published, majority are targeted toward specific and single class of water pollutants including heavy metals,[12] dyes,[13] organic solvents,[14] and oils[5,12b,c,13,14b,15] with no reviews focused on multipollutant control using graphene-based sorbent materials to date. As accentuated by several critical reviews, an enormous knowledge gap still exists to link the surface chemistry and physicochemical properties of advanced graphene sorbents with sorption performance for multiple pollutant control in water purification.[11a,c,16] Therefore, in this review, we primarily focus on the multipollutant remediation in water using advanced graphene sorbents, which has not been discussed previously. We highlight the rational design of these advanced graphene sorbents based on their functional groups to capture multipollutants in water, followed by establishing the fundamental structure–function–performance relationships with broad classes of pollutants (heavy metals, dyes, organic solvents, and oils). In particular, correlation has been made between their adsorption properties (surface area, pore size, type of functional groups, C/O, C/N, and C/S atomic ratio) with the maximum sorption capacities achieved for sorption of multipollutants using a graphene sorbent. Finally, the reality, challenges and opportunities of graphene-based materials as emerging sorbents for progressive and sustainable water purification technology are addressed.

2. Interaction Mechanisms for Multipollutants Removal

2.1. Graphene as Emerging Sorbent for Multipollutant Water Remediation: Insights of Interaction Mechanisms

Graphene, the pristine building block of graphite, is made up of crystalline and honeycomb graphene layers consisting of sp^2-hybridized carbons. Processes involving exfoliation and functionalization of graphite are necessary to introduce sp^3 domains by breaking its thermally and chemically stable sp^2 aromatic structure in order to add and activate the functionality of this carbon allotrope. These processes allow the introduction of defects, dopant-atoms, and functional groups to attract multiple classes of pollutants in water. Recent focus of water remediation materials has been shifted to the fabrication of highly porous and low density 3D macrostructures from 2D graphene nanosheets to increase the trapping capacity toward various type of water pollutants (heavy metal ions, dyestuffs, oil, and organic solvents spills).[11a,c] By adopting the design of 3D macrostructures (sponges, membranes, beads, and fibers), adsorption properties in terms of robustness, flexibility for field operations and easy recovery can be greatly enhanced. Furthermore, these 3D graphene macrostructures also prevent nanomaterials from agglomeration besides providing adequate room to accommodate more incoming pollutants and enabling mass transport of pollutants within the sorbent structure.[11a,c,17]

Pore-filling, π–π, cationic–π, hydrogen bonding, hydrophobic, and electrostatic interactions are important physical interactions take place at the outer surface of the adsorbents. Pore-filling mechanism is mainly responsible for adsorption of organic pollutants such as oils and organic solvents. Besides giving rise to high surface area, the creation of pores within the sorbent network allows the water contaminants to diffuse and fill the pores, which are initially air-filled as shown in **Figure 2**.[18] Key features of the pore structure including pore type, pore size, and pore volume determine the access and entrapment of the pollutants within the pores of adsorbents.[8]

Figure 3 provides the general interaction mechanisms between the binding sites of the advanced graphene sorbents with different classes of water pollutants (heavy metals, dyes, oils, and organic solvents). π–π interaction involves noncovalent attraction that exists between organic pollutants carrying aromatic rings and graphene sorbents with its conjugated systems in the sp^2 -hybridized domains.[19] Cationic–π binding mechanism is a type of noncovalent attraction between a positively charged pollutant and negatively charged electron cloud of π system of the advanced graphene sorbents.[20] While, hydrogen bonding; a type of dipole–dipole interaction, exists between a hydrogen atom covalently bonded to highly electronegative atoms (nitrogen, fluorine, and oxygen) on the functionalized graphene sorbents with another electronegative atom bearing a lone pair electrons. This attractive force is greatly portrayed when the functional groups (e.g., fluorine-, oxygen- and nitrogen-containing groups), grafted on the sp^3 domains of graphene interact with the polar organic contaminants. Hydrophobic interaction occurs between nonpolar organic molecules such as oils and nonpolar solvents with the hydrophobic binding sites of graphene sorbents. Electrostatic interaction (coulombic force) can significantly contribute to the adsorption of oppositely charged pollutants including cationic heavy metal ions and ionic organic dyes on the binding sites of advanced graphene sorbents.

On the other hand, chemical interaction (ion exchange, surface complexation, and Lewis acid–base interactions) involves stronger attraction between the contaminants and the sorbents with the formation of inner complexes. Taking ion-exchange

ADVANCED SCIENCE NEWS
www.advancedsciencenews.com

ADVANCED FUNCTIONAL MATERIALS
www.afm-journal.de

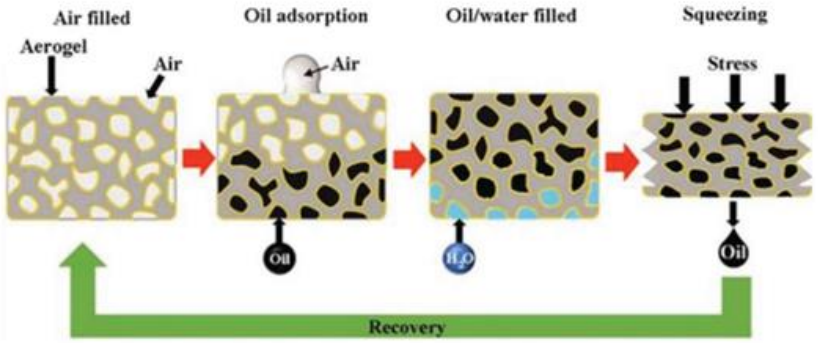

Figure 2. Physical adsorption mechanism of oil to fill the pore space within the 3D porous graphene structures such as graphene aerogel as a typical example to demonstrate influence of pore structures on oil sorption. Reproduced with permission.[18] Copyright 2018, American Chemical Society.

mechanism as an example, it describes a purification and separation process when the dissolved ions (inorganic pollutants) in an aqueous solution are exchanged with other ions of similar electrical charge on the sorbent. Surface complexation considers the interfacial equilibrium achieved between the bulk species (pollutants) with active surface groups on an adsorbent. Lewis acid–base interaction can be regarded as a concept that covers a broader range of phenomena including the hard-soft acid base theory (HSAB), coordinate bond formation, and electron pair donor–acceptor reactions.[21] A good example to exemplify this concept is by Kumar et al. that demonstrated strong interaction between Hg^{2+} ions (soft Lewis acid, electron pair acceptor) with sulfur-, and nitrogen-containing functional groups (soft Lewis bases, electron donors) on graphene

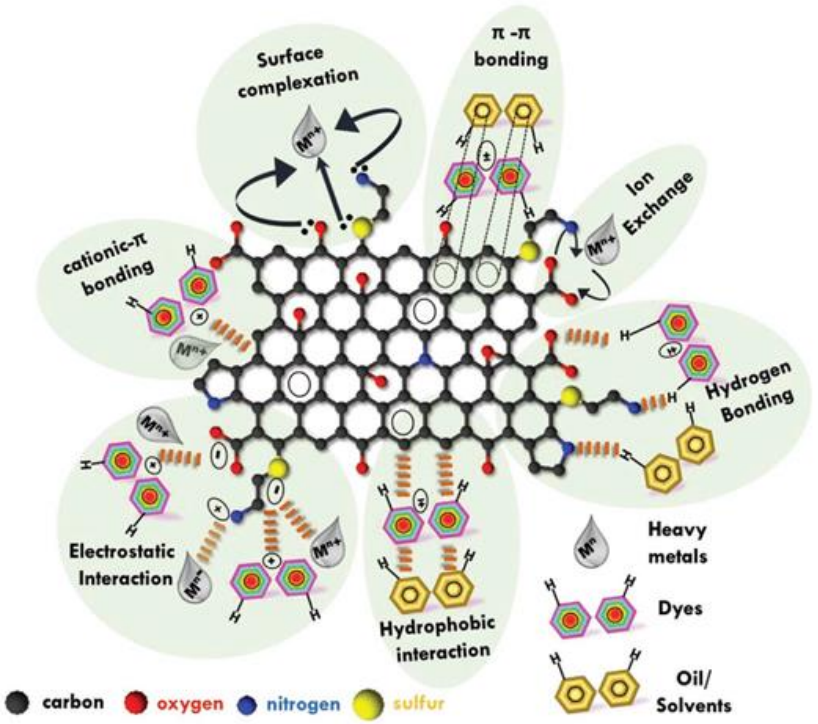

Figure 3. Overview of main interaction mechanisms between the doped atoms and functional groups showing a representative advanced graphene sorbent with ability to remove multiple water pollutants (heavy metals, dyes, oil, and solvents) from different polluted water systems. Images are not drawn to scale. Adapted with permission.[23] Copyright 2019, American Chemical Society.

adsorbents leads to the formation of coordinate bond.[22] Since the interaction mechanisms that involve multipollutants are complex, interaction mechanisms of the multipollutant sorbents reviewed in this section is individually discussed for each class of pollutant to give a better perspective on how the specific class of pollutant can be bound to the active sites of the sorbents.

2.2. Interaction Mechanism: Heavy Metals

Graphene-based sorbents offer a broad range of sorption approaches to capture heavy metal ions including electrostatic interaction, surface complexation, ion exchange, and cationic–π interactions. This can be achieved through specific design using functionalization including high-binding functional groups, elemental doping or creating defects with structural design to enhance adsorption performance. Introduction of defects on the graphene surface was found to effectively enhance the adsorption ability of heavy metals as evidenced by the vacancy defects created in graphene quantum dots for binding of cadmium, mercury and lead through charge transfer.[24] Similar findings also showcased that the single vacancy defect introduced to graphene can greatly enhance the adsorption of cadmium with substantial amount of electrons transferred from cadmium to graphene.[25] Meanwhile, doping of nitrogen/sulfur atoms in graphene has significantly increased the adsorption of heavy metals such as cadmium, mercury and lead, which could be related to van der Waals forces and electrostatic interactions.[26] Electrostatic attraction and coordination between doped nitrogen atoms and Pb^{2+} ions were responsible for the removal mechanisms of nitrogen-doped graphene aerogels that was hydrothermally fabricated.[27] In comparison to the defects and dopants crafted on the sp^3 domains of the graphene network, functional groups including oxygen-, nitrogen-, sulfur-, metals/metal oxides/ metal sulfides-containing groups are among the most explored for the uptake of heavy metal ions.

Many studies evidently demonstrated that the grafted functional groups on the graphene structure can selectively immobilize specific heavy metals that lead to enhanced heavy metals removal. Taking graphene oxide (GO) as an example, the plentiful oxygen functional groups (−COOH and −OH) on GO are responsible for the adsorption of heavy metal ions through ion exchange, surface complexation and electrostatic interactions.[28] Therefore, a great deal of work has been focused on decorating the graphene structure with precursors containing oxygen groups such as alginate and cellulose to improve the adsorption efficiency of heavy metal ions. For instance, alginate/reduced graphene oxide double network hydrogel that was laden with oxygen functional groups interacted effectively with Cu^{2+} and $Cr_2O_7^{2-}$ through electrostatic interaction mechanism.[29] Increased adsorption capacities of 35–500% toward removal of various metal ions (Pb^{2+}, Cd^{2+}, Cr^{6+}, and Cu^{2+}) due to the synergistic effect of electrostatic interaction, surface complexation and ion exchange mechanisms was proven after functionalization of GO using an oxygen functional group precursor, carboxymethyl cellulose.[30]

Apart from oxygen-containing groups, functionalization of graphene with nitrogen- and sulfur-containing precursors was also found to substantially improve the uptake of heavy metal ions. For example, simultaneous adsorption of Cd (II), Hg (II), and As (III) ions to the binding sites of GO modified with 3-aminopyrazole, a nitrogen-containing group precursor, occurred through a combined mechanism of physical adsorption, surface complexation, and electrostatic interaction.[31] Another example of GO functionalized with nitrogen-containing group, 2,2-dipyridylamine (GO-DPA), demonstrated high affinity toward simultaneous adsorption of Pb (II), Cd (II), Ni (II), and Cu (II) ions that could be attributed to the surface complexation and electrostatic interaction.[32] Effective removal of $Pb^{2+}$and Cd^{2+} was confirmed through the modification of GO using thiacalix[4]arenetetrasulfonate, a sulfur-containing group modifier. Good performance could be attributed to the surface complexation between the functional groups and the studied metal ions as illustrated in **Figure 4**a.[33] Surface complexation and electrostatic interaction were the dominant mechanisms that described the binding chemistry between As (V) ion to a metal/metal oxide modified graphene sorbent, manganese ferrite-graphene oxide (MFO-GO) nanocomposites (Figure 4b).[34] Functionalization of GO with magnetic Fe_3O_4 nanoparticles showed that the incorporated iron oxide nanoparticles enhanced the adsorption of Cd (II) through electrostatic interaction.[35] Due to the formation of different arsenic species at varied pH, chitosan modified GO was found to interact with arsenic species through a series of mechanisms including surface complexation, cationic–π, anionic–π, and electrostatic interactions.[36]

2.3. Interaction Mechanism: Organic Dyes

Typically, dyes are colored organic macromolecules that can be categorized based on their molecular structure, charge, solubility or the chromophores present in their structure.[37] Examples of water-soluble dyes include acid, base, direct and reactive dyes, while azo, disperse, sulfur and vat dyes can be regarded as water-insoluble dyes.[38] Presence of the aromatic ring in their structure enables the interaction of the delocalized electrons in their benzene ring with the delocalized π electrons that exist in the basal plane of the graphene structure. Interaction mechanism between the organic dyes and the binding sites of graphene often involves the basal plane of the graphene structure (sp^2 domains) such as π–π and cationic–π interactions in addition to electronic interaction, and hydrogen bonding resulting from the sp^3 domains of the graphene structure. Adsorption performance of graphene-based materials is more pronounced with the use of functionalized graphene to target the removal of organic dyes based on the charged group carried by the organic dyes. For instance, GO, a common derivative of graphene carrying negatively charged groups on its surface, demonstrates better performance towards adsorption of cationic dyes than anionic dyes.[11a] While, anionic dyes are more successfully removed using graphene modified with cationic functional groups such as chitosan, polyethyleneimine and amine.[11a]

For successful adsorption of organic dyes, numerous concepts based on the interactions between functionalized graphene and organic dyes have been explored. Fabrication of polydopamine coated graphene nanosheets was demonstrated for removal of methyl violet, methyl blue and 4-nitrophenol through electrostatic

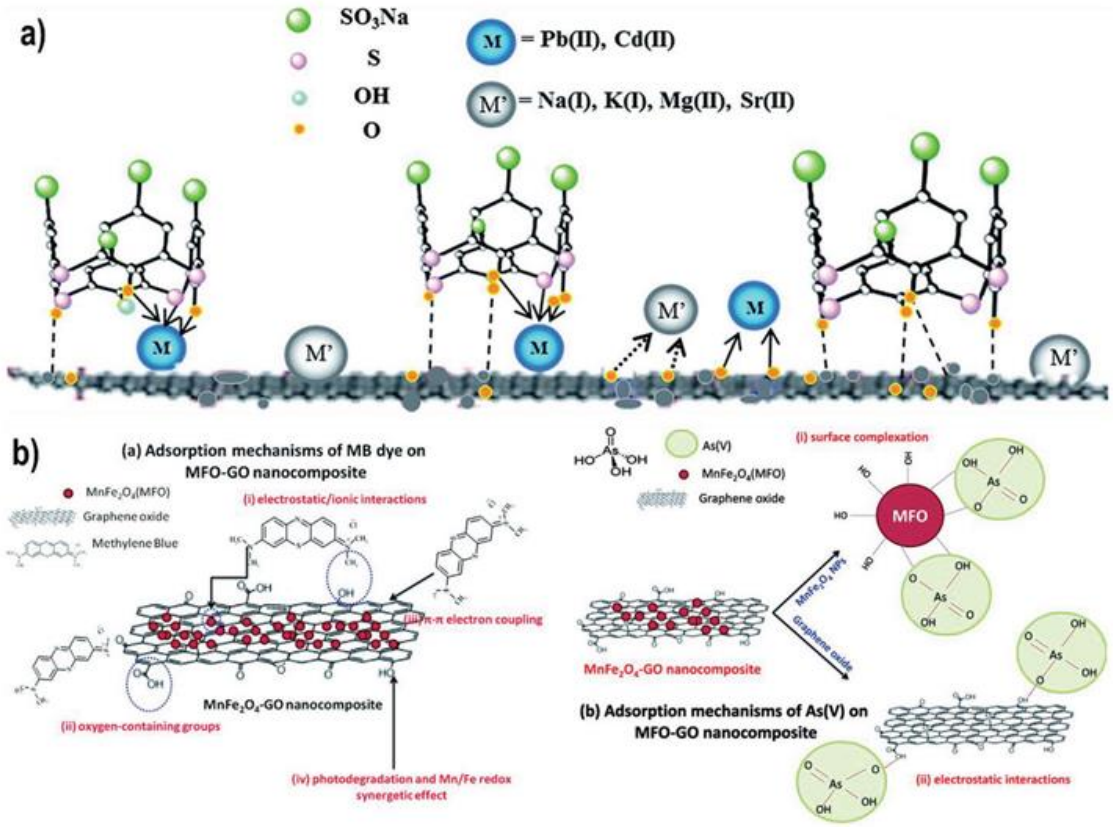

Figure 4. Interaction mechanisms of advanced graphene sorbents with multiple water pollutants: a) interaction of thiacalix[4] arenetetrasulfonate-functionalized reduced graphene oxide (TCAS-rGO) toward multiple metal ions. Reproduced with permission.[33] Copyright 2016, Royal Society of Chemistry and b) proposed adsorption mechanism of methylene blue and arsenic (V) ions on GO-$MnFe_2O_4$ nanocomposites. Reproduced under the terms of the Creative Commons Attribution 3.0 Unported License.[34] Copyright 2018, Royal Society of Chemistry.

and π–π interactions between polydopamine (precursor carrying oxygen- and nitrogen-functional groups) with the organic dyes.[39] Electrostatic interaction was found to be the main driving force for the adsorption of methylene blue toward the adsorption site of sulfonated graphene nanosheets carrying $-SO_3H$, $-COOH$, and $-OH$ functional groups apart from minor contribution from π–π interaction.[40] A similar concept was shown using a GO/chitosan aerogel, which exhibited dual functionality and interactions based on electrostatic and π–π interactions between the oxygen-containing groups on GO with cationic dyes. While, electrostatic interaction was responsible for the adsorption of anionic dyes to the amino groups on chitosan chains.[41]

To further improve adsorption efficiency, magnetic graphene oxide (MGO) was reported to remove methylene blue and orange G due to electrostatic attraction between the negatively charged MGO surface and π–π interaction between the aromatic structure of the dyes and the π conjugation domain of MGO nanosheets.[35] Benefited from the presence of highly porous structure with macro- and micropore sizes, photoinitiated thiol-modified multifunctional graphene biopolymer foam (Alg-Fe_3O_4-rGO-4S) was designed to tackle simultaneous water pollutants including dyes. Electrostatic interaction mechanism was dominantly showcased in the binary competitive dyes (methylene blue and rhodamine B) removal experiments performed using Alg-Fe_3O_4-rGO-4S. The developed sorbent exhibited stronger affinity toward methylene blue although both tested dyes are cationic dyes, which are expected to have similar binding affinity toward the negatively charged functionalized graphene composite. The poor performance of rhodamine B was due to the reduced positive charge density of rhodamine B molecule in the presence of the zwitterions (N^+ and COO^-) at pH >3 that decreased its interaction with the negatively charged functionalized sorbent.[42]

2.4. Interaction Mechanism: Oils and Organic Solvents

Spilled oils (crude oils, diesel, gasoline, motor, and engine oils) and organic solvents (toluene, methanol, ethanol, chloroform, and xylene) can be regarded as hydrocarbons with low

ADVANCED SCIENCE NEWS
www.advancedsciencenews.com

ADVANCED FUNCTIONAL MATERIALS
www.afm-journal.de

solubility in water, which are detrimental to the aquatic life and environments.[11c,43] Unlike heavy metal ions and certain organic dyes, removal of oils and organic solvents is mainly governed by noncovalent interactions and physical absorption in the pores of the functionalized graphene sorbents. Depending on the viscosity of the fluids to be removed, efficient removal of oil and organic solvents can be achieved using graphene and GO sponges with high surface area, tunable surface chemistry, large pore volume, and appropriate pore size.[11a] Reports suggested that the restoration of the hydrophobic and sp^2 domains of the graphene structure can feasibly enhance the uptake of oils and organic solvents via non-covalent interactions including hydrophobic and π–π interactions.[11a] Interactions between oil and organic solvents with the functionalized graphene sorbents are further discussed using examples as the following.

Spongy graphene fabricated via hydrothermal reaction using ammonia efficiently absorbed not only petroleum products and fats, but also toluene and chloroform resulting from its highly porous structure and hydrophobic effect. Appropriate hydrophilic groups in the graphene network is necessary to increase the interaction between the polar solvents for improved absorption capacity.[44] An ultralight nitrogen-doped graphene framework fabricated using pyrrole through hydrothermal method showed its excellent adsorption capacity for various types of organic solvents and oils due to its porous structure.[45] Apart from hydrophobic interaction, Pei et al. have shown that π–π interaction is the primary mechanism responsible for the enhanced adsorption of 1,2,4-trichlorobenzene (TCB), 2,4,6-trichlorophenol (TCP), and 2-naphthol on graphene. While the adsorption of TCP and 2-naphthol on GO can be attributed to hydrogen bonding resulting from the oxygen-containing groups on GO.[46] As depicted in **Figure 5**, the superior adsorption capability of chitosan modified GO aerogel toward phenol can be ascribed to π–conjugation interaction between the partially nonoxidized GO regions and the aromatic phenol.[41] Excellent absorption capacity of polydopamine functionalized GO aerogel towards oils and organic solvents was owing to its hydrophobic effect, large surface area, and high porosity.[39]

3. Advancing Multipollutant Sorbents through Materials Design

In the previous section, the key concepts for the removal of pollutants (heavy metals, dyes, organic solvents and oils) based on functionalized graphene to achieve specific interactions were discussed. In this section, rational materials design is explored to combine these interaction mechanisms to achieve simultaneous multipollutant removal. For that purpose, graphene-based sorbents are designed in several ways including optimizing their textural properties, engineering their porous architecture, shaping them into different sorbent forms (hydrogel, aerogel, particle, fluids, and powder) and tailoring their chemical functionality for different wastewater treatment applications. Use of 3D graphene-based porous sorbents with lightweight, interconnected porous structure and high surface area is proven as an effective material design strategy to tackle heavy metals, dye pollutants and oils spills in water.[11a,47] In particular, trapping of nonpolar organic contaminants such as oils and organic solvents is mainly governed by pore-filling mechanism.[16] This feature can be demonstrated by engineering highly porous 3D structures with large pore volume, low density, and high specific surface area.[11a,43] Sorption of oil and organic solvents is also dictated by surface wettability of sorbents with numerous surface modifiers including silanes, hydrophobic polymers (polyfluorowax, pyrrole, spiropyran, and etc), TiO_2 nanoparticles,

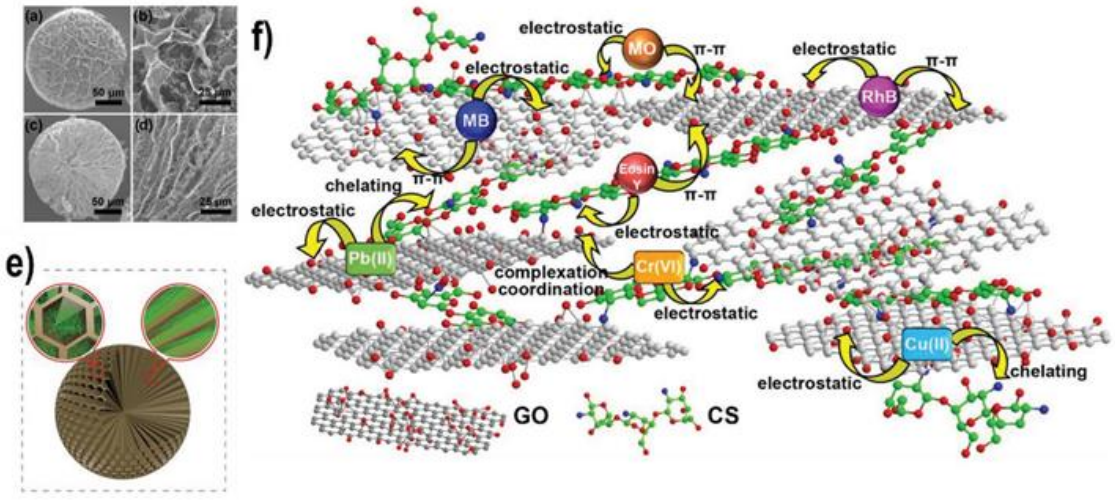

Figure 5. a–d) SEM images of GO/chitosan aerogel microspheres (GCAM). e) Schematic diagram of GCAM with honeycomb-cobweb and radially oriented microchannel structures. f) Type of interaction mechanisms of advanced graphene sorbents with multiple water pollutants: adsorption mechanism of GCAMs for numerous pollutants. Adapted with permission.[41] Copyright 2017, American Chemical Society.

ADVANCED SCIENCE NEWS
www.advancedsciencenews.com

ADVANCED FUNCTIONAL MATERIALS
www.afm-journal.de

kaolinite, carbon nanotubes (CNT), and graphene have been adopted to tailor the surface wettability of the sorbent materials.[43] Since several reviews have considerable coverage on the design of 3D graphene porous structure for water treatment, this area will not be expanded in this review.[11a,c,17,47–48] Despite numerous advantages including lightweight, rich porous structure, and high surface area can be achieved following the structural modification of graphene through tuning of 2D graphene sheets to 3D graphene aerogels, introduction of specific surface functional groups and heteroatoms are necessary to modify the graphene framework for improved binding affinity toward heavy metal ions and organic dyes. Through heteroatom doping and functionalization, surface charge generated on the surface of graphene and its counterparts can increase the binding tendency of charged pollutant species (e.g. heavy metal ions and certain organic dyes) towards their surface. Typically, across all the studied graphene-based materials, oxygen-, nitrogen-, and sulfur- containing groups are among the most common chemical species introduced to the graphene framework. These chemical species can be grafted on the graphene framework through wet chemical methods, thermal annealing, hydrothermal, solvothermal, microwave synthesis and plasma treatments using different precursors with specific examples provided in the following discussion to promote the adsorption of heavy metal ions and organic dyes in particular.[11b,15a]

Synthesis of graphene-based sorbents for capturing multipollutants in water is still restricted by low water dispersion, chemical inertness, high hydrophobicity and tendency to undergo π–π stacking of graphene.[23,49] To address these key challenges, modification strategies such as chemical functionalization and heteroatom doping have been extensively explored to tune the inherent properties of pristine graphene for improved adsorption performance in capturing environmental contaminants in water. Our focus in this section is to review the removal of multiple types of water pollutants through the rational design of graphene sorbents using heteroatom doping and functionalization strategies. Overview of the common dopants and functionalizing agents with their corresponding active groups are summarized in **Figure 6**. Heteroatom dopants, oxygen-containing groups, nitrogen-containing groups, sulfur-containing groups, metal/metal oxides/metal sulfides, sulfur-containing groups and mixed functional groups are among the important categories in designing an ideal sorbent toward the remediation of multiple water pollutants. The advanced graphene sorbents reviewed in this section demonstrated their sorption affinity towards either a single, binary, or ternary water pollutant systems.

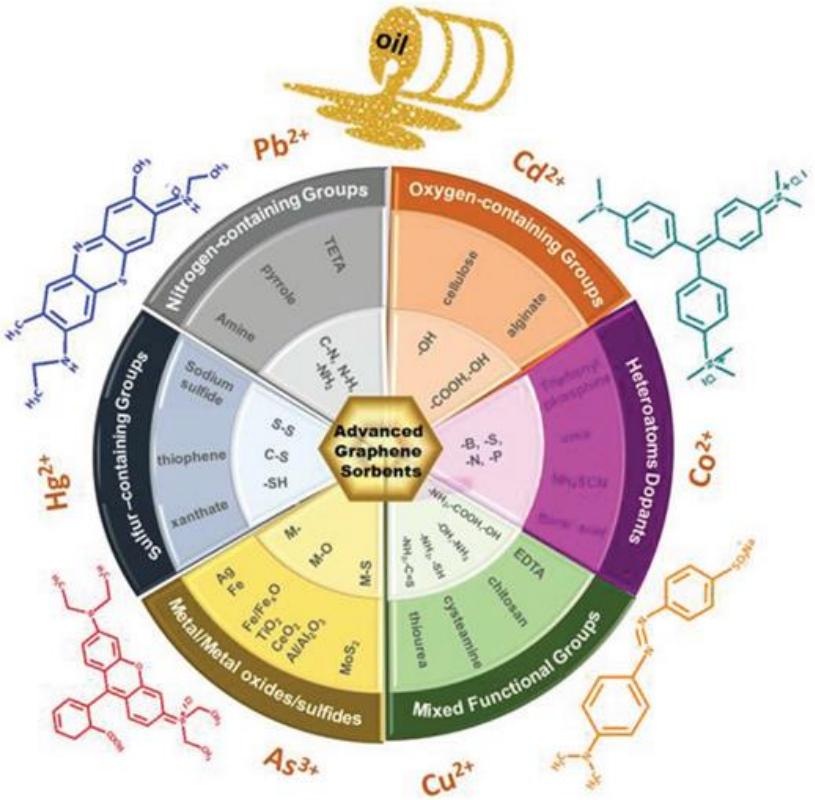

Figure 6. Overview of common dopants and functionalizing agents with their corresponding functional groups on advanced graphene sorbents for multiwater pollutants (heavy metals, dyes, oil, and organic solvents) removal.

3.1. Heteroatoms Doped-Graphene Sorbents

Doped-graphene with heteroatoms such as nitrogen, sulfur, boron, and phosphorus have been reported to effectively bind heavy metals and organic pollutants.[11b] Heteroatom doping results in either the substitution or insertion of heteroatoms of/at the carbon atom from the hexagonal honeycomb lattice of graphene.[23,49] Several approaches of heteroatom doping of graphene and GO were reported based on chemical vapor deposition, arc discharge, solvothermal, thermal annealing, wet chemical synthesis, pyrolysis, microwave treatment, and hydrothermal reactions.[11b] Heteroatoms such as −P, −B, −S, and −N are the most common dopants introduced to modify the graphene framework by adopting precursors such as boric acid, triphenyl phosphorus, urea, thiophene, cysteine, and ammonium thiocyanate for environmental protection. To achieve desired surface chemistry, these heteroatoms can be inserted individually or codoped to have single or dual atoms introduced simultaneously to the structure of graphene.[11b] In the study by Liu et al., a 3D nitrogen and boron-co-doped graphene aerogel (BN-GAs) was prepared through a combined solvothermal and freeze drying method by treating GO with $BN(OH)_x$ that was pretreated via thermal substitution process. Binary doping of nitrogen and boron atoms not only prevented GO from restacking during the solvothermal process, but also created adsorption active sites with uneven charge distribution on the surface of the graphene composites for enhanced trapping of water pollutants. The simultaneous codoped graphene aerogel (BN-GA) was hydrophobic and highly porous that exhibited outstanding absorption capacities up to 23 g g^{-1} for different oils and solvents from 10–23 times of its original weight.[50]

3D nitrogen and sulfur codoped graphene hydrogels (N/S-GHs) developed using a green thermal assembly approach demonstrated superior adsorption capacity toward organic dyes (methylene blue, malachite green, and crystal violet). N/S-GH has pronounced binding affinity toward a single pollutant system of organic dyes containing methylene blue, malachite green and crystal violet. In this doping modification process (**Figure 7**), glutathione carrying $-NH_2$, −SH, and −COOH groups, was employed not only as nitrogen and sulfur sources but also as binding and reducing agents to modify the graphene sheets. The enhanced features of N/S-GH including the highly porous structure, larger surface area, hydrophobicity and better durability significantly lifted the maximum adsorption capacities of cationic dyes, methylene blue, malachite green and crystal violet, to 625, 750, and 600 mg g^{-1}, respectively.[51]

Similarly, another example of a nitrogen and sulfur codoped graphene aerogel, N/S-GBA, was hydrothermally modified for simultaneous adsorption of a binary pollutant system consisting of a heavy metal (Cd^{2+}) and organic dyes (safranin, crystal violet, and methylene blue). 2,5-dithiobisurea was adopted as a crosslinker, reducing agent, and a nitrogen and sulfur doping agent to react with GO. XPS analysis confirmed the successful doping of GO with 7.95 at% and 3.80 at% of nitrogen and sulfur, respectively. High adsorption capacities of 200.88, 326.98, 226.02, 129.54 mg g^{-1} were recorded for Cd (II), safranin-O, crystal violet, and methylene blue, respectively, after the heteroatom doping of GO.[52]

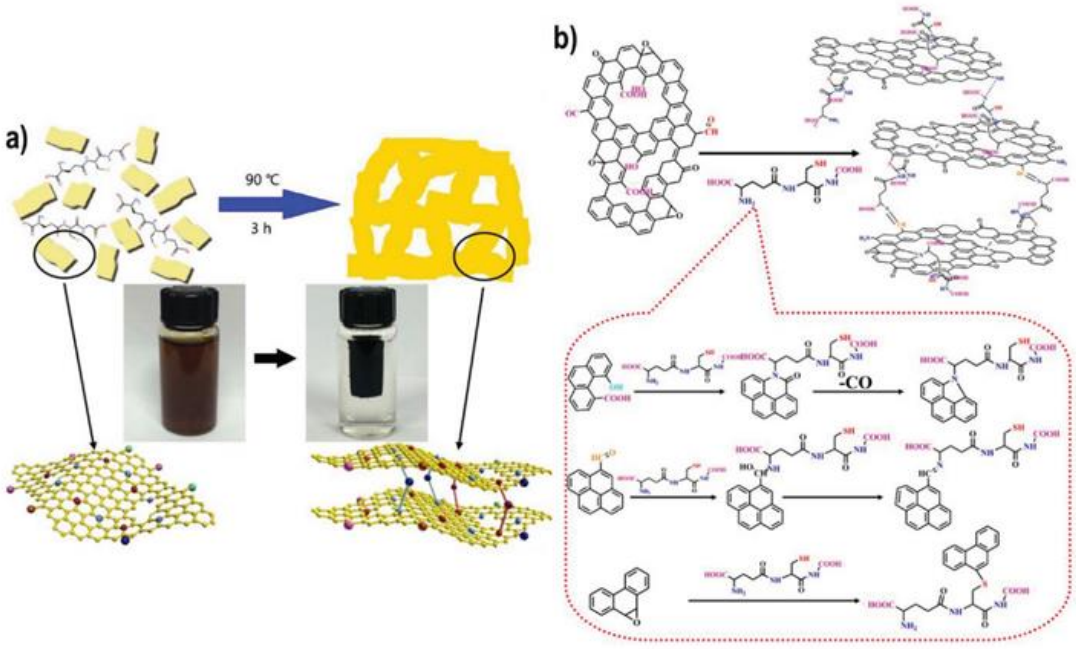

Figure 7. a) Illustration of formation of nitrogen and sulfur codoped –3D graphene hydrogels (N/S-GHs) from GO (2.0 mg mL^{-1}). b) Controlled assembly of N/S-GHs by glutathione with possible reaction pathways for nitrogen and sulfur doping. Adapted with permission.[51] Copyright 2016, Elsevier.

ADVANCED SCIENCE NEWS
www.advancedsciencenews.com

ADVANCED FUNCTIONAL MATERIALS
www.afm-journal.de

3.2. Oxygen-Containing Groups-Based Graphene Sorbents

The well-explored chemical functionalization of graphene involves the rehybridization of sp^2 to sp^3 carbon on the graphene basal plane based on the covalent attachment of organic functional groups to its sp^3 carbon, incorporating the grafting of oxygen-, sulfur-, nitrogen-containing groups.[49] One of the most common functionalized graphene derivatives is GO that can be prepared using wet chemical methods utilizing different oxidizing agents through Brodie (HNO_3, $KClO_3$), Staudenmaier (HNO_3, $KClO_3$, H_2SO_4), Hofmann (HNO_3, $KClO_3$, H_2SO_4), Hummers ($KMnO_4$, $NaNO_3$, H_2SO_4), Tour ($KMnO_4$, H_2SO_4, H_3PO_4), and Gao (K_2FeO_4, H_2SO_4) methods as summarized in **Figure 8**a.[11e] These surface oxidation modification techniques can generate myriads of oxygen groups such as hydroxyl (−OH), carboxyl (−COOH), carbonyl (−C=O) and epoxides (−C−O) on the surface of the graphene, which are also active for further functionalization of graphene.

Alternative oxidation treatments including oxygen plasma etching process and irradiation of high energy electron beam are also adopted to etch the graphene structure.[53] Oxygen enhancement treatment using irradiation of high energy electron beam for the preparation of GO also demonstrated promising introduction of oxygen-containing groups with controllable oxygen content in GO. It was confirmed that oxygen-containing groups are more inclined to decorate on the additional defects created in the carbon lattice during irradiation, which was responsible for improved Pb (II) adsorption compared to the untreated GO.[53b] Although GO is enriched with oxygen functional groups, research studies have shown that further modification of GO using precursors with oxygen-containing functional groups can effectively enhance the adsorption performance towards water pollutants, particularly for heavy metal ions and organic dyes. This was demonstrated through the fabrication of carboxymethyl cellulose/GO (CMC/GO) using cellulose as the oxygen-containing group modifier by spray-drying method. The formation of hydrogen bonds between the

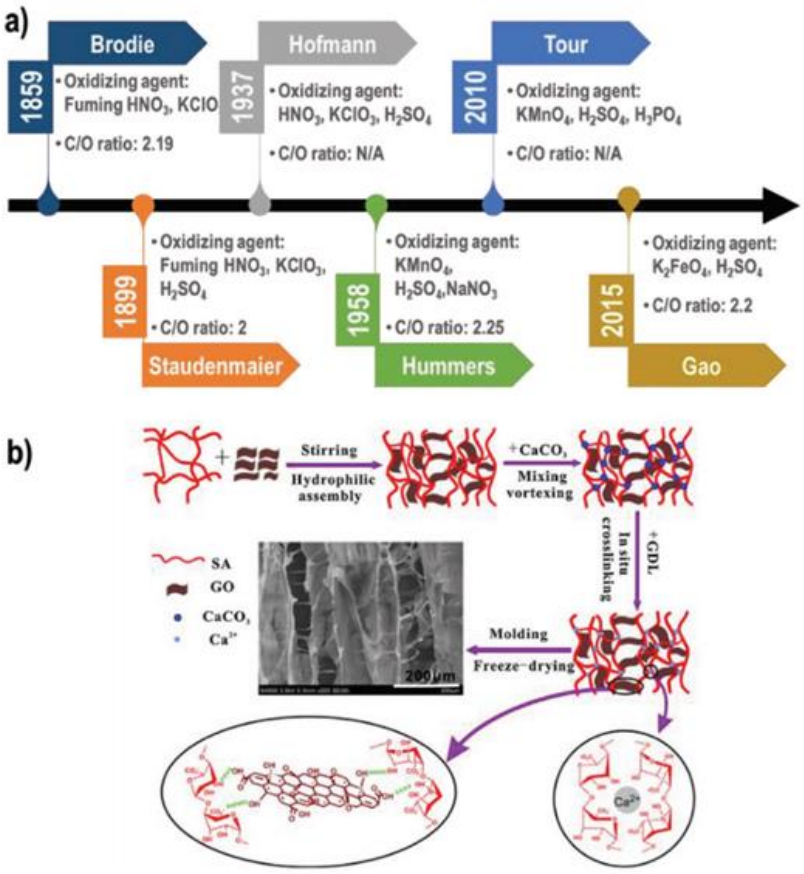

Figure 8. a) Timeline of developed oxidation methods for GO fabrication with oxidizing agents and C/O ratio included. Adapted with permission.[11e] Copyright 2016, Royal Society of Chemistry. b) Fabrication and formation mechanism of SAGO aerogel. Reproduced with permission.[54] Copyright 2016, Elsevier.

ADVANCED SCIENCE NEWS
www.advancedsciencenews.com

ADVANCED FUNCTIONAL MATERIALS
www.afm-journal.de

oxygen-containing groups in GO sheets and cellulose improved both the mechanical strength and swelling properties of the adsorbent. The additional grafted hydroxyl groups after the functionalization of GO significantly improved the adsorption performance toward multiple classes of pollutants (methylene blue, eosin Y, Pb^{2+}, Cd^{2+}, Cu^{2+}).[30] Fabrication of porous sodium alginate/GO (SA/GO) through crosslinking and freeze-drying methods (Figure 8b) demonstrated high adsorption capacities of 267.4 and 98.0 mg g^{-1} for Pb^{2+} and Cu^{2+}, respectively. Incorporation of additional oxygen functional groups has significantly enhanced the morphology and mechanical property of SA/GO besides the adsorption performance towards the examined pollutants.[54] Similarly, Pan et al. developed a macroporous calcium alginate/GO (mp-CA/GO) by utilizing oxygen containing-group precursor, alginate, to capture Pb^{2+}, Cu^{2+} and Cd^{2+}. In this work, polystyrene colloidal particles were used as a sacrificial template while GO was a reinforcing filler to achieve high adsorption capacities and outstanding regeneration ability. Maximum adsorption capacities of 368.2, 98.1, and 183.6 mg g^{-1} were attained for Pb^{2+}, Cu^{2+}, and Cd^{2+}, respectively, along with consistent removal efficiency achieved after 20 adsorption-desorption cycles using mp-CA/GO.[55]

3.3. Nitrogen-Containing Group-Based Graphene Sorbents

Functionalized graphene sorbents grafted with nitrogen-containing group such as hyperbranched polyamine modified GO (HPA-GO) were developed to address a binary pollutant system consisting of Pb (II) and methylene blue. Unlike linear polymers, the hyperbranched polyamine functionalization was found to be more effective to interact with the desired pollutants due to its nearly spherical structure with numerous decorated functional groups. Multifunctional hyperbranched polyamine functionalized graphene oxide (HPA-GO) was developed through the nucleophilic ring opening reaction between the amine groups of HPA and the epoxy group of GO in a KOH solution utilizing N-ethylethylene diamine as the nitrogen functionalizing precursor. Owing to the abundant hydroxyl and amino groups on HPA-GO, exceptional adsorption capacities of 819.7 and 740.7 mg g^{-1} were achieved for Pb^{2+} and methylene blue, respectively.[56]

While, GO chemically modified using 2,2-dipyridylamine (DPA), a functionalizing precursor with nitrogen containing group, exhibited strong binding affinity toward a single pollutant system containing Pb^{2+}, Cd^{2+}, Ni^{2+}, and Cu^{2+}. The oxygen-containing groups on GO was first activated using pentachloride phosphine, followed by functionalization using DPA under nitrogen blanket at room temperature for 6 h. GO-DPA achieved high adsorption capacity and good recyclability for simultaneous adsorption of Pb (II), Cd (II), Ni (II) and Cu (II) from aqueous solutions. The adsorption experiments using GO-DPA were ultrasonic-assisted to achieve high maximum adsorption capacities, 369.749, 257.201, 180.893 and 358.824 mg g^{-1}, for different heavy metal ions, Pb^{2+}, Cd^{2+}, Ni^{2+} and Cu^{2+}, respectively.[32]

Modification of GO using 3-aminopyrazole, a nitrogen-containing group functionalizing agent, to form GO-f for simultaneous uptake of three different heavy metal ions (Cd^{2+}, Hg^{2+} and As^{3+}). Excellent maximum adsorption capacities, 285.714, 227.273, and 131.579 mg g^{-1}, were accomplished for Cd^{2+}, Hg^{2+}, and As^{3+} ions, respectively, owing to the presence of functional moieties, high surface area and hydrophilic character of GO-f.[31] Another promising nitrogen-containing group functionalized graphene sorbent, poly(ethyleneimine) functionalized GO, GO/PEI, was effectively used to target two different types of organic dyes, anionic methyl orange and cationic methylene blue. Remarkably, GO/PEI was found to be stable in various types of environments including acidic and basic aqueous media, as well as several organic solvents. Due to the tunable surface charge of GO/PEI, high maximum adsorption capacities, 331.0 and 249.6 mg g^{-1}, were achieved for anionic methyl orange and cationic methylene blue, respectively.[57]

3.4. Sulfur-Containing Group-Based Graphene Sorbents

Functionalized graphene sorbents decorated with sulfur-containing groups such as thiacalix[4]arenetetrasulfonate-rGO (TCAS-rGO) has shown strong binding affinity toward a single pollutant system composed of Pb^{2+} and Cd^{2+}. Presence of various sulfur containing species on the TCAS–rGO composite was found to enhance the maximum sorption capacities of Pb^{2+} (230 mg g^{-1}) and Cd^{2+} (128 mg g^{-1}) with good regeneration ability >70% after the fifth adsorption–desorption cycles.[33] Sulphur functionalized graphene oxide (GO-SO_xR) sorbent developed using Na_2S as the functionalizing precursor exhibited excellent adsorption performance over a single pollutant system containing heavy metal ions such as Pb^{2+}, Cd^{2+}, Ni^{2+} and Zn^{2+}. Outstanding maximum adsorption capacities, 285, 217, 175, and 196 mg g^{-1}, were attained for Pb^{2+}, Cd^{2+}, Ni^{2+} and Zn^{2+}, respectively. Attempts have been made to coat GO-SO_xR sorbent with TiO_2 and SiO_2. Notably, further coating of GO-SO_xR sorbent with TiO_2 has immensely uplifted the maximum adsorption capacities of Pb^{2+}, Cd^{2+}, Ni^{2+} and Zn^{2+} to 312, 384, 344, and 285 mg g^{-1}, respectively. However, GO-SO_xR coated with SiO_2 showed improved maximum adsorption capacities only for Cd^{2+}. The comprehensive studies clearly demonstrated the effect of different functionalizing precursor toward enhancing the adsorption affinity of water pollutants.[58]

3.5. Metals/Metal Oxides/Metal Sulfide-Based Graphene Sorbents

For functional groups covering metals, metal oxides, and metal sulfides, several functionalized graphene sorbents such as $CoFe_2O_4$-rGO, G/CeO_2, and rGO-MoS_2 were found to effectively tackle multiple water pollutants especially heavy metal ions.[59] For instance, decoration of graphene sheets with magnetic $CoFe_2O_4$ not only facilitated the adsorption of pollutants and magnetic separation after adsorption, but also promoted excellent chemical stability and mechanical strength on the $CoFe_2O_4$-rGO adsorbent. This metal oxide functionalized graphene sorbent demonstrated high maximum adsorption capacities, 299.4 and 157.9 mg g^{-1} toward Pb^{2+} and Hg^{2+} respectively.[59a]

Ceria nanoparticles (CeO_2) deposited on graphene nanosheets sorbent was applied to extract Se (IV), As (V), As

(III), Cu (II) and Pb (II) ions. This metal oxide functionalized graphene sorbent (CeO_2-rGO) demonstrated high maximum sorption capacities of 8.4, 14.1, 50, and 75.6 mg g^{-1} for several heavy metal ions including As(V), Se (IV), Cu(II) and Pb(II) ions.[59b] Another functionalized graphene hybrid made up of molybdenum disulfide and rGO was hydrothermally reacted to form rGO-MoS_2 for tackling a single pollutant system containing Pb^{2+} and Ni^{2+}. Enhanced maximum sorption capacities, 322 and 294 mg g^{-1}, were recorded for rGO–MoS_2 in comparison to bare MoS_2, 107 and 98 mg g^{-1} for Pb^{2+} and Ni^{2+} ion, respectively. The improved performance achieved by rGO-MoS_2 greatly manifested the importance of the functionalization process.[59c]

Use of magnetic graphene oxide (MGO) was successfully fabricated to cope with a binary pollutant system containing heavy metal ion (Cd^{2+}) and organic dyes (methylene blue and orange G). High maximum sorption capacities, 91.29, 64.23, and 20.85 mg g^{-1} were achieved for Cd^{2+}, methylene blue and orange G, respectively, using GO decorated with magnetic Fe_3O_4 nanoparticles through coprecipitation method. Nevertheless, MGO showed decreased removal efficiency of 33.78%, 42.25%, and 47.32% after the fourth adsorption–desorption cycle for the uptake of Cd^{2+}, methylene blue, and orange G, respectively. This may imply that the chemical resistance and stability of the functionalized graphene sorbent in terms of their reusability and recyclability.[35] Manganese ferrite/GO ($MnFe_2O_4$-GO) nanocomposites were developed through a modified coprecipitation method for managing a binary pollutant system containing methylene blue and As (V) ion. Enhanced maximum adsorption capacities, 177.3 and 240.4 mg g^{-1} for methylene blue and As (V) ions, respectively, were attained using a $MnFe_2O_4$-GO adsorbent. This can be attributed to the synergistic effects of both magnetic metal oxide nanoparticles and GO nanosheets.[34]

3.6. Mixed Functional Group-Based Graphene Sorbents

A combination of various functionalizing precursors including carboxyl chitosan (CMC), sodium alginate (SA) and magnetite (Fe_3O_4) were adopted to modify GO for the fabrication of CMC/SA/GO@Fe_3O_4 magnetic gel beads as depicted in **Figure 9**a. Apart from oxygen-containing groups, the functionalized gel beads also contain iron oxide nanoparticles and amino moieties, which boosted up the binding affinity toward a single water pollutant system (heavy metal ion) with maximum adsorption capacity of 55.96, 86.28, and 189.04 mg g^{-1} for Cu^{2+}, Cd^{2+}, and Pb^{2+} ions, respectively. These crosslinked-magnetic gel beads also exhibited good regenerability property that attained 90% adsorption efficiency even after five recurring adsorption–desorption cycles.[60]

Multifunctional graphene biopolymer foam, Alg-Fe_3O_4-rGO-4S, on the other hand, modified using pentaerythritol tetrakis(mercaptopropionate) through potoinitiated thiolene click reaction (Figure 9b) was proven to simultaneously remove heavy metal ions (Cu^{2+}, Hg^{2+}), dye (methylene blue), solvents and oils. Besides high density of sulfur-containing group, Alg-Fe_3O_4-rGO-4S was designed with the decoration of myriads functional groups including hydroxyl and carboxylate groups from alginate as well as iron oxide nanoparticles that outperformed the commercial adsorbent with excellent stability and recyclability. The developed sorbent was initially attested using single pollutant removal experiments with maximum sorption capacities of 789.7, 107.0, and 73.5 mg g^{-1} achieved for methylene blue, Hg (II) and Cu (II), respectively. High sorption capacity (11–18 g g^{-1}) and rapid oil-water separation were attained. It was astounding that this functionalized biopolymer foam conformed to the maximum contaminant level for copper and mercury after the simultaneous sorption experiments.[42] Similarly, chitosan/sulfydryl-functionalized GO composite (CS/GO-SH), another functionalized graphene sorbent with mixed functional groups, was studied for a single pollutant system consisting of multi-metal ions (Cu^{2+}, Cd^{2+}, and Pb^{2+} ions). High maximum sorption capacities, 447, 425, and 177 mg g^{-1}, were accomplished for the studied metal ions, Pb^{2+}, Cu^{2+} and Cd^{2+} ions, respectively. CS/GO-SH showed excellent recovery (≈85%) after three consecutive adsorption–desorption cycles. Incorporation of multifunctional groups such as −OH, −COOH, −SH and $-NH_2$ groups in CS/GO-SH not only improved the binding affinity towards the pollutants, it also facilitated the exposure of binding sites of the functionalized sorbent with the investigated pollutants due to increased surface area.[61] Polysiloxane-graphene oxide (PS-GO) gel developed using sol-gel method showcased excellent adsorption performance toward a single pollutant system (heavy metal ion). A maximum uptake (256 and 137 mg g^{-1} for Pb (II) and Cd (II) ions, respectively) could be achieved by functionalizing GO with siloxane to enrich PS-GO gel with oxygen- and nitrogen-containing groups. Remarkably, this mechanically strong functionalized graphene sorbent tested using actual industrial effluent in a fixed bed column could be regenerated (in situ) that can be feasibly operated for a large-scale wastewater treatment.[62]

Ethylene diamine tetraacetic acid (EDTA) was anchored on magnetic Fe_3O_4 nanoparticles functionalized GO for improved adsorption toward different types of heavy metal ions (Pb^{2+}, Hg^{2+} and Cu^{2+} ions). Due to the synergistic functionalization effect from metal oxides, oxygen- and nitrogen- groups, EDTA functionalized magnetic GO (EDTA-mGO) showed high maximum adsorption capacity towards Pb^{2+}(508.4 mg g^{-1}), Hg^{2+} (268.4 mg g^{-1}) and Cu^{2+} (301.2 mg g^{-1}) ions. This promising functionalized graphene sorbent also demonstrated rapid magnetic separation (25 s) and good recyclability with >80% removal efficiency achieved for all the studied ions even after five repeating adsorption–desorption cycles.[63] For GO/chitosan aerogel microspheres (GCAMs), GO was modified with chitosan (functional groups: −OH, NH_2, −O−) in the presence of glutaraldehyde as a crosslinker. It appeared as a superior adsorbent for a ternary system of multi-pollutant control, including heavy metal ions (Pb (II), Cu (II), Cr (VI)), organic dyes (methylene blue, rhodamine B, methyl orange, Eosin Y) and organic solvent (phenol). Addition of chitosan was found to increase not only the surface area, but also the mechanical strength with the formation of a honeycomb-coweb structure in the final sorbent composite. Although chitosan greatly improved the adsorption efficiency, high chitosan content led to a stunted uptake rate of heavy metal ions and organic dyes as a result of elongated diffusion path due to larger composite size and pore size. Therefore, an optimized content of functionalizing agent is

ADVANCED SCIENCE NEWS
www.advancedsciencenews.com

ADVANCED FUNCTIONAL MATERIALS
www.afm-journal.de

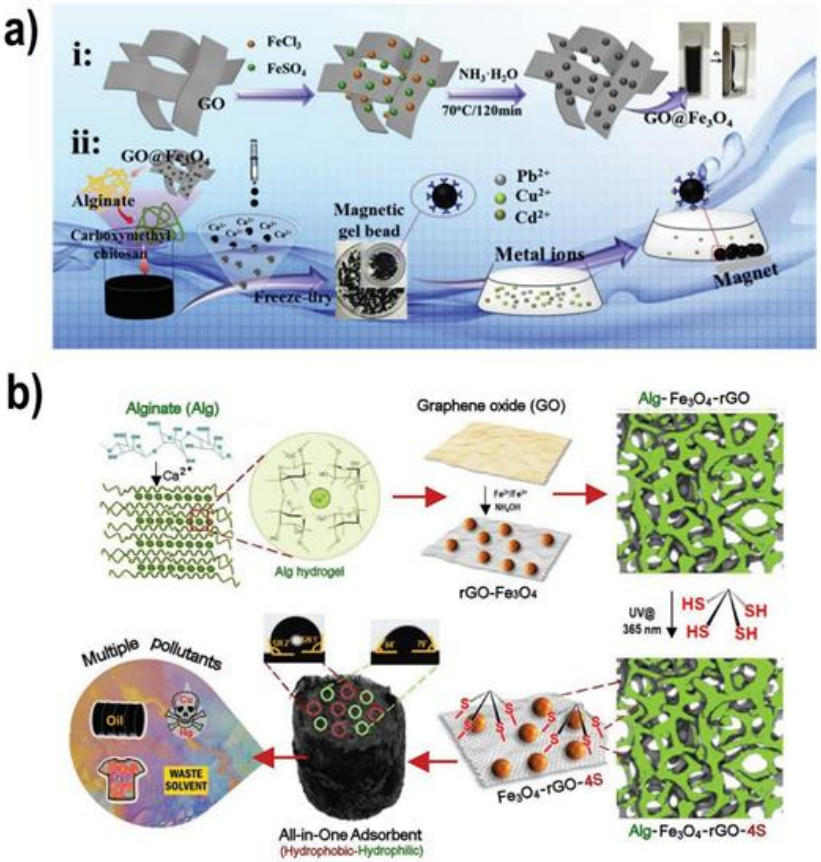

Figure 9. Exemplars of advanced graphene sorbents through materials design for multipollutant control in water: a) Fabrication of CMC/SA/GO@Fe_3O_4 gel beads. Reproduced with permission.[60] Copyright 2019, Elsevier. b) Fabrication of multifunctional graphene biopolymer foam for simultaneous removal of multiple water pollutants. Reproduced with permission.[42] Copyright 2020, Wiley-VCH.

crucial to ensure enhanced adsorption performance of sorbent material. The developed multifunctional GCAMs demonstrated outstanding maximum sorption capacity, rapid adsorption, increased structural stability that could retain up to six cycles of adsorption–desorption performance to tackle a broad spectrum of water pollutants.[41]

Another ternary multipollutant control system was showcased by polydopamine coated reduced GO (PRGO) to tackle a vast category of water pollutants. GO was reduced and surface coated through π–π stacking and aryl–aryl coupling mechanisms by dopamine, a functionalizing agent consists of −OH and $-NH_2$ groups. The biomimetic polydopamine (PDA) graphene aerogel was not only a promising adsorbent, but also a catalyst to tackle a broad class of water contaminants including oils, organic solvents, and dyes. The fabricated PRGO was adopted as a template for the construction of a 2D architecture decorated with mineralized inorganic and metal nanoparticles, as well as the 3D aerogel. Further functionalization approaches including the decoration of calcite and gold nanoparticles were introduced to the bioinspired surface of PRGO to promote binding affinity towards heavy metal ions and catalytic activity of 4-nitrophenol. Apart from facilitating the catalytic reduction of 4-nitrophenol, PDA assembled graphene aerogel also exhibited outstanding performance to adsorb different types of heavy metal ions (Pb^{2+} and Cd^{2+}), dyes (methyl violet, methyl orange, methylene blue, and congo red), oils and solvents (vegetable oil, paraffin oil, chlorobenzene, hexane, toluene, cyclohexane, and gasoline). The hydrophobic and highly porous 3D hydrogel showed good trapping ability for organic dyes (89–380 mg g^{-1}), oils and organic solvents (26–42.5 g g^{-1}). Functionalization of GO by adopting dopamine not only enhanced the binding affinity toward multiple pollutants, but also rendered greater dispersibility in various solvents, higher chemical and thermal stability, as well as higher mechanical strength with excellent regeneration capability.[39] Xanthate functionalized magnetic graphene oxide (Fe_3O_4-xGO) has been attested for its excellent binding affinity in a binary water pollutant system consisting of Hg^{2+} and methylene blue. Excellent adsorption capacities of 526.32 and 118.55 mg g^{-1} were achieved for methylene blue and Hg^{2+}, respectively attributed to the presence of iron oxide nanoparticles,

ADVANCED SCIENCE NEWS
www.advancedsciencenews.com

ADVANCED FUNCTIONAL MATERIALS
www.afm-journal.de

amino and xanthate groups on GO sheets after functionalization process. Additionally, Fe_3O_4–xGO can be easily recovered within one minute after the adsorption process through a magnetic separation approach.[64] Microporous spongy chitosan graphene oxide (CSGO) is another exemplar that demonstrated promising adsorption capability toward a binary pollutant system (heavy metal ion and organic dye). The highly porous and biodegradable CSGO was prepared through lyophilization using chitosan, a precursor containing −OH and $-NH_2$ groups, was effective in removal of methyl orange and Cu^{2+} with 567.07 and 53.69 mg g^{-1}, respectively, recorded for their saturated adsorption capacity.[65]

Based on the reviewed graphene sorbents presented in previous sections, a comprehensive doped/functional groups–sorption performance relationship (**Figure 10**) is established to correlate sorption performance toward different types of water pollutant using a single advanced graphene material modified by heteroatoms and functionalized groups.[29–35,39–42,50–52,54–66] On average, sorption capacity achieved for multipollutants include heavy metal ions, organic dyes, oils, and organic solvents are within 1000 mg g^{-1} for organic dyes and heavy metal ions. While, less than 100 g g^{-1} recorded for organic solvents and oils using the advanced graphene sorbents. By grafting the basal plane of graphene sheets with specific dopants and functional groups, performance of advanced graphene sorbents toward sorption of multipollutants can be greatly intensified in terms of their dispersion in water, creation of surface charge, and mechanical strength. Modification on the surface wettability and structural architecture to create pores in graphene sorbent can give rise to 3D graphene sorbent with large pore volume, lightweight, and high porosity for larger capacity of storing pollutants. Advanced

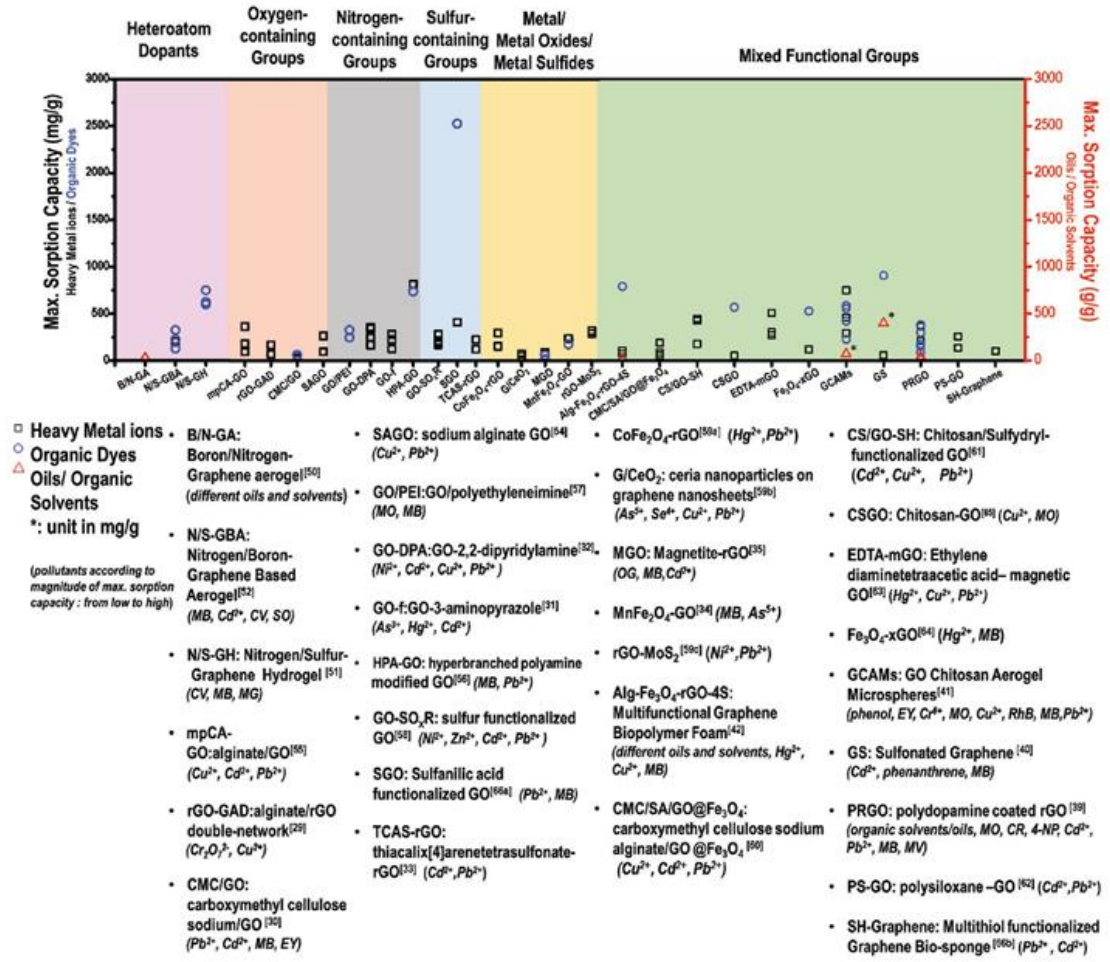

Figure 10. Correlation of sorption capacity of advanced graphene sorbents grafted with heteroatom dopants and different functional groups for sorption of multipollutants (heavy metal ions, organic dyes, oils, and organic solvents) in water. MB: methylene blue; CV: crystal violet; SO: safranin orange; MG: malachite green; EY: Eosin Y; MO: methyl orange; OG: Orange G; RhB: Rhodamine B; CR: Congo Red; 4-NP: 4-nitrophenol.

graphene sorbents can be synergistically benefited from the combination of these design approaches using different precursors for targeting multiclasses of pollutants in water.

3.7. Benchmarking of Functionalized Graphene Sorbents

In the previous section, we established links between material design and engineering through the integration of 3D porous structures and grafting of dopants as well as functional groups with their environmental performance showing several key examples toward the removal of multiwater pollutants. These results are promising but further improvement is still needed. One barrier in designing these enhanced graphene sorbents for the removal of multipollutants is the lack of accepted benchmark comparison. Therefore, in the following section, four case studies involving graphene and its derivatives modified with nitrogen-doped precursor and different functional groups (sulfur-, nitrogen-, and metal oxide) were selected for benchmarking studies to compare their sorption performance with their respective controls (GO and rGO) and to understand the impact of dopants and functional groups towards multi pollutants removal.

A 3D nitrogen-doped graphene aerogel (N-GA) was hydrothermally prepared by adopting urea as a doping precursor to tackle methylene blue and methyl orange in water. In this synthesis, N-GA was grafted with nitrogen-containing groups (−CONH, $-NH_2$) apart from −OH group, which was also present in its control form (GA). Enhanced adsorption efficiency of 57.80% and 74.66% for MB and MO, respectively, for N-GA in relative to its control (GA) as shown in **Table 1**, suggesting that the uplift of adsorption efficiency was attributed to the effect of nitrogen doping that offers more adsorption sites for uptake of both dyes. In order to resolve the aggregation issue of graphene sheets in N-GA, polyvinyl alcohol (PVA) was crosslinked between the graphene sheets by hydrogen bond and provided a supporting skeleton in constructing the porous structure of PVA-N-GA. Owing to the electrostatic attraction, π–π and hydrogen bonds between the dyes and adsorbent, the crosslinked composite (PVA-N-GA) effectively increased the adsorption capacity of MB and MO to 216.96 and 165.1 mg g^{-1} compared to N-GA from 133.85 and 94.21 mg g^{-1}, respectively. Moreover, PVA-N-GA also showed excellent recycling stability even after five cycles and great affinity toward other anionic and cationic dyes with >70% removal efficiency achieved. Hence, it is apparent that graphene doping can efficiently improve the sorption performance of graphene-based sorbent.[67]

Sulfonated graphene (GS), functionalized by diazotization approach using sulfanilic acid showed improved sorption performance for multiple classes of pollutants (Cd^{2+}, methylene blue and phenanthrene) relative to GO (prepared using

Table 1. Comparison of doped- and functionalized graphene-based sorbents with their respective controls for multiple water pollutant control.

Type of sorbent	Sorbent	Main functional group	Pollutants	Maximum sorption capacity [mg g^{-1}]	Percentage change of maximum sorption capacity w.r.t. control [%]	Refs.
Nitrogen-doped group	N-GA	−CONH $-NH_2-$	Methylene blue	133.85	+57.80% (GA)	[67]
			Methyl orange	94.21	+74.66% (GA)	
Control	GA	−O− −OH	Methylene blue Methyl orange	84.82 53.94	NA	[67]
Sulfur-containing group	GS	$-SO_3H$	Cd (II)	57.6	+31.8% (GO); +448.6% (rGO)	[40]
			Methylene blue	906	+45.4% (GO); +566.2% (rGO)	
			Phenanthrene	400	+6533.5% (GO); +163.2% (rGO)	
Control	GO	−O− −OH −COOH	Cd (II) Methylene blue Phenanthrene	43.7 623 6.03	NA	[40]
Control	rGO	-Conjugated π system (sp^2-hybridized carbon)	Cd (II) Methylene blue	10.5 136	NA	[40]
			Phenanthrene	152		
Metal oxide-containing group	rGO–$ZrO(OH)_2$	−O− −OH −COOH	As (III)	95.15	+254.1% (Control)	[68]
		Metal oxides/hydroxides	As (V)	84.89	+363.6% (Control)	
Control	$ZrO(OH)_2$	Metal oxides/hydroxides	As (III)	26.87	NA	[68]
			As (V)	18.31		
Nitrogen-containing group	GO-f	−CONH	Cd (II) Hg (II)	285.714 227.273	+20.0% (Control) +6.8% (Control)	[31]
			As (III)	131.579	+77.6% (Control)	
Control	GO	−O− −OH −COOH	Cd (II) Hg (II) As (III)	238.095 212.766 74.074	NA	[31]

graphite precursor by modified Hummers method) and rGO (prepared using GO precursor by chemical reduction method). The design of sulfonated graphene was presented by adopting sulfanilic acid, a precursor augmented with $-SO_3H$, $-NH_2$ and benzene groups, to overcome the aggregation issue of graphene and hydrophilic surface of GO in regulating the effective adsorption sites for three different classes of water pollutants. Among the three tested water pollutants, GS surpassed GO and rGO with 906, 400, and 57.6 mg g^{-1} maximum sorption capacity for methylene blue, phenanthrene and Cd^{2+}, respectively. Meanwhile, GO demonstrated greater removal performance for methylene blue (623 mg g^{-1}) and Cd^{2+} (43 mg g^{-1}) compared to rGO with 136 mg g^{-1} reported for methylene blue and 10.5 mg g^{-1} for Cd^{2+}. For phenanthrene, rGO (152 mg g^{-1}) showed higher sorption capacity than GO (6.03 mg g^{-1}). Despite an immense reduction of oxygen groups observed in GS after the functionalization reaction, the grafting of sulfur- and nitrogen-containing groups at the sp^3 domains of graphene endowed stronger binding affinity toward the studied water pollutants. π–π and hydrophobic interactions are the primary mechanisms that facilitate the adsorption of phenanthrene onto the functionalized graphene adsorbent. The introduced functional groups, $-SO_3H$, allowed the formation of a stable suspension, higher surface area, and the resulting defects created on the edge and planes of GS, leading to a more effective interaction with phenanthrene. Electrostatic attraction is found to be the dominant interaction mechanism between the negatively charged GS and positively charged methylene blue. Functional groups including $-COOH$ and $-SO_3H$ are chiefly responsible for the adsorption of methylene blue with an inferior impact from π–π interaction as evidenced by the lower sorption capacity of rGO. The adsorption of Cd^{2+} to the binding site of GS can be attributed to cationic–π interaction, which was not observed for GO. As shown in Table 1, drastic improvement of sorption performance was observed for GS compared to its respective controls with >30% for Cd (II), >45% for methylene blue and >160% for phenanthrene. Superior adsorption performance of GS for the uptake of water pollutants from different classes was due to the sulfanilic acid functionalization which enabled a stable dispersion by decreasing the aggregation of nanosheets during adsorption process. The $-SO_3H$ functional group also gave rise to the recovery of sp^2 hybridized plane and effectively exposed the binding sites for different classes of water pollutants. This study reaffirmed that the fabrication of an ideal functionalized sorbent to tackle distinct category of water pollutants is possible through a methodical and rational functionalization approach[40]

Modification of GO with hydrated zirconium oxide, GO-$ZrO(OH)_2$, by hydrothermal and coprecipitation reactions for simultaneous removal of As (III) and As (V) from water is another evidence of the effect of functionalization in enhancing the uptake of water pollutants. The grafted zirconium oxide on the graphene structure greatly improved the removal efficiency of As (III) and As (V), by 3.54 and 4.64 times, respectively, compared to bare $ZrO(OH)_2$ nanoparticles. Despite the same equilibrium time (15 mins) attained in both cases, GO-$ZrO(OH)_2$ achieved higher adsorption capacity, 95.15 and 84.89 mg g^{-1} for As (III) and As (V), respectively in relative to 26.87 and 18.31 mg g^{-1} recorded for $ZrO(OH)_2$ nanocomposite. Interestingly, 1:100 of GO:$ZrO(OH)_2$ is the optimum mass ratio for efficient uptake of As (III) and As (V) ions among the two other investigated mass ratios, 1:40 and 1:150. It was surmised that electrostatic attraction is the interaction mechanism that governed the adsorption of arsenic ions to the binding sites of the functionalized nanocomposite adsorbent. This study exhibited enhanced sorption performance (>250% for As (III) and >350% for As (V)) after the incorporation of graphene compared to pristine $ZrO(OH)_2$ as tabulated in Table 1. Hydrated zirconium oxide modified GO demonstrated its simultaneous As (III) and As (V) removal ability in water with excellent recyclability, portraying as a promising adsorbent for arsenic uptake from drinking water.[68]

Chemically modified GO with 3-aminopyrazole (GO-f) consisting of nitrogen-containing group exhibited highly efficient simultaneous adsorption of Cd (II), Hg (II), and As (III) from aqueous solutions. GO-f was prepared by first refluxing GO in a mixture containing $SOCl_2$ and DMF to form acyl chloride-functionalized GO, followed by heating it with 3-aminopyrazole in DMSO. The grafted nitrogen-containing functional groups have improved the uptake of the three studied heavy metal ions with a surge of 20%, 6.8% and 77.6% for Cd (II), Hg (II) and As (III) ions, respectively, in comparison to bare GO (Table 1). The good adsorption performance of the functionalized GO can be attributed to the combined adsorbent-adsorbate interaction including physisorption, surface complexation, and electrostatic interactions.[31]

It is evident that modification of graphene with dopants and chemical functional groups can effectively improve the adsorption capacity toward water pollutants from the four case studies summarized above. Impressively, these case studies also confirmed that uptake of multiple class of pollutants using a single sorbent can be achieved with comprehensive understanding on the adsorption characteristics of adsorbents, binding chemistry between the water pollutants and the grafted functional groups. Rational design of multipollutant sorbents can be achieved with controlled-tuning of the dispersion, wettability and type of modifier to target the removal of pollutants from different classes.

4. Sorption Properties–Performance Relationship

Numerous criteria in designing an ideal sorbent in terms of its structural and physical properties, mechanical and chemical resistance have been identified to dictate the success of wastewater treatment.[69] **Figure 11** depicts the typical physicochemical properties required in a sorbent to target different classes of water contaminants. Characteristics including surface wettability, porosity, surface area, mechanical strength, and bulk density are important parameters to clean up oil and nonpolar organic solvents but some (wettability, bulk density and thermal resistance) may not be applicable to effectively remove heavy metal ions and organic dyes.[43,47] The requirements of an ideal sorbent for coping both heavy metal ions and organic dyes are quite similar due to their interaction nature between these water pollutants and the graphene-based adsorbents. Adsorption properties such as chemical composition, chemical resistance, surface area, mechanical strength, and pore structure are

Figure 11. Summary of prominent adsorption properties of advanced graphene sorbents towards shaping an ideal multifunctional sorbent in coping different classes of water pollutants including heavy metal ions, organic dyes, oils and organic solvents.

vital for enhanced removal of heavy metal ions and organic dyes. However, no link is made between the physicochemical features, particularly the chemical properties of the advanced graphene sorbents and their sorption performance over multiple water pollutants to date. There is a huge information gap in terms of the comprehensive characterization profiles of the graphene-based materials to correlate with their environmental performance in the current literature.[11a] Record of a complete coverage of the characterization profiles along with their respective sorption performance is scarce and nearly not established for advanced graphene sorbents.[11a] Inadequate data on their chemical properties also hampers a reliable link to be made between the surface chemistry and the environmental performance of graphene-based materials.[11a] Therefore, a meticulous approach has been adopted to correlate the physicochemical properties of advanced graphene sorbents including the chemical composition, surface area and pore size with the sorption performance of multiple classes of pollutants in this section.

4.1. Chemical Properties–Sorption Performance Relationship

Chemical properties of advanced graphene sorbents including functional groups, chemical states, and electronic states of the elements in the adsorbent can be complementarily unraveled using Fourier transmission infra-red (FTIR), nuclear magnetic resonance (NMR) and X-ray photoelectron spectroscopy (XPS) qualitatively and quantitatively. Relationship between the chemical properties of the advanced graphene sorbents with the sorption performance (**Figure 12**) is established for the first time to correlate the underlying chemistry of the chemical composition with the maximum sorption capacity achieved by the advanced graphene sorbents. Chemical composition of advanced graphene sorbents can be determined using XPS, energy dispersive X-ray (EDX) and CHNS organic combustion techniques. CHNS technique can be regarded as a bulk elemental composition analysis involving major components in an organic sample undergo oxidative decomposition to form carbon dioxide, water, elemental nitrogen and sulfur dioxides. Relatively speaking, EDX can be considered as a subsurface technique with a depth resolution of 0.3–5 µm while XPS, a more surface-sensitive analysis, that quantitatively determines the chemical composition of sample depth at <10 nm.[70] A general expression of elemental composition in terms of common atomic ratio including carbon-to-oxygen (C/O), carbon-to-nitrogen (C/N) and carbon-to-sulfur (C/S) atomic ratio allows comparison made on the effectiveness of functionalization level across the reviewed advanced graphene sorbents in affecting the sorption performance of water pollutants. With limited data available on the chemical composition of advanced graphene sorbents, a few examples (Figure 12) were identified to establish a correlation between the common atomic ratios of advanced graphene sorbents with the maximum adsorption capacities of the pollutants investigated, which has previously never been reported.[31–33,35,42,52,58,60,66b,71]

Generally, effectiveness of the oxidation process of graphite can be gauged by the proportion of C/O atomic. A well-oxidized graphitic oxide carries a C/O atomic ratio between 2.1 and 2.9.[72] Taking magnetic CMC/SA/GO@ Fe_3O_4 as example, precursors such as chitosan, alginate and iron oxide were adopted to modify GO to adsorb three different heavy metal ions (Cu^{2+}, Cd^{2+} and Pb^{2+}) commonly found in industrial wastewater. Calculated C/O atomic ratio (2.3) determined from XPS survey peaks of C1s and O1s for CMC/SA/GO@ Fe_3O_4 after functionalization reaction. The C/O atomic ratio that falls within 2.1–2.9 clearly shows that the functionalized graphene sorbent is a well-oxidized graphene composites even after grafting with Fe_3O_4 nanoparticles using ammonium hydroxide that tends to reduce the oxygen content. The nitrogen content contributed from the $-NH_2$ group in chitosan gave rise to C/N atomic ratio of 27.5 in CMC/SA/GO@ Fe_3O_4, indicating a low nitrogen content in CMC/SA/GO@ Fe_3O_4 in comparison to other functionalized graphene sorbents. Maximum sorption capacities of 189.04 mg g^{-1}, 86.28 mg g^{-1} and 55.96 were attained for Pb^{2+}, Cd^{2+}, and Cu^{2+} using this functionalized graphene sorbent.[60] Single pollutant system containing Pb^{2+}, Cd^{2+}, Ni^{2+} and Cu^{2+} was targeted using GO-DPA sorbent modified by 2,2-dipyridylamine (DPA) that led to C/O and C/N atomic ratio of 2.7 and 10.5, respectively. In relative to GO (C/O atomic ratio of 1.6), GO-DPA with C/O atomic ratio of 2.7 can be regarded as a well-oxidized functionalized graphene material despite a reduction in its oxygen content after functionalization. Nitrogen content as high as 6.22 atomic % was detected on GO-DPA after the functionalization of GO that facilitated the attraction of the tested heavy metal ions towards GO-DPA.[32]

GO-f modified by 3-aminopyrazole, a functionalizing agent with abundant of nitrogen containing groups, resulted in C/O and C/N atomic ratio of 7.4 and 13.7, respectively, was used for simultaneous adsorption of Cd^{2+}, Hg^{2+}, and As^{3+}. Elemental composition results from EDX analysis demonstrated that the C/O atomic ratio of GO-f (7.4) has been greatly increased

ADVANCED SCIENCE NEWS
www.advancedsciencenews.com

ADVANCED FUNCTIONAL MATERIALS
www.afm-journal.de

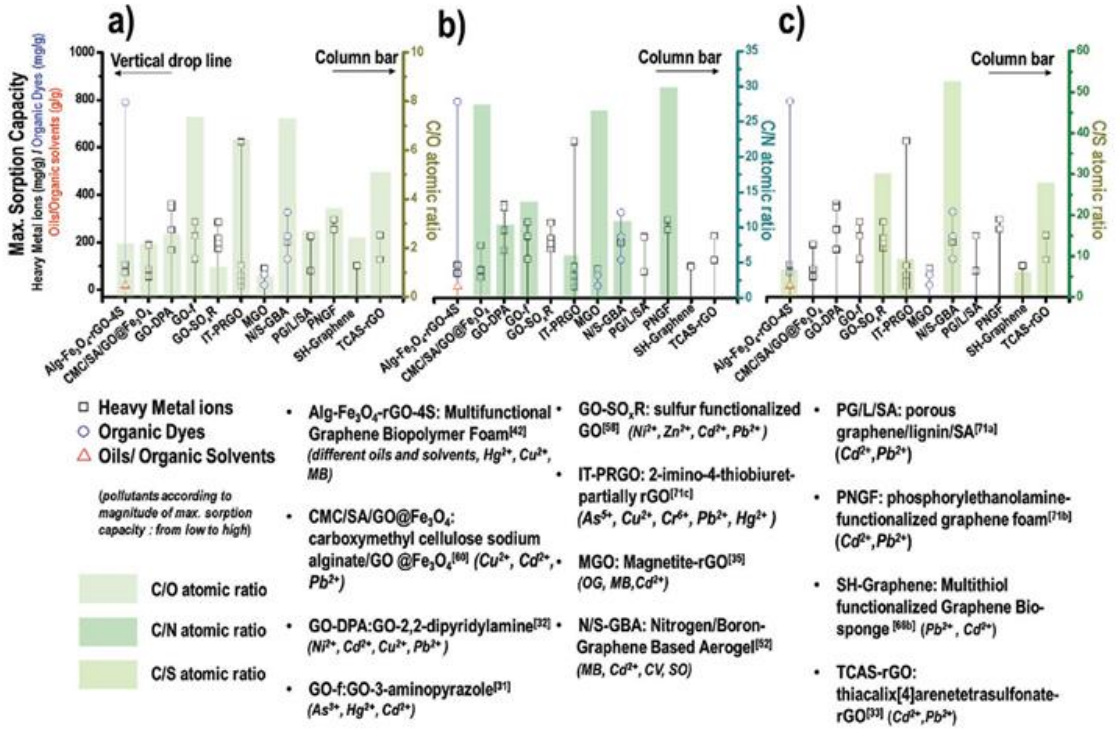

Figure 12. Relationship between adsorption properties of a) C/O, b) C/N, and c) C/S atomic ratio of advanced graphene sorbents with their adsorption performance in tackling multiple water pollutants. MB: methylene blue; OG: Orange G; CV: crystal violet; SO: safranin orange.

from GO (1.5), signifying a significant reduction of oxygen content after modification using 3-aminopyrazole, which could be attributed to the reaction between 3-aminopyrazole with epoxide and carbonyl moieties on the surface of GO. Relatively high nitrogen content (5.81 at%) was grafted on GO-f, which could be responsible for the excellent adsorption performance of the examined heavy metal ions.[31] Chemical composition of GO-SO_xR was studied using XPS and CHNS analyses to provide a more comprehensive information in terms of its surface and bulk chemical composition. Based on XPS analysis, C/O atomic ratio of GO-SO_xR has significantly reduced to 1.27 from 2.0 (GO), suggesting an uplift of oxygen content after functionalization using Na_2S. Notably, enormous difference of C/S atomic ratio was found between the surface (30.1) and bulk (1.7) analysis of GO-SO_xR, suggesting that higher sulfur-containing species was deposited in the bulk vicinity of the functionalized sorbent compared to its surface. Coupling with the high oxygen- and sulfur-containing groups found in GO-SO_xR, excellent maximum sorption capacities, 285, 217, 175, and 196 mg g^{-1}, were attained for Pb^{2+}, Cd^{2+}, Ni^{2+} and Zn^{2+}.[58] Combination of oxygen-, nitrogen- and sulfur-containing groups precursor was adopted to fabricate 2-imino-4-thiobiurent-partially rGO (IT-PRGO) for adsorption of different heavy metal ions such as Hg^{2+}, Pb^{2+}, Cr^{6+}, Cu^{2+}, and As^{5+}. EDX analysis showed that IT-PRGO possessed C/O, C/N and C/S atomic ratio of 6.5, 7.6, and 9.4, respectively, signifying successful modification of GO. Although a significant reduction of oxygen level observed in IT-PRGO, the high loading of sulfur and nitrogen could be responsible for the highest maximum adsorption capacity, 624 mg g^{-1}, observed for Hg (II).[71c]

As confirmed by XPS analysis, magnetic graphene oxide (MGO) developed with high oxygen loading (C/O atomic ratio of 0.9) was found to possess good binding affinity towards Cd (II), methylene blue, and orange G. A decline of C/O atomic ratio from 2.3 (GO) to 0.9 (MGO) after functionalization using iron ammonium salts and ammonia, clearly indicated an intense rise of oxygen content attributed to the decoration of magnetite nanoparticles on GO. Great adsorption capacities, 91.29, 64.23, and 20.85 mg g^{-1}, achieved by MGO could be due to the high loading of oxygen in MGO. Trace 1.4 at% of nitrogen (C/N atomic ratio of 26.6) found in MGO could be due to the presence of remaining impurities found in the sample and may not be relevant to be included in the discussion since a higher nitrogen content (2.16 at%) was also detected in GO prior to functionalization.[35] N/S-GBA, a nitrogen and sulfur codoped graphene aerogel, recorded a higher C/O atomic ratio of 7.4 in relative to 1.9 (GO), signifying an obvious drop of oxygen content after functionalization using 2,5-dithiobisurea. N/S-GBA also recorded a relatively low C/N and high C/S atomic ratio of 11.0 and 52.5, respectively, in comparison to other functionalized graphene sorbents. As verified by XPS analysis, loading of 7.95 at% nitrogen and 3.80 at% sulfur in

N/S-GBA could be accountable for good maximum adsorption capacities (200.878, 326.98, 226.02 and 129.54 mg g^{-1}) toward a binary pollution system (Cd^{2+}, safranin-O, crystal violet and methylene blue, respectively).[52]

3D porous graphene/lignin/sodium alginate (PG/L/SA) with its calculated C/O atomic ratio of 2.8 has pronounced binding effect towards Cd^{2+} and Pb^{2+}. Based on XPS analysis, composition of oxygen detected on PG/L/SA (26.1 at% oxygen) has been tremendously increased from nonfunctionalized porous graphene (16.91 at% oxygen) after modification using lignin and alginate. Alginate and lignin are polymeric chains laden with oxygen functional groups that could greatly enhance the maximum adsorption capacities, 79.88 mg g^{-1} and 226.24 mg g^{-1}, of Cd^{2+} and Pb^{2+}, respectively.[71a] Phosphorylethanolamine-functionalized graphene foam (PNGF), grafted with phosphorus, oxygen and nitrogen-containing groups, has great adsorption affinity towards Pb^{2+} and Cd^{2+}. Relatively high C/O atomic ratio (3.7) and C/N atomic ratio of 29.9 were recorded in PNGF as verified by XPS analysis. Although only 2.53 at% nitrogen and 1.57 at% of phosphorus were detected in PNGF, maximum adsorption capacities as high as 296 g g^{-1} and 254.9 mg g^{-1} were achieved for Pb^{2+} and Cd^{2+} adsorption in water.[71b] An increased C/O atomic ratio (5.2) was found in TCAS-rGO, compared to the pristine GO (2.2), indicating that a significant reduction of oxygen level in TCAS-rGO after the modification using TCAS. According to XPS analysis, nearly half atomic concentration of oxygen (15.59 at%) was detected in TCAS-rGO in comparison to GO (31.29 at%) with addition of 2.88 at% sulfur found in TCAS-rGO. The decline of oxygen content and increment of sulfur atomic concentration in TCAS-rGO clearly indicated successful functionalization of GO for high maximum adsorption capacities, 230 and 128 mg g^{-1}, for Pb^{2+} and Cd^{2+}, respectively.[33]

4.2. Structural Properties–Sorption Performance Relationship

Since adsorption process is a surface phenomenon, structural properties including pore size, total pore volume, and surface area are critical in affecting the adsorption efficiency.[69] Specific surface area, often expressed in m^2 g^{-1}, is inversely proportional to the particle size of a material based on the exposure of binding sites of a sorbent with the water contaminants. The smaller the particle size, the larger the surface area per unit volume for greater interaction between the binding sites of sorbents with pollutants. Specific surface area of graphene related materials can be measured based on the amount of physisorbed gas (nitrogen gas) using BET (Brunauer–Emmett–Teller) technique or adsorption of organic dyes that can be determined using UV-Vis spectrometry.[11a,73]

Adsorption efficiency of an adsorbent can be greatly influenced by pore size as water pollutants that tend to remain on the adsorbent surface will diffuse into the internal pores of the adsorbent. Sorption capacity of an adsorbent is therefore directly correlated to the pore size ratio of adsorbent, which is linked to the size or dimension of the targeted pollutants.[69] Pore size of an adsorbent, can be classified based on the pore width: micropore (<2 nm), mesopore (2–50 nm) and macropore (>50 nm) according to International Union of Pure and Applied Chemistry (IUPAC).[69,74] Presence of micro-, meso-, and macropores in a sorbent material renders many benefits to the adsorption of water pollutants. Macroporosity allows accessibility of pollutants ranging from large to small size, thus enables rapid diffusion into the sorbent materials. It is also advantageous in terms of the recyclability of the sorbent material that offers quick diffusion of heat without damaging the structure of the sorbent during the removal of absorbed oil.[17] Adsorption of smaller pollutant species such as inorganic ions occurs at the micropores of an adsorbent while larger molecules such as dyes are mainly trapped in the mesopores of an adsorbent.[69] Pore size is inversely proportional to the surface area of 3D graphene sorbent materials to tackle viscous water pollutants such as crude oil. Graphene sponges with larger opened pores, thinner pore walls and interconnected pores are found to be more desirable to capture oils.[11a] The interconnected pore structure is also favorable for the diffusion of metal ions that often follows the intraparticle diffusion model. Rate of removal is usually higher at the beginning of the reaction, which could be attributed to the large surface area of 3D graphene-based materials[17]

It is therefore paramount to correlate the pore size of advanced graphene sorbents with their corresponding maximum sorption capacities as depicted in **Figure 13**.[34,39,40,42,50,51,57–59,c,62–63,66b,68,71a,75] Taking 3D nitrogen and boron codoped graphene aerogel (B/N-GA) as an example, enhanced textural properties including the specific surface area and pore volume were observed in B/N-GA after the doping process. With pore width ranging from 2.5 to 11 nm, mesoporous B/N-GA exhibited a larger surface area (169.9 m^2 g^{-1}) and higher total pore volume (2.21 cm^3 g^{-1}) compared to its undoped material (graphene aerogel, GA), 52.3 m^2 g^{-1} and 0.94 cm^3 g^{-1}, respectively. The enhanced textural characteristics of B/N-GA led to excellent maximum absorption capacity (23 g g^{-1}) of different types of oil and solvent pollutants in water.[50]

Magnetic cobalt ferrite-rGO ($CoFe_2O_4$-rGO) exhibited pore volume and pore size of 0.1490 cm^3 g^{-1} and 4.054 nm, respectively, after modification using a mixed phase metal oxide. High maximum sorption capacities of 299.4 mg g^{-1} for Pb^{2+} and 157.9 mg g^{-1} for Hg^{2+} were achieved by $CoFe_2O_4$-rGO with a measured surface area of 169.9 m^2 g^{-1}.[59a] Despite relatively low surface area measured for EDTA-mGO (49.97 m^2 g^{-1}) among the reviewed functionalized graphene sorbents, great binding affinity was attained towards a single type of pollutant system containing Pb^{2+}, Hg^{2+}, and Cu^{2+} ions. Significant improved surface area was observed in EDTA-mGO (49.97 m^2 g^{-1}) compared to its controls including EDTA-Fe_3O_4 (10.1 m^2 g^{-1}) and Fe_3O_4 (12.5 m^2 g^{-1}) that led to high adsorption capacities in EDTA-mGO.[63] Although low surface area, 30.13 m^2 g^{-1}, was detected in Fe_3O_4–xGO, high maximum sorption capacities, 526.32 and 118.55 mg g^{-1}, were recorded for a binary pollutant system consisting of methylene blue and Hg^{2+}.[64] GO/polyamidoamine (GO-PAMAM) was found to possess excellent adsorption affinity toward a single pollution system containing Pb^{2+}, Cd^{2+}, Cu^{2+}, and Mn^{2+} ions even with its low surface area (25 m^2 g^{-1}). The low surface area observed in GO-PAMAM could be due to incomplete exfoliation of GO and agglomeration in the fabrication process. Notably, GO-PAMAM, although had low surface area, it still exhibited high adsorption capacities, 568.18, 253.81, 68.68, and 18.29 mg g^{-1}, toward the studied

ADVANCED SCIENCE NEWS
www.advancedsciencenews.com

ADVANCED FUNCTIONAL MATERIALS
www.afm-journal.de

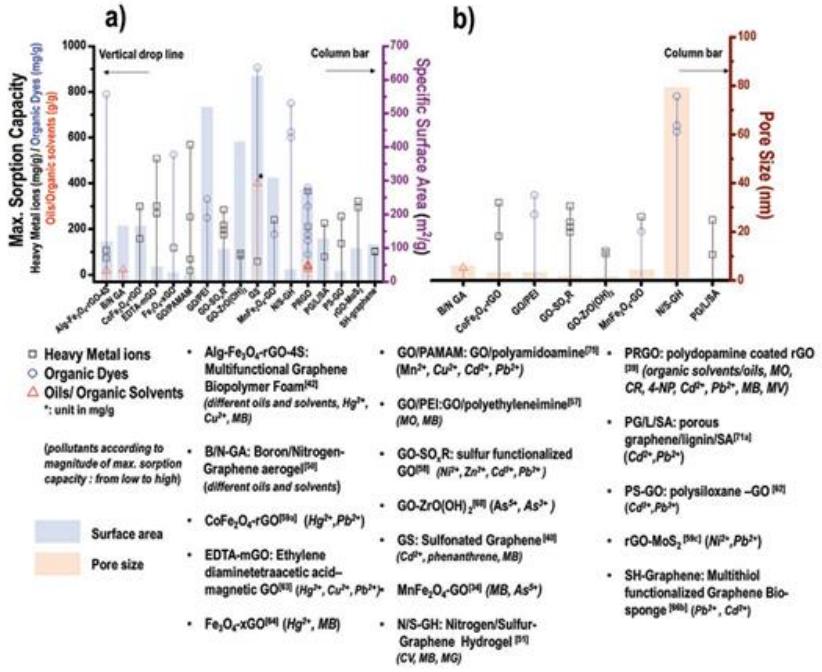

Figure 13. Relationship between adsorption properties of a) surface area and b) pore size of advanced graphene sorbents with their adsorption performance in tackling multiple water pollutants. MB: methylene blue; MO: methyl orange; CV: crystal violet; SO: safranin orange; MG: malachite green; CR: Congo Red; 4-NP: 4-nitrophenol; MV: methyl violet.

heavy metal ions including Pb^{2+}, Cd^{2+}, Cu^{2+}, and Mn^{2+} ions, respectively.[75] 3D GO/polyethyleneimine (GO-PEI), a functionalized graphene sorbent featured with its relatively high SSA (526.4 $m^2\ g^{-1}$), exhibited high adsorption capacities of 331 and 249.6 mg g^{-1}, toward a single pollutant system containing anionic methyl orange and cationic methylene blue, respectively. Higher surface area attained in GO/PEI compared to its pristine GO could be attributed to the internal spacing created by the insertion of PEI between the lamellar structure of GO after the modification process. Combination of the mesoporous properties including high surface area and micropores with the pore width between 3 and 4 nm of GO/PEI contributed to its potential application in water purification.[57]

Surface area of GO-SO_xR (102 $m^2\ g^{-1}$) decorated with multitude of sulfur- and oxygen-containing groups was nearly twofold higher than its pristine GO (57 $m^2\ g^{-1}$) after functionalization using sodium sulfide. Outstanding adsorption capacities (285, 217, 175, and 196 mg g^{-1} for Pb^{2+}, Cd^{2+}, Ni^{2+} and Zn^{2+} ions, respectively) were achieved with merely an average pore diameter of 2.5 nm of GO-SO_xR. This study implied that the surface area of graphene sorbent material can be greatly enhanced by functionalization using a sulfur-containing group precursor.[58] Nevertheless, it is sometimes challenging to determine if the good sorption performance achieved is the effect from the increased surface area or from the effect of doping or modification with functional groups. One way to attest if the increase in sorption capacity is due to the increased surface area rather than the grafted functional groups is by designing an experiment to prepare the same sorbent materials with different sizes since particle size is inversely proportional to the specific surface area of a material. Correlation between the sorption performance and the effect of surface area can be established by performing sorption experiments on these different sized-sorbents materials. The outcomes from these sorption experiments using the same sorbent material with different sizes (or surface area) can be used to confirm if these factors (surface area or functional groups) make an impact on the sorption performance of a sorbent material. Decoration of $MnFe_2O_4$ nanocrystals on GO nanosheets has tremendously increased the surface area of $MnFe_2O_4$-GO to 316.8 $m^2\ g^{-1}$ compared to bare $MnFe_2O_4$, 67.5 $m^2\ g^{-1}$. The mesoporous characteristic of $MnFe_2O_4$- GO with an average pore size of 4.2–5.6 nm was found to render promising water purification application as evidenced by its high adsorption capacities for a binary pollution system containing methylene blue and As (V).[34] Polydopamine-coated graphene nanosheets (PDA-rGO) with its relatively high surface area, 280 $m^2\ g^{-1}$, demonstrated promising adsorption performance toward a ternary pollution system. PDA-rGO was used as a template with decorated gold nanoparticles that catalyzed 4-nitrophenol at approximately 175 mg g^{-1} maximum adsorption capacity. Grafting of $CaCO_3$ onto PDA-rGO exhibited excellent binding affinity towards Pb^{2+} and Cd^{2+}, at 365 and 210 mg g^{-1}, respectively. About 25–42.5 g g^{-1} sorption capacities were attained for different kinds of oils and solvents using PDA-rGO aerogel. This comprehensive study clearly revealed that different types of water pollutants can be effectively

captured by manipulating the functionalizing agents and form of the sorbent.[39]

5. Reality, Challenges and Opportunities

With the growing number of publications on the development of graphene-related sorbents in this recent decade, it is no doubt that advanced graphene materials have demonstrated their promising potential in water purification treatment. Despite the good research progress already made using graphene-related materials, however, in reality, certain challenges as summarized in **Figure 14** should be overcome to maximize the full potential of advanced graphene sorbents and their integration into advanced water purification technologies.

5.1. Multipollutant Removal Approach

Although graphene sorbents have demonstrated satisfactory sorption capabilities to remove different class of contaminants ranging from heavy metals, organic dyes and to oils, majority of these research studies focused on the removal of single water pollutant under an ideal model system condition. Realizing that this ideal condition may not exist as the polluted water systems are often made up of a wide array of pollutants, an urgent call for a multipollutant modeling approach aimed to target simultaneous uptake of coexisting water pollutants is needed.[2] In particular, the performance efficiency for simultaneous uptake of coexisting water pollutants from different pollutant classes using advanced graphene sorbents has rarely been reported in the literature and can be considered as one of the major gaps in adsorption studies. A shift of current conventional single-pollutant modelling toward multipollutant approach should be undertaken for a more inclusive coverage of water pollutants assessment using emerging advanced graphene sorbents.[2–3,8] Hence, future sorption studies should be extended to cover multi-pollutant control assessment rather than just focusing on a single-pollutant investigation.

5.2. Separation, Regeneration and Valorization

Effective separation and regeneration of advanced graphene sorbents from trapped pollutants have become increasingly vital to prevent the generation of secondary pollutants after the adsorption process. Majority of the published work focus on the sorption of pollutants with minimal efforts devoted to the separation, recovery, and valorization of the spent sorbents. In terms of separation, the use of magnetic separation concept could be advantageous due to its time-, energy- and cost-saving benefits to achieve sorbent separation from the treated water using advanced graphene sorbents decorated with synthetic or natural magnetic nanoparticles.[60,76] For regeneration of spent sorbents, systematic studies to investigate experimental parameters including regeneration methods, type of eluents, stability of sorbent materials and recycling times are essential criteria to assure the stability and reusability of the sorbent materials. Promising opportunities could be visualized on the valorization of the postsorption sorbents that could reduce the potential environmental footprint. This opens the door for economically-viable alternatives to convert the spent sorbents to value-added green products such as catalysts, soil conditioners, feed additives and bioactive compounds.[77]

5.3. Standardization and Database

One of the critical issues is dealing with the inconsistency of experimental sorption parameters reported in the literature. Incomplete studies of primary experimental sorption conditions (pH, initial pollutant concentration, sorbent amount, contact time, temperature and ionic strength) may result in insufficient data that affects the evaluation outcomes of reaction spontaneity, type of sorption mechanism and sorption nature between the studied sorbent and pollutants. Taking GO as an example, different maximum sorption capacities were reported for the same studied contaminants despite the same sorbent material (GO) used in the studies.[11d] This discrepancy could be due to the varied experimental conditions adopted in the sorption studies. Therefore, it is challenging to make an impartial comparison on the performance of sorbents. It is

Figure 14. Reality, challenges, and opportunities of advanced graphene sorbents as emerging water purification technology.

crucial to ensure that the details of the experimental conditions used are explicitly recorded.

It should be highlighted that current literature has shown inadequate characterization analysis performed on graphene sorbent materials. As a result, formulating a correlation between the sorption properties of the advanced graphene sorbents with their corresponding sorption performances is difficult.[11a] It is surprising to find that although sorption properties (surface area, particle size, pore size, chemical composition, and wettability) can greatly affect the sorption performance, a number of these essential characterization results are found missing after a thorough exploration in the literature. Given that varied measurement conditions were used to characterize the sorbent materials, the reliability of the characterization outcomes can be sometimes arguable. The disagreement found on the sorption performance outcomes due to inconsistency of the investigated experimental conditions and the sorption properties of advanced graphene sorbents have been an unconsciously pressing issue that hinders the commercialization of these emerging sorbents in water purification treatment. A more rigorous standardization and quality control over the sorbents properties and their respective sorption parameters should be implemented for future publication of sorbent-related work. Characterization techniques to probe the sorption properties (morphology, textural, structural, physical, chemical, and thermal properties) and experimental sorption parameters (pH, contact time, initial concentration of pollutant, sorbent amount, temperature, ionic strength, competing ions, recycling times, and real sample assessment) should be made mandatory for studies conducted on sorbents. A universal comprehensive database pertaining the novel advanced graphene sorbents should be developed with the outputs generated to improve the understanding of sorption properties–performance relationship for appropriate sorbent material selection in wastewater discharged from different sectors such as agricultural, textile, mining, or chemical manufacturing plants as well as natural waters including groundwater, lake, river, and seawater.

5.4. Upscaling and Technology Integration

Current water purification technologies using advanced graphene sorbents are also impeded by the up-scaling limitation to transform laboratory batch studies to large-scale wastewater treatment plants. It is discouraging that most of these novel advanced graphene sorbents remain as laboratory-based technology despite outperforming the commercial sorbent material (AC). The failure to extend the laboratory batch studies to continuous investigations or pilot-scale testing could be attributed to the lack of integration of data science into the advanced water purification technology. Thorough sorption performance evaluation of the advanced graphene sorbents in the field operation could be first predicted using data mining and machine learning approaches to accurately gauge the optimized condition under the practical and realistic pollutants removal environment. The interaction of the sorbents with pollutants could be greatly affected due to the complexity of water components in real assessments. Fitting of batch sorption performance data and characteristics of sorbent materials into machine learning models could rapidly attest the practicability of the sorbent materials based on the type of treated water systems that could promise higher success rate of upscaling the laboratory technology for field operations.[78]

5.5. Environmental Impact and Sustainability

The boom in nanotechnology has shown promising prospect of advanced graphene sorbents in water purification. However, debate over the environmental impact and its potential risks due to the introduction of nanomaterials including graphene and its derivatives in water has been an on-going concern. A cytotoxicity study revealed that GO with smaller nanosheets was more cytotoxic than larger sheets with accumulation of nanomaterial detected in the kidney and lung tissues of mice in an vivo toxicological test.[79] Nonetheless, the cytotoxic effects of these nanomaterials can be dramatically reduced after converting them into nanocomposites as proven by the decreased cytotoxic activity of NIH 3T3 fibroblast cells in poly-*N*-vinyl carbazole graphene nanocomposites compared to graphene and GO alone.[80] Integration of advanced graphene nanomaterials with biocompatible polymers (alginate, cellulose, and chitosan) by converting the nanomaterials in the form of a powder or suspension to macroscopic polymers such as sponges could help prevent the potential leaching of nanomaterials in water by promoting water security and sustainability.[17,66b] Although remarkable removal efficiency achieved by advanced graphene sorbents in water purification, more research studies should be propagated to understand their potential risks and toxicological impacts upon exposure towards the environment and human health.

5.6. Cost and Funding

Cost can be considered as one of the major barriers that restricts the full scale translation and application of advanced graphene sorbents as an alternative for existing sorbents in the field operation. It is undeniable that AC beats graphene in terms of its lower market price and availability. However, the overall pollutant treatment cost should also take into account the performance efficiency, treatment time and regeneration feasibility for a sustainable water purification technology. Considering the outstanding performance efficiency and highly regenerability portrayed by the graphene-based sorbents, only a small amount of these sorbents is necessary to treat a large pool of polluted water. This promises a more economically feasible water treatment process in relative to the commercial sorbents. It is worth noting that the market price of emerging carbon sorbents based on CNTs, graphene, and its derivatives is considerably dropping to values that can be competitive to AC considering their greater performance.[81] Today, the market price of graphene and its derivatives has dramatically plunged to ca $100 per kg due to an increase in graphene and its derivatives production using more economically feasible manufacturing methods. It is essential to highlight that graphene and its derivatives are produced from a cheap raw source, graphite,

with a price ≈$1000 per tonne. With the increase in number of graphene producers in the market, it is expected that the market price of graphene and its derivatives could hit even further lower price in the near future. In addition, it has become increasingly vital to incorporate the cost analysis to achieve a more holistic cost projection on the novel sorbents developed as showcased in some of the published work.[44,82] Finally, more opportunities including commercialization of sorbent materials, water-related research grants and scholarships from both the academia and industry should be devoted in this area to ensure the sustainability of on-going research and cope with the pressing global water stress issue.

6. Conclusions and Prospects

We have reviewed the current progress on designing of graphene sorbents and their performances for multipollutants remediation in water based on heteroatoms dopants, oxygen-, nitrogen-, sulfur-, metals/metal oxides/metal sulfides- and mixed-functional groups. It has shown that understanding the building blocks of graphene could help define the interaction mechanisms between them and the multipollutants in water. Based on these findings, it is possible to build a roadmap for rational design of emerging graphene sorbents to tackle the challenging multipollutant control in water. The fundamental structure–function–performance relationships have been evaluated, establishing correlation between the sorption performance of multi-pollutants in water and particular adsorption properties (surface area, pore size, type of functional groups, C/O, C/N, and C/S atomic ratio) of advanced graphene sorbents.

The reality, challenges, and opportunities of graphene materials as emerging sorbents for advanced and sustainable water purification technology have been critically discussed in a broad perspective. Five identified challenges still remain to be addressed:

1. Limited focus given on the treatment of practical multicomponent water systems using sorbents
2. Separation, regeneration and valorization of sorbents
3. Standardization of testing conditions and establishment of a sorbent–performance database
4. Upscaling and sorbent technology integration for multipollutant water purification
5. Sustainability of accepted technologies
6. Cost and funding involved to ensure research and development of advanced graphene sorbents that can be optimistically resolved in parallel with the fast-growing body of fundamental research.

Due to increasing level of water pollution, and worsening climate change, the dwindling of clean water supplies is a "silent" global challenge that could constraint future development. Over decades of development, these graphene-based sorbents have shown great improvement and promising results to meet the requirements for the next-generation commercial water purification technology. We foresee the integration of advanced graphene-based materials with other cutting-edge water generation technologies including solar energy water evaporation, fog harvesting and desalination of sea water to further address the shortage of clean water globally.

Acknowledgements

This work was supported by the ARC Research Hub for Graphene Enabled Industry Transformation (IH150100003).

Conflict of Interest

The authors declare no conflict of interest.

Keywords

adsorbent, dyes, graphene, heavy metals, oils, water purification

Received: August 28, 2020
Revised: October 2, 2020
Published online:

[1] World Health Organization (WHO), Geneva (accessed: March 2020).
[2] M. Strokal, J. E. Spanier, C. Kroeze, A. A. Koelmans, M. Flörke, W. Franssen, N. Hofstra, S. Langan, T. Tang, M. T. H. van Vliet, Y. Wada, M. Wang, J. van Wijnen, R. Williams, *Curr. Opin. Environ. Sustainability* **2019**, *36*, 116.
[3] a) G. N. Hlongwane, P. T. Sekoai, M. Meyyappan, K. Moothi, *Sci. Total Environ.* **2019**, *656*, 808; b) P. J. J. Alvarez, C. K. Chan, M. Elimelech, N. J. Halas, D. Villagrán, *Nat. Nanotechnol.* **2018**, *13*, 634.
[4] a) N. B. Singh, G. Nagpal, S. Agrawal, Rachna, *Environ. Technol. Innovation* **2018**, *11*, 187; b) M. Pei, B. Zhang, Y. He, J. Su, K. Gin, O. Lev, G. Shen, S. Hu, *Environ. Int.* **2019**, *131*, 105026.
[5] S. Bolisetty, M. Peydayesh, R. Mezzenga, *Chem. Soc. Rev.* **2019**, *48*, 463.
[6] M. Pescod, *Wastewater Treatment and Use in Agriculture*, Food and Agriculture Organization of the United Nations, Italy **1992**.
[7] a) P. L. Yap, S. Kabiri, D. N. H. Tran, D. Losic, *ACS Appl. Mater. Interfaces* **2019**, *11*, 6350; b) J. Tang, Y. Huang, Y. Gong, H. Lyu, Q. Wang, J. Ma, *J. Hazard. Mater.* **2016**, *316*, 151; c) F. Luo, J. L. Chen, L. L. Dang, W. N. Zhou, H. L. Lin, J. Q. Li, S. J. Liu, M. B. Luo, *J. Mater. Chem. A* **2015**, *3*, 9616.
[8] L. Wang, C. Shi, L. Wang, L. Pan, X. Zhang, J.-J. Zou, *Nanoscale* **2020**, *12*, 4790.
[9] R. Gusain, N. Kumar, S. S. Ray, *Coord. Chem. Rev.* **2020**, *405*, 213111.
[10] a) M. Sweetman, S. May, N. Mebberson, P. Pendleton, K. Vasilev, S. Plush, J. Hayball, *C* **2017**, *3*, 18; b) S. De Gisi, G. Lofrano, M. Grassi, M. Notarnicola, *Sustainable Mater. Technol.* **2016**, *9*, 10.
[11] a) N. Yousefi, X. Lu, M. Elimelech, N. Tufenkji, *Nat. Nanotechnol.* **2019**, *14*, 107; b) L. Feng, Z. Qin, Y. Huang, K. Peng, F. Wang, Y. Yan, Y. Chen, *Sci. Total Environ.* **2020**, *698*, 134239; c) H. Wang, X. Mi, Y. Li, S. Zhan, *Adv. Mater.* **2020**, *32*, 1806843; d) I. Ali, A. A. Basheer, X. Y. Mbianda, A. Burakov, E. Galunin, I. Burakova, E. Mkrtchyan, A. Tkachev, V. Grachev, *Environ. Int.* **2019**, *127*, 160; e) K. Yang, J. Wang, X. Chen, Q. Zhao, A. Ghaffar, B. Chen, *Environ. Sci. Nano* **2018**, *5*, 1264; f) S. Kim, C. M. Park, M. Jang, A. Son, N. Her, M. Yu, S. Snyder, D.-H. Kim, Y. Yoon, *Chemosphere* **2018**, *212*, 1104.
[12] a) M. Kumar, J. S. Chung, S. H. Hur, *Appl. Sci.* **2019**, *9*, 2925; b) J. Xu, Z. Cao, Y. Zhang, Z. Yuan, Z. Lou, X. Xu, X. Wang, *Chemosphere*

2018, *195*, 351; c) L. Xu, J. Wang, *Crit. Rev. Environ. Sci. Technol.* **2017**, *47*, 1042; d) W. Peng, H. Li, Y. Liu, S. Song, *J. Mol. Liq.* **2017**, *230*, 496; e) İ. Duru, D. Ege, A. R. Kamali, *J. Mater. Sci.* **2016**, *51*, 6097.

[13] N. Baig, Ihsanullah, M. Sajid, T. A. Saleh, *J. Environ. Manage* **2019**, *244*, 370.

[14] a) D. Gaber, M. Abu Haija, A. Eskhan, F. Banat, *Water, Air, Soil Pollut.* **2017**, *228*, 320; b) W. Shu, B. Hengchang, S. Litao, *Nanotechnol. Rev.* **2016**, *5*, 3.

[15] a) X. Yang, Y. Wan, Y. Zheng, F. He, Z. Yu, J. Huang, H. Wang, Y. S. Ok, Y. Jiang, B. Gao, *Chem. Eng. J.* **2019**, *366*, 608; b) A. I. A. Sherlala, A. A. A. Raman, M. M. Bello, A. Asghar, *Chemosphere* **2018**, *193*, 1004.

[16] Z. Yin, C. Cui, H. Chen, Duoni, X. Yu, W. Qian, *Small* **2020**, *16*, 1902301.

[17] Y. Shen, Q. Fang, B. Chen, *Environ. Sci. Technol.* **2015**, *49*, 67.

[18] J. Huang, Z. Yan, *Langmuir* **2018**, *34*, 1890.

[19] R. Thakuria, N. K. Nath, B. K. Saha, *Cryst. Growth Des.* **2019**, *19*, 523.

[20] A. S. Mahadevi, G. N. Sastry, *Chem. Rev.* **2013**, *113*, 2100.

[21] W. B. Jensen, *Chem. Rev.* **1978**, *78*, 1.

[22] A. S. Krishna Kumar, S.-J. Jiang, W.-L. Tseng, *J. Environ. Chem. Eng.* **2016**, *4*, 2052.

[23] P. L. Yap, S. Kabiri, Y. L. Auyoong, D. N. H. Tran, D. Losic, *ACS Omega* **2019**, *4*, 19787.

[24] I. Shtepliuk, R. Yakimova, *Phys. Chem. Chem. Phys.* **2018**, *20*, 21528.

[25] J. Liao, L. Yang, C. Z. Wang, S. Lin, *Mater. Technol.* **2017**, *32*, 840.

[26] H. R. Ghenaatian, M. Shakourian-Fard, G. Kamath, *J. Mater. Sci.* **2019**, *54*, 13175.

[27] Y. Wei, L. Xu, Y. Tao, C. Yao, H. Xue, Y. Kong, *Ind. Eng. Chem. Res.* **2016**, *55*, 1912.

[28] W. Wu, Y. Yang, H. Zhou, T. Ye, Z. Huang, R. Liu, Y. Kuang, *Water, Air, Soil, Pollut.* **2012**, *224*, 1372.

[29] Y. Zhuang, F. Yu, H. Chen, J. Zheng, J. Ma, J. Chen, *J. Mater. Chem. A* **2016**, *4*, 10885.

[30] J. Liu, H. Chu, H. Wei, H. Zhu, G. Wang, J. Zhu, J. He, *RSC Adv.* **2016**, *6*, 50061.

[31] M. Alimohammady, M. Jahangiri, F. Kiani, H. Tahermansouri, *New J. Chem.* **2017**, *41*, 8905.

[32] R. Zare-Dorabei, S. M. Ferdowsi, A. Barzin, A. Tadjarodi, *Ultrason. Sonochem.* **2016**, *32*, 265.

[33] C. Liu, D. X. Zhang, L. T. Zhao, X. Lu, P. Zhang, S. N. He, G. W. Hu, X. Q. Tang, *RSC Adv.* **2016**, *6*, 113352.

[34] P. T. Lan Huong, N. Tu, H. Lan, L. H. Thang, N. Van Quy, P. A. Tuan, N. X. Dinh, V. N. Phan, A. T. Le, *RSC Adv.* **2018**, *8*, 12376.

[35] J.-H. Deng, X.-R. Zhang, G.-M. Zeng, J.-L. Gong, Q.-Y. Niu, J. Liang, *Chem. Eng. J.* **2013**, *226*, 189.

[36] A. S. K. Kumar, S.-J. Jiang, *J. Environ. Chem. Eng.* **2016**, *4*, 1698.

[37] a) M. A. Rauf, S. Salman Ashraf, *Chem. Eng. J.* **2012**, *209*, 520; b) V. Katheresan, J. Kansedo, S. Y. Lau, *J. Environ. Chem. Eng.* **2018**, *6*, 4676.

[38] K. Singh, S. Arora, *Crit. Rev. Environ. Sci. Technol.* **2011**, *41*, 807.

[39] C. Cheng, S. Li, J. Zhao, X. Li, Z. Liu, L. Ma, X. Zhang, S. Sun, C. Zhao, *Chem. Eng. J.* **2013**, *228*, 468.

[40] Y. Shen, B. Chen, *Environ. Sci. Technol.* **2015**, *49*, 7364.

[41] R. Yu, Y. Shi, D. Yang, Y. Liu, J. Qu, Z.-Z. Yu, *ACS Appl. Mater. Interfaces* **2017**, *9*, 21809.

[42] P. L. Yap, K. Hassan, Y. L. Auyoong, N. Mansouri, F. Farivar, D. N. Tran, D. Losic, *Adv. Mater. Interfaces* **2020**, *7*, 14.

[43] S. Gupta, N.-H. Tai, *J. Mater. Chem. A* **2016**, *4*, 1550.

[44] H. Bi, X. Xie, K. Yin, Y. Zhou, S. Wan, L. He, F. Xu, F. Banhart, L. Sun, R. S. Ruoff, *Adv. Funct. Mater.* **2012**, *22*, 4421.

[45] Y. Zhao, C. Hu, Y. Hu, H. Cheng, G. Shi, L. Qu, *Angew. Chem., Int. Ed.* **2012**, *51*, 11371.

[46] Z. Pei, L. Li, L. Sun, S. Zhang, X.-q. Shan, S. Yang, B. Wen, *Carbon* **2013**, *51*, 156.

[47] M. A. Riaz, G. McKay, J. Saleem, *Environ. Sci. Pollut. Res.* **2017**, *24*, 27731.

[48] a) M. Peng, Y. Zhu, H. Li, K. He, G. Zeng, A. Chen, Z. Huang, T. Huang, L. Yuan, G. Chen, *Chem. Eng. J.* **2019**, *373*, 213; b) V. Chabot, D. Higgins, A. Yu, X. Xiao, Z. Chen, J. Zhang, *Energy Environ. Sci.* **2014**, *7*, 1564.

[49] V. Georgakilas, M. Otyepka, A. B. Bourlinos, V. Chandra, N. Kim, K. C. Kemp, P. Hobza, R. Zboril, K. S. Kim, *Chem. Rev.* **2012**, *112*, 6156.

[50] Y. Liu, M. Xiang, L. Hong, *RSC Adv.* **2017**, *7*, 6467.

[51] Y.-C. Shi, A.-J. Wang, X.-L. Wu, J.-R. Chen, J.-J. Feng, *J. Colloid Interface Sci.* **2016**, *484*, 254.

[52] Q. Kong, C. Wei, S. Preis, Y. Hu, F. Wang, *Environ. Sci. Pollut. Res.* **2018**, *25*, 21164.

[53] a) S. P. Surwade, S. N. Smirnov, I. V. Vlassiouk, R. R. Unocic, G. M. Veith, S. Dai, S. M. Mahurin, *Nat. Nanotechnol.* **2015**, *10*, 459; b) J. Bai, H. Sun, X. Yin, X. Yin, S. Wang, A. E. Creamer, L. Xu, Z. Qin, F. He, B. Gao, *ACS Appl. Mater. Interfaces* **2016**, *8*, 25289.

[54] C. Jiao, J. Xiong, J. Tao, S. Xu, D. Zhang, H. Lin, Y. Chen, *Int. J. Biol. Macromol.* **2016**, *83*, 133.

[55] L. Pan, Z. Wang, Q. Yang, R. Huang, *Nanomaterials* **2018**, *8*, 957.

[56] L. Hu, Z. Yang, L. Cui, Y. Li, H. H. Ngo, Y. Wang, Q. Wei, H. Ma, L. Yan, B. Du, *Chem. Eng. J.* **2016**, *287*, 545.

[57] Q. Zhao, X. Zhu, B. Chen, *Chem. Eng. J.* **2018**, *334*, 1119.

[58] M. Pirveysian, M. Ghiaci, *Appl. Surf. Sci.* **2018**, *428*, 98.

[59] a) Y. Zhang, L. Yan, W. Xu, X. Guo, L. Cui, L. Gao, Q. Wei, B. Du, *J. Mol. Liq.* **2014**, *191*, 177; b) A. Baranik, A. Gagor, I. Queralt, E. Marguí, R. Sitko, B. Zawisza, *Microchim. Acta* **2018**, *185*, 264; c) M. J. Aghagoli, F. Shemirani, *Microchim. Acta* **2017**, *184*, 237.

[60] Z. Wu, W. Deng, W. Zhou, J. Luo, *Carbohydr. Polym.* **2019**, *216*, 119.

[61] X. Li, H. Zhou, W. Wu, S. Wei, Y. Xu, Y. Kuang, *J. Colloid Interface Sci.* **2015**, *448*, 389.

[62] G. Zhou, C. Liu, Y. Tang, S. Luo, Z. Zeng, Y. Liu, R. Xu, L. Chu, *Chem. Eng. J.* **2015**, *280*, 275.

[63] L. Cui, Y. Wang, L. Gao, L. Hu, L. Yan, Q. Wei, B. Du, *Chem. Eng. J.* **2015**, *281*, 1.

[64] L. Cui, X. Guo, Q. Wei, Y. Wang, L. Gao, L. Yan, T. Yan, B. Du, *J. Colloid Interface Sci.* **2015**, *439*, 112.

[65] Y. Wang, X. Liu, H. Wang, G. Xia, W. Huang, R. Song, *J. Colloid Interface Sci.* **2014**, *416*, 243.

[66] a) M. Wei, H. Chai, Y. Cao, D. Jia, *J. Colloid Interface Sci.* **2018**, *524*, 297; b) P. L. Yap, Y. L. Auyoong, K. Hassan, F. Farivar, D. N. H. Tran, J. Ma, D. Losic, *Chem. Eng. J.* **2020**, *395*, 124965.

[67] Y. Ding, Z. Tian, H. Li, X. Wang, *New Carbon Mater.* **2019**, *34*, 315.

[68] X. Luo, C. Wang, L. Wang, F. Deng, S. Luo, X. Tu, C. Au, *Chem. Eng. J.* **2013**, *220*, 98.

[69] C. P. Bergmann, F. M. Machado, *Carbon Nanomaterials as Adsorbents for Environmental and Biological Applications*, Springer, New York **2015**.

[70] E. I. Braun, P. Pantano, *Carbon* **2014**, *77*, 912.

[71] a) F. Zhou, X. Feng, J. Yu, X. Jiang, *Environ. Sci. Pollut. Res.* **2018**, *25*, 15651; b) Y. Chen, X. Song, T. Zhao, Y. Xiao, Y. Wang, X. Chen, *J. Hazard. Mater.* **2018**, *343*, 298; c) F. S. Awad, K. M. AbouZeid, W. M. A. El-Maaty, A. M. El-Wakil, M. S. El-Shall, *ACS Appl. Mater. Interfaces* **2017**, *9*, 34230.

[72] W. S. Hummers, R. E. Offeman, *J. Am. Chem. Soc.* **1958**, *80*, 1339.

[73] A. Kovtun, E. Treossi, N. Mirotta, A. Scidà, A. Liscio, M. Christian, F. Valorosi, A. Boschi, R. J. Young, C. Galiotis, I. A. Kinloch, V. Morandi, V. Palermo, *2D Mater.* **2019**, *6*, 025006.

[74] K. S. W. Sing, D. H. Everett, R. A. W. Haul, L. Moscou, R. A. Pierotti, J. Rouquérol, T. Siemieniewska, *Pure Appl. Chem.* **1982**, *54*, 2201.

[75] F. Zhang, B. Wang, S. He, R. Man, *J. Chem. Eng. Data* **2014**, *59*, 1719.

[76] I. Andjelkovic, S. Azari, M. Erkelens, P. Forward, M. F. Lambert, D. Losic, *RSC Adv.* **2017**, *7*, 3941.
[77] D. Harikishore Kumar Reddy, K. Vijayaraghavan, J. A. Kim, Y.-S. Yun, *Adv. Colloid Interface Sci.* **2017**, *242*, 35.
[78] G. S. Fanourgakis, K. Gkagkas, E. Tylianakis, G. Froudakis, *J. Phys. Chem. C* **2020**, *124*, 7117.
[79] K. Wang, J. Ruan, H. Song, J. Zhang, Y. Wo, S. Guo, D. Cui, *Nanoscale Res. Lett.* **2010**, *6*, 8.
[80] a) C. M. Santos, J. Mangadlao, F. Ahmed, A. Leon, R. C. Advincula, D. F. Rodrigues, *Nanotechnology* **2012**, *23*, 395101; b) I. E. Mejías Carpio, C. M. Santos, X. Wei, D. F. Rodrigues, *Nanoscale* **2012**, *4*, 4746.
[81] S. C. Smith, D. F. Rodrigues, *Carbon* **2015**, *91*, 122.
[82] a) H. Fan, H. Ren, X. Ma, S. Zhou, J. Huang, W. Jiao, G. Qi, Y. Liu, *Chem. Eng. J.* **2020**, *390*, 124639; b) R. Xu, G. Zhou, Y. Tang, L. Chu, C. Liu, Z. Zeng, S. Luo, *Chem. Eng. J.* **2015**, *275*, 179.

Pei Lay Yap completed her Bachelor of Science (Applied Chemistry) and Master of Science (Material Science and Nanotechnology) degrees at The University of Malaya, Malaysia with her research focus on materials design and characterizations for mercury removal from water systems. Currently, she is pursuing a Ph.D. degree under the supervision of Prof. Dusan Losic at the School of Chemical Engineering and Advanced Materials, The University of Adelaide, Australia, where she focuses on the development of new methodologies for the design of novel functionalized graphene-based materials for environmental applications.

Diana N. H. Tran completed a Bachelor of Engineering, majoring in Chemical Engineering, at the University of Adelaide and is currently a lecturer in the School of Chemical Engineering & Advanced Materials. She obtained her Ph.D. degree in Engineering (Minerals and Materials) from The Ian Wark Research Institute, University of South Australia in 2010. She has worked on the development of new technologies for processing graphite and 2D-based nanomaterials for different applications, as well as in the field of colloid and interface science related to mineral processing.

Dusan Losic is a professor at School of Chemical Engineering and Advanced Materials, University of Adelaide, a leader of Research Group and Director of the ARC Research Hub for Graphene Enable Industry Transformation. He completed Ph.D. in Nanotechnology at Flinders University (2003). His research is focused on engineering nanomaterials, properties and applications for addressing environmental, health, energy and agriculture problems.

CHAPTER 3

FUNDAMENTAL UNDERSTANDING ON SURFACE ENGINEERING OF FUNCTIONALIZED GRAPHENE MATERIALS

3. FUNDAMENTAL UNDERSTANDING ON SURFACE ENGINEERING OF FUNCTIONALIZED GRAPHENE MATERIALS

3.1. Overview and Significance of Work

Chapter 3 highlights the fundamental understanding on surface engineering and structural design of functionalized graphene materials through the combined modifications of chemical doping, reduction and thiol-ene click reaction. Resulting derivatives from the combined modifications with varying levels and configurations of oxygen, nitrogen and sufur within the graphene framework are comprehensively studied using a series of characterization techniques (UV-Vis, Raman, XRD, TGA-DTG, FTIR and XPS analyses). Fundamental mastery of functionalized graphene materials with tailorable doping levels, functional groups and interfacial properties at varied oxidation levels is developed. Findings from this chapter fulfil Objective 2 and are consolidated in a published peer-reviewed research article.

3.2. Statement of Authorship

Statement of Authorship

Title of Paper	Tuning the Multifunctional Surface Chemistry of Reduced Graphene Oxide via Combined Elemental Doping and Chemical Modifications
Publication Status	☒ Published ☐ Accepted for Publication ☐ Submitted for Publication ☐ Unpublished and Unsubmitted work written in manuscript style
Publication Details	Yap, P. L., Kabiri, S., Auyoong, Y. L., Tran, D. N. H., & Losic, D. (2019). Tuning the multifunctional surface chemistry of reduced graphene oxide via combined elemental doping and chemical modifications. ACS Omega, 4(22),

Principal Author

Name of Principal Author (Candidate)	Pei Lay Yap		
Contribution to the Paper	Prepared and characterized on all the samples, interpreted data as well as wrote the manuscripts		
Overall percentage (%)	85%		
Certification:	This paper reports on original research I conducted during the period of my Higher Degree by Research candidature and is not subject to any obligations or contractual agreements with a third party that would constrain its inclusion in this thesis. I am the primary author of this paper.		
Signature		Date	07/10/20

Co-Author Contributions

By signing the Statement of Authorship, each author certifies that:

i. the candidate's stated contribution to the publication is accurate (as detailed above);

ii. permission is granted for the candidate in include the publication in the thesis; and

iii. the sum of all co-author contributions is equal to 100% less the candidate's stated contribution.

Name of Co-Author	Yow Loo Au Yoong		
Contribution to the Paper	Helped to evaluate and edit the manuscript.		
Signature		Date	07/10/20

Name of Co-Author	Shervin Kabiri		
Contribution to the Paper	Edited and revised the manuscript.		
Signature		Date	07/10/20

Please cut and paste additional co-author panels here as required.

Statement of Authorship

Title of Paper	Tuning the Multifunctional Surface Chemistry of Reduced Graphene Oxide via Combined Elemental Doping and Chemical Modifications
Publication Status	☒ Published ☐ Accepted for Publication ☐ Submitted for Publication ☐ Unpublished and Unsubmitted work written in manuscript style
Publication Details	Yap, P. L., Kabiri, S., Auyoong, Y. L., Tran, D. N. H., & Losic, D. (2019). Tuning the multifunctional surface chemistry of reduced graphene oxide via combined elemental doping and chemical modifications. ACS Omega, 4(22),

Principal Author

Name of Principal Author (Candidate)	Pei Lay Yap
Contribution to the Paper	Prepared and characterized on all the samples, interpreted data as well as wrote the manuscripts
Overall percentage (%)	85%
Certification:	This paper reports on original research I conducted during the period of my Higher Degree by Research candidature and is not subject to any obligations or contractual agreements with a third party that would constrain its inclusion in this thesis. I am the primary author of this paper.
Signature	Date 01/10/20

Co-Author Contributions

By signing the Statement of Authorship, each author certifies that:

i. the candidate's stated contribution to the publication is accurate (as detailed above);

ii. permission is granted for the candidate in include the publication in the thesis; and

iii. the sum of all co-author contributions is equal to 100% less the candidate's stated contribution.

Name of Co-Author	Diana N.H. Tran
Contribution to the Paper	Co-supervised and revised manuscript.
Signature	Date 02/10/20

Name of Co-Author	Dusan Losic
Contribution to the Paper	Supervised the development of work, edited, revised the manuscript and acted as the corresponding author.
Signature	Date 02/10/20

Please cut and paste additional co-author panels here as required.

3.3. Published work

This section is presented as a published article as ***Yap, P. L.***, *Kabiri, S., Auyoong, Y. L., Tran, D. N. H., & Losic, D. (2019). Tuning the multifunctional surface chemistry of reduced graphene oxide via combined elemental doping and chemical modifications. ACS Omega, 4(22), 19787-19798.* Reproduced with permission.[22] Copyright (2019) American Chemical Society.

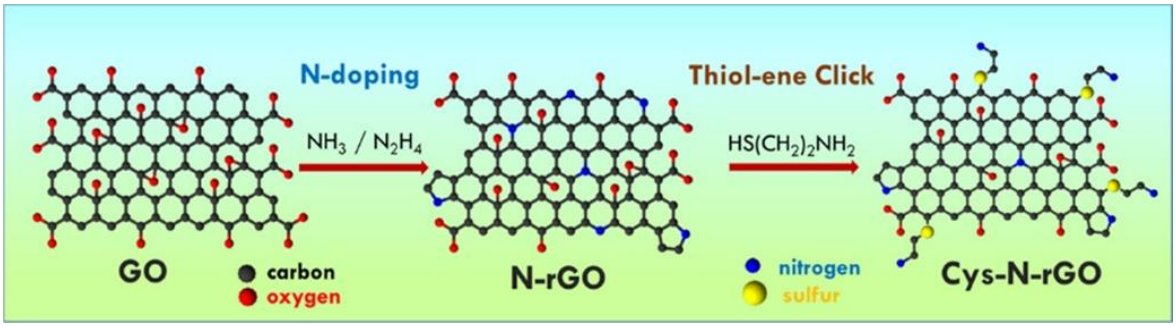

Figure 12. Graphical abstract of *"Tuning the multifunctional surface chemistry of reduced graphene oxide via combined elemental doping and chemical modifications". Reproduced with permission.[22] Copyright (2019) American Chemical Society.*

ACS OMEGA

Article

Cite This: ACS Omega 2019, 4, 19787−19798

http://pubs.acs.org/journal/acsodf

Tuning the Multifunctional Surface Chemistry of Reduced Graphene Oxide via Combined Elemental Doping and Chemical Modifications

Pei Lay Yap,[†,‡] Shervin Kabiri,[‡,§] Yow Loo Auyoong,[∥] Diana N. H. Tran,[†,‡] and Dusan Losic*[,†,‡]

[†]School of Chemical Engineering and Advanced Materials and [‡]ARC Hub for Graphene Enabled Industry Transformation, The University of Adelaide, Adelaide, SA 5005, Australia

[§]School of Agriculture, Food and Wine, The University of Adelaide, PMB 1, Waite Campus, Glen Osmond, SA 5064, Australia

[∥]Research & Business Partnerships, Research Services, The University of Adelaide, Adelaide, SA 5000, Australia

Supporting Information

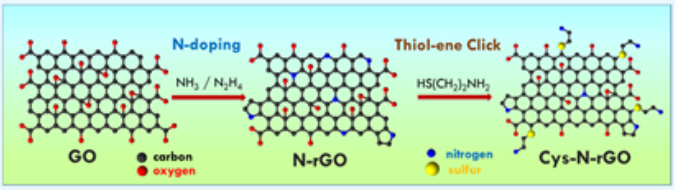

ABSTRACT: The synthesis of graphene materials with multiple surface chemistries and functionalities is critical for further improving their properties and broadening their emerging applications. We present a simple chemical approach to obtain bulk quantities of multifunctionalized reduced graphene oxide (rGO) that combines chemical doping and functionalization using the thiol-ene click reaction. Controllable modulation of chemical multifunctionality was achieved by simultaneous nitrogen doping and gradual chemical reduction of graphene oxide (GO) using ammonia and hydrazine, followed by covalent attachment of amino-terminated thiol molecules using the thiol-ene click reaction. A series of N-doped rGO (N-rGO) precursors with different levels of oxygen groups were synthesized by adjusting the amount of reducing agent (hydrazine), followed by subsequent covalent attachment of cysteamine via the thermal thiol-ene click reaction to yield different ratios of mixed functional groups including N (pyrrolic N, graphitic N, and aminic N), S (thioether S, thiophene S, and S oxides), and O (hydroxyl O, carbonyl O, and carboxyl O) on the reduced GO surface. Detailed XPS analysis confirmed the disappearance of unstable pyridinic N in cys-N-rGO and the reduction degree threshold of N-rGO for effective cysteamine modification to take place. Our study establishes a strong correlation between different reduction degrees of N-rGO with several existing oxygen functional groups and addition of new tunable functionalities including covalently attached nitrogen (amino) and sulfur (C−S−C, C═S, and S−O). This simple and versatile approach provides a valuable contribution for practical designing and synthesis of a broad range of functionalized graphene materials with tailorable functionalities, doping levels, and interfacial properties for potential applications such as polymer composites, supercapacitors, electrocatalysis, adsorption, and sensors.

1. INTRODUCTION

Graphene has sparked tremendous research interest over the last two decades owing to its unique 2D structure, high surface area, extraordinary electron mobility, notable mechanical strength, thermal conductivity, and structural and optical properties in a diverse range of applications across industrial sectors including composites, supercapacitors, batteries, fuel cells, inks, protective and functional coatings.[1] Many of these applications require specific chemical functionalizations of graphene to achieve its integration with other materials, which are different in nature including polymers, organic molecules, biomolecules, metals, semiconductors, nanoparticles, or other 2D materials. Chemical functionalization of graphene powder materials is particularly needed to make stable graphene−water dispersions for improved processability to achieve better incorporation of these materials for engineering new functional and hybrid materials needed for broad applications.[2]

Many functionalization strategies of graphene have been explored over the last two decades based on covalent or noncovalent chemical binding of organic molecules and functional groups containing oxygen (i.e., graphene oxide), nitrogen (amino), sulfur (mercapto), fluorine, or hydrogen to the carbon atoms. These methods are mostly inherited from the developments of "older" carbon nanoforms such as fullerenes and carbon nanotubes that have paved the way for the functionalization of graphene and its derivatives today. Graphene oxide (GO), prepared from the oxidation and exfoliation of graphite in the presence of strong acids and oxidants, is one of the most popular forms of chemically (oxygen) functionalized graphene used not only as an important precursor to convert the intermediate, reduced

Received: August 16, 2019
Accepted: October 28, 2019
Published: November 11, 2019

DOI: 10.1021/acsomega.9b02642
ACS Omega 2019, 4, 19787−19798

GO (rGO), into produce bulk graphene but also for other applications such as membranes, sensors, and composites. GO addresses some inherent disadvantages of pristine graphene such as high hydrophobicity, chemical inertness, and a lack of dispersibility in water. However, GO also has some drawbacks such as low conductivity and amorphous structure, which hinder its broader applications.[2] Hence, a balance is required between the desirable properties of both GO and graphene to harness the benefits of both materials. Controllable reduction and chemical functionalization are considered as a rational approach in achieving these requirements is needed for many applications.

Chemical functionalization of graphene bulk materials can significantly lead to the generation of a new type of graphene-based materials, which facilitates the unprecedented properties of graphene with other compound classes.[3] Among many explored reactions, the thiol-ene click route based on the targeted attack on the sp^2 carbon using thiol radicals generated by the action of either heat or light appears to be one of the most efficient and promising strategies to achieve these tasks.[4,5] The assimilation of graphene with the thiol-ene click reaction has recently gained remarkable attention in advanced macromolecular engineering and materials chemistry given the attributes that this approach is highly efficient, versatile, simple, catalyst-free, and proceeds in benign solvents under mild reaction conditions in addition to the high yield conversion.[4,6]

On the other hand, elemental doping of graphene with selected elements (with N, S, B, and P) has been recognized as a desirable approach for controlling the band gap and tailoring the electrical and electron transport properties, as well as electrocatalytic performances, of graphene. This approach offers a unique way to extend the limited zero band-gap energies of graphene by the hybridization of electronic orbitals from sp^2 to sp^3 and opening large band gaps (>4 eV), which are important for many applications.[7−9] Numerous strategies were reported for individual (N) or co-doping (N and S) to insert the dual atoms simultaneously into the carbon network using gaseous, hydrothermal, and solvothermal processes with different precursors such as ammonia,[10] thiophene,[10] L-cysteine,[11] hydrazine,[12] ammonium thiocyanate,[13] etc. These hybrid materials are used as catalysts to enhance the electrocatalytic oxygen reduction,[14] as the anode material to improve the adsorption capability of sodium ions in sodium-ion batteries,[15] and as metal-free cathode catalysts for the application in direct biorenewable alcohol fuel cells.[10] However, there are still limited studies on combining these two concepts to target the heteroatom insertion in the graphene lattice with surface functionalization, which can be regarded as a highly valuable approach for engineering of a broad range of bulk graphene hybrid materials needed for many emerging applications.

The aim of this study was to demonstrate the combination of simultaneous binary-heteroatom doping and click chemistry to create bulk multifunctional graphene materials with tunable surface chemistry for more diverse electronic, sensing, catalytic, and adsorption properties and applications following our previous study, which showed promising performance for water remediation by applying multifunctional graphene composites synthesized via the thiol-ene click reaction.[19] In this work, the controllable modulation of chemical multi-functionality is proposed by consequent elemental doping and gradual chemical reduction of GO using ammonia and hydrazine followed by covalent attachment of amino-terminated thiol molecules (cysteamine) via the thermal thiol-ene click reaction, which has not been addressed previously. Our primary focus is targeted on the fundamental understanding of the changes in the surface property to identify the chemical species (functional groups) of the thiol-ene-clicked graphene composites using reduced graphene oxide (rGO) with varied oxidation levels. The formation of the resulting derivative of nitrogen-doped and cysteamine-functionalized reduced graphene oxide (cys-N-rGO) with varying levels and configurations of oxygen, nitrogen, and sulfur atoms within the graphene framework was confirmed by a series of characterization techniques including UV−vis, Raman, XRD, TGA−DTA, FTIR, and XPS analyses. Results from this study underpin the fundamental mastery of controllable functionalization to tailor the properties of graphene and its derivatives using the combination of simultaneous binary-heteroatom doping and click chemistry, which is needed for a broad range of applications.

2. RESULTS AND DISCUSSION

2.1. Simultaneous Nitrogen Doping and Gradual Chemical Reduction of GO. In the first experiment, synthesis of N-doped reduced graphene oxide with a controllable level of oxygen functional groups was performed by simultaneous doping and chemical reduction of GO using ammonia and hydrazine (details of synthesis conditions are included in Table S1, Supporting Information). A series of characterization results including TEM, SEM, and XPS are summarized in Figure 1 and Table S2 to confirm the structural, elemental, and chemical compositions of the prepared N-doped rGO precursors. Figure 1A presents the SEM and TEM images of the typical structure of GO sheets with sizes in the nanometer range and thickness of a few graphene layers, which are used for the entire experiments. The wrinkled and fairly smooth surface of GO can be clearly observed from its SEM

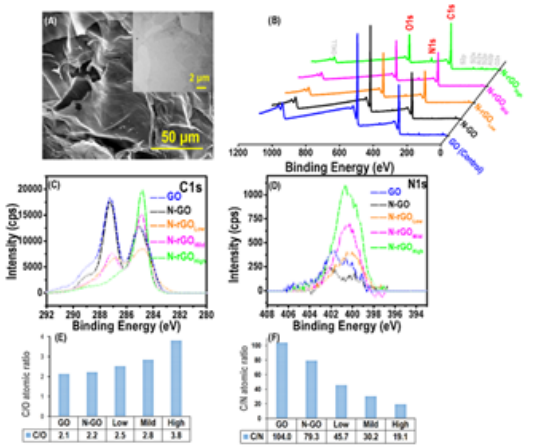

Figure 1. (A) FESEM image with the inset displaying the TEM image of exfoliated GO nanosheets used for the synthesis of N-doped rGO precursors. Plots of (B) XPS survey spectra with characteristic C 1s, O 1s, and N 1s peaks; high-resolution XPS of (C) C 1s scan and (D) N 1s scan with background subtracted; (E) C/O atomic ratios, and (F) C/N atomic ratios for GO, N-GO, and N-rGO precursors (low, mild, and high).

DOI: 10.1021/acsomega.9b02642
ACS Omega 2019, 4, 19787−19798

image, whereas the ultrathin stacked GO layers can be seen from the TEM image as incorporated in the inset of Figure 1A.

Figure 1B shows a series of survey XPS spectra recorded from GO (control), N-doped GO (N-GO), and N-doped rGO (N-rGO) with different levels of reduction (low, mild, and high) showing characteristic C 1s, O 1s, and N 1s peaks detected at ~285, ~532, and ~400 eV, respectively, indicating the presence of carbon, oxygen, and nitrogen on the surface of N-doped precursors. A series of individual high-resolution peaks showing carbon, nitrogen, and oxygen peaks for all prepared N-GO and N-rGO precursors to confirm their chemical functionalities are depicted in Figures 1C,D and S1, respectively. These spectra clearly demonstrated changes of the peak intensity as a result of the reduction in oxygen functionalities and the increased N-doping effect after treatment with ammonia and hydrazine. Normalized atomic percentages of C, O, and N calculated from the area of the survey spectra under C 1s, O 1s, and N 1s peaks, respectively, and their aspect ratios are summarized in Table S2 and Figure 1E and F, correspondingly. The XPS results showed that the highest amount of oxygen was found in control GO, with nearly 32% of oxygen detected. As expected, the atomic percentage of oxygen was slightly reduced to ~31% for N-GO and progressively to ~20% for the N-rGO precursor with the highest reduction degree as the amount of hydrazine and reduction time increased. The carbon-to-oxygen (C/O) atomic ratio determined from the XPS survey scans (Figure 1E) confirmed these changes in reduction, showing a gradual increase in the value (2.13, which is typical for GO) to 2.21 (N-GO), 2.52 (low N-rGO), 2.84 (mild N-rGO), and 3.80 (high N-rGO), which verified the gradual reduction of GO. From the literature, it is reported that upon reduction, the C/O atomic ratio can increase to 12 for highly reduced GO, depending on the type and amount of the reducing agent and the reduction conditions used.[20−22] However, the primary goal in this work was having a series of rGO precursors with different levels of oxygen functional groups (C/O atomic ratio between 2 and 4), which suited the next functionalization step to attach thiol organic molecules with amino functional groups.

In addition to the decreased oxygen level, the use of hydrazine treatment with ammonia on GO provides simultaneous N-doping by the integration of nitrogen atoms into the graphene network, while ammonia can also be used to change the charge state of rGO sheets, preventing the agglomeration of graphene sheets upon reduction.[23,24] The doping of N in the graphene network is confirmed from the XPS survey spectra and reflected by the progressive increase of N concentrations (Table S2) and surface-carbon-to-nitrogen (C/N) atomic ratio, as illustrated in Figure 1F. Contrary to the increasing trend of the C/O atomic ratio, the C/N atomic ratio of rGO precursors was pronouncedly decreased from the control to N-rGO of high reduction degree, implying the growing amount of N incorporated into the rGO network as the reduction degree increased. By adjusting the amount of hydrazine and reduction time progressively, the atomic percentage of O was found to decrease visibly, whereas that of N was increased simultaneously. This finding suggests that the elemental compositions of O and N on GO can be easily dictated by varying the amount of hydrazine and reduction time.

Further peak fitting analysis of the high-resolution XPS scans of C 1s, O 1s, and N 1s was carried out to determine the chemical environment and species present on the surface of GO, N-GO, and N-rGOs. To ensure that the peak fitting outcomes remain mathematically and chemically realistic, we prudently fitted and deconvoluted the high-resolution C 1s peaks into two main components (nonoxygenated and oxygenated carbon) after imposing parameter constraints as mentioned in the characterization section on their respective position and full width at half-maximum (fwhm) of the components. The nonoxygenated C components include C−C (sp^3 C, ~285 eV), C═C (sp^2 C, ~284.6 eV), C−N (~285.7 eV), and C−S (~285.2 eV), while the oxygenated C components consist of C−O−C (epoxide, ~287.2 eV), C−OH (hydroxyl, ~286.6 eV), C═O (carbonyl, ~288.1 eV), and HO−C═O (carboxyl, ~289.0 eV). It is noteworthy that the component assignments are conforming to the reported literature, despite that some slight shifts in terms of the position of the components were observed after the reduction treatment.[25−29] The peak deconvolution studies of high-resolution C 1s spectra of GO (Figure S2A), N-GO, and N-rGO are displayed in Figure 2A−D. Control GO and N-doped

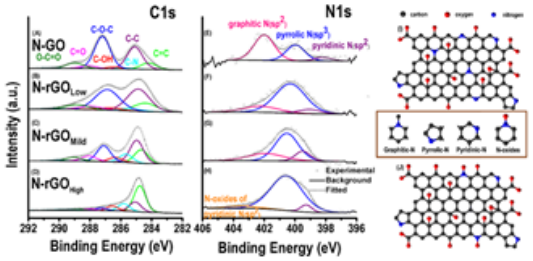

Figure 2. Plots of deconvoluted high-resolution spectra of (A−D) C 1s and (E−H) N 1s, and possible chemical structures determined from XPS deconvolution analysis of (I) N-GO, N-rGO$_{Low}$, and N-rGO$_{Mild}$ and (J) N-rGO$_{High}$ after simultaneous N-doping and reduction by ammonia and hydrazine (not drawn on scale).

GO (N-GO) showed typical characteristics of C 1s species for GO with strongly oxidized surface and oxygenated functional groups predominantly made up of epoxides (C−O−C), carboxyls (HO−C═O), carbonyls (C═O), and hydroxyls (C−OH). A higher peak intensity exhibited by C−O−C (287 eV) relative to C−C (285 eV) is an indication of an ordinary well-oxidized GO decorated with a plethora of oxygen functional groups under a harsh oxidization process.[30,31] The deconvoluted C 1s spectra of other rGOs with low, mild, and high reduction degrees showed the same oxygen-containing groups, however with weaker peak intensities, clearly demonstrating a gradual reduction of oxygen groups. For low and mild N-rGOs (Figure 2B and C), the spectra show similar peaks of carbon species C−O−C (287 eV) and the C−C peak (285 eV) with the only difference that peak intensities are decreased. However, for high N-rGO, its spectrum (Figure 2D) exhibits relatively weak C−O−C (287 eV) than C−C (285 eV) peaks, revealing the formation of a highly reduced graphene structure, which is in agreement with the previous reports.[18,32] In agreement with the C 1s narrow-scan analysis, the O 1s XPS plots of all of these samples characterized by their respective binding energies also indicated the formation of different oxygen-containing groups including quinone, aromatic C═O, aliphatic C−O, and aromatic C−O, which are detailed in Figures S2B (GO) and S3(N-GO and N-rGOs). On the other hand, a very intense C═C peak (284 eV) is

DOI: 10.1021/acsomega.9b02642
ACS Omega 2019, 4, 19787−19798

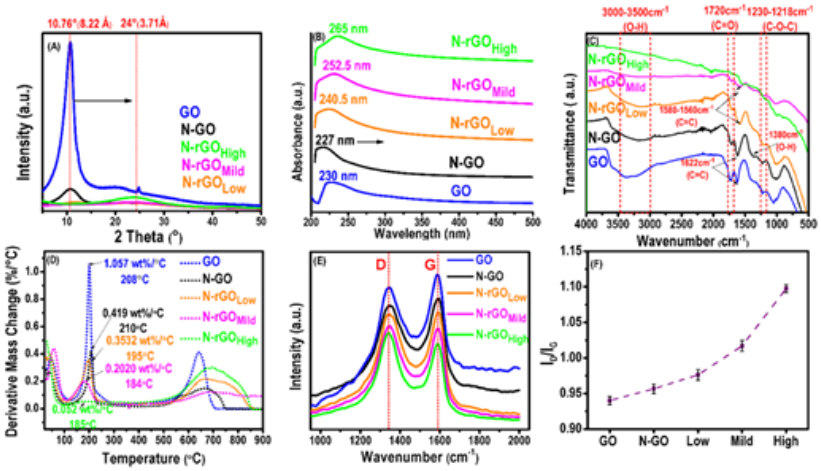

Figure 3. Plots of (A) XRD, (B) UV−vis, (C) FTIR, (D) DTA, (E) Raman analyses, (F) I_D/I_G ratio measured from Raman spectra of GO, N-GO, and N-rGO (low, mild, and high) samples prepared by simultaneous doping and reduction using hydrazine and ammonia.

observed for these materials for the product with the highest degree of graphene reduction, as illustrated in Figure 2D.

The high-resolution and peak deconvolution studies of N 1s spectra positioned at around 401 eV for N-GO and N-rGOs are presented in Figure 2E−H. These results obviously indicate a considerable buildup of nitrogen species in all of the hydrazine-reduced GO. It could be seen that N-GO low and mild N-rGOs could be resolved into three different nitrogen-bonding configurations within the graphene lattice including pyridinic N (bonded to sp^2 C in a hexagonal configuration) at around 398.1−399.5 eV, pyrrolic N (bonded to sp^3 C in a pentagonal configuration) at 399.8−401.2 eV, and quaternary or graphitic N, which is sp^3-hybridized found at 401.1−402.7 eV, as depicted in Figure 2E−H.[24] According to Park et al., the peak at around 400 eV can be allotted to pyrazoline groups (non-aromatic 5-membered rings), which can be further resolved into two N 1s peaks at 398.6 and 400.5 eV representing two N atoms in different chemical environments, as illustrated in Figure 2E−H.[12] Interestingly, the high N-rGOs exhibited dissimilar chemical N environments with their corresponding narrow peaks deconvoluted into pyridinic N at 399.3 eV, pyrrolic N at 400.6 eV, and N-oxides of pyridinic nitrogen at around 403 eV.[24] The N-oxides detected in high N-rGO are commonly attached to nitrogen-containing dangling bonds or physisorbed species, which is concordant with the findings in the reported literature.[7,33] As proposed by Stankovich et al., hydrazine is well known to feasibly ring-open epoxides and form hydrazine alcohols. Although the chemical environment of N species was not resolved in their work, the significant nitrogen incorporation in the graphene network further rendered the intriguing query on how the mechanism of deoxygenation and re-establishment of the graphene conjugated network can take place via hydrazine treatment. The mechanism of simultaneous deoxygenation and insertion of N in the graphene structure still remains an open question.[21] In the work conducted by Park et al., hydrazine treatment of GO was proven to insert an aromatic nitrogen moiety in a 5-membered ring at the platelet edges of graphene, and the aromaticity of the pyrazole moiety can enhance electron conduction in the rGO due to the reduced band gap and localized electronic states of the sp^2 configuration of N. They also proposed that hydrazine-reduced/substituted graphene oxide is a more precise description for GO treated by hydrazine due to the doped N in the graphene structure.[12] Meanwhile, it was reported that hydrazine also resulted in nitrogen doping, evidenced by the XPS technique with about 2.86 at % nitrogen content detected as well as resolved pyridinic N, pyrrolic N, and graphitic N discovered in the graphene structure, demonstrating the excellent capacity stability and improved cyclic performance in lithium-sulfur batteries.[34] Xie et al. found that graphene designed with high percentages of doped pyridinic N and pyridone N (6.8−8 at % of total nitrogen content) can be achieved by the combination of ammonia and hydrazine under hydrothermal treatment, which enhanced the capacitance and cycling performance for electrochemical applications.[33] Based on the literature references and the detailed XPS analysis of high-resolution C 1s, N 1s, and O 1s in the present study, a series of N-doped rGOs with varying oxygen levels can be simply prepared using the chemical reduction approach, and the chemical structure of the obtained N-doped precursors is schematically proposed in Figure 2I and J. It should be highlighted that hydrazine exhibits dual roles as a reductant and an N-dopant for graphene oxide, which enables simultaneous N-doping and GO reduction to achieve rGO with different functionalities including several types of N groups (pyridinic, pyrolytic, and graphitic N) combined with different levels of O groups (quinone, aliphatic, and aromatic O).[33,34]

To further verify these observations and the proposed chemical structure of the prepared precursors, XRD, UV−vis, FTIR, Raman, and DTA analyses were carried out and are presented in Figure 3. XRD patterns in Figure 3A reveal the characteristic peaks for GO (2θ = 10.78°) and N-GO (2θ = 10.76°), which were found to progressively reduce and disappear in all of the prepared N-rGOs. A new broad peak at around 2θ = 24° was observed for high-reduction-degree N-rGO, indicating the re-establishment of the conjugated rGO network, which could be attributed to the elimination of the oxygen-containing groups intercalated between the GO layers after the reduction reaction.[35,36] Meanwhile, a weak peak at

DOI: 10.1021/acsomega.9b02642
ACS Omega 2019, 4, 19787−19798

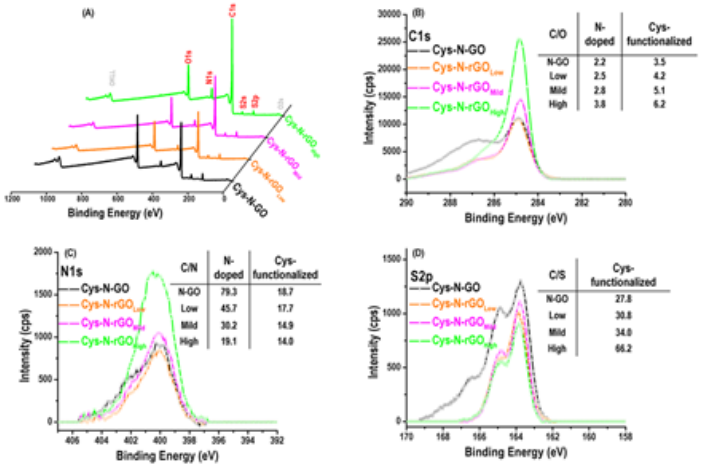

Figure 4. (A) Plots of XPS survey spectra with characteristic C 1s, O 1s, and N 1s peaks and high-resolution XPS of (B) C 1s scan, (C) N 1s scan, and (D) S 2p with background subtracted and their corresponding C/O, C/N, and C/S atomic ratios before and after cysteamine functionalization of N-GO and N-rGOs.

around $2\theta \sim 43°$ was also found for high-reduction-degree N-rGO, which could be associated with the turbostratic band of the disordered carbon materials.[37] The obvious peak shift observed in the XRD patterns of GO and N-rGO from approximately 11 to 24° further affirmed the presence of different reduction degrees of the N-rGOs due to varied oxygen contents and doped N that resulted after the chemical reduction treatment, as evidenced by the XPS analysis discussed previously.

The reduction degree of the N-rGO precursors was also confirmed by the UV−vis technique, and their respective UV−vis spectra are illustrated in Figure 3B, which all show a single absorption peak attributed to the $\pi-\pi^*$ transition of a C═C bond in the aromatic carbon. The strong absorption plasmon peak recorded for the N-GO at 227 nm is found to be almost similar to that for GO at 230 nm, suggesting that oxygen groups were not significantly reduced by the ammonia treatment. On the other hand, different reduction degrees of N-rGOs exhibited significant variations in their absorption maxima, which can also be visibly recognized by the color of their dispersions (Figure S4, Supporting Information). In Figure 3B, the absorption maximum has progressively shifted to the right, moving from GO to N-rGO of high reduction degree. The red-shifted spectra to a longer wavelength indicated that there is a gradual increase in π-electron density and the restoration of sp^2 carbon in the graphene network.[38,39] Complementing with the outcomes from XPS and XRD techniques, the UV−vis results strongly suggest the formation of N-rGO with different reduction degrees.

The FTIR spectra as depicted in Figure 3C show the characteristic bands of GO and N-GO precursors in the regions of 3100−3500, 1720, 1380, and 1218−1230 cm^{-1}, which can be ascribed to the stretching mode of hydroxyl and the vibration modes of the carbonyl, C−OH, and epoxy groups, respectively.[40] These transmittance bands are also present in the N-rGO precursors but were slightly shifted after the hydrazine treatment.[40] It can be observed that the intensity of the O−H (3000−3500 cm^{-1}) and C−O−C (1218−1230 cm^{-1}) bands gradually decreased and eventually the bands disappeared, particularly for N-rGO of the highest reduction degree. This result indicated that oxygen moieties such as O−H and C−O−C groups can be prominently removed when using a large amount of hydrazine for a prolonged reaction time. This finding is consistent with the previous studies, where hydrazine is effective in removing in-plane oxygen functional groups such as epoxy and hydroxyls, leaving the edge moieties such as carboxyls and carbonyls on GO.[39,40] The declining peak intensity particularly for OH and C−O−C groups on rGO precursors clearly manifested that N-rGO precursors with gradual removal of oxygen groups were effectively created, in good agreement with the outcomes from the C/O atomic ratio determined using the XPS technique.

The thermal stabilities of GO, N-GO, and N-rGO samples were evaluated by both TGA and differential thermogravimetric (DTA) analyses (Figures S5 and 3D, respectively). Overall, it could be detected that all N-rGOs exhibited higher thermal stability relative to GO, which reflects the success of the reduction process of GO and the chemical reduction via the removal of attached oxygen functional groups by hydrazine. The calculated derivative mass change at ~200 °C (from 1.057 to 0.052 wt %/°C for GO control to N-rGO with the highest reduction degree) displayed in the DTA plots (Figure 3D) verified that the oxygen moieties were removed progressively by controlled chemical reduction using hydrazine. This peak can be ascribed to the decomposition of labile oxygen-containing functional groups, such as hydroxyl (−OH), epoxy [−CH (O) CH−], and carboxyl (−COOH) groups, between the layers of GO nanosheets.[32] This finding demonstrates that the effective stepwise oxygen reduction degree was introduced into the N-rGO, which correlates well with the XPS elemental composition, UV−vis, FTIR, and XRD results discussed in the previous section. More details on the mass-loss events are provided in Figure S5, Supporting Information.

Finally, Raman spectra (Figure 3E) of GO, N-GO, and N-rGO with different reduction degrees were recorded to confirm the structural features and defects formed during the doping and chemical reduction processes. Two apparent peaks at approximately 1344 and 1591 cm^{-1} corresponding to the D and G bands, respectively, are observed, in which the D band

DOI: 10.1021/acsomega.9b02642
ACS Omega 2019, 4, 19787−19798

arises due to the breathing mode of aromatic rings, which requires a defect for its activation, whereas the G band can be related to the bond stretching of sp^2 carbon pairs in both rings and chains.[39] The intensity ratio of the D to G bands, I_D/I_G (measure for the degree of disorder), as illustrated in the inset of Figure 3E, shows that the I_D/I_G ratio increases gradually from control GO to N-rGO with the highest reduction degree. The steady rise of I_D/I_G values strongly reflects that defects were created in the reduced samples due to the removal of oxygen groups and doping of nitrogen atoms during the reduction of GO using hydrazine.[39,41,42] This finding shows that the amount of defect sites present in the N-rGO precursors of different reduction degrees can be effectively controlled via the amount of hydrazine and reaction time used.

2.2. Chemical Functionalization of N-rGO via the Thermal Thiol-ene Click Reaction. In the second step, we performed further chemical functionalization on N-doped GO and N-rGO with different levels of reduction using amino-terminated thiol (cysteamine) via thiol-ene click chemistry to demonstrate the synthesis of graphene with a broad range of multifunctionalities, which includes doped nitrogen, oxygen, amino, and sulfur functional groups. A series of characterization methods were used again including XPS, XRD, FTIR, TGA−DTA, and Raman analyses to confirm the structural and chemical composition changes.

The XPS survey spectra of click-chemistry cysteamine-functionalized N-rGOs (cyst-N-rGO) are shown in Figure 4A, and the corresponding peaks of C 1s, O 1s, N 1s, and S 2p located at ∼285, ∼400, and ∼164 eV, respectively (Figure 4B−D), clearly indicate the successful incorporation of new nitrogen and sulfur species into the rGO framework. The atomic concentrations of all the cysteamine-functionalized N-GO and N-rGOs are tabulated in Table S3, and the elemental ratios of C/O, C/N, and C/S were also calculated to determine the chemical composition of cys-N-rGOs after the covalent attachment of cysteamine, which are depicted in Figure 4B−D. These figures and ratio numbers indicate that the C/O ratio of cys-N-rGOs increases when compared to that of their respective N-rGO intermediates. It should be noted that the C/O atomic ratio of cys-N-rGOs was found to be in the range of 3.50−6.17 compared to 2.21−3.80 for N-rGOs, revealing that a further reduction event had occurred with more oxygen atoms being removed in the treatment using cysteamine, indicating the role of cysteamine both as covalently attaching molecules and as an additional reducing agent in this thiol-ene click chemical reaction. Meanwhile, a substantial drop of the C/N atomic ratio is observed in cys-N-rGOs (Figure 4C) when compared to their respective N-rGO precursors (Figure 1F) visibly indicating that cysteamine is adding more nitrogen into the graphene network by having amino groups on their ends. It is important to mention that the C atomic percentage of functionalized cys-N-rGO increases (Table S3) when compared to that of its respective N-rGO precursors (Table S2), signifying the effective functionalization of N-rGOs and attachment of new cysteamine molecules since each cysteamine molecule has two C atoms, which enhanced the total amount of C. An interesting trend showed that cysteamine modification tends to attach more nitrogen per carbon atom onto N-GO compared with N-rGO. An increasing C/S atomic ratio was observed for cys-N-GO (2.62 at %S) and cys-N-rGO with low (2.45 at %S) and mild (2.28 at %S) reduction levels, implying that a slightly greater amount of sulfur per carbon atom was grafted into the graphene network. Interestingly, high cys-N-rGO with N-rGO of the highest reduction degree exhibited the lowest amount of sulfur being anchored. The significant trend found in the C/N and C/S ratios of cys-N-GO and cys-N-rGOs could be related to the presence of oxygen functionalities on the GO surface, which may imply the presence and the role of oxygen groups as activation agents of C═C in the thiol-ene click reaction, as also highlighted by Luong et al.[6]

The peak deconvolution studies of the C 1s profile for cys-N-rGOs are displayed in Figure 5A−D. A significant decrease

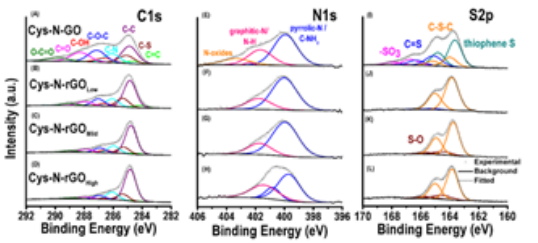

Figure 5. Plots of deconvoluted high-resolution (A−D) C 1s, (E−H) N 1s, and (I−L) S 2p peaks of cys-N-GO and cys-N-rGOs formed from their corresponding N-rGO precursors at different reduction levels.

of the C═C signal (284 eV) was observed for all cys-N-rGOs relative to their respective N-rGO precursors (Figure S6, Supporting Information), suggesting that C═C species were prominently involved in the functionalization using cysteamine. On the other hand, a substantial decline in the C−O−C (287 eV) peak was also noticed for cys-N-GO and mild and low cys-N-rGOs in contrast to their respective N-rGO precursors. The cysteamine-directed reduction events, i.e., hydrogenation and oxygen removal on these carbon species, could be greatly responsible for the diminished signals.[43] The dramatic decline of the C−O−C peak could be linked to the reduction process, whereas the obvious fall trend observed for the C═C bond can be associated with the thiol-ene reaction, which targeted the sp^2 C on the graphene network to click the −SH group on the cysteamine molecule via the thermal thiol-ene click reaction. Remarkably, the C−S species (285 eV) was detected in all the spectra of cys-N-rGOs. The formation of C−S species in all cys-N-rGOs can be prominently attributed to the successful anchoring of cysteamine onto the graphene oxide surface via the thermal thiol-ene click reaction. Apparently, the results showed that both the reduction and modification processes occurred simultaneously. This discovery divulges and confirms the synergistic role of cysteamine not only as an effective functionalization agent but also as a reducing agent, which was evident in our studies and has been supported in the literature.[43]

From the N 1s deconvolution analysis, two major N 1s peak components at around 399.8−401.2 and 401.1−402.7 eV (Figure 5E−H), which could be assigned to pyrrolic and graphitic N, respectively, were detected in all of the cys-N-rGO derivatives. Simultaneously, the binding energies positioned at around 399 and 401 eV are also known to be attributed to C−NH_2 and N−H bonds (N connected to a single C), respectively, which could contribute to the same peaks as found in the high-resolution N 1s spectra of all cys-N-rGOs.[24,44−46] The presence of C−NH_2 and N−H in all final products revealed that cysteamine molecules have been

DOI: 10.1021/acsomega.9b02642
ACS Omega 2019, 4, 19787−19798

successfully clicked on their respective N-rGOs via the thiol-ene click reaction, as verified in the previous analyses. For cys-N-GO, an additional peak at 403.4 eV due to the formation of oxide-N species on top of the pyrrolic and quaternary N was also identified in its N 1s narrow spectrum (Figure 5E).[46] On the other hand, only two dominant peaks, corresponding to pyrrolic (399.8−401.2 eV) and graphitic (401.1−402.7 eV) nitrogen, were observed for the rest of the cys-N-rGO samples.[24] Further quantification details for the N1 scan can be found in Table S4, Supporting Information. It should be highlighted that pyridinic N, which was initially present after hydrazine treatment, disappeared in all of the derivatives after the cysteamine functionalization. Despite the low amount of pyridinic N present initially after the N-doping process, the diminished pyridinic N could also be linked to the favorable degradation of this N species in the form of NH_3 after recombination with NH_2 through the diffusion during the cysteamine functionalization.[47] It has been reported that the control of the type of N species formed in the doped graphene network plays a very important role in affecting the electrochemical behavior of supercapacitors.[48,49] From the previous studies, pyrrolic N is found to increase the wettability of graphene in aqueous electrolytes besides its enhanced contribution to pseudocapacitance. Quaternary N can give rise to better electron transfer by decreasing the intrinsic resistance of carbon, particularly at high current loads, which affects the energy storage performance of supercapacitors.[11,49] In the presence of a lone pair of electrons and higher electronegativity (relative to carbon) exhibited by nitrogen, the doped N can unreservedly play its roles as the Lewis basic sites to enhance the charge transfer, which aids in disrupting the chemically inert graphene network in terms of its electronic properties.[42] Moreover, the doped N can also act as an electron pair donor to form a metal complex with heavy metals for water purification applications.[19] Therefore, the development of the cys-N-rGOs with controlled content and tailorable N species, as described in this contribution, is important to provide insights into the material design for applications with a specific interest.

The peak deconvolution analysis of S 2p for cys-N-rGOs was performed by fitting the S 2p doublet ($2p_{3/2}$ and $2p_{1/2}$) at a peak area ratio of 2:1 with 1.2 eV of spin−orbit splitting between these two doublet peaks, and the results are depicted in Figure 5I−L. In general, all cys-N-rGOs displayed similar peak profiles, except for N-GO, which exhibited an extra shoulder in the contour with the presence of a variety of S species including thioether S, C−S−C, (164.0 eV), thiophene S (163.6 eV), thioketone C═S (165.1 eV), and SO_3 (166.7 eV), as shown in Figure 5I.[50−52] For cys-N-rGO with low reduction level, only sulfur species of C−S−C and C═S were found, whereas C−S−C and S−O species were discovered in the rest of the cys-N-rGOs, as demonstrated in Figure 5I−L. One of the most apparent findings from this high-resolution S 2p deconvolution analysis is the detection of C−S−C species in all of the cys-N-rGOs, as evidenced by its corresponding doublet (S $2p_{3/2}$ at ∼163.9 eV and S $2p_{1/2}$ at ∼165 eV).[52] The quantification details of each S species are included in Table S5, Supporting Information. The formation of C−S−C species on the surface of the final products strongly proves the successful event of clicking −SH species from the cysteamine molecule on the N-rGO precursors via the surface-functionalized thermal thiol-ene click reaction.[52] Given the chemical structure of cysteamine as $HS-CH_2CH_2-NH_2$, the detection of the C−S−C peak on all cys-N-rGOs clearly revealed that the cysteamine molecules are neither physically attached nor chemically bonded via amino groups but covalently bonded through the active functional group (−SH) to the rGO surface via the thermal thiol-ene click reaction, as proposed in this work. Our results also indicate that the fixed GO/cysteamine ratio used in this study is the main factor to determine the amount of S being grafted onto the surface of graphene, with the reduction degree threshold at the ratio of hydrazine/GO = 0.15 for 24 h reduction time. Moreover, owing to the lone pair of electrons possessed by sulfur, the sulfur-rich graphene composites including cys-N-GOs prepared herein can also act as an additional functional group providing an electron pair to form coordinate bonds that can be used for many applications such as the binding of the heavy metals (electron pair acceptor) for remediation of contaminants in the environment.[19,53] As reported in the literature, the variation of chemical states of sulfur specifically related to the oxidized sulfur species incorporated into the carbon network plays significant roles in modulating the surface chemistry for designing high-performance capacitors.[48,54] In our present study, it can be clearly observed that a combination of different S environments existing in a tunable amount was created when GO with different reduction degrees was subjected to the thiol-ene click reaction. This is an important finding and a new strategy for the design of graphene materials with properties of both graphene and GO with a specific combination of chemical elements and functionalities required for catalysis, environmental remediation, and energy storage applications.

Based on the XPS analysis of high-resolution peaks of C 1s, N 1s, and S 2p and literature data, the chemical functionalities of the obtained cys-N-rGO derivatives are identified and schematically presented in Figure 6. It could be seen that by attaching the amino-terminated thiol molecules on N-doped rGO via thiol-ene click chemistry, it is possible to create a more complex multifunctionality on graphene with additional amino and sulfur functional groups. To further confirm the presence of nitrogen, oxygen, and sulfur functional groups in the prepared cys-N-rGO derivatives, further analyses using Raman, FTIR, TGA−DTA, and XRD techniques were performed, with their results summarized in Figures 7 and S7.

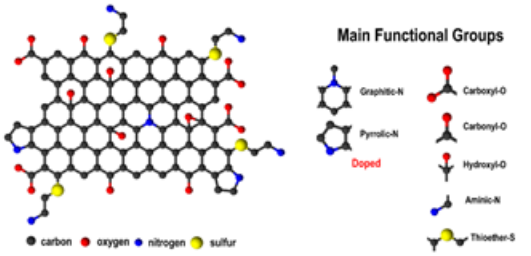

Figure 6. Proposed general chemical structure with main functional groups detected on the multifunctional derivative, cys-N-rGO, formed from the N-rGO precursor.

The presence of functional groups in cys-N-rGOs was investigated using FTIR analysis, and the results are displayed in Figure 7A. The first transmittance signal we can locate in the spectra is the −OH group stretching vibrations at ∼3400 cm^{-1} where this peak can also be found in GO, N-GO, and low and mild N-rGO precursors (Figure 3C). Among all of the cys-N-

DOI: 10.1021/acsomega.9b02642
ACS Omega 2019, 4, 19787−19798

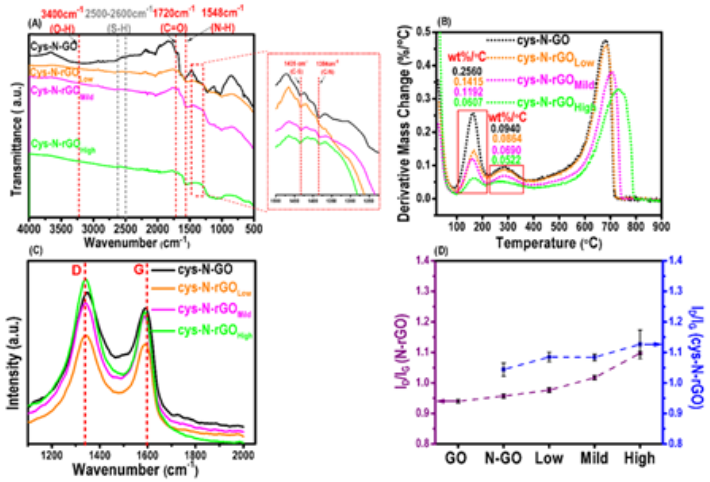

Figure 7. Plots of (A) FTIR, (B) DTA, and (C) Raman analyses and (D) I_D/I_G ratio for cys-N-GO and cys-N-rGOs formed from their corresponding N-GO and N-rGO precursors at different reduction levels.

rGOs synthesized, this specific −OH moiety was observed only in the spectrum of cys-N-GO, implying that some hydroxyl groups that are originally present in its respective N-GO precursor (Figure 3C) still remained intact in the cys-N-GO network after cysteamine functionalization. From the FTIR analysis, it can be observed that the chemical reduction by cysteamine via the removal of the O−H group is incomplete for cys-N-GO, whereas it is complete for the rest of the cys-N-rGOs. This discovery is in good correlation with the XRD result of all cys-N-rGOs discussed in Figure S7A, Supporting Information. Furthermore for all of the cys-N-rGOs studied, the appearance of a new peak near 1435 cm^{-1} (enlarged Figure 7A), which can be attributed to C−S vibrations, was also detected.[55] A detailed inspection of the two peaks positioned at 1384 and 1548 cm^{-1} (enlarged Figure 7A), which can be attributed to the stretching vibrations of C−N and N−H, respectively, was also identified.[56−58] It is essential to note that all the peaks corresponding to N−H, C−N, and S−H vibrations were not detected in the FTIR spectra of their respective N-rGO precursors. Moreover, no absorption associated with the stretching vibration of the S−H group, commonly recorded between 2500 and 2600 cm^{-1} was observed, signifying the breaking of the S−H bond in cysteamine to covalently attach on the reduced graphene sheets via thiol-ene click functionalization.[59,60] Coupled with the strong evidence from these observations, we can infer the successful grafting of the cysteamine functional groups onto the graphene framework via the thermal thiol-ene click reaction, which converted the N-GO and N-rGO precursors to cys-N-GO and cys-N-rGOs, respectively.

The TGA−DTA graphs of all cys-N-GO and cys-N-rGOs (Figures S7B and 7B) show a stepwise decreasing trend at approximately 200 °C in which this pattern is very similar to that of their respective N-rGO precursor thermograms (Figure 3D). The percentage mass loss for all cys-N-rGOs in this temperature range is significantly lower compared to that of their respective N-rGO precursors, which implies that the amount of the oxygen moiety in cys-N-rGOs is lesser compared to that in their respective N-rGO precursors. Cysteamine was proven, with its reducing ability, to carry out reduction by removing the labile oxygen functional group, which could explain this result of mass loss observed at approximately 200 °C. The thermograms of cys-N-rGOs also demonstrated a final steep mass loss starting at around 600−700 °C in which this could be linked to the pyrolysis of the more stable and labile oxygen-containing residuals attached to the skeleton of carbon atoms. It was observed that the final mass loss for most of the cys-N-rGOs (Figure 7B) produced was slightly shifted to a higher temperature compared to that of their respective N-rGO precursors (Figure 3D). This implies that higher thermal stability can be attained for the end product, cys-N-rGOs, in contrast to their respective N-rGO precursors, which can be explained by a higher reduction rate induced by additional reduction by cysteamine. The appearance of a weak shoulder at around 250 °C for all cys-N-rGOs (Figure 7B) and its absence in the thermograms of their respective N-rGO precursors (Figure 3D) further confirm that the N-rGO precursors have been successfully modified with cysteamine. This weak signal can be highly correlated to the detachment of cysteamine from cys-N-rGOs, which evidently suggests the successful incorporation of cysteamine into cys-N-rGOs sheets. This finding is also consistent with our previous study showing cysteamine can also be anchored onto graphene oxide via a one-pot modification approach.[19]

The structural features and defects formed in the end product, cys-N-rGOs, investigated using Raman spectroscopy (Figure 7C) with two intense characteristic bands (D band at 1342 cm^{-1} and G band at 1589 cm^{-1}), were identified. The intensity ratios of the D and G bands (I_D/I_G) for all cys-N-rGOs were calculated and compared with those of their respective N-rGOs demonstrated in Figure 7D. In comparison to all N-rGO precursors, it can be seen that all cys-N-rGOs exhibit higher I_D/I_G values. This observation revealed that more defects were being created in cys-N-rGOs after the modification using cysteamine. Additionally, the amount of defect sites generated in cys-N-rGOs is highly dependent on the reduction degree of N-rGO precursors used, as manifested by the enhanced I_D/I_G ratio after cysteamine-directed modification. In short, the higher the reduction degree of the N-rGO precursor used, the more defect sites eventually created

DOI: 10.1021/acsomega.9b02642
ACS Omega 2019, 4, 19787−19798

in the end product, cys-N-rGOs, which is an indication of successful anchoring of cysteamine on the surface of the N-rGO precursor.

3. CONCLUSIONS

In summary, we have demonstrated a simple modification approach of graphene materials that combines chemical doping and functionalization, which is able to control their chemical composition and level of multiple functional groups with O, N, and S elements. The synthesis of a broad range of graphene precursors (N-rGO) with different functionalities was performed by simultaneous nitrogen doping and gradual chemical reduction of GO using ammonia and hydrazine, followed by covalent attachment of amino-terminated thiol molecules (cysteamine) using the thiol-ene click reaction. Controllable modulation of the chemical multifunctionality of synthesized cys-N-doped rGO (cys-N-rGO) derivatives with different levels of oxygen groups (carboxyl, hydroxyl, and carbonyl) and different ratios of mixed functional groups including N (pyrrolic N, quaternary N, and aminic N) and S (thioether S, thiophene S, and S oxides) is confirmed by comprehensive characterization techniques including UV−vis, FTIR, Raman, XRD, TGA−DTA, and XPS analyses. Thorough XPS analysis showed the introduction of doped binary nitrogen- and sulfur-containing groups, in particular of pyrrolic N and quaternary N as well as thioether S and thiophenic S, whose level can be controlled by modulating the reduction degree of GO prior to modification using cysteamine. In addition, the XPS analysis also confirmed the disappearance of unstable pyridinic N after cysteamine modification, which unveils the protocol for the future design of N-doped graphene derivatives, in particular for oxygen reduction catalysts. This study provides mechanistic insights into the role of reduction degree of GO to be used as a synthetic platform combined with other functionalization methods such as click chemistry to create graphene materials with complex chemical multifunctionality and desirable interfacial properties such as doping level needed for a wide range of polymer composites, sensors, environmental, catalysis, and energy storage applications.

4. EXPERIMENTAL SECTION

4.1. Materials. Natural graphite rocks were obtained from a local mining site (Uley, Eyre Peninsula, South Australia, Australia), crushed into powder using a benchtop ring mill (Rocklabs), and sifted using a 25 μm sieve. Potassium permanganate (Sigma-Aldrich), 85% w/w phosphoric acid (Chem-Supply), 98% sulfuric acid (Chem-Supply), 30% hydrogen peroxide (Chem-Supply), 36% hydrochloric acid (Chem-Supply), 64−65% hydrazine monohydrate (Sigma-Aldrich), 30% ammonia (Chem-Supply), cysteamine hydrochloride (Sigma-Aldrich), *N*,*N*-dimethylforamide (DMF, Chem-Supply), 2,2-azobis-2-methylpropionitrile (AIBN, Sigma-Aldrich), hexane (Chem-Supply), ethyl acetate (Chem-Supply), and ethanol (Chem-Supply) were used directly without prior purification.

4.2. Preparation of Graphene Oxide (GO). GO was synthesized by the oxidation of graphite according to improved Hummer's method.[16] Briefly, sieved graphite powder (≤25 μm, 3.0 g) was added to a round-bottom flask containing $KMnO_4$ (18.0 g). The acid mixture (9:1 H_2SO_4/H_3PO_4) was cooled to 4 °C and slowly poured onto the graphite powder in the presence of $KMnO_4$ and stirred at room temperature before heating (60 °C, 16 h) to form a thick paste. The formed paste was cooled to room temperature; poured onto ice cubes in the presence of hydrogen peroxide (3 mL); washed with distilled water and 30% hydrochloric acid, followed by distilled water and ethanol. The product was centrifuged at 4200 rpm for each successive wash. The obtained GO was dispersed in ethanol and freeze-dried to give a brown product.[17]

4.3. Preparation of N-Doped Reduced Graphene Oxide (N-rGO). A series of N-rGO samples with several reduction degrees were prepared by the reduction of GO according to reported methodology by Morimoto et al.[18] Prepared GO (400 mg) was dispersed in distilled water (2 mg mL^{-1}) in a glass reaction flask. Hydrazine monohydrate (32, 6030, and 120 μL) was added into separate reaction flasks containing GO dispersion. The mixtures were sonicated (10 min), ammonia (80 μL) was added, and the mixtures were heated with magnetic stirring (90 °C, 2 h). N-GO was prepared as a control without hydrazine monohydrate. Subsequently, the as-formed products were cooled to room temperature, washed several times with distilled water and ethanol, and dried (40 °C, 24 h) prior to characterizations.

4.4. Synthesis of Cysteamine-Functionalized N-GO and N-rGO (cys-N-GO and cys-N-rGO). Cysteamine-functionalized N-rGO (cys-N-rGO) was prepared as previously described in our work with some modifications.[19] N-rGO (100 mg) was added to DMF (50 mL), sonicated (30 min) to obtain a homogeneous dispersion, and purged with N_2 gas (30 min) to create an inert environment. The cysteamine reaction mixture consisting of AIBN (200 μL), cysteamine hydrochloride (200 mg), and DMF (100 mL) was sonicated (30 min) and added into the N-rGO dispersion. The dispersion was purged with N_2 gas for further 30 min and transferred into a round-bottom flask, which was sealed and heated (70 °C, 12 h) in a silicon oil bath. Similarly, N-GO was treated with the cysteamine reaction mixture to produce cys-N-GO. The resulting product was cooled to room temperature and washed with a mixture of 1:1 hexane/ethyl acetate, followed by ethanol and distilled water. The product was then freeze-dried and characterized to obtain the corresponding cysteamine-functionalized derivatives.

4.5. Characterizations. Prepared GO, N-GO, N-rGO, cys-N-GO, and cys-N-rGO were characterized using several techniques including UV−visible absorbance (UV−vis), Fourier transform infrared (FTIR) spectroscopy, Raman spectroscopy, thermogravimetric analysis (TGA), and X-ray photoelectron spectroscopy (XPS). Scanning electron microscopy (SEM) (Quanta 450 FEG, FEI) at an operating voltage of 10 kV and transmission electron microscopy (TEM) (Tecnai G2 Spirit) at an operating voltage of 100 kV were used to characterize the morphology of the GO. UV−vis analysis was conducted using a Shimadzu UV−vis spectrometer (UV-1601) in the range of 200−800 cm^{-1} to probe the reduction degree of the samples prepared. All of the samples were diluted in ethanol prior to measurements at room temperature, with at least three independent runs of reproducible results obtained for each sample. FTIR spectroscopy (Nicolet 6700, Thermo Fisher) in the range of 500−4000 cm^{-1} was carried out under attenuated total reflection (ATR) mode to identify the functional groups in the materials. Raman spectroscopy (LabRAM HR Evolution, Horiba Jvon Yvon Technology, Japan) with a 532 nm laser (mpc 3000) as the excitation source was used to determine the vibrational properties of the materials. All of the spectra were recorded with an integration

DOI: 10.1021/acsomega.9b02642
ACS Omega 2019, 4, 19787−19798

time of 10 s, each on three different spots. An X-ray diffractometer (600 Miniflex, Rigaku, Japan) equipped with a Cu X-ray tube was used for analysis on GO, N-doped and cysteamine-functionalized materials to unveil the composition of the materials in the range of 2θ = 5−80° at 40 kV and 15 mA with a 10° min^{-1} scan speed. The thermal stabilities, reduction degrees, and functionalization levels of the materials were investigated using TGA (Q500, TA Instruments) under a nitrogen atmosphere with the samples heated to 900 °C at a heating rate of 10 °C min^{-1}. The elemental compositions and chemical states of the materials were determined using XPS [AXIS Ultra_DLD (Kratos, U.K.) equipped with a monochromatic Al Kα radiation source ($h\nu$ = 1486.7 eV)] at 225 W, 15 kV, and 15 mA. XPS wide scans were acquired at 0.5 eV step size over 10−1100 eV at the pass energy of 160 eV, whereas the narrow scans were obtained at a 0.1 eV step size and pass energy of 20 eV. The deconvolution and fitting of peaks were performed using Casa XPS software. All of the core-level spectra involved in this work were calibrated to the primary peak (C−C/C−H peak) of the adventitious carbon at 285 eV; the relative sensitivity factor (RSF) values were set at 0.278 for C 1s, 0.668 for S 2p, 1.8 for N 1s, and 2.93 for O 1s. Meanwhile, the components in C 1s were deconvoluted by referencing to the adventitious carbon (C−C peak), with their respective fwhm confined between 1 and 1.2 eV; a constraint was also imposed on the position of the C 1s components relative to the adventitious carbon (C−C peak), and the area of the satellite peak was restricted to 0.069634 relative to the C═C peak.

■ ASSOCIATED CONTENT

Supporting Information

The Supporting Information is available free of charge on the ACS Publications website at DOI: 10.1021/acsomega.9b02642.

Synthesis conditions for N-doped and cysteamine-functionalized derivatives; high-resolution XPS O 1s scans for GO, N-GO, and N-rGOs; normalized atomic percentages of C, O, and N for GO, N-GO, and N-rGOs; high-resolution XPS deconvoluted C 1s and O 1s peaks for GO; high-resolution XPS deconvoluted O 1s peaks for N-GO and N-rGOs; photographs of GO, N-GO, and N-rGO with varied reduction degrees dispersed in ethanol; TGA plots of GO, N-GO, and N-rGO precursors; normalized atomic percentages of C, O, and N for cys-N-GO and cys-N-rGOs; plots of relative contributions of C 1s C═C and C−O−C components for N-GO, N-rGOs, cys-N-GO, and cys-N-rGOs; relative surface concentrations of nitrogen and sulfur species of cys-N-rGOs; XRD patterns of cys-N-GO and cys-N-rGOs; and TGA plots of cys-N-GO and cys-N-rGOs (PDF)

■ AUTHOR INFORMATION

Corresponding Author

*E-mail: dusan.losic@adelaide.edu.au.

ORCID

Diana N. H. Tran: 0000-0002-4023-3373

Dusan Losic: 0000-0002-1930-072X

Author Contributions

The manuscript was written through contributions of all authors. All authors have given approval to the final version of the manuscript.

Notes

The authors declare no competing financial interest.

■ ACKNOWLEDGMENTS

The authors acknowledge the funding by the ARC Research Hub for Graphene Enabled Industry Transformation (IH150100003). We thank Dr Nathan Stanley for the drawing of the chemical structure, Australian Microscopy and Microanalysis Research Facility (AMMRF) for XPS analysis, and Adelaide Microscopy for the access of SEM and TEM facilities.

■ ABBREVIATIONS

GO,graphene oxide; N-GO,nitrogen-doped graphene oxide; N-rGO,nitrogen-doped reduced graphene oxide; cys-N-rGO,-cysteamine-functionalized nitrogen-doped reduced graphene oxide; H_2SO_4,sulfuric acid; H_3PO_4,phosphoric acid; H_2O_2,hydrogen peroxide; HCl,hydrochloric acid; C_2H_7NS,cysteamine; DMF,*N*,*N*-dimethylforamide; TEM,-transmission electron microscopy; SEM,scanning electron microscopy; FTIR,Fourier transform infrared spectroscopy; TGA,thermogravimetric analysis; DTA,derivative thermogravimetric analysis; XRD,X-ray diffraction; XPS,X-ray photoelectron spectroscopy; UV−vis,UV−visible spectroscopy; I_D/I_G,intensity ratio of D and G bands; C/O,carbon-to-oxygen atomic ratio; C/N,carbon-to-nitrogen atomic ratio; C/S,carbon-to-sulfur atomic ratio; C,carbon; O,oxygen; S,sulfur; N,nitrogen; OH,hydroxyl; CH(O)CH,epoxy; COOH,carboxyl; C═O,carbonyl; COOR,ester; C−O−C,epoxide; C−S−C,thioether; C═S,thioketone; SO_3,sulfur trioxide

■ REFERENCES

(1) Mohan, V. B.; Lau, K.-T.; Hui, D.; Bhattacharyya, D. Graphene-Based Materials and Their Composites: A Review on Production, Applications and Product Limitations. *Composites, Part B* **2018**, *142*, 200−220.

(2) Georgakilas, V.; Otyepka, M.; Bourlinos, A. B.; Chandra, V.; Kim, N.; Kemp, K. C.; Hobza, P.; Zboril, R.; Kim, K. S. Functionalization of Graphene: Covalent and Non-Covalent Approaches, Derivatives and Applications. *Chem. Rev.* **2012**, *112*, 6156−6214.

(3) Hirsch, A.; Englert, J. M.; Hauke, F. Wet Chemical Functionalization of Graphene. *Acc. Chem. Res.* **2013**, *46*, 87−96.

(4) Salavagione, H. J. Promising Alternative Routes for Graphene Production and Functionalization. *J. Mater. Chem. A* **2014**, *2*, 7138−7146.

(5) Lowe, A. B. Thiol-ene "click" reactions and recent applications in polymer and materials synthesis: a first update. *Polym. Chem.* **2014**, *5*, 4820−4870.

(6) Luong, N. D.; Sinh, L. H.; Johansson, L. S.; Campell, J.; Seppälä, J. Functional Graphene by Thiol-ene Click Chemistry. *Chem. - Eur. J.* **2015**, *21*, 3183−3186.

(7) Hwang, J. O.; Park, J. S.; Choi, D. S.; Kim, J. Y.; Lee, S. H.; Lee, K. E.; Kim, Y.-H.; Song, M. H.; Yoo, S.; Kim, S. O. Workfunction-Tunable, N-Doped Reduced Graphene Transparent Electrodes for High-Performance Polymer Light-Emitting Diodes. *ACS Nano* **2012**, *6*, 159−167.

(8) Xu, X.; Liu, C.; Sun, Z.; Cao, T.; Zhang, Z.; Wang, E.; Liu, Z.; Liu, K. Interfacial Engineering in Graphene Bandgap. *Chem. Soc. Rev.* **2018**, *47*, 3059−3099.

(9) Son, J.; Lee, S.; Kim, S. J.; Park, B. C.; Lee, H.-K.; Kim, S.; Kim, J. H.; Hong, B. H.; Hong, J. Hydrogenated Monolayer Graphene with

DOI: 10.1021/acsomega.9b02642
ACS Omega 2019, 4, 19787−19798

Reversible and Tunable Wide Band Gap and Its Field-Effect Transistor. *Nat. Commun.* **2016**, *7*, No. 13261.
(10) Qiu, Y.; Huo, J.; Jia, F.; Shanks, B. H.; Li, W. N- and S-Doped Mesoporous Carbon as Metal-Free Cathode Catalysts for Direct Biorenewable Alcohol Fuel Cells. *J. Mater. Chem. A* **2016**, *4*, 83−95.
(11) Wang, T.; Wang, L.-X.; Wu, D.-L.; Xia, W.; Jia, D.-Z. Interaction between Nitrogen and Sulfur in Co-Doped Graphene and Synergetic Effect in Supercapacitor. *Sci. Rep.* **2015**, *5*, No. 9591.
(12) Park, S.; Hu, Y.; Hwang, J. O.; Lee, E.-S.; Casabianca, L. B.; Cai, W.; Potts, J. R.; Ha, H.-W.; Chen, S.; Oh, J.; Kim, S. O.; Kim, Y.-H.; Ishii, Y.; Ruoff, R. S. Chemical Structures of Hydrazine-Treated Graphene Oxide and Generation of Aromatic Nitrogen Doping. *Nat. Commun.* **2012**, *3*, No. 638.
(13) Rivera, L. M.; Fajardo, S.; Arévalo, M. D. C.; García, G.; Pastor, E. S- and N-Doped Graphene Nanomaterials for the Oxygen Reduction Reaction. *Catalysts* **2017**, *7*, 278.
(14) Amiinu, I. S.; Zhang, J.; Kou, Z.; Liu, X.; Asare, O. K.; Zhou, H.; Cheng, K.; Zhang, H.; Mai, L.; Pan, M.; Mu, S. Self-Organized 3D Porous Graphene Dual-Doped with Biomass-Sponsored Nitrogen and Sulfur for Oxygen Reduction and Evolution. *ACS Appl. Mater. Interfaces* **2016**, *8*, 29408−29418.
(15) Shi, J.; Wang, Y.; Su, Q.; Cheng, F.; Kong, X.; Lin, J.; Zhu, T.; Liang, S.; Pan, A. N-S Co-Doped C@SnS Nanoflakes/Graphene Composite as Advanced Anode for Sodium-Ion Batteries. *Chem. Eng. J.* **2018**, *353*, 606−614.
(16) Marcano, D. C.; Kosynkin, D. V.; Berlin, J. M.; Sinitskii, A.; Sun, Z.; Slesarev, A.; Alemany, L. B.; Lu, W.; Tour, J. M. Improved Synthesis of Graphene Oxide. *ACS Nano* **2010**, *4*, 4806−4814.
(17) Kabiri, S.; Tran, D. N. H.; Azari, S.; Losic, D. Graphene-Diatom Silica Aerogels for Efficient Removal of Mercury Ions from Water. *ACS Appl. Mater. Interfaces* **2015**, *7*, 11815−11823.
(18) Morimoto, N.; Kubo, T.; Nishina, Y. Tailoring the Oxygen Content of Graphite and Reduced Graphene Oxide for Specific Applications. *Sci. Rep.* **2016**, *6*, No. 21715.
(19) Yap, P. L.; Kabiri, S.; Tran, D. N. H.; Losic, D. Multifunctional Binding Chemistry on Modified Graphene Composite for Selective and Highly Efficient Adsorption of Mercury. *ACS Appl. Mater. Interfaces* **2019**, *11*, 6350−6362.
(20) Dreyer, D. R.; Park, S.; Bielawski, C. W.; Ruoff, R. S. The Chemistry of Graphene Oxide. *Chem. Soc. Rev.* **2010**, *39*, 228−240.
(21) Stankovich, S.; Dikin, D. A.; Piner, R. D.; Kohlhaas, K. A.; Kleinhammes, A.; Jia, Y.; Wu, Y.; Nguyen, S. T.; Ruoff, R. S. Synthesis of Graphene-Based Nanosheets via Chemical Reduction of Exfoliated Graphite Oxide. *Carbon* **2007**, *45*, 1558−1565.
(22) Pei, S.; Cheng, H.-M. The Reduction of Graphene Oxide. *Carbon* **2012**, *50*, 3210−3228.
(23) Li, D.; Müller, M. B.; Gilje, S.; Kaner, R. B.; Wallace, G. G. Processable Aqueous Dispersions of Graphene Nanosheets. *Nat. Nanotechnol.* **2008**, *3*, 101.
(24) Wang, H.; Maiyalagan, T.; Wang, X. Review on Recent Progress in Nitrogen-Doped Graphene: Synthesis, Characterization, and Its Potential Applications. *ACS Catal.* **2012**, *2*, 781−794.
(25) Shang, Y.; Zhang, D.; Liu, Y.; Guo, C. Preliminary Comparison of Different Reduction Methods of Graphene Oxide. *Bull. Mater. Sci.* **2015**, *38*, 7−12.
(26) Baskoro, F.; Wong, C.-B.; Kumar, S. R.; Chang, C.-W.; Chen, C.-H.; Chen, D. W.; Lue, S. J. Graphene Oxide-Cation Interaction: Inter-Layer Spacing and Zeta Potential Changes in Response to Various Salt Solutions. *J. Membr. Sci.* **2018**, *554*, 253−263.
(27) Li, Y.; Bao, L.; Zhou, Q.; Ou, E.; Xu, W. Functionalized Graphene Obtained via Thiol-Ene Click Reactions as an Efficient Electrochemical Sensor. *ChemistrySelect* **2017**, *2*, 9284−9290.
(28) Tadjarodi, A.; Moazen Ferdowsi, S.; Zare-Dorabei, R.; Barzin, A. Highly Efficient Ultrasonic-Assisted Removal of Hg(II) Ions on Graphene Oxide Modified with 2-Pyridinecarboxaldehyde Thiosemicarbazone: Adsorption Isotherms and Kinetics Studies. *Ultrason. Sonochem.* **2016**, *33*, 118−128.
(29) Tian, Z.; Li, J.; Zhu, G.; Lu, J.; Wang, Y.; Shi, Z.; Xu, C. Facile Synthesis of Highly Conductive Sulfur-Doped Reduced Graphene Oxide Sheets. *Phys. Chem. Chem. Phys.* **2016**, *18*, 1125−1130.
(30) Sun, W.; Wang, L.; Yang, Z.; Zhu, T.; Wu, T.; Dong, C.; Liu, G. Tuning the Oxidation Degree of Graphite toward Highly Thermally Conductive Graphite/Epoxy Composites. *Chem. Mater.* **2018**, *30*, 7473−7483.
(31) Ganguly, A.; Sharma, S.; Papakonstantinou, P.; Hamilton, J. Probing the Thermal Deoxygenation of Graphene Oxide Using High-Resolution In Situ X-ray-Based Spectroscopies. *J. Phys. Chem. C* **2011**, *115*, 17009−17019.
(32) Peng-Gang, R.; Ding-Xiang, Y.; Xu, J.; Tao, C.; Zhong-Ming, L. Temperature Dependence of Graphene Oxide Reduced by Hydrazine Hydrate. *Nanotechnology* **2011**, *22*, No. 055705.
(33) Xie, B.; Chen, Y.; Yu, M.; Shen, X.; Lei, H.; Xie, T.; Zhang, Y.; Wu, Y. Carboxyl-Assisted Synthesis of Nitrogen-Doped Graphene Sheets for Supercapacitor Applications. *Nanoscale Res. Lett.* **2015**, *10*, 332.
(34) Han, J.; Xi, B.; Feng, Z.; Ma, X.; Zhang, J.; Xiong, S.; Qian, Y. Sulfur−Hydrazine Hydrate-Based Chemical Synthesis of Sulfur@Graphene Composite for Lithium−Sulfur Batteries. *Inorg. Chem. Front.* **2018**, *5*, 785−792.
(35) Wu, N.; She, X.; Yang, D.; Wu, X.; Su, F.; Chen, Y. Synthesis of Network Reduced Graphene Oxide in Polystyrene Matrix by a Two-Step Reduction Method for Superior Conductivity of the Composite. *J. Mater. Chem.* **2012**, *22*, 17254−17261.
(36) Hou, D.; Liu, Q.; Wang, X.; Quan, Y.; Qiao, Z.; Yu, L.; Ding, S. Facile Synthesis of Graphene via Reduction of Graphene Oxide by Artemisinin in Ethanol. *J. Materiomics* **2018**, *4*, 256−265.
(37) Dave, K.; Park, K. H.; Dhayal, M. Two-Step Process for Programmable Removal of Oxygen Functionalities of Graphene Oxide: Functional, Structural and Electrical Characteristics. *RSC Adv.* **2015**, *5*, 95657−95665.
(38) Cui, X.; Fang, X.; Zhao, H.; Li, Z.; Ren, H. An Electrochemical Sensor for Dopamine Based on Polydopamine Modified Reduced Graphene Oxide Anchored with Tin Dioxide and Gold Nanoparticles. *Anal. Methods* **2017**, *9*, 5322−5332.
(39) Eda, G.; Chhowalla, M. Chemically Derived Graphene Oxide: Towards Large-Area Thin-Film Electronics and Optoelectronics. *Adv. Mater.* **2010**, *22*, 2392−2415.
(40) Ţucureanu, V.; Matei, A.; Avram, A. M. FTIR Spectroscopy for Carbon Family Study. *Crit. Rev. Anal. Chem.* **2016**, *46*, 502−520.
(41) Tran, D. N.; Kabiri, S.; Wang, L.; Losic, D. Engineered Graphene−Nanoparticle Aerogel Composites for Efficient Removal of Phosphate from Water. *J. Mater. Chem. A* **2015**, *3*, 6844−6852.
(42) Duan, X.; O'Donnell, K.; Sun, H.; Wang, Y.; Wang, S. Sulfur and Nitrogen Co-Doped Graphene for Metal-Free Catalytic Oxidation Reactions. *Small* **2015**, *11*, 3036−3044.
(43) Dutta, S.; Chatterjee, S.; Mukherjee, I.; Saha, R.; Singh, B. P. Fabrication of ZnS Hollow Spheres and RGO-ZnS Nanocomposite Using Cysteamine as Novel Sulfur Source: Photocatalytic Performance on Industrial Dyes and Effluent. *Ind. Eng. Chem. Res.* **2017**, *56*, 4768−4778.
(44) Jalani, G.; Cerruti, M. Nano Graphene Oxide-Wrapped Gold Nanostars as Ultrasensitive and Stable SERS Nanoprobes. *Nanoscale* **2015**, *7*, 9990−9997.
(45) Xu, J.; He, S.; Zhang, H.; Huang, J.; Lin, H.; Wang, X.; Long, J. Layered Metal-Organic Framework/Graphene Nanoarchitectures for Organic Photosynthesis under Visible Light. *J. Mater. Chem. A* **2015**, *3*, 24261−24271.
(46) Kondo, T.; Casolo, S.; Suzuki, T.; Shikano, T.; Sakurai, M.; Harada, Y.; Saito, M.; Oshima, M.; Trioni, M. I.; Tantardini, G. F.; Nakamura, J. Atomic-Scale Characterization of Nitrogen-Doped Graphite: Effects of Dopant Nitrogen on the Local Electronic Structure of the Surrounding Carbon Atoms. *Phys. Rev. B* **2012**, *86*, No. 035436.
(47) Naumov, O.; Naumov, S.; Abel, B.; Varga, A. The Stability Limits of Highly Active Nitrogen Doped Carbon ORR Nano-

DOI: 10.1021/acsomega.9b02642
ACS Omega 2019, 4, 19787−19798

Catalysts: A Mechanistic Study of Degradation Reactions. *Nanoscale* **2018**, *10*, 6724−6733.
(48) Zhang, D.; Zheng, L.; Ma, Y.; Lei, L.; Li, Q.; Li, Y.; Luo, H.; Feng, H.; Hao, Y. Synthesis of Nitrogen- and Sulfur-Codoped 3D Cubic-Ordered Mesoporous Carbon with Superior Performance in Supercapacitors. *ACS Appl. Mater. Interfaces* **2014**, *6*, 2657−2665.
(49) Hulicova-Jurcakova, D.; Seredych, M.; Lu, G. Q.; Bandosz, T. J. Combined Effect of Nitrogen- and Oxygen-Containing Functional Groups of Microporous Activated Carbon on its Electrochemical Performance in Supercapacitors. *Adv. Funct. Mater.* **2009**, *19*, 438−447.
(50) Wang, D. H.; Xia, X. H.; Xie, D.; Niu, X. Q.; Ge, X.; Gu, C. D.; Wang, X. L.; Tu, J. P. Rational In-Situ Construction of Three-Dimensional Reduced Graphene Oxide Supported Li_2S/C Composite as Enhanced Cathode for Rechargeable Lithium−Sulfur Batteries. *J. Power Sources* **2015**, *299*, 293−300.
(51) Wu, F.; Li, J.; Tian, Y.; Su, Y.; Wang, J.; Yang, W.; Li, N.; Chen, S.; Bao, L. 3D Coral-Like Nitrogen-Sulfur Co-Doped Carbon-Sulfur Composite for High Performance Lithium-Sulfur Batteries. *Sci. Rep.* **2015**, *5*, No. 13340.
(52) Huang, B.; Liu, Y.; Huang, X.; Xie, Z. Multiple Heteroatom-Doped Few-Layer Carbons for the Electrochemical Oxygen Reduction Reaction. *J. Mater. Chem. A* **2018**, *6*, 22277−22286.
(53) Kumar, A. S. K.; Jiang, S.-J. Preparation and Characterization of Exfoliated Graphene Oxide-L-cystine as an Effective Adsorbent of Hg (II) Adsorption. *RSC Adv.* **2015**, *5*, 6294−6304.
(54) Zhao, X.; Zhang, Q.; Chen, C.-M.; Zhang, B.; Reiche, S.; Wang, A.; Zhang, T.; Schlögl, R.; Sheng Su, D. Aromatic Sulfide, Sulfoxide, and Sulfone Mediated Mesoporous Carbon Monolith for Use in Supercapacitor. *Nano Energy* **2012**, *1*, 624−630.
(55) Awad, F. S.; AbouZeid, K. M.; El-Maaty, W. M. A.; El-Wakil, A. M.; El-Shall, M. S. Efficient Removal of Heavy Metals from Polluted Water with High Selectivity for Mercury(II) by 2-Imino-4-thiobiuret−Partially Reduced Graphene Oxide (IT-PRGO). *ACS Appl. Mater. Interfaces* **2017**, *9*, 34230−34242.
(56) Liu, J.; Zhu, K.; Jiao, T.; Xing, R.; Hong, W.; Zhang, L.; Zhang, Q.; Peng, Q. Preparation of Graphene Oxide-Polymer Composite Hydrogels via Thiol-ene Photopolymerization as Efficient Dye Adsorbents for Wastewater Treatment. *Colloids Surf., A* **2017**, *529*, 668−676.
(57) Luo, X.; Ma, K.; Jiao, T.; Xing, R.; Zhang, L.; Zhou, J.; Li, B. Graphene Oxide-Polymer Composite Langmuir Films Constructed by Interfacial Thiol-Ene Photopolymerization. *Nanoscale Res. Lett.* **2017**, *12*, 99.
(58) Tiwari, I.; Gupta, M.; Pandey, C. M.; Mishra, V. Gold Nanoparticle Decorated Graphene Sheet-Polypyrrole Based Nanocomposite: Its Synthesis, Characterization and Genosensing Application. *Dalton Trans.* **2015**, *44*, 15557−15566.
(59) Ke, J.; Li, X.; Zhao, Q.; Hou, Y.; Chen, J. Ultrasensitive Quantum Dot Fluorescence Quenching Assay for Selective Detection of Mercury Ions in Drinking Water. *Sci. Rep.* **2014**, *4*, No. 5624.
(60) Cai, Y.; Du, G.; Gao, G.; Chen, J.; Fu, J. Colour-Tunable Quantum Dots/Poly(NIPAM-co-AAc) Hybrid Microgels Based on Electrostatic Interactions. *RSC Adv.* **2016**, *6*, 98147−98152.

DOI: 10.1021/acsomega.9b02642
ACS Omega 2019, 4, 19787−19798

Supporting Information

Tuning the Multifunctional Surface Chemistry of Reduced Graphene Oxide via Combined Elemental Doping and Chemical Modifications

Pei Lay Yap[†,‡], *Shervin Kabiri*[‡,ℊ], *Yow Loo Auyoong*[§], *Diana, N.H. Tran*[†,‡] *and Dusan Losic*[*,†,‡]

[†]School of Chemical Engineering and Advanced Materials, [‡]ARC Hub for Graphene Enabled Industry Transformation, The University of Adelaide, Adelaide, SA 5005, Australia

[ℊ]School of Agriculture, Food and Wine, The University of Adelaide, PMB 1, Waite Campus, Glen Osmond, SA 5064, Australia

[§]Research & Business Partnerships, The University of Adelaide, Adelaide, SA 5000, Australia

*Corresponding author: dusan.losic@adelaide.edu.au

Table S1. Synthesis conditions of the GO, N-doped precursors and cys- functionalized N-rGO derivatives synthesized in this work.

N-precursor	GO	N-GO	N-rGO-$_{Low}$	N-rGO-$_{Mild}$	N-rGO-$_{High}$
Ammonia/GO (µL/mg)	0	0.20	0.20	0.20	0.20
Hydrazine/GO (µL/mg)	0	0	0.08	0.15	0.30
Reduction time (hrs)	2	2	2	2	24
N-precursor: cysteamine= 1:2 at 70 ˚C for 12 hours					
cys-N-rGO	-	cys-N-GO	cys-N-rGO-$_{Low}$	cys-N-rGO-$_{Mild}$	cys-N-rGO-$_{High}$

* *N-rGO= N-doped reduced graphene oxide*
* *Cys-N-rGO =cysteamine functionalized N-doped reduced graphene oxide*

Table S2. Normalized atomic percentage of C, O and N calculated from the area of the XPS survey spectra under C1s, O1s and N1s peaks respectively for GO, N-GO and N-rGOs.

N-rGO precursors		GO	N-GO	N-rGO$_{Low}$	N-rGO$_{Mild}$	N-rGO$_{High}$
At %	C	67.57	68.28	70.49	72.18	76.00
	O	31.78	30.86	27.97	25.43	20.01
	N	0.65	0.86	1.54	2.39	3.98

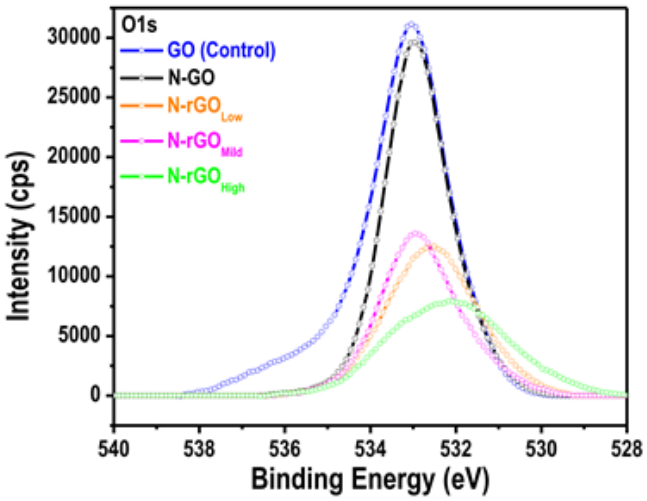

Figure S1. Plot of experimental high resolution XPS O1s scan with background subtracted for GO, N-GO and N-rGO (low, mild and high).

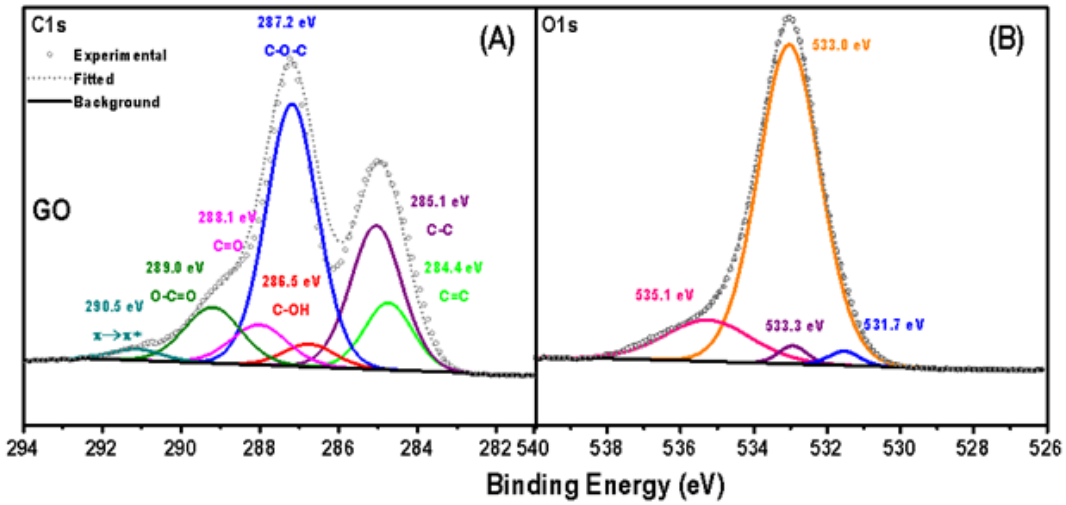

Figure S2. High resolution XPS deconvoluted (A) C1s and (B) O1s peaks for GO. The peak fitting of O1s experimental curve for GO indicates the presence of oxygen species including C=O (531.7 eV), C-O (533.0 eV), O-H (533.3 eV) and adsorbed water (535.1 eV).[1-3]

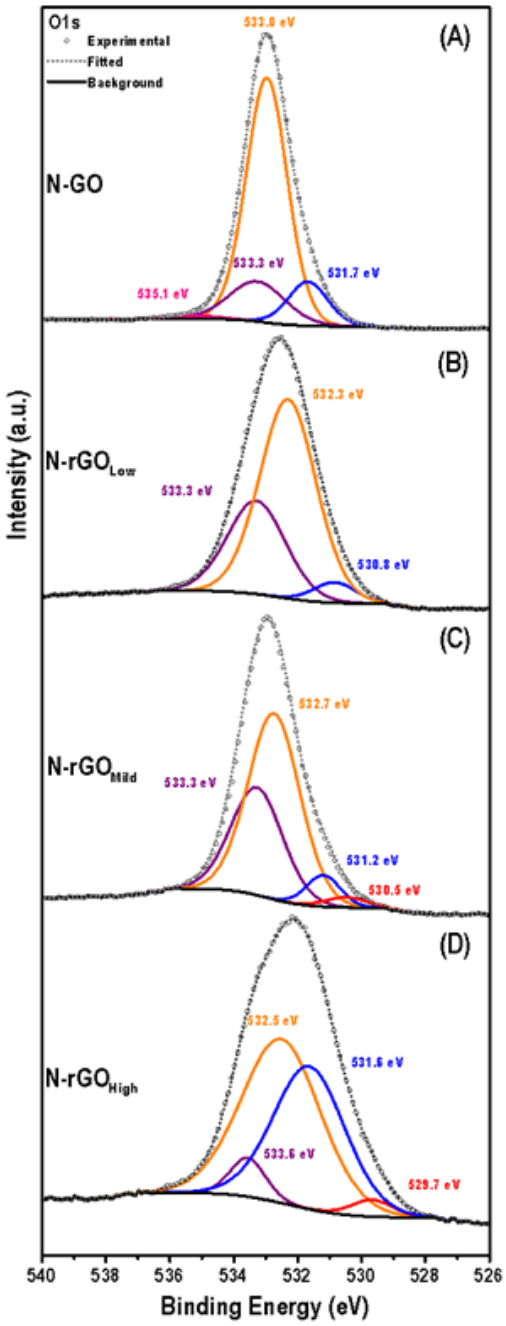

Figure S3. High resolution XPS deconvoluted O1s peaks for (A) N-GO (B) N-rGO$_{Low}$ (C) N-rGO$_{Mild}$ and (D) N-rGO$_{High}$. The deconvolution analysis of O1s region for N-GO and N-rGO shows four O components corresponding to quinone (red curve at ~530.5 eV), C=O (blue curve at 531-531.7 eV), C-O (orange curve at 532.3-533.0 eV), O-H (purple curve at 533.3-533.6 eV) and adsorbed water (pink curve 535.1 eV).[1-3]

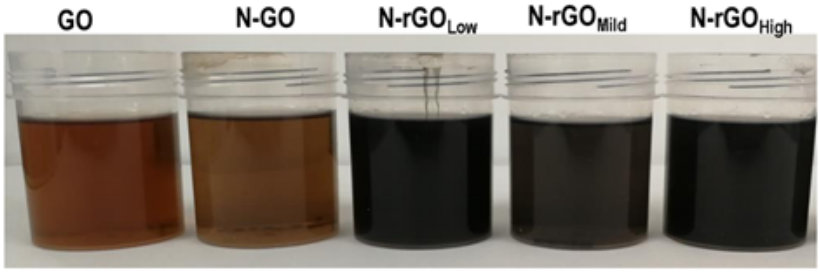

Figure S4. Photograph of GO, N-GO and N-rGOs dispersed in ethanol. Dispersions of GO and N-GO show typical yellow-brown colour. The dispersions transformed to black when GO was reduced by hydrazine, indicating the reduction event based on their dispersion visual appearance.[4]

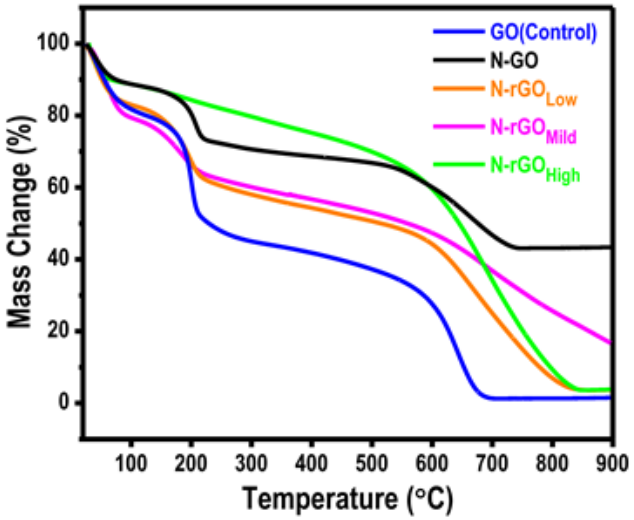

Figure S5. TGA plot of GO, N-GO and N-rGO precursors. From the TGA plot, similar to GO, the oxygen element embedded in N-rGO precursors can be eliminated in the form of water, oxygen, carbon monoxide, and carbon dioxide upon heating. Under the inert atmosphere, GO exhibits a mass loss of about 17 % at 100 °C, the boiling point of water, which can be attributed to the desorption of adsorbed water. With the raise of temperature from 150 °C to 250 °C, the mass loss of GO rose up to 33.2 %, this result was unreservedly corroborated with a gradual stepped drop in their derivative mass change at about 200 ˚C with the highest peak detected at 1.057 weight %/˚C for GO (Figure 3B). This event can be ascribed to the decomposition of labile oxygen-containing functional groups, such as hydroxyl (-OH), epoxy (-CH(O)CH-) and carboxyl (-COOH) groups between the layers of GO nanosheets. The final mass loss step of GO appearing at 640 °C (loss of 48%), involves the pyrolysis of remaining of more stable and labile oxygen-containing moieties,

including carbonyl (C=O) and ester (-COOR) groups attached to the edge of GO nanosheets and the skeleton of carbon atoms.[5, 6] For all N-rGO precursors, their first mass loss below 100 ˚C is also due to the removal of adsorbed water between their graphitic layers.[6] It is worth noting that the second and third mass loss for all N-rGOs at 150- 250 °C and 650-700 ˚C are significantly lower than GO showing removal of oxygen-containing functional group.[5]

Table S3. Normalized atomic percentage of C, O, N and S calculated from the area of the survey spectra under C1s, O1s, N1s and S2p peaks respectively for cys-N-GO and cys-N-rGOs.

cys-N-rGO derivatives		cys-N-GO	cys-N-rGO$_{Low}$	cys-N-rGO$_{Mild}$	cys-N-rGO$_{High}$
At %	C	72.71	75.36	77.46	80.09
	O	20.76	17.97	15.08	12.99
	N	3.91	4.22	5.19	5.71
	S	2.62	2.45	2.28	1.21

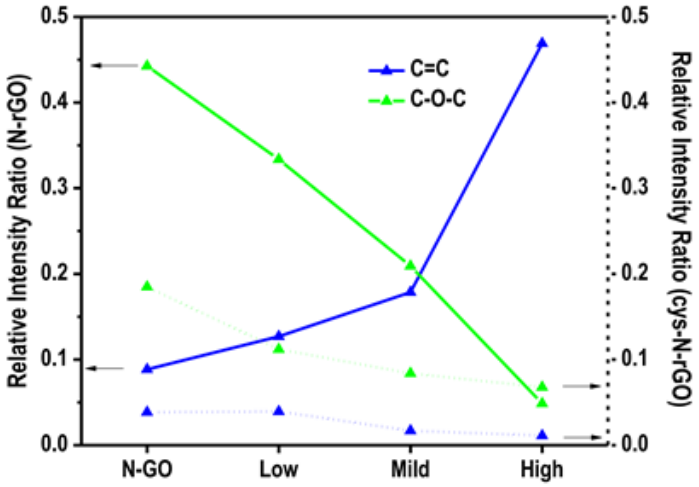

Figure S6. Plots of relative contribution of C1s C=C and C-O-C peak components estimated by dividing the area under each component by whole C1s peak-area of deconvoluted C1s peak components for cys-N-GO and cys-N-rGOs (dotted line) prepared using their respective N-GO and N-rGOs (solid line).

Table S4. Relative surface concentrations of nitrogen species by fitting the N1s core level XPS spectra as a function of reduction degree for cys-N-rGOs prepared using respective N-rGO at N-rGO: cysteamine= 1:2 at 70 ˚C for 12 hours with varied reduction degree of rGO.

Binding energy (eV)	Relative Peak Area of N1s (%)		
	399.8-401.2 Pyrrolic-N	401.1-402.7 Quaternary-N	402.8 Oxides-N
cys-N-GO	56.28	29.91	13.81
cys-N-rGO$_{Low}$	74.70	25.30	-
cys-N-rGO$_{Mild}$	76.91	23.09	-
cys-N-rGO$_{High}$	67.82	32.18	-

Table S5. Relative contribution of deconvoluted S2p peak components as a function of reduction degree for cys-N-rGO samples prepared using respective N-rGO at N-rGO: cysteamine= 1:2 at 70 ˚C for 12 hours using N-rGO with varied reduction degree.

Binding energy (eV)	Relative Peak Area of S2p (%)				
	164.0, 165.0 C-S-C	165.1, 166.3 C=S	163.6, 164.8 Thiophene S	166.7, 167.9 SO_3	164.5, 165.7 S-O
cys-N-GO	17.09	21.76	48.67	12.48	-
cys-N-rGO$_{Low}$	96.72	3.28	-	-	-
cys-N-rGO$_{Mild}$	87.33	-	-	-	12.67
cys-N-rGO$_{High}$	83.00	-	-	-	17.00

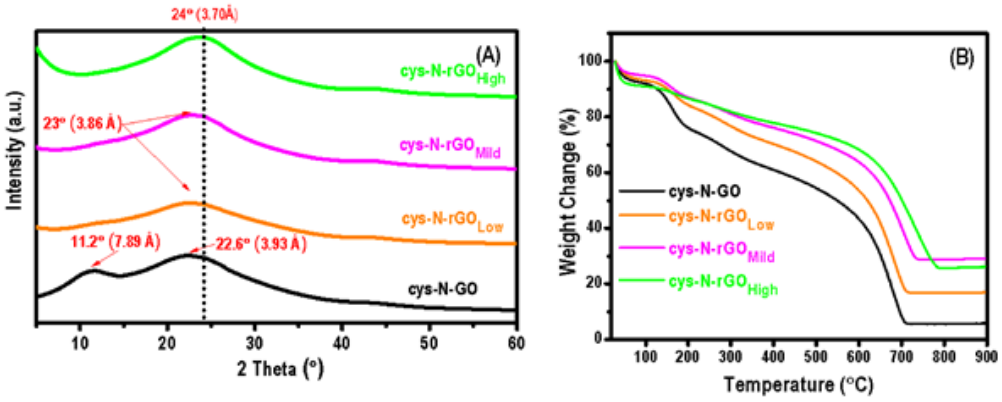

Figure S7. (A) XRD patterns of cys-N-GO and cys-N-rGOs. For cys-N-GO, it can be observed that the XRD profile has changed significantly when compared to its previous N-rGO precursor (Figure 3A). A very prominent change occurred on the cys-N-GO with two broad peaks identified at $2\theta = 11.2^{\circ}$ and 22.6° compared to only one peak found at $2\theta = 10.78^{\circ}$ as in N-GO. The change of these XRD profiles could be highly related to the removal of oxygen functional groups from the GO sheets as well as the substantial exfoliation and disruption in the interlayer structure of GO. Apparently, cysteamine demonstrates the reducing agent properties as also shown in hydrazine and it can be found that N-GO has been reduced partially by cysteamine. For low cys-N-rGO, the XRD pattern has changed from a partially reduced form to a fully reduced form (also detected in mild, and high cys-N-rGO). This again revealed the ability of cysteamine in further reducing rGO precursors in thermal thiol-ene click reaction.[7-11] (B) TGA plot of cys-N-GO and cys-N-rGO (low, mild and high).

References

1. Zhou, L.-N.; Zhang, X.-T.; Shen, W.-J.; Sun, S.-G.; Li, Y.-J., Monolayer of Close-Packed Pt Nanocrystals on a Reduced Graphene Oxide (RGO) Nanosheet and Its Enhanced Catalytic Performance Towards Methanol Electrooxidation. *RSC Adv.* **2015,** 5, (57), 46017-46025.
2. Fan, X.; Yu, C.; Yang, J.; Ling, Z.; Qiu, J., Hydrothermal Synthesis and Activation of Graphene-Incorporated Nitrogen-Rich Carbon Composite for High-Performance Supercapacitors. *Carbon* **2014,** 70, 130-141.
3. Yu, B.; Wang, X.; Qian, X.; Xing, W.; Yang, H.; Ma, L.; Lin, Y.; Jiang, S.; Song, L.; Hu, Y.; Lo, S., Functionalized Graphene Oxide/Phosphoramide Oligomer Hybrids Flame Retardant Prepared Via In Situ Polymerization For Improving the Fire Safety of Polypropylene. *RSC Adv.* **2014,** 4, (60), 31782-31794.
4. Pei, S.; Cheng, H.-M., The Reduction of Graphene Oxide. *Carbon* **2012,** 50, (9), 3210-3228.
5. Xialie, W.; Xiaohong, W.; Zhanpeng, L.; Yi, T.; Ye, Y.; Ping, Z., Rapid and Efficient Synthesis of Soluble Graphene Nanosheets Using N-Methyl-p-Aminophenol Sulfate as a Reducing Agent. *Nanotechnology* **2012,** 23, (48), 485604.
6. Peng-Gang, R.; Ding-Xiang, Y.; Xu, J.; Tao, C.; Zhong-Ming, L., Temperature Dependence of Graphene Oxide Reduced by Hydrazine Hydrate. *Nanotechnology* **2011,** 22, (5), 055705.
7. Orth, E. S.; Fonsaca, J. E. S.; Domingues, S. H.; Mehl, H.; Oliveira, M. M.; Zarbin, A. J. G., Targeted Thiolation of Graphene Oxide and its Utilization as Precursor for Graphene/Silver Nanoparticles Composites. *Carbon* **2013,** 61, 543-550.
8. Pham, V. H.; Cuong, T. V.; Hur, S. H.; Oh, E.; Kim, E. J.; Shin, E. W.; Chung, J. S., Chemical Functionalization of Graphene Sheets by Solvothermal Reduction of a Graphene Oxide Suspension in N-Methyl-2-Pyrrolidone. *J. Mater. Chem.* **2011,** 21, (10), 3371-3377.

9. Thakur, S.; Das, G.; Raul, P. K.; Karak, N., Green One-Step Approach to Prepare Sulfur/Reduced Graphene Oxide Nanohybrid for Effective Mercury Ions Removal. *J. Phys. Chem. C* **2013,** 117, (15), 7636-7642.

10. Navaee, A.; Salimi, A., Efficient Amine Functionalization of Graphene Oxide through the Bucherer Reaction: an Extraordinary Metal-Free Electrocatalyst for the Oxygen Reduction Reaction. *RSC Adv.* **2015,** 5, (74), 59874-59880.

11. Dutta, S.; Chatterjee, S.; Mukherjee, I.; Saha, R.; Singh, B. P., Fabrication of ZnS Hollow Spheres and RGO-ZnS Nanocomposite Using Cysteamine as Novel Sulfur Source: Photocatalytic Performance on Industrial Dyes and Effluent. *Ind. Eng. Chem. Res.* **2017,** 56, (16), 4768-4778.

CHAPTER 4

FUNCTIONALIZED GRAPHENE COMPOSITES THROUGH HYDROTHERMAL AND CHEMICAL REDUCTION APPROACHES FOR WATER PURIFICATION

4. FUNCTIONALIZED GRAPHENE COMPOSITES VIA HYDROTHERMAL AND CHEMICAL REDUCTION APPROACHES FOR WATER PURIFICATION

4.1. Overview and Significance of Work

Chapter 4 addresses several key issues of the commercial adsorbent (AC) including its high energy consumption for the activation process and ineffectiveness in removing heavy metals, especially mercury ions at low concentration in water. In this work, functionalized graphene composites are demonstrated using a mixed polyamine precursor (nitrogen-containing group) through hydrothermal and chemical reduction approaches. This work aims to:

- develop a low cost, low energy, environmentally friendly and scalable production method for an adsorbent, and
- design adsorbents with a fast adsorption rate, high affinity and selectivity towards removing low concentrations of mercury in water

Findings from this chapter achieved Objectives 3 and 4, which are combined in a published peer-reviewed research article.

4.2. Statement of Authorship

Statement of Authorship

Title of Paper	Polyamine-modified reduced graphene oxide: A new and cost-effective adsorbent for efficient removal of mercury in waters.
Publication Status	☒ Published ☐ Accepted for Publication ☐ Submitted for Publication ☐ Unpublished and Unsubmitted work written in manuscript style
Publication Details	Yap, P. L., Tung, T. T., Kabiri, S., Matulick, N., Tran, D. N. H., & Losic, D. (2020). Polyamine-modified reduced graphene oxide: A new and cost-effective adsorbent for efficient removal of mercury in waters. Separation and Purification Technology, 238, 116441.

Principal Author

Name of Principal Author (Candidate)	Pei Lay Yap		
Contribution to the Paper	Prepared, characterized and conducted performance testing on all the samples, interpreted data as well as wrote the manuscripts		
Overall percentage (%)	85%		
Certification:	This paper reports on original research I conducted during the period of my Higher Degree by Research candidature and is not subject to any obligations or contractual agreements with a third party that would constrain its inclusion in this thesis. I am the primary author of this paper.		
Signature		Date	01/09/20

Co-Author Contributions

By signing the Statement of Authorship, each author certifies that:

i. the candidate's stated contribution to the publication is accurate (as detailed above);
ii. permission is granted for the candidate in include the publication in the thesis; and
iii. the sum of all co-author contributions is equal to 100% less the candidate's stated contribution.

Name of Co-Author	Tran Thanh Tung		
Contribution to the Paper	Helped in sample synthesis, edited and revised the manuscript.		
Signature		Date	02/10/20

Name of Co-Author	Shervin Kabiri		
Contribution to the Paper	Edited and revised the manuscript.		
Signature		Date	02/10/20

Please cut and paste additional co-author panels here as required.

Statement of Authorship

Title of Paper	Polyamine-modified reduced graphene oxide: A new and cost-effective adsorbent for efficient removal of mercury in waters.
Publication Status	☒ Published ☐ Accepted for Publication ☐ Submitted for Publication ☐ Unpublished and Unsubmitted work written in manuscript style
Publication Details	Yap, P. L., Tung, T. T., Kabiri, S., Matulick, N., Tran, D. N. H., & Losic, D. (2020). Polyamine-modified reduced graphene oxide: A new and cost-effective adsorbent for efficient removal of mercury in waters. Separation and Purification Technology, 238, 116441.

Principal Author

Name of Principal Author (Candidate)	Pei Lay Yap		
Contribution to the Paper	Prepared, characterized and conducted performance testing on all the samples, interpreted data as well as wrote the manuscripts		
Overall percentage (%)	85%		
Certification:	This paper reports on original research I conducted during the period of my Higher Degree by Research candidature and is not subject to any obligations or contractual agreements with a third party that would constrain its inclusion in this thesis. I am the primary author of this paper.		
Signature		Date	01/09/20

Co-Author Contributions

By signing the Statement of Authorship, each author certifies that:

i. the candidate's stated contribution to the publication is accurate (as detailed above);

ii. permission is granted for the candidate in include the publication in the thesis; and

iii. the sum of all co-author contributions is equal to 100% less the candidate's stated contribution.

Name of Co-Author	Nicola Matulick		
Contribution to the Paper	Helped in synthesis.		
Signature		Date	22/09/2020

Name of Co-Author	Diana N.H. Tran		
Contribution to the Paper	Co-supervised and revised manuscript.		
Signature		Date	02/10/20

Please cut and paste additional co-author panels here as required.

Statement of Authorship

Title of Paper	Polyamine-modified reduced graphene oxide: A new and cost-effective adsorbent for efficient removal of mercury in waters.
Publication Status	☒ Published ☐ Accepted for Publication ☐ Submitted for Publication ☐ Unpublished and Unsubmitted work written in manuscript style
Publication Details	Yap, P. L., Tung, T. T., Kabiri, S., Matulick, N., Tran, D. N. H., & Losic, D. (2020). Polyamine-modified reduced graphene oxide: A new and cost-effective adsorbent for efficient removal of mercury in waters. Separation and Purification Technology, 238, 116441.

Principal Author

Name of Principal Author (Candidate)	Pei Lay Yap		
Contribution to the Paper	Prepared, characterized and conducted performance testing on all the samples, interpreted data as well as wrote the manuscripts		
Overall percentage (%)	85%		
Certification:	This paper reports on original research I conducted during the period of my Higher Degree by Research candidature and is not subject to any obligations or contractual agreements with a third party that would constrain its inclusion in this thesis. I am the primary author of this paper.		
Signature		Date	01/07/20

Co-Author Contributions

By signing the Statement of Authorship, each author certifies that:

i. the candidate's stated contribution to the publication is accurate (as detailed above);

ii. permission is granted for the candidate in include the publication in the thesis; and

iii. the sum of all co-author contributions is equal to 100% less the candidate's stated contribution.

Name of Co-Author	Dusan Losic		
Contribution to the Paper	Supervised the development of work, edited, revised the manuscript and acted as the corresponding author.		
Signature		Date	02/10/20

Name of Co-Author			
Contribution to the Paper			
Signature		Date	

Please cut and paste additional co-author panels here as required.

4.3. Published work

This section is presented as a published review article as ***Yap, P. L.,*** *Tung, T. T., Kabiri, S., Matulick, N., Tran, D. N. H., & Losic, D. (2020). Polyamine-modified reduced graphene oxide: a new and cost-effective adsorbent for efficient removal of mercury in waters. Separation and Purification Technology, 238, 116441.* Reproduced with permission.[23] Copyright (2019) Elsevier.

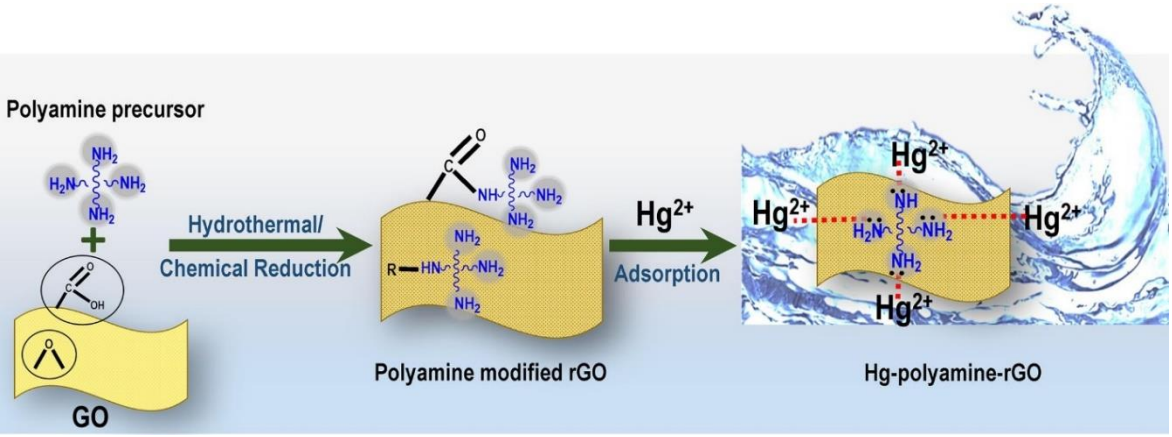

Figure 13. Graphical abstract of *"Polyamine-modified reduced graphene oxide: a new and cost-effective adsorbent for efficient removal of mercury in waters". Reproduced with permission.[23] Copyright (2019) Elsevier.*

Separation and Purification Technology 238 (2020) 116441

Contents lists available at ScienceDirect

Separation and Purification Technology

journal homepage: www.elsevier.com/locate/seppur

Polyamine-modified reduced graphene oxide: A new and cost-effective adsorbent for efficient removal of mercury in waters

Pei Lay Yap[a,b], Tran Thanh Tung[a,b], Shervin Kabiri[a,b,c], Nicola Matulick[a,b], Diana N.H. Tran[a,b], Dusan Losic[a,b,*]

[a] School of Chemical Engineering and Advanced Materials, The University of Adelaide, Adelaide, SA 5005, Australia
[b] ARC Hub for Graphene Enabled Industry Transformation, The University of Adelaide, Adelaide, SA 5005, Australia
[c] School of Agriculture, Food and Wine, The University of Adelaide, PMB 1, Waite Campus, Glen Osmond, SA 5064, Australia

ARTICLE INFO

Keywords:
Polyamine-modified reduced graphene oxide
Hydrothermal process
Graphene composites
Water treatment
Mercury removal

ABSTRACT

This paper describes the synthesis and characterization of polyamine modified reduced graphene oxide rich with mixed amino groups as a cost- and performance- efficient adsorbent for mercury removal from waters. The synthetic approach is based on a simple process to functionalize graphene oxide (GO) with low-cost commercial polyamine epoxy hardener followed by the reduction of created polyamine-GO hybrid by hydrothermal (HT) or chemical reduction (CM) process with hydrazine. Both polyamine modified reduced graphene oxide (rGO), referred as HT-rGO-N and CM-rGO-N, exhibited 8.28% and 5.47% N content, respectively. Mercury adsorption study showed that these rGO functionalized composites have high adsorption kinetics, reaching equilibrium within the first ten minutes. The adsorption kinetics and equilibrium of their adsorption process can be well described using pseudo-second order and Freundlich isotherm models with estimated sorption capacity of 63.8 mg/g and 59.9 mg/g for HT-rGO-N and CM-rGO-N respectively. The adsorption capacity for Hg is achieved in broad range of pH (pH 5–9) and can be described as high-performing compared with other amino based adsorbents reported in the literature. More importantly, these adsorbents showed very high selectivity towards Hg(II), outperformed the commercial activated carbon adsorbent with only ~16% mercury removal efficiency achieved in multimetallic solution consisting of Hg(II), Cd(II), Co(II), Cu(II) and Pb(II) ions in both solid and dispersed forms. Finally, these polyamine functionalized rGO adsorbents confirmed their notable performance in regeneration and removal of spiked mercury from natural waters mimicking real applications. These results demonstrated realistic water remediation capabilities of developed polyamine functionalized rGO adsorbents as promising candidates for environmental applications.

1. Introduction

The pollution emerging from the presence of heavy metals in surface waters due to rapid urbanization and industrial revolution has led to alarming environmental and health concerns [1]. In particular, mercury, a ubiquitous metal with long range atmospheric transport can bioaccumulate and biomagnify in the food chain poses a major threat to global food security [2]. Exposure to mercury even at low concentration can lead to disastrous health consequences like vision, speech and hearing impairments, as well as damage to the central nervous and nephrotic systems [3]. Due to the limitation of access to clean water in meeting the growing global demand, the development of efficient water purification systems to remove mercury from our precious yet most wasted natural resource, water, is a now-urgent pursuit [4].

Existing water treatment technologies for mercury removal such as chemical precipitation, ion exchange, flocculation, membrane filtration, and adsorption have been broadly adopted to remediate mercury contaminated water. Among the available technologies, adsorption is regarded as one of the most promising and favourable techniques owing to its ease of operation, low cost, and practical design for real water applications [5]. Currently, driven by the economic factor, activated carbon still remains the most cost effective environmental solution for water treatment [6]. Although activated carbon is known for its remarkable characteristics such as high surface area, high porosity and flexibility for surface modification, it is still bounded by several drawbacks including pore blockage which limits the diffusion of smaller contaminants including heavy metal ions into its porous structure [7]. Moreover, most activated carbons adsorbents available on market are

* Corresponding author at: School of Chemical Engineering and Advanced Materials, The University of Adelaide, Adelaide, SA 5005, Australia.
E-mail address: dusan.losic@adelaide.edu.au (D. Losic).

https://doi.org/10.1016/j.seppur.2019.116441
Received 20 August 2019; Received in revised form 11 November 2019; Accepted 16 December 2019
Available online 16 December 2019
1383-5866/

impregnated with heteroatoms (silver, sulfur, iodide and etc) to enhance their removal efficiency may pose leaching risk including sulfur contamination and other operational issues during the decontamination process [8].

Unlike activated carbon, graphene-based adsorbents on the other hand are not affected by internal diffusion and possess higher stability apart from its faster adsorption kinetics towards heavy metal ions than activated carbon due to the opened-up layer structure of graphene [9,10]. From the energy consumption perspective, the production of graphene-based materials is less energy-intensive compared to activated carbon which requires high temperature treatment to create porosity in its carbon network. In relative to activated carbon, graphene-based adsorbents are still in their infancy compared to activated carbon which require more research efforts before these technologies can be feasibly converted to industrial end-products [6]. Although some graphene adsorbents in the literature showed considerable high adsorption capacity, the complexity, sustainability and scalability of their preparation process are still the key barriers for practical implementation in the field operation [11,12]. Therefore, to address these limitations that include the operational issues, possible leaching complications and lack of efficiency, the development of new and advanced mercury remediation solutions with low cost and sustainable technologies is an urgent pursuit.

Adsorbents bearing chelating functional groups containing sulphur, nitrogen and oxygen atoms are known to possess strong binding affinity towards mercury [13]. Hence, majority of the research have been focusing on the use of adsorbents decorated with these three atoms that is achieved by surface functionalization of different porous scaffold with broad range of organic molecules with these functional groups such as mercapto-silanes, polypyrrole, chitosan, cysteamine, dithiocarbamate and etc [14–17]. The thiol surface modification by thiol groups showed the highest binding affinity for mercury followed by amino groups that are also highly recommended to be used as the binding functional groups. However, in designing these amino- based adsorbent, most of the previous studies were focused on single molecule functionalization which limit the potential to provide high density of binding sites and high adsorption capacity. Thus, there is a need to explore and develop new adsorbents containing multi-type of nitrogen species for mercury removal to achieve high-efficient mercury adsorption with environmentally-friendly and scalable adsorbent preparation.

Inspired by the respectable binding chemistry of N and the pressing demand for mercury decontamination solutions, in this paper, we present our work to engineer new graphene adsorbents functionalized with multiple amino groups for efficient and low-cost removal of mercury from water. To achieve the scalability and fabrication simplicity, an approach is designed to use low-cost and commercially available polyamine epoxy hardener as precursors combined by simple chemical and hydrothermal processes as depicted in Fig. 1. The concept, is based on the covalent grafting of polyamine precursor on epoxides and carboxyls rich functional groups on GO. The polyamine precursor was chosen due to the presence of multi-type amino groups including polyethylenepolyamine, triethyelenpolyamine and tetraethylenepentamine which acts as the electron donor and chelating agent to immobilize mercury in waters [5]. This readily available polyamine blend is cheap and water soluble which facilitates the chemical reaction to take place between GO and the polyamine mixture without the use of volatile organic solvents. The polyamine functionalized GO is further reduced by hydrothermal and chemical reduction process using hydrazine in order to make the adsorbent in robust solid form applicable for adsorption application. Herein, we also compared the sorption efficiency of the hydrothermally fabricated polyamine modified rGO composite (HT-rGO-N) with chemically (hydrazine)-reduced polyamine modified rGO composite (CM-rGO-N) developed in our previous study [18]. The morphology, structural, chemical and thermal properties of the prepared adsorbents were thoroughly studied using a broad range of characterization techniques comprising of SEM-EDX, CHN combustion, UV–Vis, Raman, FTIR, zeta potential, XRD, XPS and TGA-DTA analyses. A comprehensive evaluation on their process efficiency based on the influence of sorption conditions including the contact time, initial Hg(II) concentration, solution pH, recycling times, competing ions in both dispersed and solid forms towards Hg(II) removal was performed. The kinetic and equilibrium behaviours of these two adsorbents were also studied in detailed using non-linear regression analysis on kinetic and equilibrium models. The performance of the adsorbents was also explored at a realistic level using Hg(II) spiked river and sea waters to demonstrate their practicability in surface waters. This study proposes to fill the research gaps by developing a new type polyamine modified rGO adsorbents using low-cost multi -polyamine blend and scalable hydrothermally process to graft the N-containing species on GO (HT-rGO-N) for efficient sequester of Hg (II) from waters.

2. Experimental

2.1. Materials and chemicals

Natural graphite flakes were received from a local mining site (Uley, Eyre Peninsula, South Australia, Australia), milled into powder using a benchtop ring mill (Rocklabs). Potassium permanganate ($KMnO_4$, Sigma Aldrich), 98% sulphuric acid (H_2SO_4, Chem-Supply), 85% w/w phosphoric acid (H_3PO_4, Chem-Supply), 30% hydrogen peroxide (H_2O_2,Chem-Supply), 36% hydrochloric acid (HCl, Chem-Supply), 67–69% nitric acid (HNO_3, Seastar Chemicals), 1 N sodium hydroxide (NaOH, Chem-Supply), 205 fast hardener (a blend of polyamine and polyamine adducts, West System), hydrazine monohydrate (N_2H_4, Sigma Aldrich) mercury (II) chloride ($HgCl_2$, Chem-Supply), lead(II) nitrate ($Pb(NO_3)_2$, Univar), cobalt(II) nitrate ($Co(NO_3)_2$, Ajax), copper (II) nitrate ($Cu(NO_3)_2$, ChemSupply), cadmium(II) nitrate ($Cd(NO_3)_2$, Mallinckrodt), thiourea (CH_4N_2S, Sigma Aldrich), and ethanol (Chem-Supply) were used directly without prior purification. High purity milli-Q water (18.2 $M\Omega cm^{-1}$) was used throughout the work, unless otherwise stated.

2.2. Preparation of polyamine modified chemically- and hydrothermally-reduced graphene oxide composites (CM-rGO-N and HT-rGO-N)

Graphene oxide was prepared via the improved Hummer's method as detailed in our previous work [19]. The synthesis of polyamine modified rGO composites was performed according to the adapted methodology from our previous studies [18]. In a typical procedure, 225 mg of GO was first dispersed in 100 mL water using probe sonication for 20 min at 60% power to obtain a well-dispersed GO suspension. The dispersed polyamine hardener solution (composition as detailed in Table S1) containing 1100 mg in 20 mL deionized water was added into the GO suspension (polyamine-based crosslinker: GO mass ratio of 5:1) under magnetic stirring at room temperature. The mixture was then stirred for another one hour. To prepare HT-rGO-N composite, the well-stirred aqueous dispersion was equally poured into two 100 mL Teflon-lined autoclaves, sealed and heated at 150 °C for three hours. For the synthesis of CM-rGO-N composite, 100 µL hydrazine monohydrate was added into the well-stirred aqueous dispersion contained in a 250 mL round bottom flask, placed in a silicon oil bath and heated at 95 °C under reflux with magnetic stirring for five hours. Subsequently, the as- formed products from two different methods were left to cool to room temperature and were washed several times with distilled water via vacuum filtration. All the control samples (GO, HT-rGO-C and CM-rGO-C) were fabricated according to the procedures described hereby without the addition of polyamine hardener solution. The obtained products were freeze-dried for overnights and stored. The details of the materials characterization are provided in the Supplementary Material.

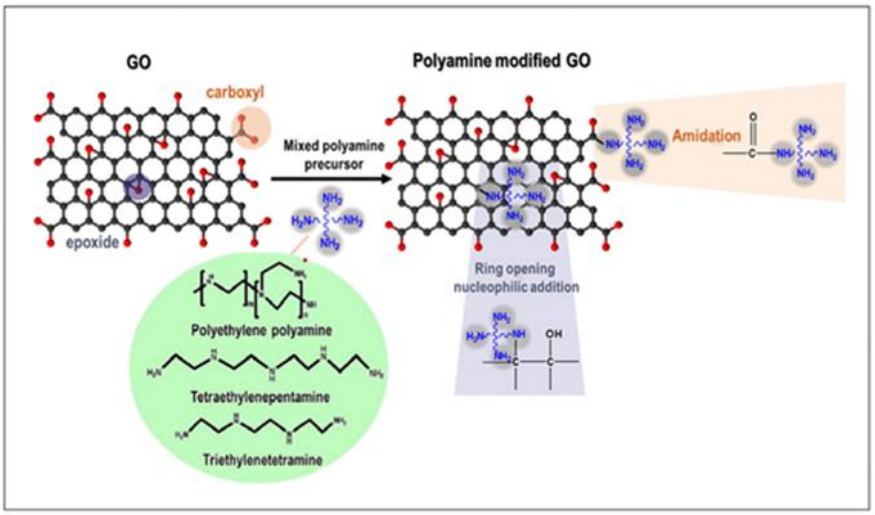

Fig. 1. Schematic diagram of the reaction mechanisms for covalent attachment of mixed polyamine molecules on graphene oxide (GO) which is followed by hydrothermal (HT) and chemical (CM) reduction to create polyamine-rGO adsorbent.

2.3. Adsorption studies

In this work, all the heavy metal ions removal experiments were conducted via batch study in triplicate by oscillating the desired amount of adsorbent in the metal ion solution using an orbital mixer (Ratek, Model OM7, Australia) at 200 rpm with a control (without adsorbent) running in parallel. The adsorption studies were performed using adsorbents dispersed in milli-Q water (via sonication) with the same volume of milli-Q water as blank added into the control. The pH of the metal ion solution was measured using a pH meter FiveGO FG2, Mettler Toledo) and adjusted using diluted HCl or NaOH at ambient temperature. At the end of the adsorption experiment, 10 mL aliquot was withdrawn and centrifuged immediately at 12000 rpm for five minutes. The remaining metal ion concentration in the sample was then acidified with 2% HCl (for mercury analysis) or 2% HNO_3 (for other metal ions analysis) prior to ICP-MS measurement. Milli-Q water was used throughout the study unless otherwise stated. The amount of mercury(II) ions adsorbed per unit of adsorbent mass, at a given time, t (q_t, mg g^{-1}) was deduced using the following equation [16]:

$$q_t = \frac{(C_0 - C_t)V}{m} \quad (1)$$

where C_o and C_t are initial and mercury (II) concentrations at time t (mg L^{-1}), while V is the volume of solution (L) and m is the mass of adsorbent (g). The removal efficiency (R_t, %) at a given time, t, was calculated based on the following equation [16]:

$$R_t = \frac{(C_0 - C_t)}{C_0} \times 100 \quad (2)$$

2.3.1. Kinetic study

The rate of the mercury uptake was investigated using 2.5 mg adsorbent added into approximately 11 ppm of 20 mL mercury (II) solution at pH ~5 with the liquid samples withdrawn at time intervals 0–24 h. The obtained experimental data was fitted into two mathematical models, i.e. Lagergren pseudo-first-order [20] and the Ho's pseudo-second-order [21] in their non-linear forms.

The pseudo-first order equation:

$$q_t = q_e\left(1 - e^{-k_1 t}\right) \quad (3)$$

The pseudo-second order equation:

$$q_t = \frac{q_e^2 k_2 t}{1 + q_e k_2 t} \quad (4)$$

where q_e and q_t represent the amount of Hg(II) ions adsorbed (mg g^{-1}) at equilibrium and at time t respectively; k_1 *and* k_2 are the rate constants for the pseudo-first order and pseudo-second order kinetic models respectively; t is the time.

2.3.2. Equilibrium study

A series of known concentration (1.5 to 11 mg L^{-1}) Hg(II) working solutions (20 mL) at pH 5–5.5 was allowed to reach the equilibrium for 2 h using 2.5 mg adsorbent. The residual mercury concentration was determined following the same procedure described above. The adsorption process between the adsorbent and Hg(II) ions was studied using two equilibrium models in their non-linear forms, i.e. the two-parameters Langmuir and Freundlich isotherms:

The Langmuir equation [22]:

$$q_e = \frac{q_m b_L C_e}{1 + b_L C_e} \quad (5)$$

where q_e and q_m are the adsorption capacity at equilibrium and maximum monolayer coverage capacity respectively (mg g^{-1}), C_e denotes the concentration of mercury (II) ions at equilibrium (mg L^{-1}) and b_L is the Langmuir constant.

The Freundlich equation[23]:

$$q_e = K_F C_e^{1/n} \quad (6)$$

where K_F signifies the Freundlich adsorption constant ($mg^{1-1/n}$ $L^{1/n}$ g^{-1}), C_e represents the concentration of mercury(II) ions at equilibrium (mg L^{-1}) and $1/n$ is the adsorption intensity.

2.3.3. Influence of solution pH

The effect of pH of the materials towards mercury uptake was conducted at pH range 3–10 of mercury(II) solution (~1.5 mg L^{-1}) using 1.0 mg of adsorbent with the pH adjusted using HCl or NaOH before the adsorption experiments. Same procedure as described above was used to determine the remaining Hg(II) concentration after mercury adsorption.

2.3.4. Influence of competing ions

The effect of competing ions was conducted by adding 2.5 mg of adsorbent into a quintuple metal ion mixture containing about 5 mg L^{-1} of Hg, Pb, Cu, Co and Cd ions at pH 5–5.5 for 2 h. This study was conducted in two approaches, namely dispersed and solid (freeze dried) forms in order to demonstrate the selectivity of the materials in different forms towards metal ions adsorption. The remaining concentration of metal ions was determined using ICP-MS after the selectivity experiments.

2.3.5. Influence of recycling times

The regeneration of the prepared adsorbents was investigated by adding them separately into 50 mL of *ca.* 1.50 mg L^{-1} Hg(II) at pH 5.3 at ambient temperature. The desorption cycles were carried out by mixing the spent adsorbent with 30 mL 2% (w/v) thiourea in 0.1 M HCl as eluent at 250 rpm on the orbital shaker for 1 h to wash out the bound Hg(II) from the adsorbent. The spent adsorbent was then washed with large amount of milli-Q water to bring the pH to above five and followed by drying of the adsorbents at ambient temperature. The remaining Hg(II) concentration in each cycle was probed using ICP-MS after three repeating adsorption–desorption cycles.

2.3.6. Influence of water matrix: Adsorption study using real waters

The efficiency of the fabricated materials towards Hg(II) adsorption was evaluated using Hg(II) spiked river and sea waters without pH adjustment to simulate real natural water samples. Water samples were collected from Torrens River (Adelaide, South Australia, 34°55′02.7″S 138°36′ 14.6″E) and Henley Beach (Adelaide, South Australia, 34°54′51.1″S 138°29′ 30.0″E). Both the natural water samples were spiked with *ca.* 0.5 mg L^{-1} Hg(II) solution and 2.5 mg of adsorbents (CM-rGO-N and HT-rGO-N composites) were separately added into 20 mL of each spiked water sample, stirring at 200 rpm for 2 h at ambient temperature. The concentration of mercury solution remained in the collected aliquots were determined by ICP-MS.

3. Results and discussion

3.1. Structural and chemical composition characterizations

The topography of the resulting materials was studied using SEM and TEM techniques. GO control sample demonstrates smooth, thin and wrinkled layers before the modification process (Fig. S1a). As depicted in Fig. 2 a-d, the SEM micrographs visibly show that both polyamine functionalized rGO solid materials prepared by hydrothermal and chemical reduction processes exhibit similar porous rough surface with randomly oriented and burgeoned overlapping GO sheets after the modification with polyamine precursor. Meanwhile, Fig. 2e shows typical wrinkled and corrugated morphology of rGO sheets. After the polyamine precursor modification, the structures of the rGO sheets preserved with stacking layers of polyamine modified rGO composite were observed (Fig. 2f).

Elemental quantification by combustible technique used for bulk analysis as tabulated in Table 1 shows that the N concentration was substantially increased to 6.51 wt% for HT-rGO-N after the modification using polyamine precursor via hydrothermal reaction. Meanwhile, 3.80 wt% of N was found for CM-rGO-C and it was dramatically increased to 10.34% for CM-rGO-N after modification via chemical reduction. This significant increase in N atomic percentage recorded in both the modified materials strongly suggests the successful incorporation of N-containing groups onto GO network. Remarkably, almost similar net N wt % determined from both modified graphene composites (HT-rGO-N: 6.51 wt% and CM-rGO-N: 6.54 wt%) contributed by the grafting of polyamine precursor, indicated that graphene composites enriched with N species can be obtained irrespective of the modification route applies.

The chemical composition of the functionalized materials determined using EDX analysis presented in Fig. S1b and c also confirmed high N atomic composition after modifications (HT-rGO-N: 7.4 at%, CM-rGO-N: 9.8 at%), corroborating the attachment of N-containing species on GO. Similar to the result determined using combustion technique, the slightly higher N composition recorded in CM-rGO-N compared to HT-rGO-N could be due to the cumulative contribution of nitrogen species doped on the GO structure after the chemical reaction using hydrazine [24]. Nevertheless, the chemical quantification from both the combustion and EDX analyses verified the effective functionalization using polyamine-based crosslinker via these two approaches. The presence of N element and its distribution on rGO surface was further confirmed by the elemental mapping as depicted in Fig. 3. These images clearly demonstrated homogeneous distribution of N elements on both polyamine functionalized rGO composites using two reduction processes.

The UV–vis absorption spectra of the amino modified rGO composites and control samples are presented in Fig. 4a and Fig. S2a respectively. The sharp absorption at 225 nm for GO indicates the transition of π-π^* for C=C bond in the GO structure which is almost similar to the typical absorption peak for GO (230 nm), while the broad absorptions at 260 nm for HT-rGO-C and 265 nm for CM-rGO-C samples evidently imply the reduction of GO via both the hydrothermal and chemical approaches [18,25–27]. It was found that the absorption peaks of both the functionalized rGO composites were red-shifted to 280 nm and 265 nm for the hydrothermal and chemical polyamine modified rGO composites respectively in relative to GO (225 nm) after the reaction. This signifies an enhancement in the π-electron concentration as well as the restoration of sp^2 carbon of the graphene system.

The chemical species found on the modified graphene composites were determined by FTIR analysis as illustrated in Fig. 4b. As visualized from the FTIR spectra, the appearance of the bands at around 1568 cm^{-1} which can be assigned to amide II, representing the combination of N–H stretching and C–N stretching while the peak identified at 1205 cm^{-1} could be ascribed to pyrrole ring breathing on both the modified rGO sample verified the successful capping of nitrogen functional groups on the GO [14,28,29]. An intense peak at about 3200 cm^{-1}corresponding to N–H stretching mode was visibly recorded on the FTIR spectra of both the hydrazine and hydrothermal modified rGO composites [16]. The significant disappearance of the peak at 1720 cm^{-1} on the FTIR spectrum of GO (Fig. S2b) with the combination of a new vibration mode arose at around 1450 cm^{-1} denoting the C–N stretching of amide found in both the hydrothermal and hydrazine functionalized rGO composite revealed the formation of amide linkage which could be resulting from the amidation reaction between carboxylic group in GO and the amine moieties in polyamine precursor [30]. It is worth noting that the notable disappearance of the band at 1044 cm^{-1} which could be referenced to epoxide group indicates the involvement of epoxide groups in GO (Fig. S2b) to react with amine groups in the polyamine hardener [31]. This reaction is also evidenced by the appearance of a peak located at around 1345 cm^{-1} (bending of –OH group) resulting from the nucleophilic addition reaction between amine and epoxide moieties [32].

The Raman spectra of both prepared polyamine modified rGO composites to elucidate their structural characteristics are summarized in Fig. 4c. Two typical peaks of the D-band (1347 cm^{-1}) and G-band (1590 cm^{-1}) are identified in both the samples were found to be shifted from GO (D-band, 1358 cm^{-1} and G-band, 1592 cm^{-1}) as displayed in Fig. S2c. The increased intensity ratio of D to G bands (I_D/I_G ratio) for HT-rGO-N (1.05 ± 0.016) and CM-rGO-N (1.04 ± 0.017) implies that defects have been created on the surface of both the materials in comparison to GO (0.96 ± 0.004). The significant difference of the I_D/I_G ratio for both the modified rGO composites in relative to the control sample (GO) also signifies the enhancement of the disordered graphene sheets with an increase in sp^2 clusters [33].

TGA was performed to confirm the attachment of the N functional groups on the modified rGO composites aside from studying the

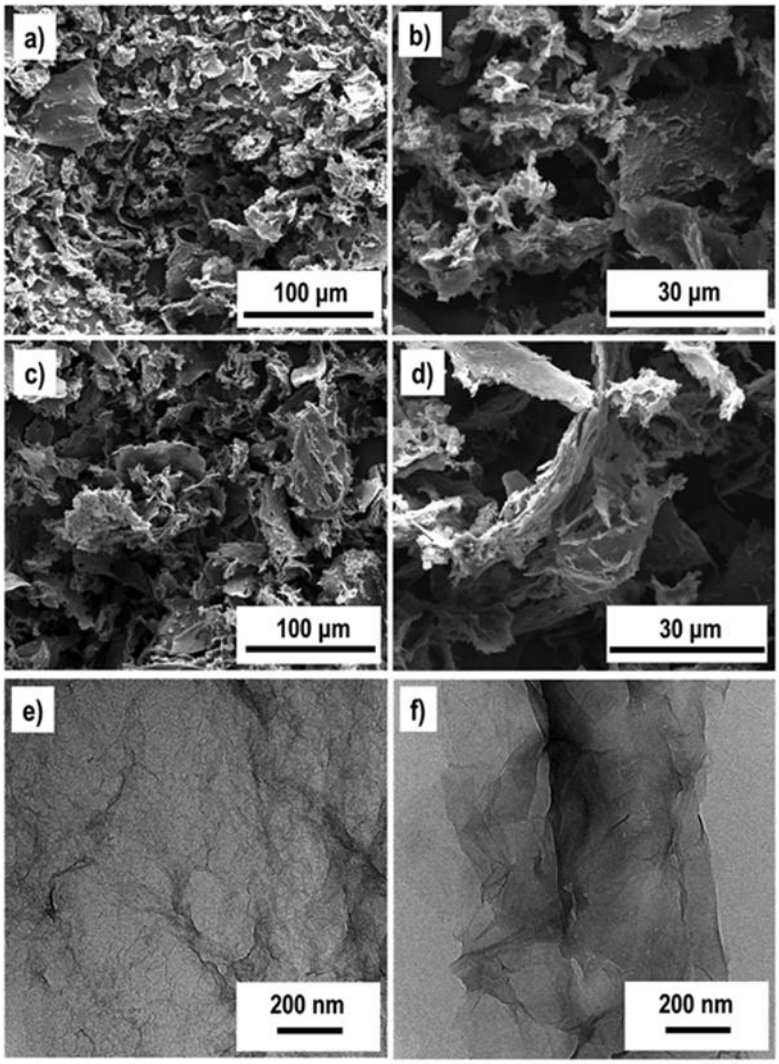

Fig. 2. SEM micrographs of (a-b) HT-rGO-N and (c-d) CM-rGO-N composites at different magnifications after freeze-drying. TEM images of (e) CM-rGO-C and (f) CM-rGO-N composites.

Table 1
Normalized chemical composition of samples determined using combustible elemental analysis in wt %.

Element	Weight %			
	C	H	N	O
GO	41.11	2.90	0.00	55.99
HT-rGO-C	62.76	2.07	0.00	35.17
HT-rGO-N	44.48	6.40	6.51	42.61
CM-rGO-C	61.90	2.29	3.80	32.01
CM-rGO-N	59.69	4.09	10.34	25.88

thermal properties of the functionalized rGO composites. As expected, it could be visible that GO is highly thermal unstable in comparison to HT-rGO-C and CM-rGO-C as shown in Fig. S2d. Under the inert environment, 2 main mass losses were identified in GO as displayed in Fig. S2d with the first decomposition took place below 100 °C due to the loss of solvent trapped in the GO network. Meanwhile, the second mass loss happened at about 200 °C which can be accounted for the decomposition of bountiful of unstable oxygen functional groups including hydroxyl (−OH), epoxy (−CH (O) CH−) and carboxyl (−COOH) groups in the form of H_2O, O_2, CO, and CO_2 [16]. Correspondingly, both the control samples (HT-rGO-C and CM- rGO-C) encountered mass loss at similar decomposition temperatures as GO (total mass loss of 60%) but with lower total percentage loss (GO: 62%, HT-rGO-C: 38% and CM-rGO-C: 32%) recorded (Fig. S2d). On the contrary, both hydrothermal and chemical modified rGO composites experienced a major mass loss (~30.6% and ~ 23.0% respectively) at around 320 °C which can be associated with the breakdown of the functional groups grafted on the modified graphene composites as evidenced in Fig. 4d. This

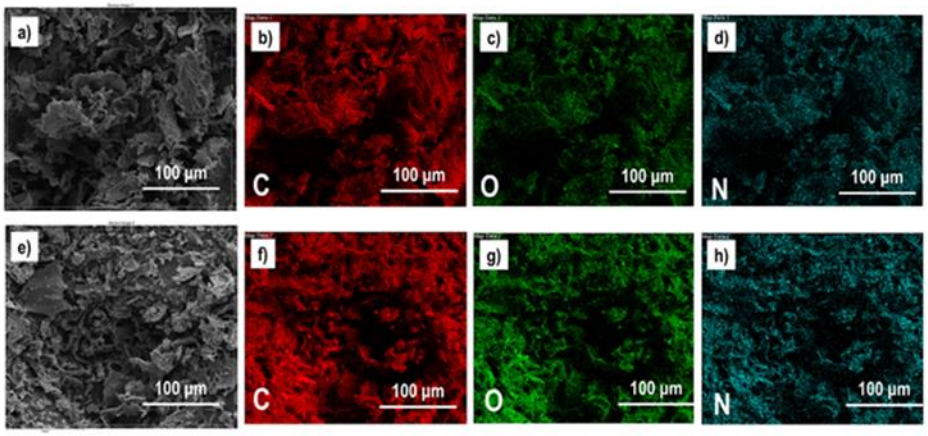

Fig. 3. (a) SEM image (black and white) and EDS mapping (color) of (a-d) CM-rGO-N (e-h) HT-rGO-N containing C, O and N elements.

observation was not detected on the thermograms of the control samples including the GO, HT-rGO-C and CM-rGO-C (Fig. S2d) which ascertained the presence of the grafted functional groups in the GO framework coupling with the results from the elemental and FTIR analyses discussed previously.

XRD technique was applied to reveal the structural characteristic of the materials prepared. As illustrated in Fig. S2e, the sharp peak at $2\theta = 11.6^{\circ}$ (d-spacing = 7.6 Å) found on the XRD profile of GO implies the complete oxidation of graphite. The increased d-spacing of the peak in GO (7.6 Å) compared to graphite (3.34 Å) is due to the intercalation of the water molecules and oxygen groups between the interlayer of graphene during the oxidation process [34,35]. Meanwhile, prominent changes were observed for HT-rGO-N and CM-rGO-N on their broad peaks at 21.2° (d-spacing = 4.2 Å) and 23.3° (d-spacing = 3.8 Å) respectively as demonstrated in Fig. 4e. As compared to the peak arose at 24° with d-spacing of 3.7 Å (Fig. S2e) for both the hydrothermal and hydrazine reduced control samples, the augmented d-spacing of the modified rGO samples could be associated with the successful attachment of functional groups from the polyamine crosslinker which broadens the distance between the rGO layers after the functionalization process [34,36,37].

XPS characterization results including survey graphs showing characteristics C1s, O1s and N1s peaks at around 285 eV, 532 eV and 399.5 eV respectively are presented in Fig S3a-b as well as high resolution C1s and N1s peaks in Fig. 5a and Fig. S3c. These results clearly confirmed the successful modification of graphene oxide using polyamine-based crosslinker. Both the samples demonstrated increased N atomic % (Table S2) after the modification process. CM-rGO-N exhibited 8.28 N atomic % compared to its control (CM-rGO-C, 2.83 atomic %), while HT-rGO-N showed 5.47 N atomic % in relative to its control HT-rGO-C with no detection of nitrogen. For CM-rGO-C, the 2.83 atomic % N arose from hydrazine added during the reduction process. Remarkably, the difference of N atomic % in CM-rGO-N (5.45 atomic %) after the subtraction from its control sample agrees well with the N atomic % recorded in HT-rGO-N (5.47 atomic %) after the modification using the polyamine-based crosslinker. Similar to the bulk chemical analysis (combustible technique) discussed in the previous section, the same net amount of N (≈5.5 atomic %) found in both samples obviously indicates that the polyamine crosslinker has been effectively grafted on GO regardless of the modification method applied. Further fitting of the C1s and N1s narrow spectra (Fig. 5) verified the chemical reaction between GO and the polyamine-based crosslinker. The deconvolution of the C1s spectra of HT-rGO-N and CM-rGO-N showed additional peak positioned at around 286.0 eV which could be ascribed to C−N besides the characteristic peaks of GO (Fig. S3c). The N1s deconvoluted peaks of both materials (Fig. 5b) exhibit multiple N configurations including $-NH_2$, HNC═O, N−H and protonated amine centered at 399.4, 400.2, 401 and 402eV respectively, indicating the presence of rich N species decorated on the surface of the composites. Interestingly, another peak at 402.7 eV which could be referenced to N-oxides was found only in CM-rGO-N [38–41]. The presence of HNC═O species in both the materials implies that carboxyls on GO has been reacted with amine on the polyamine crosslinker via amidation process which correlates well with the FTIR result discussed previously.

The presence of several types of oxygen functional groups in GO including epoxide and carboxyl groups allows the covalent bonding of amine groups to form via ring opening nucleophilic addition and amidation respectively with the amine hydrogens in the multi-amine precursor [42,43]. Coupling with the outcomes from FTIR and XPS analyses, we inferred that two chemical mechanisms took place between graphene oxide and the polyamine crosslinker as summarized in Fig. 1. The deduction of both the reaction mechanisms in Fig. 1 is well evidenced by the prominent appearance of C−N and N species including N−H as well as HNC═O from the XPS deconvolution analysis. Moreover, the nucleophilic addition reaction is well supported by the FTIR results as discussed previously with the disappearance of epoxide group and the presence of amide II (combination of N−H stretching and C−N stretching) and hydroxyl groups generated after the modification using polyamine crosslinker. Meanwhile, the amidation reaction between carboxyl group in GO and the amine moieties in the polyamine modifier can be confirmed with the disappearance of carboxyl band and the presence of C−N of amide in both the modified graphene composites.

3.2. Adsorption studies

3.2.1. Kinetic study

The kinetic profiles in terms of the normalized Hg (II) concentration (C_t/C_0) after 24 h contact time for HT-rGO-N and CM-rGO-N adsorbents are shown in Fig. 6a. The abrupt uptake of Hg (II) for both of these materials at the first 10 min noticeably demonstrated a rapid initial adsorption rate which could be due to the presence of plethora unoccupied active sites on the surface of the adsorbents and their high specific surface area, SSA, (HT-rGO-N: 63 ± 8 m^2/g; CM-rGO-N: 270 ± 10 m^2/g). Nevertheless, further extension of the contact time did not significantly improve the uptake of Hg (II) as the two materials could have reached the saturation of their active binding sites. It could also be observed that both the materials attained equilibrium at almost similar contact time with HT-rGO-N achieving slightly higher removal

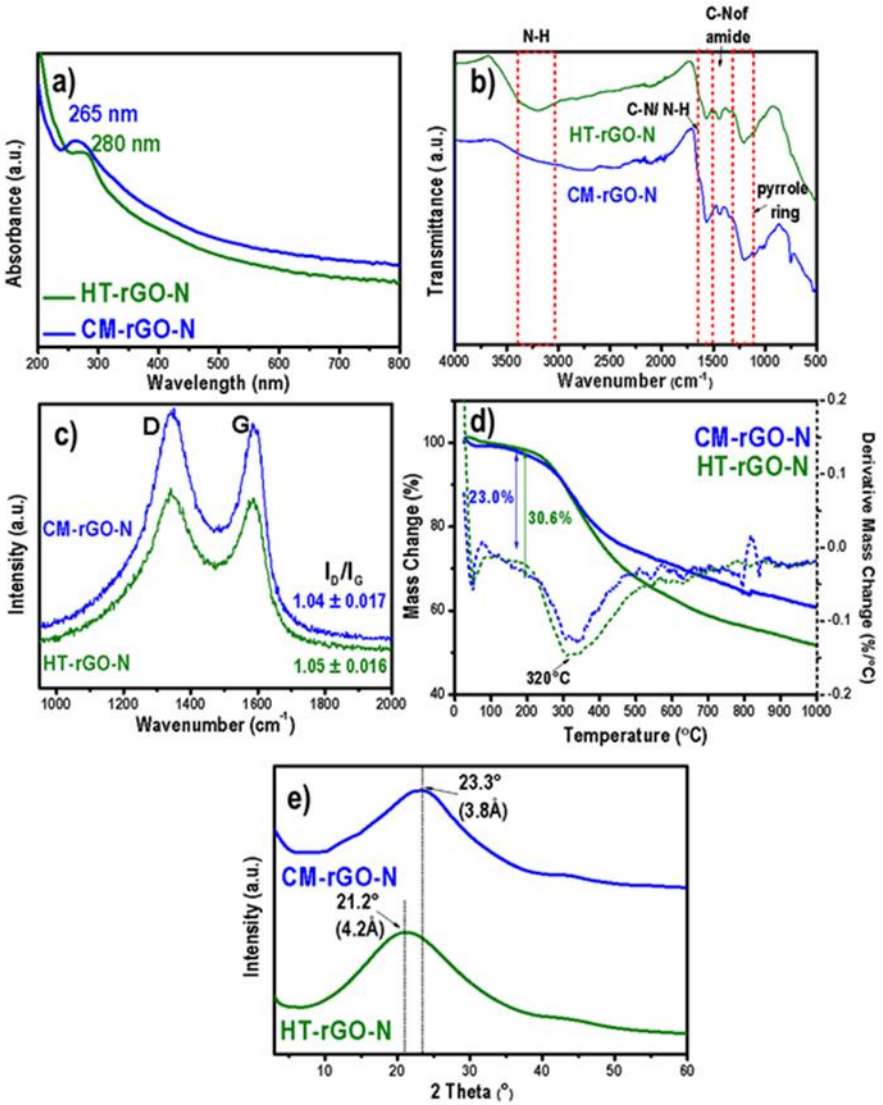

Fig. 4. Comparative graphs of HT-rGO-N and CM-rGO-N showing (a) UV–Vis, (b) FTIR, (c) Raman, (d) TGA and DTA, (e) XRD graphs.

percentage compared to CM-rGO-N when approximately 11 mg/L initial concentration of mercury was used in the study. We also found that the SSA of both adsorbents was greatly reduced in comparison to their respective controls (HT-rGO-C: 386 ± 24 m^2/g; CM-rGO-C: 680 ± 13 m^2/g) after the modification using polyamine precursor. This could be attributed to the blockage of rGO sheets by the long chain of polyamine precursor during the functionalization process. To gain further insight about the adsorption behavior of both the functionalized samples, their kinetic experimental data were then fitted into pseudo-first and pseudo-second order kinetic models (Fig. 6b and c) in order to evaluate their rate-limiting step as well as the adsorption mechanism. Based on the fitting analysis (Table 2), both the adsorbents achieved higher linear correlation coefficient using pseudo-second-order kinetic model (R^2 > 0.91) in comparison to pseudo-first order model (R^2 = 0.88 and 0.90 for HT-rGO-N and CM-rGO-N respectively). This suggests that chemisorption is the rate-limiting step for binding of Hg (II) onto the adsorbents which emphasizes on the sharing and exchange of electrons between the adsorbate (Hg^{2+}) and the adsorbent (HT-rGO-N and CM-rGO-N) at the solid-solution interface [16]. This could be accounted for the presence of N heteroatom on the surface of the adsorbents which allows the metal (Hg)-complexation to take place. A more representative comparison was made using graphene oxide adsorbents grafted with nitrogen functional groups in the literature (Table S3) to evaluate the adsorption rate of the adsorbents fabricated in this work. As reported by Liu et al.[44], ethylenediamine decorated with magnetite/graphene oxide (EDA-Fe_3O_4/GO) adsorbent was found to achieve the same equilibrium time (10 min) when higher sorbent dosage (200 mg/L) was used to remove mercury with lower initial concentration (8 ppm) in comparison to both the adsorbents (HT-rGO-N and CM-rGO-N) prepared in this work (11 ppm, 125 mg/L). Moreover,

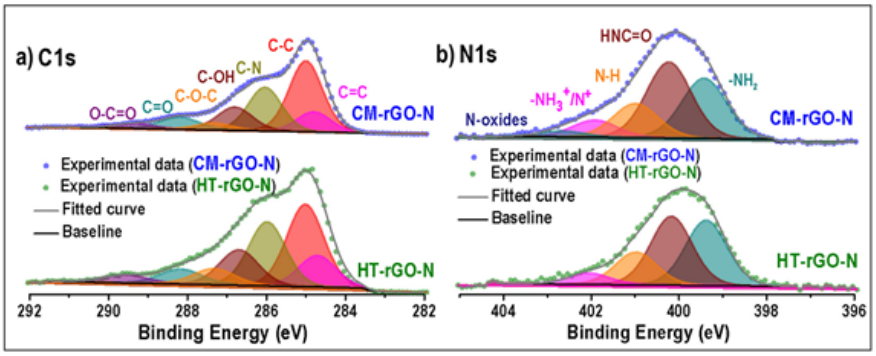

Fig. 5. XPS narrow scans of (a) C1s and (b) N1s for HT-rGO-N and CM-rGO-N confirming successful immobilization of polyamine functional groups.

with lower sorbent dosage, the sorption capacity, q_e, of HT-rGO-N (63.8 mg/g) and CM-rGO-N (59.9 mg/g) was more than 2 times higher than EDA-Fe_3O_4/GO (25 mg/g) determined using pseudo-second-order kinetic model [44]. It should also be highlighted that longer time was required for 200 mg/L of amino functionalized graphene composites, Fe_3O_4-GS, (120 min) and 10 mg/L of three dimensional graphene oxide bounded with nitrogen functional groups, 3DGON, (12 h) to reach the mercury uptake equilibrium when 5 ppm and 0.05 ppm initial mercury concentration were applied respectively in their studies [45,46]. Furthermore, both the adsorbents (23.0 mg/g for Fe_3O_4-GS and 4.5 mg/g for 3DGON respectively) also exhibit lower sorption capacity in relative to the adsorbents synthesized hereby [45,46]. With the use of 250 ppm Hg(II), thymine grafted rGO (rGO-Thy) also showed longer equilibration time (20 min) when 1000 mg/L sorbent dosage was applied to achieve 149.25 mg/g sorption capacity. This finding shows that both the polyamine modified reduced graphene oxide composites in this work are efficient mercury adsorbents in terms of their capability at attaining high sorption capacity with rapid adsorption rate.

3.2.2. Equilibrium study

The influence of different initial Hg^{2+} concentration on the sorption capacity of the prepared adsorbents was investigated in the range of 1.5–11.0 mg/L at pH around 5 in order to probe the adsorption performance for low concentration mercury removal. It should be noted that the sorption capacity of an adsorbent is strongly dependent on the initial Hg (II) concentration used in the equilibrium study. High initial Hg (II) concentration will lead to increased sorption capacity correspondingly due to stronger driving force which overcomes the mass transfer resistance to allow the transport of mercury from the metal ion solution to the surface of the adsorbent for adsorption process to take place [14,15,47]. In order to gain further insight on the adsorption behaviour of the prepared adsorbents towards mercury uptake, the experimental equilibrium data was fitted and studied using Langmuir and Freundlich isotherm models as presented in Fig. 7 a and b. Based on the non-linear regression analysis (Table 3), Freundlich isotherm model was found to be more suitable to describe the adsorption behaviour of the functionalized graphene composites with the goodness of fit > 0.94 achieved under the adsorption conditions studied. Unlike Langmuir isotherm which assumes monolayer sorption, Freundlich isotherm model is broadly used to describe the multilayer adsorption in heterogeneous systems with the adsorption process not limited to formation of monolayer. With the conformity of the high correlation coefficient (R^2) to Freundlich isotherm model, both the adsorbents are found to exhibit a heterogeneous multilayer system during the interaction of Hg(II) in the water. The adsorption intensity, 1/n, is a measure of surface heterogeneity ranges from 0 to 1 with the system becoming more heterogeneous as its value is closer to 0. A smaller 1/n value (< 0.5) was computed for both CM- and HT-rGO-N composites, implying that the interaction between Hg (II) and the adsorbents involved the heterogeneous adsorptive sites with multilayers coverage [48,49]. By employing same hydrothermal method and nitrogen functionalized graphene oxide, the sorption capacity achieved by CM-rGO-N (70 mg/g) is found to be two times higher than the nitrogen grafted 3D graphene oxide foam, 3DGON, (35 mg/g) [45]. Similarly, the magnetic graphene composite (Fe_3O_4-GS) with amino functional group developed by Guo et al. via hydrothermal approach recorded only 23.03 mg/g (> 2 times lesser than HT-rGO-N) [46]. Meanwhile, both the sorption capacity accomplished by CM-rGO-N and HT-rGO-N in this work also outperformed the oxygen and nitrogen enriched chitosan films cross-linked with genipin (2.2 mg/g) and grafted with caffeic acid (4.0 mg/g) prepared by Rocha et al.[15]. These findings clearly demonstrate the potential of the synthesized adsorbents for immobilization of Hg (II) ions

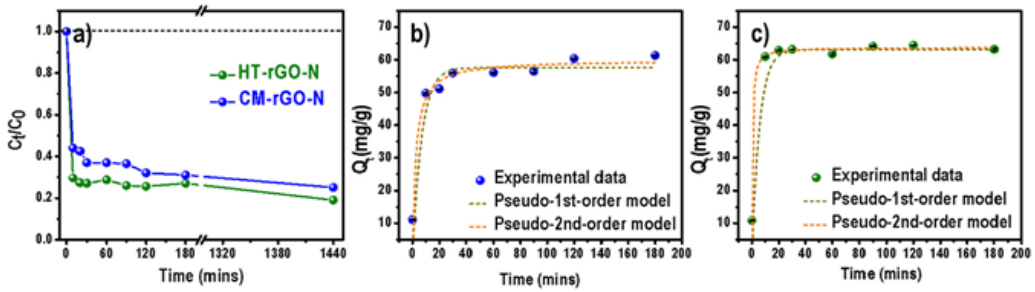

Fig. 6. (a) Variation of normalized concentration of Hg(II) (C_t/C_0) using HT-rGO-N and CM-rGO-N adsorbents with 2.5 mg adsorbent in 20 mL ~ 11 ppm Hg (II) solution at about pH 5 at 23.0 °C. Kinetic modelling of pseudo-first order and pseudo-second order for the experimental data extracted from the sorption process of Hg (II) onto (b) CM-rGO-N and (c) HT-rGO-N composites.

Table 2
Adsorption parameters of pseudo-first order and pseudo-second order kinetic models for Hg(II) adsorption on CM-rGO-N and HT-rGO-N composites.

Kinetic model	Parameter	Adsorbent	
		CM-rGO-N	HT-rGO-N
Pseudo-first order	k_1 (min^{-1})	0.148 ± 0.04	0.175 ± 0.056
	q_e (mg g^{-1})	57.55 ± 2.52	63.09 ± 2.55
	R^2	0.8810	0.9007
Pseudo-second order	k_2 (g mg^{-1} min^{-1})	0.0069 ± 0.0044	0.0359 ± 0.0077
	q_e (mg g^{-1})	59.92 ± 2.93	63.80 ± 2.48
	R^2	0.9091	0.9405

Table 3
Adsorption parameters of Langmuir and Freundlich isotherm models for Hg (II) adsorption on CM-rGO-N and HT-rGO-N.

Isotherm model	Parameter	Adsorbent	
		CM-rGO-N	HT-rGO-N
Langmuir	q_{max} (mg g^{-1})	58.05 ± 7.71	75.80 ± 12.42
	b (L mg^{-1})	3.19 ± 1.50	1.20 ± 0.54
	R^2	0.8158	0.9004
Freundlich	n	3.08 ± 0.39	2.13 ± 0.30
	K ($mg^{1-1/n}$ g^{-1} $L^{1/n}$)	39.45 ± 1.83	39.16 ± 3.00
	R^2	0.9418	0.9443

in wastewater clean-up.

3.2.3. Influence of solution pH

The effect of solution pH towards mercury (II) adsorption by both the adsorbents were investigated in the pH range of 3–9 as depicted in Fig. 7c. Different sorption stages were identified from the pH profiles with the most optimum mercury uptake occurred above pH 5 for both the adsorbents. At acidic pH, it could be evidently observed that CM-rGO-N (~20%) demonstrated significantly lower mercury uptake compared to HT-rGO-N (~70%). This could be associated with the competition of active binding sites between mercury and hydrogen ions as well as the protonation effect of the functional groups on the surface of the adsorbents at lower pH [16]. Meanwhile, both the materials behave similarly in terms of the mercury removal efficiency from the pH around 5 to 9. In order to gain further insight about the effect of the surface charge of the modified rGO composites towards mercury capturing process, an intensive zeta potential study was conducted by dispersing the adsorbents respectively in milli-Q water under different pH conditions as presented in Fig. 7c. From the zeta potential study, both the as-synthesized adsorbents recorded positive zeta potential values below pH 6 which tend to repel the positively charged mercury (II) ions, resulting in the lowest amount of mercury (II) being adsorbed on their positively charged surface. At approximately pH 5, a drastic uptake of mercury is observed for both the adsorbents which could be attributed to the less protonation of the functional groups on their surface as evident by less positive zeta potential values measured, causing a more spontaneous bond formation between the mercury (II) ions and the adsorbents. As the pH further increased to above 6, the electron rich surface of both the adsorbents becomes more negative (< -10 mV) which could be due to the deprotonation of the amine and remaining oxygen groups decorated on the adsorbents which enhances the binding affinity of the Hg (II) ions onto the negatively charged binding sites on the adsorbents. This result is in good agreement with the highest removal efficiency achieved (> 80% for CM-rGO-N; > 90% for HT-rGO-N) from pH 6 to 9 which is beneficial for real application of the prepared adsorbents in the natural water matrix with their pH lies in this region.

3.2.4. Influence of competing ions

In order to assess the feasibility of the developed adsorbents for real water purification treatment, the competitive effects of the adsorbents were examined in a quinary mixture containing Hg (II), Cu (II), Cd (II), Pb (II) and Co (II) ions. The selectivity of the metal ions uptake was studied in two approaches, i.e., the dispersed and solid (freeze-dried for both HT-rGO-N and CM-rGO-N) forms in order to compare their metal removal efficiency under competitive adsorption conditions. In essence, it could be notably visualized from the bar charts (Fig. 8) that both adsorbents have preferential strong binding affinity towards Hg(II), followed by Cu(II) and Pb(II) regardless of the forms of the adsorbents applied in the study. Interestingly, CM-rGO-N showed slightly higher mercury uptake in its solid form (~84%) compared to its dispersed form (~72%), while HT-rGO-N achieved higher mercury removal efficiency in its dispersed form (~86%) compared to its solid form (~79%). This finding was also evinced by a water dispersion study with a better dispersion of HT-rGO-N in water was observed in comparison to CM-rGO-N even after one hour sonication as illustrated in the inset of Fig. 8. It is also markedly to highlight that the metal removal efficiency for both the materials does not differ much irrespective of the sorbent forms (dispersed or freeze dried) applied in the study. This outcome further ascertains the flexibility and the practical application of these developed adsorbents to be applied in the real field operation. Furthermore, a well-established commercial adsorbent, ground activated carbon was also employed to benchmark the performance of the prepared adsorbents in this study. The obtained data revealed that the mercury removal efficiency of activated carbon was stunted with merely ~16% Hg(II) being adsorbed (approximately 4.5 folds lesser Hg (II) removed) in relative to both the adsorbents prepared (~84% for CM-rGO-N and ~79% for HT-rGO-N). This remarkable performance shows that both the prepared adsorbents outperformed the commercial

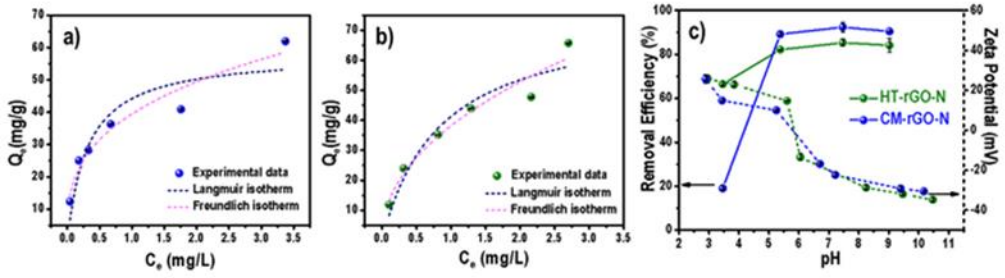

Fig. 7. Equilibrium data of (a) CM-rGO-N and (b) HT-rGO-N adsorbents at initial Hg (II) concentration = 1.5–11 mg/L fitted with Langmuir isotherm and Freundlich isotherm models. Adsorption conditions: sorbent dosage = 125 mg/L, pH ~ 5 at 23.0 °C, (c) Influence of solution pH towards Hg (II) removal efficiency and zeta potential of CM-rGO-N and HT-rGO-N composites measured at different pH. Adsorption conditions: pH = 3–10, initial concentration of Hg (II) ~ 1.5 mg/L, sorbent dosage = 50 mg/L at 23.0 °C.

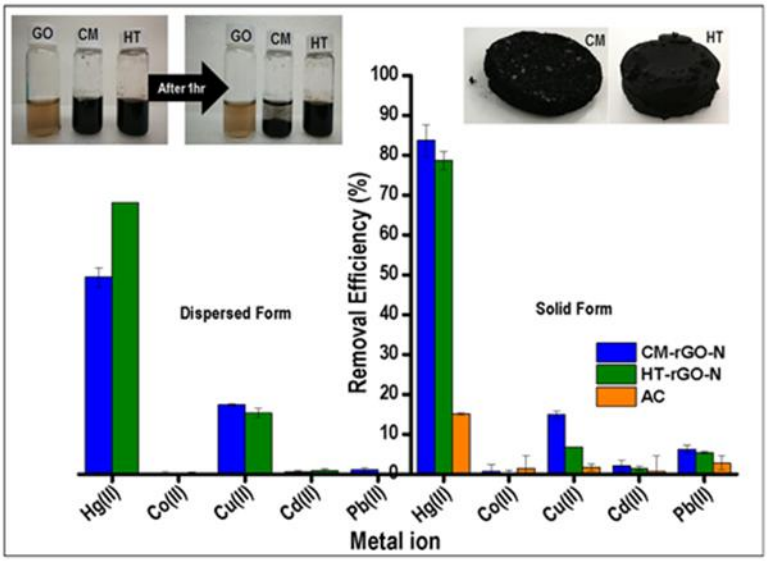

Fig. 8. Comparative study showing influence of competing ions on Hg (II) adsorption using CM-rGO-N, HT-rGO-N, adsorbents and commercial activated carbon (AC) in dispersed and solid forms. The left inset shows the dispersion of CM-rGO-N and HT-rGO-N composites in water after sonication and after 1 h standing; the right inset depicts CM-rGO-N and HT-rGO-N composites after freeze drying. Adsorption conditions: pH = ~5, $[M^{2+}]_i$ = ~5 mg L^{-1}, adsorbent dosage = 2.5 mg, volume of solution = 20 mL, equilibration time = 2 h, T = 22.5 °C.

adsorbent despite the strong competition from the multi-metallic ions solution which could serve as a low-cost alternative to trap Hg(II) ions in the water systems.

3.2.5. Influence of recycling times

The regeneration of the synthesized adsorbents was also investigated after mercury adsorption by desorbing the spent adsorbents respectively in a mixture solution of 2% (w/v) thiourea in 0.1 M HCl as the eluent. As illustrated in Fig. 9a, both the adsorbents still maintained high mercury removal efficiency (> 85%) even after third repeating adsorption–desorption cycle which manifests the reusability of both the adsorbents. This crucial aspect for both the adsorbents could have add-on economic and sustainable environmental values for water purification technology in the long run.

3.2.6. Influence of water matrix

The evaluation of the prepared adsorbents was performed on mercury spiked river and seawater in order to attest the performance of the modified rGO composites under real water conditions as summarized in Fig. 9b. Table S4 tabulates the pH and mercury concentration for the sampled natural waters with < 0.168 μg/L and 1.89 μg/L of mercury found in the river water and seawater respectively prior to mercury spiking. In relative to the water matrix used, it could be observed that both the adsorbents achieved higher removal rate on river water (~89% for CM-rGO-N and ~74% for HT-rGO-N composites) compared to sea water (88.6% for CM-rGO-N and 56.5% for HT-rGO-N composites). Interestingly, the almost identical removal efficiency achieved by CM-rGO-N in both river water and sea water could be associated with the presence of unsaturated active sites since only a low mercury concentration was used. On the other hand, the lower removal efficiency for HT-rGO-N in seawater could be due to the presence of higher flux of ions such as Na^+, Mg^{2+} and Ca^{2+} ions which compete with Hg(II) for active binding sites on the surface of the adsorbent [45]. The presence of negatively charged mercury chloro complexes such as $HgCl_4^{2-}$ and $HgCl_3^-$ due to the large amount of chloride ions in the seawater may repel with the negatively charged binding sites on the adsorbent surface, leading to lower mercury uptake seawater [15].

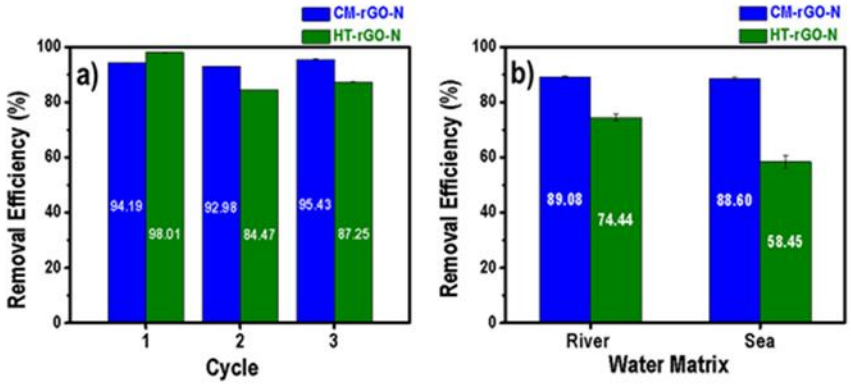

Fig. 9. Influence of (a) recycling times and (b) water matrix on Hg(II) adsorption using CM-rGO-N and HT-rGO-N composites. Adsorption conditions: $[Hg^{2+}]_i$ = ~0.5 mgL^{-1}, volume of solution = 20 mL, equilibration time = 2 h, T = 22.5 °C.

4. Conclusions

In summary, a new and cost-efficient polyamine functionalized rGO adsorbent was successfully prepared using GO and commercial polyamine-precursor followed by their HT and chemical reduction. Reaction mechanism and formation of rich and multiple type of N-containing functional groups on rGO is confirmed by detailed XPS and FTIR analyses. Both the reduction approaches showed identical and high N content (net 5.5 at % from polyamine precursor using XPS analysis; net 6.5 wt% from bulk combustion analysis) grafted on the rGO. The mercury removal efficiency of prepared nitrogen rich rGO composites were systematically investigated over numerous adsorption parameters including influence of contact time, concentration, solution pH, adsorbent form, recycling times and water matrix. Results indicated that composite made by HT reduction (HT-rGO-N) demonstrated slightly better performance than composite made by chemical reduction (CM-rGO-N) in terms of its adsorption capacity in broad range of pH. Both of these materials were found to show high adsorption rate with good fit in the pseudo-second order and Freundlich isotherm models towards Hg (II) removal. > 70% selectivity towards Hg(II) achieved in multi-metallic solutions containing Hg(II), Cd(II), Co(II), Cu(II), and Pb(II) for both of these adsorbents with CM-rGO-N performed better in its solid form than in dispersed form while HT-rGO-N exhibited higher mercury removal in its dispersed form than the solid form. Both of these adsorbents also surpassed the commercial activated carbon with only ~ 16% mercury removed and achieved > 85% removal even after three recycling times. They also demonstrated better performance for mercury removal in river water and seawater correspondingly which was advantageous towards water purification in natural waters. In essence, this work contributes to the development of facile and cost-efficient water remediation solution which can be potentially translated into industrial scale application using inexpensive and commercially available polyamine crosslinker via green one-step scalable modification approach.

Acknowledgements

This work was supported by the ARC Research Hub for Graphene Enabled Industry Transformation [IH150100003]. The authors thank Australian Microscopy and Microanalysis Research Facility (AMMRF), Adelaide microscopy for access of SEM-EDX and ICP-MS facilities.

Appendix A. Supplementary material

Characterization details for the samples prepared in this work, Table of Chemical composition of polyamine precursor, SEM image of GO, EDX spectra of HT-rGO-N and CM-rGO-N, Plots of UV-Vis, FTIR, Raman, TGA-DTA and XRD of GO and control samples, Table of normalized chemical composition of samples from XPS analysis, Plots of survey spectra (control and polyamine modified rGO composites) and C1s high resolution spectra of control samples, comparison table of Hg (II) performance, table of mercury (II) concentration and pH for river water and seawater used are included. Supplementary data to this article can be found online at https://doi.org/10.1016/j.seppur.2019.116441.

References

[1] J. Xu, Z. Cao, Y. Zhang, Z. Yuan, Z. Lou, X. Xu, X. Wang, A review of functionalized carbon nanotubes and graphene for heavy metal adsorption from water: preparation, application, and mechanism, Chemosphere 195 (2018) 351–364.
[2] Minamata convention on mercury, in: U. Nations (Ed.) Kumamoto, Japan, 2017.
[3] World Health Organization, Exposure to mercury: a major public health concern, 2007.
[4] P.H. Gleick, Water resources, Encyclopedia of climate and weather, 1996, pp. 817–823.
[5] J.-G. Yu, B.-Y. Yue, X.-W. Wu, Q. Liu, F.-P. Jiao, X.-Y. Jiang, X.-Q. Chen, Removal of mercury by adsorption: a review, Environ Sci. Pollut. R. 23 (2016) 5056–5076.
[6] N. Yousefi, X. Lu, M. Elimelech, N. Tufenkji, Environmental performance of graphene-based 3D macrostructures, Nat Nanotechnol. 14 (2019) 107–119.
[7] M. Sweetman, S. May, N. Mebberson, P. Pendleton, K. Vasilev, S. Plush, J. Hayball, Activated carbon, carbon nanotubes and graphene: materials and composites for advanced water purification, C—J. Carbon Res. 3 (2017) 18.
[8] K.S.K. Reddy, A.A. Shoaibi, C. Srinivasakannan, Mercury removal using metal sulfide porous carbon complex, Process Saf. Environ. Prot. 114 (2018) 153–158.
[9] Y. Cao, X. Li, Adsorption of graphene for the removal of inorganic pollutants in water purification: a review, Adsorption 20 (2014) 713–727.
[10] H. Sadegh, G.A.M. Ali, V.K. Gupta, A.S.H. Makhlouf, R. Shahryari-ghoshekandi, M.N. Nadagouda, M. Sillanpää, E. Megiel, The role of nanomaterials as effective adsorbents and their applications in wastewater treatment, J. Nanostructure Chem. 7 (2017) 1–14.
[11] F.S. Awad, K.M. AbouZeid, W.M.A. El-Maaty, A.M. El-Wakil, M.S. El-Shall, Efficient removal of heavy metals from polluted water with high selectivity for mercury(II) by 2-Imino-4-thiobiuret–partially reduced graphene oxide (IT-PRGO), ACS Appl. Mater. Interfaces 9 (2017) 34230–34242.
[12] C. Zhou, H. Zhu, Q. Wang, J.X. Wang, J. Cheng, Y.F. Guo, X.J. Zhou, R.B. Bai, Adsorption of mercury (II) with an Fe_3O_4 magnetic polypyrrole-graphene oxide nanocomposite, RSC Adv. 7 (2017) 18466–18479.
[13] S. Thakur, G. Das, P.K. Raul, N. Karak, Green one-step approach to prepare sulfur/reduced graphene oxide nanohybrid for effective mercury ions removal, J. Phys. Chem. C 117 (2013) 7636–7642.
[14] N. Ballav, R. Das, S. Giri, A.M. Muliwa, K. Pillay, A. Maity, L-cysteine doped polypyrrole (PPy@L-Cyst): a super adsorbent for the rapid removal of Hg^{+2} and efficient catalytic activity of the spent adsorbent for reuse, Chem. Eng. J. 345 (2018) 621–630.
[15] L.S. Rocha, Â. Almeida, C. Nunes, B. Henriques, M.A. Coimbra, C.B. Lopes, C.M. Silva, A.C. Duarte, E. Pereira, Simple and effective chitosan based films for the removal of Hg from waters: equilibrium, kinetic and ionic competition, Chem. Eng. J. 300 (2016) 217–229.
[16] P.L. Yap, S. Kabiri, D.N.H. Tran, D. Losic, Multifunctional binding chemistry on modified graphene composite for selective and highly efficient adsorption of mercury, ACS Appl. Mater. Interfaces 11 (2019) 6350–6362.
[17] T. Gao, J. Yu, Y. Zhou, X. Jiang, The synthesis of graphene oxide functionalized with dithiocarbamate group and its prominent performance on adsorption of lead ions, J. Taiwan Inst. Chem. E. 71 (2017) 426–432.
[18] T.T. Tung, R. Karunagaran, D.N.H. Tran, B. Gao, S. Nag-Chowdhury, I. Pillin, M. Castro, J.-F. Feller, D. Losic, Engineering of graphene/epoxy nanocomposites with improved distribution of graphene nanosheets for advanced piezo-resistive mechanical sensing, J. Mater. Chem. C 4 (2016) 3422–3430.
[19] D.N. Tran, S. Kabiri, L. Wang, D. Losic, Engineered graphene–nanoparticle aerogel composites for efficient removal of phosphate from water, J. Mater. Chem. A 3 (2015) 6844–6852.
[20] S.K. Lagergren, About the theory of so-called adsorption of soluble substances, Sven. Vetenskapsakad. Handingarl 24 (1898) 1–39.
[21] Y.S. Ho, G. McKay, Pseudo-second order model for sSorption processes, Process Biochem. 34 (1999) 451–465.
[22] I. Langmuir, The adsorption of gases on plane surfaces of glass, mica and platinum, J. Am. Chem. Soc. 40 (1918) 1361–1403.
[23] H. Freundlich, Over the adsorption in solution, Z. Phys. Chem. (1906) 385–470.
[24] S. Stankovich, D.A. Dikin, R.D. Piner, K.A. Kohlhaas, A. Kleinhammes, Y. Jia, Y. Wu, S.T. Nguyen, R.S. Ruoff, Synthesis of graphene-based nanosheets via chemical reduction of exfoliated graphite oxide, Carbon 45 (2007) 1558–1565.
[25] X. Cui, X. Fang, H. Zhao, Z. Li, H. Ren, An electrochemical sensor for dopamine based on polydopamine modified reduced graphene oxide anchored with tin dioxide and gold nanoparticles, Anal. Methods 9 (2017) 5322–5332.
[26] N. Morimoto, T. Kubo, Y. Nishina, Tailoring the oxygen content of graphite and reduced graphene oxide for specific applications, Sci. Rep. 6 (2016) 21715.
[27] G. Eda, M. Chhowalla, Chemically derived graphene oxide: towards large-area thin-film electronics and optoelectronics, Adv. Mater. 22 (2010) 2392–2415.
[28] H. Xie, S. Tang, Z. Gong, S. Vongehr, F. Fang, M. Li, X. Meng, 3D nitrogen-doped graphene/$Co(OH)_2$-nanoplate composites for high-performance electrochemical pseudocapacitors, RSC Adv. 4 (2014) 61753–61758.
[29] J. Ederer, P. Janoš, P. Ecorchard, J. Tolasz, V. Štengl, H. Beneš, M. Perchacz, O. Pop-Georgievski, Determination of amino groups on functionalized graphene oxide for polyurethane nanomaterials: XPS quantitation vs. functional speciation, RSC Adv. 7 (2017) 12464–12473.
[30] H. Park, S. Hyun Noh, J. Hye Lee, W. Jun Lee, J. Yun Jaung, S. Geol Lee, T. Hee Han, Large scale synthesis and light emitting fibers of tailor-made graphene quantum dots, Sci. Rep. 5 (2015) 14163.
[31] B. Yu, X. Wang, X. Qian, W. Xing, H. Yang, L. Ma, Y. Lin, S. Jiang, L. Song, Y. Hu, S. Lo, Functionalized graphene oxide/phosphoramide oligomer hybrids flame retardant prepared via in situ polymerization for improving the fire safety of polypropylene, RSC Adv. 4 (2014) 31782–31794.
[32] A. Ghosh, S. Raha, S. Dey, K. Chatterjee, A. Roy Chowdhury, A. Barui, Chemometric analysis of integrated FTIR and Raman spectra obtained by non-invasive exfoliative cytology for the screening of oral cancer, Analyst 144 (2019) 1309–1325.
[33] S. Kabiri, D.N. Tran, M.A. Cole, D. Losic, Functionalized three-dimensional (3D) graphene composite for high efficiency removal of mercury, Environ. Sci.: Water Res. Technol 2 (2016) 390–402.
[34] N. Wu, X. She, D. Yang, X. Wu, F. Su, Y. Chen, Synthesis of network reduced graphene oxide in polystyrene matrix by a two-step reduction method for superior conductivity of the composite, J. Mater. Chem. 22 (2012) 17254–17261.
[35] D.N.H. Tran, S. Kabiri, D. Losic, A green approach for the reduction of graphene oxide nanosheets using non-aromatic amino acids, Carbon 76 (2014) 193–202.

[36] D. Hou, Q. Liu, X. Wang, Y. Quan, Z. Qiao, L. Yu, S. Ding, Facile synthesis of graphene via reduction of graphene oxide by artemisinin in ethanol, J. Materiomics 4 (2018) 256–265.
[37] K. Dave, K.H. Park, M. Dhayal, Two-step process for programmable removal of oxygen functionalities of graphene oxide: functional, structural and electrical characteristics, RSC Adv. 5 (2015) 95657–95665.
[38] H. Min, P.-L. Girard-Lauriault, T. Gross, A. Lippitz, P. Dietrich, W.E.S. Unger, Ambient-ageing processes in amine self-assembled monolayers on microarray slides as studied by ToF-SIMS with principal component analysis, XPS, and NEXAFS spectroscopy, Anal. Bioanal. Chem. 403 (2012) 613–623.
[39] L. Wang, Q. Yao, H. Bi, F. Huang, Q. Wang, L. Chen, PANI/graphene nanocomposite films with high thermoelectric properties by enhanced molecular ordering, J. Mater. Chem. A 3 (2015) 7086–7092.
[40] J. Xu, S. He, H. Zhang, J. Huang, H. Lin, X. Wang, J. Long, Layered metal-organic framework/graphene nanoarchitectures for organic photosynthesis under visible light, J. Mater. Chem. A 3 (2015) 24261–24271.
[41] T. Susi, T. Pichler, P. Ayala, X-ray photoelectron spectroscopy of graphitic carbon nanomaterials doped with heteroatoms, Beilstein J. Nanotechnol. 6 (2015) 177–192.
[42] M.R. Saeb, E. Bakhshandeh, H.A. Khonakdar, E. Mäder, C. Scheffler, G. Heinrich, Cure kinetics of epoxy nanocomposites affected by MWCNTs functionalization: a review, Sci. World J. 2013 (2013) 14.
[43] E.J.C. Amieva, J. López-Barroso, A.L. Martínez-Hernández, C. Velasco-Santos, Graphene-based materials functionalization with natural polymeric biomolecules, Recent Advances in Graphene Research, In Tech, 2016.
[44] M. Liu, Z. Tao, H. Wang, F. Zhao, Q. Sun, Study on the adsorption of Hg(II) by one-pot synthesis of amino-functionalized graphene oxide decorated with a Fe_3O_4 microsphere nanocomposite, RSC Adv. 6 (2016) 84573–84586.
[45] B. Henriques, G. Gonçalves, N. Emami, E. Pereira, M. Vila, P.A.A.P. Marques, Optimized graphene oxide foam with enhanced performance and high selectivity for mercury removal from water, J. Hazard. Mater. 301 (2016) 453–461.
[46] X. Guo, B. Du, Q. Wei, J. Yang, L. Hu, L. Yan, W. Xu, Synthesis of amino functionalized magnetic graphenes composite material and its application to remove Cr (VI), Pb(II), Hg(II), Cd(II) and Ni(II) from contaminated water, J. Hazard. Mater. 278 (2014) 211–220.
[47] H. Aydın, Y. Bulut, Ç. Yerlikaya, Removal of copper (II) from aqueous solution by adsorption onto low-cost adsorbents, J. Environ. Manage. 87 (2008) 37–45.
[48] L. Cui, Y. Wang, L. Gao, L. Hu, L. Yan, Q. Wei, B. Du, EDTA functionalized magnetic graphene oxide for removal of Pb(II), Hg(II) and Cu(II) in water treatment: adsorption mechanism and separation property, Chem. Eng. J. 281 (2015) 1–10.
[49] K.Y. Foo, B.H. Hameed, Insights into the modeling of adsorption isotherm systems, Chem. Eng. J. 156 (2010) 2–10.

Supplementary Material

Polyamine-modified reduced graphene oxide: a new and cost-effective adsorbent for efficient removal of mercury in waters

Pei Lay Yap[a,b], *Tran Thanh Tung* [a,b], *Shervin Kabiri*[c], *Nicola Matulick*[a,b], *Diana, N.H. Tran*[a,b] *and Dusan Losic**[a,b]

[a] School of Chemical Engineering and Advanced Materials, The University of Adelaide, Adelaide, SA 5005, Australia

[b]ARC Hub for Graphene Enabled Industry Transformation, The University of Adelaide, Adelaide, SA 5005, Australia

[c]School of Agriculture, Food and Wine, The University of Adelaide, PMB 1, Waite Campus, Glen Osmond, SA 5064, Australia

**Corresponding author:* dusan.losic@adelaide.edu.au

Materials Characterization

The prepared samples were characterized by several techniques including scanning electron microscopy equipped with EDX Silicon Drift Detectors (FE-SEM, Quanta 450 FEG, FEI, USA; EDX, Ultim Max 170mm SDD, Oxford Instruments, UK) to study the morphology and elemental distribution of the materials. TEM technique (TEM, Tecnai G2 Spirit) was also applied to study the morphology of the pre- and post-polyamine functionalized rGO composites using drop casting method on the TEM grid.

Elemental analysis of the samples were performed using a Perkin Elmer 2400 series II CHNS/O Elemental Analyzer in CHNS configuration. The combined combustion/reduction tube was packed using Perkin Elmer EA6000 and Perkin Elmer 'Hi-Purity' copper with a reaction temperature of 975°C. Results were calibrated to 2mg of Perkin Elmer Organic Analytical Standard of Cystine (formula: $(SCH_2CH(NH_2)CO_2H)_2$) with known abundances of carbon (29.99%), hydrogen (5.07%), nitrogen (11.67%) and sulphur (26.69%). The accepted error range between standards was ±0.3 % for carbon, hydrogen and nitrogen and ±0.39 % for sulphur calculated against 12 replicates.

The specific surface area (SSA) of the materials was determined via methylene blue (MB) adsorption method using UV-Vis spectroscopy (Shimadzu UV-1601, Japan) as described in our previous work [1, 2].

Fourier Transform Infrared spectroscopy (FTIR, Nicolet 6700, Thermo Fisher) in the range of 500-4000 cm^{-1} was recorded to detect the functional groups present in the materials. Raman spectroscopy (LabRAM HR Evolution, Horiba Jvon Yvon Technology, Japan) with a 532 nm laser (mpc 3000) as excitation source was used to determine the vibrational characteristics of the materials. All the spectra were collected with an integration time of 10 seconds each on 3 different

spots. The X-ray diffraction (600 Miniflex, Rigaco, Japan) was used to unveil the composition of the materials in the range of 2θ = 5-80° at 40 kV and 15 mA with the scan speed of $10^{\circ}min^{-1}$. Thermal decomposition of the samples was studied using thermogravimetric analysis (TGA/DSC 2, STAR^{e} System, Mettler Toledo, Switzerland) under nitrogen atmosphere with the samples heated to 1000 °C at a heating rate of 10 °C min^{-1}.

XPS measurement was performed using AXIS Ultra_DLD (Kratos, UK) equipped with a monochromatic Al Kα radiation source (hv =1486.7 eV) at 225 W, 15 kV and 15 mA. XPS wide scans were carried out at 0.5 eV step size over -10-1100 eV at the pass energy of 160 eV while the narrow scans were acquired at a 0.1 eV step size and pass energy of 20 eV. The deconvolution and fitting of peaks were performed using Casa XPS^{TM} software. The binding energy scale was calibrated with the primary peak (C-C/C-H peak) of adventitious carbon at 285.0 eV; the full width at half maximum (fwhm) for all component peaks were constrained within the difference of ± 0.2 eV.

The zeta potential of the prepared adsorbent was measured as a function of pH in triplicate using a Malvern Zetasizer (Nanoseries, Australia). The adsorbent was dispersed in Milli-Q water with the pH of the mixture adjusted using HCl or NaOH in the range of 3-10. Solution ICP-MS (QQQ 8900, Agilent) was used to measure the remaining concentration of Hg(II) solution after the adsorption experiments.

Table S1. Main chemical composition of commercial polyamine precursor (West System 205 Fast Hardener)*

Chemical identity	Concentration (%)
Product of triethylenetetramine with phenol and formaldehyde	45-70

polyethylenepolyamines	10-30
triethylenetetramine	5-13
Triethylenetetramine, reaction product with propylene oxide	5-10
tetraethylenepentamine	3-10
hydroxybenzene	1-7

*The exact chemical identity and concentration is held as confidential business information (CBI).

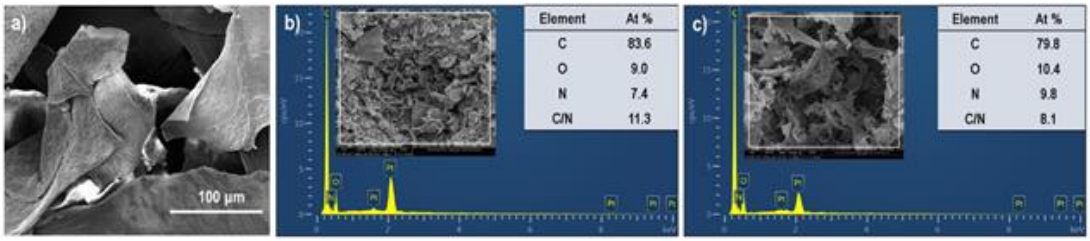

Fig. S1. (a) SEM image of GO, EDX spectra and normalized atomic percentage for (b) HT-rGO-N and (c) CM-rGO-N.

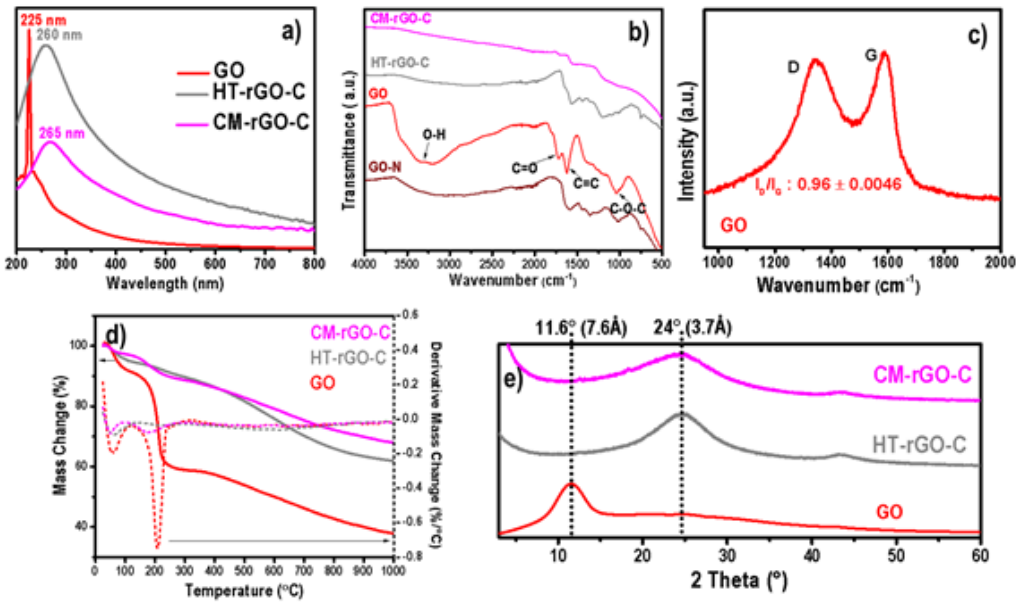

Fig. S2. Plots of (a) UV-Vis, (b) FTIR, (c) Raman, (d) TGA-DTA and (e) XRD of GO and control samples.

Table S2. Normalized chemical composition of samples determined from their respective XPS survey curves (Fig. S3 and Fig. 6) in atomic %.

Element	Atomic %		
	C	O	N
GO	71.11	28.89	0
HT-rGO-C	82.40	17.60	0
HT-rGO-N	81.92	12.60	5.47
CM-rGO-C	82.99	14.17	2.83
CM-rGO-N	80.10	11.60	8.28

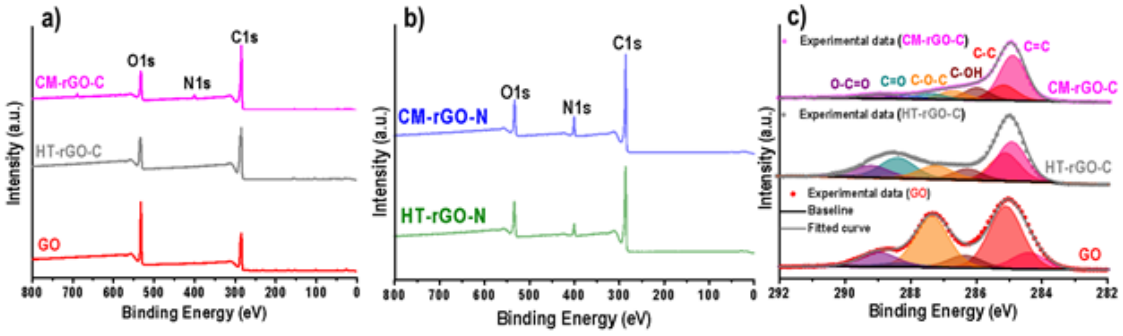

Fig. S3. Plots of XPS survey scan of (a) GO and control samples, (b) polyamine modified rGO composites and (c) C1s high resolution scan of GO and control samples. Fitting of C1s high resolution spectrum for GO, HT-rGO-C and CM-rGO-C show characteristic of GO peaks centered around 284.4eV, 285.1 eV, 286.3 eV, 287.3 eV, 288.4 eV and 289.0 eV which can be assigned to C=C, C-C, C-OH, C-O-C, C=O and O-C=O respectively [3, 4].

Table S3. Comparison of Hg (II) adsorption kinetics conditions and performance of various adsorbents.

Type of Adsorbent	Specific surface area ($m^2\ g^{-1}$)	Time to reach equilibrium	Initial Hg (II) concentration (mg/ L)	Sorbent dosage in Hg (II) solution (mg/ L)	T (°C)	pH	Sorption capacity q_e* (mg/ g)	Ref
HT-rGO-N	63[a]	10 mins	11	125	23.0	5.3	70.4	**This work**
CM-rGO-N	270[a]	10 mins	11	125	23.0	5.3	67.1	**This work**
EDA-Fe_3O_4/GO	97.56[b]	10 mins	8	200	25	5.3	25.57	[5]
3DGON	400[b]	12 hrs	0.05	10	21.0	4.5	4.5	[6]
Amino functionalised graphene composites (Fe_3O_4-GS)	62.43[b]	120 mins	5	200	25.0	NA	23.03	[7]

Thymine grafted rGO (rGO-Thy)	N.A.	20 mins	250	1000	NA	6	149.25	[8]

q_e determined using pseudo second order model

[a] corresponds to methylene blue adsorption method and [b] refers to Brunauer–Emmett–Teller (BET) method for specific surface area determination

N.A.- Not Available

Table S4. Mercury (II) concentration and pH of river water and seawater used in the sorption experiments.

Type of water matrix	River water	Seawater
pH	8.17	8.13
Temperature (˚C)	21.50	20.40
[Hg (II)], μg/L	< 0.168	1.89

References

[1] P.L. Yap, S. Kabiri, D.N.H. Tran, D. Losic, Multifunctional binding chemistry on modified graphene composite for selective and highly efficient adsorption of mercury, ACS Appl. Mater. Interfaces 11 (2019) 6350-6362.

[2] D.N. Tran, S. Kabiri, L. Wang, D. Losic, Engineered graphene–nanoparticle aerogel composites for efficient removal of phosphate from water, J. Mater. Chem. A 3 (2015) 6844-6852.

[3] F. Baskoro, C.-B. Wong, S.R. Kumar, C.-W. Chang, C.-H. Chen, D.W. Chen, S.J. Lue, Graphene oxide-cation interaction: inter-layer spacing and zeta potential changes in response to various salt solutions, J. Membr. Sci. 554 (2018) 253-263.

[4] B. Lesiak, L. Kövér, J. Tóth, J. Zemek, P. Jiricek, A. Kromka, N. Rangam, C sp2/sp3 hybridisations in carbon nanomaterials – XPS and (X)AES study, Appl. Surf. Sci. 452 (2018) 223-231.

[5] M. Liu, Z. Tao, H. Wang, F. Zhao, Q. Sun, Study on the adsorption of Hg(II) by one-pot synthesis of amino-functionalized graphene oxide decorated with a Fe_3O_4 microsphere nanocomposite, RSC Adv. 6 (2016) 84573-84586.

[6] B. Henriques, G. Gonçalves, N. Emami, E. Pereira, M. Vila, P.A.A.P. Marques, Optimized graphene oxide foam with enhanced performance and high selectivity for mercury removal from water, J. Hazard. Mater. 301 (2016) 453-461.

[7] X. Guo, B. Du, Q. Wei, J. Yang, L. Hu, L. Yan, W. Xu, Synthesis of amino functionalized magnetic graphenes composite material and its application to remove Cr(VI), Pb(II), Hg(II), Cd(II) and Ni(II) from contaminated water, J. Hazard. Mater. 278 (2014) 211-220.

[8] L. Liu, L. Ding, X. Wu, F. Deng, R. Kang, X. Luo, Enhancing the Hg(II) removal efficiency from real wastewater by novel thymine-grafted reduced graphene oxide complexes, Ind. Eng. Chem. Res. 55 (2016) 6845-6853.

CHAPTER 5

FUNCTIONALIZED GRAPHENE COMPOSITES VIA THERMAL THIOL-ENE CLICK APPROACH FOR WATER PURIFICATION

5. FUNCTIONALIZED GRAPHENE COMPOSITES VIA THERMAL THIOL-ENE CLICK APPROACH FOR WATER PURIFICATION

5.1. Overview and Significance of Work

Production process of the commercial adsorbent (AC) is energy-intensive and inefficient to remove residual mercury at low concentration in water systems even after conventional water treatment. Engineering of functionalized graphene composites is demonstrated using cysteamine (sulfur- and nitrogen-containing precursor) through a thermal thiol-ene click approach. This work targets to:

- develop a mild, low energy, environmentally friendly and scalable production method for an adsorbent, and
- design an adsorbent with a fast adsorption rate, high affinity and selectivity towards removing low concentrations of mercury in water

Findings from this work accomplished Objectives 3 and 4, which are colligated in a published peer-reviewed research article.

5.2. Statement of Authorship

Statement of Authorship

Title of Paper	Multifunctional binding chemistry on modified graphene composite for selective and highly efficient adsorption of mercury
Publication Status	☒ Published ☐ Accepted for Publication ☐ Submitted for Publication ☐ Unpublished and Unsubmitted w ork w ritten in manuscript style
Publication Details	Yap, P. L., Kabiri, S., Tran, D. N. H., & Losic, D. (2019). Multifunctional binding chemistry on modified graphene composite for selective and highly efficient adsorption of mercury. ACS Applied Materials & Interfaces, 11(6), 6350-6362.

Principal Author

Name of Principal Author (Candidate)	Pei Lay Yap		
Contribution to the Paper	Prepared, characterized and conducted performance testing on all the samples, interpreted data as well as wrote the manuscripts		
Overall percentage (%)	85%		
Certification:	This paper reports on original research I conducted during the period of my Higher Degree by Research candidature and is not subject to any obligations or contractual agreements with a third party that would constrain its inclusion in this thesis. I am the primary author of this paper.		
Signature		Date	01/10/20

Co-Author Contributions

By signing the Statement of Authorship, each author certifies that:

i. the candidate's stated contribution to the publication is accurate (as detailed above);

ii. permission is granted for the candidate in include the publication in the thesis; and

iii. the sum of all co-author contributions is equal to 100% less the candidate's stated contribution.

Name of Co-Author	Shervin Kabiri		
Contribution to the Paper	Helped in data intepretation, edited and revised the manuscript.		
Signature		Date	02/10/20

Name of Co-Author	Diana N.H. Tran		
Contribution to the Paper	Co-supervised and revised the manuscript.		
Signature		Date	02/10/20

Please cut and paste additional co-author panels here as required.

Statement of Authorship

Title of Paper	Multifunctional binding chemistry on modified graphene composite for selective and highly efficient adsorption of mercury
Publication Status	☒ Published ☐ Accepted for Publication ☐ Submitted for Publication ☐ Unpublished and Unsubmitted w ork w ritten in manuscript style
Publication Details	Yap, P. L., Kabiri, S., Tran, D. N. H., & Losic, D. (2019). Multifunctional binding chemistry on modified graphene composite for selective and highly efficient adsorption of mercury. ACS Applied Materials & Interfaces, 11(6), 6350-6362.

Principal Author

Name of Principal Author (Candidate)	Pei Lay Yap		
Contribution to the Paper	Prepared, characterized and conducted performance testing on all the samples, interpreted data as well as wrote the manuscripts		
Overall percentage (%)	85%		
Certification:	This paper reports on original research I conducted during the period of my Higher Degree by Research candidature and is not subject to any obligations or contractual agreements with a third party that would constrain its inclusion in this thesis. I am the primary author of this paper.		
Signature		Date	07/10/20

Co-Author Contributions

By signing the Statement of Authorship, each author certifies that:

i. the candidate's stated contribution to the publication is accurate (as detailed above);

ii. permission is granted for the candidate in include the publication in the thesis; and

iii. the sum of all co-author contributions is equal to 100% less the candidate's stated contribution.

Name of Co-Author	Dusan Losic		
Contribution to the Paper	Supervised the development of work, edited, revised the manuscript and acted as the corresponding author.		
Signature		Date	07/10/20

Name of Co-Author			
Contribution to the Paper			
Signature		Date	

Please cut and paste additional co-author panels here as required.

5.3. Published work

This section is presented as a published article as ***Yap, P. L.***, *Kabiri, S., Tran, D. N. H., & Losic, D. (2019). Multifunctional binding chemistry on modified graphene composite for selective and highly efficient adsorption of mercury. ACS Applied Materials & Interfaces, 11(6), 6350-6362.* Reproduced with permission.[14] Copyright (2019) American Chemical Society.

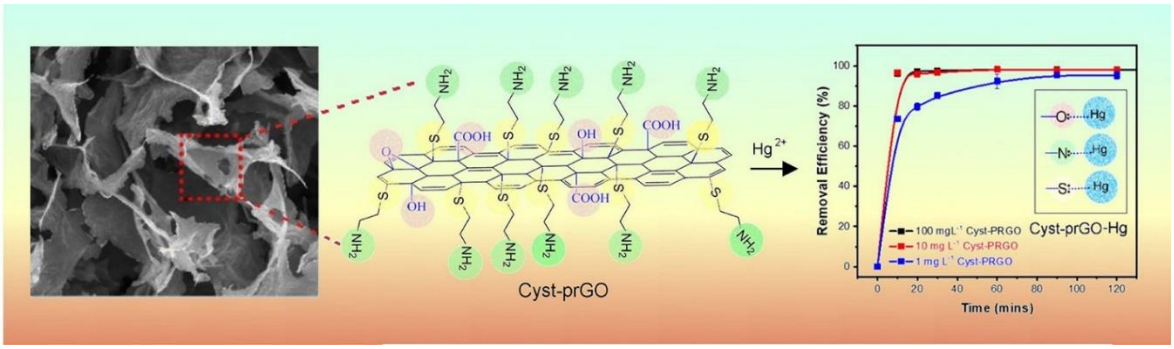

Figure 14. Graphical abstract of "*Multifunctional binding chemistry on modified graphene composite for selective and highly efficient adsorption of mercury*". *Reproduced with permission.[14] Copyright (2019) American Chemical Society.*

ACS APPLIED MATERIALS & INTERFACES

Research Article

Cite This: ACS Appl. Mater. Interfaces 2019, 11, 6350−6362

www.acsami.org

Multifunctional Binding Chemistry on Modified Graphene Composite for Selective and Highly Efficient Adsorption of Mercury

Pei Lay Yap,[†,‡] Shervin Kabiri,[†,‡] Diana N. H. Tran,[†,‡] and Dusan Losic*[,†,‡]

[†]School of Chemical Engineering, The University of Adelaide, Adelaide, South Australia 5005, Australia

[‡]ARC Hub for Graphene Enabled Industry Transformation, The University of Adelaide, Adelaide, South Australia 5005, Australia

Supporting Information

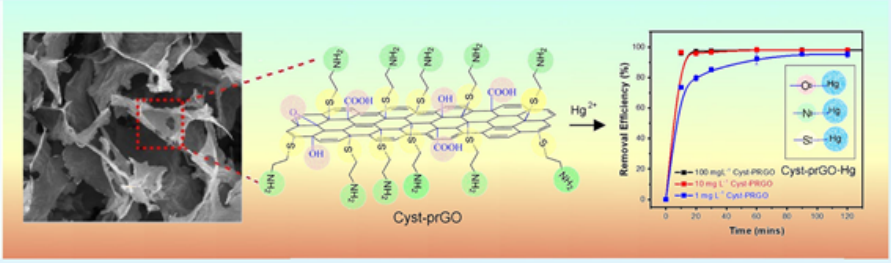

ABSTRACT: Engineering of multifunctional binding chemistry on graphene composites using thiol−ene click reaction for selective and highly efficient adsorption of mercury(II) is demonstrated. Graphene oxide (GO) is used as an initial material for covalent attachment of cysteamine molecules by thiol−ene click reaction on C═C groups to achieve a partially reduced graphene surface with multiple binding chemistry such as O, S, and N. Batch adsorption studies showed remarkable adsorption rate with only 1 mg L^{-1} dosage of adsorbent used to remove 95% Hg (II) (~1.5 mg L^{-1}) within 90 min. The high adsorption capacity of 169 ± 19 mg g^{-1}, high selectivity toward Hg in the presence of 30 times higher concentration of competing ions (Cd, Cu, Pb) and high regeneration ability (>97%) for five consecutive adsorption−desorption cycles were achieved. Comparative study with commercial activated carbon using spiked Hg (II) river water confirmed the high performance and potential of this adsorbent for real mercury remediation of environmental and drinking waters.

KEYWORDS: *thiol−ene, cysteamine, graphene oxide, mercury, adsorbent, adsorption*

1. INTRODUCTION

The increasing level of heavy metals in our environment caused by rapid industrialization and population growth with their high toxicity and bioaccumulation is causing serious global concerns. Numerous conventional water purification technologies including precipitation, membrane filtration, reduction, ion exchange, and adsorption have been commonly used to remove heavy metals from aqueous systems.[1,2] However, most of these technologies are ineffective particularly when facing the removal of very low concentration of heavy metals (ppb level) such as mercury. To address this challenging problem, the adsorption process emerged as a promising method to be used alone or combined with conventional methods. Thus far, activated carbons and synthetic silica mesoporous materials (MCM-41 and SBA-15) are the most successful adsorbents that are developed and commercially available on the market.[3−5] However, these adsorbents have some disadvantages including lack of selectivity, versatility, high cost, energy- and labor-intensive, as well as their production involving the use and waste of toxic materials. To address these limitations, the development of new adsorbents with chemical versatility based on natural or waste materials such as, graphite, zeolites, clays, starch, fly ash, chitosan, etc. with sustainable and green production is recognized as a favorable approach.[6]

Graphene with a unique 2D structure which can be produced at large scale from cheap raw material (graphite), having large specific surface area, ability to tailor surface chemistry, and designed in different 3D forms has received considerable interest for the development of advanced adsorbents in heavy metals removal.[7,8] Many approaches using graphene materials including graphene oxide (GO), reduced graphene oxide (rGO), pristine graphene and their composites with nanoparticles and polymers in different forms of 3D composites (hydrogels, aerogels, foams, and membranes) have been explored.[6,9−11] GO having high density of different oxygen functional groups (i.e., carboxyl, phenol, lactone) with strong electron donating property and binding affinity toward heavy metals including mercury has been in particular an attractive choice.[11] In addition to oxygen functionalities, GO can be modified with specific functional groups containing sulfur, nitrogen, phosphorus through doping

Received: October 1, 2018
Accepted: December 3, 2018
Published: December 3, 2018

DOI: 10.1021/acsami.8b17131
ACS Appl. Mater. Interfaces 2019, 11, 6350−6362

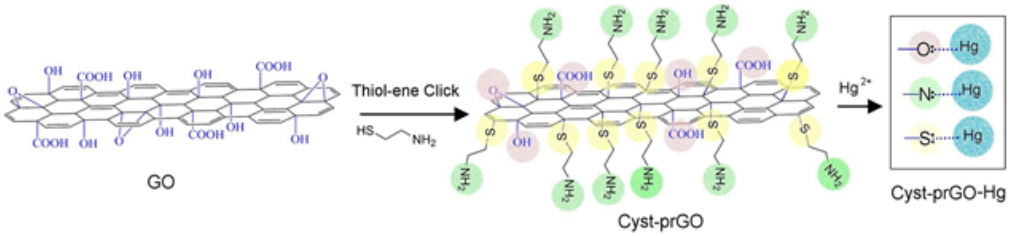

Figure 1. Schematic illustration of the functionalization of GO with thiol−ene click reaction to achieve a graphene composite with multifunctional binding chemistry for high performing adsorption of mercury.

or covalent immobilization providing new prospects to design advanced adsorbents with high adsorption capacity and selectivity for heavy metals.[6] Kumar et al. used this idea in their work to make graphene oxide-L-cystine adsorbent via the reaction between amino group bound in L-cysteine with hydroxyl and carboxyl groups on GO showing the maximum adsorption capacity of 79.36 mg g^{-1} for mercury.[12] In their latter work, the synthesis of GO-MBT (2-mercaptobenzothiazole) adsorbent through the reaction between the carbonyl groups (after chlorination with $SOCl_2$) on GO with MBT was demonstrated which outperformed their previous work recording an adsorption capacity of 107.52 mg g^{-1} for mercury.[13] In a study reported by Aghdam et al., a high maximum adsorption capacity of 282.7 mg g^{-1} was determined when a series of multistep reaction between GO with divinyl sulfone, allyl acetoacetate and *N*,*N*-dimethyl acrylamide was carried out to fabricate poly(allyl acetoacetate)-grafted graphene oxide (GO-GAA).[14]

To combine a synthetic polymer grafted with specific functional groups on the GO surface, another approach has been reported to increase the specific surface chemistry to improve the adsorption capacity of mercury to 277.0 mg g^{-1}.[15] Most of these functionalization with polymers have also been achieved via the reaction of polymers with the oxygen functional groups (carboxyls, hydroxyls or carbonyls) on GO which limits their involvement in the adsorption process. In our previous studies, we demonstrated the development of a unique 3D graphene hybrid composite decorated with iron nanoparticles interconnected with diatom silica (graphene-DE-αFeOOH) microparticles[6] that was then modified with silane chemistry using 3-mercaptopropyltrimethoxysilane (graphene-DE-αFeOOH-SH)[9] to increase the density of thiol active sites, and to enhance its affinity and adsorption capacity toward mercury binding. The best performing adsorbent for the removal of both high and low concentration of mercury in water with adsorption capacity of >800 mg g^{-1} was achieved. However, the preparation step of this hybrid is too complex and hard to scale up, which prompted our team to explore a more simplified method to produce a graphene adsorbent with high density of mercury binding chemistry.

It is worth noting that most studies on the development of graphene-based mercury adsorbents presented results with less consideration on the relevant mercury removal conditions, such as the use of extremely high mercury concentrations and large adsorbent dosages.[10] There are only few studies performed for the removal of low mercury concentrations in water, which is more important and the most challenging. For these applications, it is critical to have high surface area adsorbing matrix with optimized surface chemistry and maximized number of strong binding sites.

To address these limitations, in this paper, we report a facile approach for functionalization of GO surface with high density of multiple functional groups including sulfur, amine, and oxygen to design high performing adsorbents with efficient removal of ultralow concentration of heavy metals including mercury. Our concept, as presented in Figure 1, is based on the covalent attachment of cysteamine on the sp^2 carbon of GO via thermal thiol−ene click reaction. The cysteamine and thiol−ene click reaction were specifically selected to achieve the attachment of thiol and amino binding functionality through targeted sp^2 carbon binding without compensating the merits of oxygen functionalities on GO. The ultimate goal is to introduce the additional sulfur and amino functional groups and combine them with existing oxygen groups in GO to achieve a graphene composite with multiple surface chemistry and an enhanced binding performance for mercury. In this context, thiol−ene click reaction is recognized as one of the most promising routes as it allows targeted addition to the C=C using a thiol precursor by the action of heat (thermally) or light (photochemically) which enables the desired functional group (thiol) to attack the sp^2 carbon on GO.[16] Owing to its modular nature, highly efficient, catalyst-free, simple, and mild reaction conditions, thiol−ene click reaction appears to be a very popular approach for surface modifications and materials applications which may provide scalable production of the graphene adsorbents.[17] The structural, chemical and thermal characteristics of the prepared cysteamine modified partially reduced graphene oxide (Cyst-prGO) composite were studied in details using a broad range of characterization techniques followed by systematic batch studies for adsorption kinetics, isotherms, influence of pH, co-ions, sorbent dosage, and recyclability to evaluate the performance of the adsorbent toward Hg (II) ions. Finally, in order to demonstrate the practical application of this adsorbent at a realistic level, the as-prepared adsorbent was tested on Hg (II) spiked river water.

2. EXPERIMENTAL SECTION

2.1. Materials and Chemicals. Natural graphite flakes were obtained from a local mining site (Uley, Eyre Peninsula, South Australia, Australia), milled into powder using a benchtop ring mill (Rocklabs) and sieved using a 25 μm sieve. Activated carbon (Haycarb), potassium permanganate ($KMnO_4$, Sigma-Aldrich), 98% sulfuric acid (H_2SO_4, Chem-Supply), 85% w/w phosphoric acid (H_3PO_4, Chem-Supply), 30% hydrogen peroxide (H_2O_2, Chem-Supply), 36% hydrochloric acid (HCl, Chem-Supply), 67−69% nitric acid (HNO_3, Seastar Chemicals), 1M sodium hydroxide (NaOH, Chem-Supply), cysteamine hydrochloride (C_2H_7NS, Sigma-Aldrich), mercury(II) chloride ($HgCl_2$, Sigma-Aldrich), thiourea (CH_4N_2S, Sigma-Aldrich), *N*,*N*-dimethylforamide (DMF, Chem-Supply), 2,2-azobis-2-methylpropionitrile ($C_8H_{12}N_4$ (AIBN), Sigma-Aldrich), hexane (C_6H_{14}, Chem-Supply), ethyl acetate ($C_4H_8O_2$, Chem-

DOI: 10.1021/acsami.8b17131
ACS Appl. Mater. Interfaces 2019, 11, 6350−6362

Supply), and ethanol (C_2H_6O, Chem-Supply) were used directly without prior purification. High purity Milli-Q water (18.2 MΩ·cm) was used throughout the work, unless otherwise stated.

2.2. Preparation of Graphene Oxide (GO). GO was prepared by the oxidation of natural graphite based on the improved Hummer's method.[18] In the preparation, 3.0 g of graphite powder (≤25 μm) was used to synthesize GO. A 9:1 ratio of concentrated sulfuric acid and phosphoric acid (360:40) mL was mixed and cooled to ∼4 °C in the fridge. This mixture was slowly added to the graphite powder in the presence of 18.0 g potassium permanganate upon stirring at room temperature. The mixture was then heated to 60 °C for about 16 h to form a thick paste. The thick paste was left to cool to room temperature and was poured onto ice cubes in the presence of 3 mL hydrogen peroxide. Subsequently, the mixture was washed several times with distilled water, 5% hydrochloric acid, followed by acetone and ethanol. For each successive wash, the product was centrifuged at 4200 rpm. The obtained brown GO was dispersed in ethanol and freeze-dried to obtain a brown product.[6]

2.3. Synthesis of Cysteamine Modified Partially Reduced Graphene Oxide (Cyst-prGO). Functionalization of GO was performed according to the adaptation of the reported methodology by Luong et al.[19] In order to achieve maximum loading of functional groups and retain the oxygen functionalities on GO for better dispersion during mercury adsorption in aqueous systems, a few attempts were performed to optimize the modification parameters (Further details in SI, Figure S1A and B). The most optimized condition was at 70 °C, 12 h with the mass ratio of GO: cysteamine = 10:5. In a typical procedure, GO (200 mg) was added into 100 mL of DMF and ultrasonicated for 30 min to obtain a homogeneous exfoliated GO dispersion. This was then followed by purging of nitrogen gas for 30 min to create an inert environment. A separate mixture containing 100 μL AIBN (radical initiator), 100 mg of cysteamine hydrochloride and 50 mL DMF was ultrasonicated for 30 min and was added into the exfoliated GO dispersion. Subsequently, this dispersion was continued with purging of nitrogen gas for another 30 min. The reaction mixture was then poured into a round-bottom flask, sealed and heated in a 70 °C silicon oil bath for 12 h. After the reaction, the resulting product was cooled to room temperature and washed with a mixture of hexane and ethyl acetate in the ratio of 1:1, followed by ethanol and distilled water using centrifuge at 4200 rpm (SI, Figure S1C). The product was finally freeze-dried to obtain the corresponding Cyst-prGO (SI, Figure S1D).

2.4. Batch Adsorption Studies. The batch adsorption performance toward mercury(II) removal was conducted using 100 mL Hg (II) working solution at the desired pH, initial concentration, and amount of adsorbent on an orbital mixer (Ratek, model OM7, Australia). All the adsorption experiments were carried out using Cyst-prGO dispersed in ethanol in triplicate with a control (in the absence of adsorbent) running in parallel. For kinetic study, Cyst-prGO was added at the desired adsorbent amount into various vials containing 100 mL mercury(II) solution and these mixtures were stirred at ambient temperature on an orbital mixer at 170 rpm. Liquid samples were withdrawn at particular time intervals and immediately centrifuged prior to ICP−MS analysis. After the adsorption experiment, liquid samples were withdrawn and immediately centrifuged at 11 000 rpm for 5 min to separate the supernatant from the remaining mercury(II) solution. The collected liquid sample was then acidified with 2% HNO_3 for ICP−MS measurement to determine the remaining concentration of mercury(II) in the solution. The amount of mercury(II) ions adsorbed per unit of adsorbent mass, at a given time, t (q_t, mg g^{-1}) was deduced using the following equation:[6]

$$q_t = \frac{(C_0 - C_t)V}{m} \quad (1)$$

where C_0 and C_t are initial and mercury(II) concentrations at time t (mg L^{-1}), while V is the volume of solution (L) and m is the mass of adsorbent (g). The removal efficiency (R_t, %) at a given time, t, was calculated based on the following equation:[10]

$$R_t = \frac{(C_0 - C_t)}{C_0} \times 100 \quad (2)$$

2.5. pH Dependence Study. The effect of pH toward mercury uptake was investigated at pH range 3−10 of mercury(II) solution (∼1.5 mg L^{-1}) with the pH adjusted using HCl or NaOH before the adsorption experiments. Same procedure as described above was used to determine the remaining Hg (II) concentration after mercury adsorption.

2.6. Equilibrium Study. The adsorption capacity of the adsorbent was determined by adding 1 mg Cyst-prGO in a series of known concentration (1−10 mg L^{-1}) of Hg (II) working solutions at pH 5.3. The mixtures were stirred at 170 rpm on an orbital shaker at ambient temperature for 2 h. The liquid samples were withdrawn, analyzed with ICP−MS following the same procedure described above.

Kinetic Models. The rate of the sorption process was investigated by fitting the experimental data into two mathematical models, namely Lagergren pseudo-first-order[21] and the Ho's pseudo-second-order[22] (SI, Adsorption Kinetics).

Equilibrium Models. The adsorption process between Cyst-prGO and mercury(II) ions was evaluated using two popular equilibrium models, which are, Langmuir[23] and Freundlich[24] models (SI, Adsorption Isotherms).

2.7. Selectivity Study. The selectivity of Cyst-prGO toward Hg (II) was performed by adding 1 mg of Cyst-prGO into a quadruple metal ion mixture containing Hg (II), M (II) = Pb, Cu, and Cd stirred at 170 rpm at pH 5.3 for 2 h. This study was conducted in two approaches: $[Hg\ (II)]_i$: $[M\ (II)]_i$ = 1:1 and $[Hg\ (II)]_i$: $[M\ (II)]_i$ = 0.03:1 in order to demonstrate the selectivity of this material toward Hg (II). The remaining concentration of Hg (II) and M (II) was determined using ICP−MS after the selectivity experiments.

2.8. Regeneration Study. The regeneration of Cyst-prGO was investigated by loading Cyst-prGO adsorbent in ca. 1.00 mg L^{-1} Hg (II) at pH 5.3 at ambient temperature. The desorption cycles were carried out by stirring the spent adsorbent with 30 mL 2% (w/v) thiourea in 0.1 M HCl as eluent at 250 rpm on the orbital shaker for 1 h to wash out the bound Hg (II) from Cyst-prGO. This was then followed by washing the spent adsorbent with large amount of Milli-Q water to bring the pH to above five and drying process. Five adsorption−desorption cycles were repeated and the remaining Hg (II) concentration in each cycle was probed using ICP−MS.

2.9. Real Application Study. The efficiency of Cyst-prGO was evaluated using Hg (II) spiked river water (pH ∼ 7, without pH adjustment) collected from Torrens River (Adelaide, South Australia, 34°55′01.4″S 138°36′ 10.9″E) to simulate real application scenario. The river water was filtered using filter paper prior spiking with ca. 4.0 mg L^{-1} Hg (II) solution. In this study, 5.00 mg of adsorbents (Cyst-prGO, GO and commercial activated carbon) were separately added into 100 mL spiked Hg (II) river water. These mixtures were then stirred at 170 rpm for 2 h at ambient temperature. The collected liquid samples were then subjected for ICP−MS analysis to determine the remaining Hg (II) concentration.

3. RESULTS AND DISCUSSION

3.1. Characterizations of GO and Cyst-prGO. TEM was employed to distinguish the morphological difference between GO and the synthesized Cyst-prGO as visualized in Figure 2A and B. GO shows a typical ultrathin and wrinkled sheet-like structure with different sizes while Cyst-prGO displays a highly connected, aggregated and corrugated hybrid structure with multilayered assembly of the sheet-like individual GO sheets.[9] SEM analysis of the fractured hybrid revealed interconnected 3D microporous skeleton of Cyst-prGO after functionalization with cysteamine as displayed in Figure 2C confirming its unique architecture. A close-up image (Figure 2D) unveils the wrinkled, thin and paper-like structure of Cyst-prGO analogous to the structure determined from TEM analysis.

DOI: 10.1021/acsami.8b17131
ACS Appl. Mater. Interfaces 2019, 11, 6350−6362

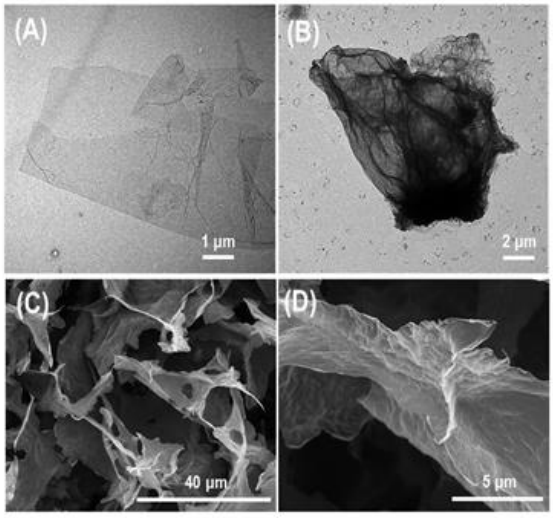

Figure 2. TEM images of (A) graphene oxide (GO) sheets and (B) cysteamine functionalized reduced graphene oxide (Cyst-prGO) sheets. (C and D) SEM images of Cyst-prGO after freeze-drying.

FTIR analysis was performed to verify the attachment of functional groups on GO and Cyst-prGO. As depicted in Figure 3A, the spectra of both materials exhibit a strong broad band at ~3400 cm^{-1} for O−H stretching vibrations, 1720 cm^{-1} corresponding to C═O stretching of −COOH, and peaks at 1030 and 1384 cm^{-1} conform to the C−O and C−OH bonds, respectively. The band at nearly 3200 cm^{-1} due to N−H stretching was also recorded on the spectrum of Cyst-prGO although insignificant in relative to other peaks due to the overlapping peak with O−H band.[6,9,20,25] It should also be noted that the band at 1620 cm^{-1} (C═C skeleton stretching vibration of the aromatic ring) on GO was shifted to 1644 cm^{-1} on Cyst-prGO which could be attributed to N−H vibration after the functionalization reaction.[26,27] In addition, the targeted thiolation on GO via thiol−ene click reaction was evidenced by the presence of new peaks near 1435, 1410, and 1350 cm^{-1} on Cyst-prGO which can be allotted to C−S vibrations.[28,29] Significantly, peaks at 1247 and 660 cm^{-1} which could be ascribable to $-CH_2-S$ wagging and vibrational C−S bonds respectively were also found after the functionalization process.[30,31] The absence of the common peak at around 2500 cm^{-1} which could be associated with S−H stretching on Cyst-prGO suggests that the thiol−ene click reaction has taken place via the reaction between −SH group on cysteamine with C═C on GO. A small peak at 2929 cm^{-1} which could be linked to the symmetric stretching mode of $-CH_2$ moiety on the carbon chain of cysteamine was also found on the spectrum of Cyst-prGO.[9,32] The FTIR results further corroborated the successful grafting of functional groups in cysteamine on GO and the partially retained oxygen functional groups through thiol−ene click reaction.

Comparative TGA thermograms of GO and Cyst-prGO as shown in Figure 3B was employed to confirm the thiol−ene click reaction in Cyst-prGO. Both GO and Cyst-prGO showed thermal instability before 650 °C with step-like profiles unlike graphite, which displayed no significant weight loss (SI, Figure S2A). Three major mass losses were identified on GO, whereas four were detected on Cyst-prGO. The first stage of mass loss below 110 °C could be attributed to the loss of moisture content and interstitial water which accounts for 13.36% for GO and 7.66% for Cyst-prGO[33] (SI, Figure S2B and C). The second mass loss of 46.79% and 24.07% which occurred at 190 and 160 °C for GO and Cyst-prGO, respectively can be associated with the removal of oxygen-containing functional groups.[34] Interestingly, a moderately small mass loss along with a tiny shoulder peak at 251 °C (18.11%) was only found on the derivative mass loss plot of Cyst-prGO (SI, Figure S2C), but not on GO, which could be related to the attachment of additional functional groups via thiol−ene click reaction. Subsequently, the last mass loss with nearly 40% on the TGA curves of both (39.85% for GO and 39.31% for Cyst-prGO) samples taking place at 538 °C (GO) and 592 °C (Cyst-prGO) could be related to the bulk pyrolysis of carbon skeleton.[34] A relative appreciable amount of residue (~11%) was left at 600 °C for Cyst-prGO in contrast to GO (0%)

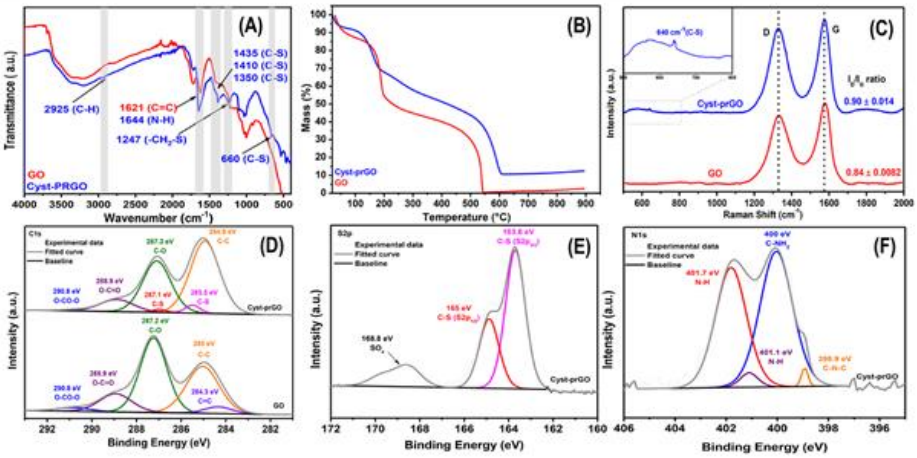

Figure 3. (A) FTIR, (B) TGA, (C) Raman, (D) XPS high resolution for C 1s spectra of graphene oxide (GO) and cysteamine functionalized partially reduced graphene oxide (Cyst-prGO), XPS high resolution spectra for (E) S 2p and (F) N 1s of Cyst-prGO.

DOI: 10.1021/acsami.8b17131
ACS Appl. Mater. Interfaces 2019, 11, 6350−6362

further confirming the successful insertion of other functionalities such as sulfur and amine from cysteamine and increase in thermal stability.[32]

The XRD patterns of GO and Cyst-prGO are displayed in (SI, Figure S3A). The peak at 2θ = 11.32° (d-spacing = 7.81 Å) on GO confirms the complete oxidation of graphite commonly existing at 2θ = 26.62° (SI, Figure S3B).[35] On the other hand, a shift of the peak at 2θ = 11.32° on GO to 10.65° with corresponding higher interlayer spacing of 8.30 Å was observed on the XRD pattern of Cyst-prGO. This signifies the increased distance between the exfoliated GO layers after the introduction of cysteamine which could be due to the insertion of functionalities, including sulfur and amine groups, playing the role as spacers between the GO interlayers after the functionalization process.[36,37] Meanwhile, the broad peak in the range of 2θ = 20−26° on the XRD pattern of Cyst-prGO can be associated with the stacking of few layers graphene sheets.[37,38]

Figure 3C depicts the Raman spectra of GO and Cyst-prGO where two characteristic peaks at 1330 and 1575 cm^{-1} related to the D and G bands, respectively are observed. The D band can be related to the defects or disorder in the graphitic structure, whereas the G band corresponds to the in-plane vibration of the sp^2 carbon to sp^3 hybridized carbon resulting from the destruction of the sp^2 structures of graphite or covalent attachment of functional groups.[6,9] Typically, the intensity ratio of D and G bands (I_D/I_G) measures the degree of functionalization, which provides an indicator of the structural defects of carbon. Cyst-prGO exhibits a higher I_D/I_G ratio (0.90) compared to GO (0.84) which suggests an increase in the degree of disorder on the partially reduced GO sheets. Moreover, the presence of a weak band near 640 cm^{-1} (inset of Figure 3C) representing the gauche conformation of the vibrational stretching of C−S bond is also identified on the Raman spectrum for Cyst-prGO which further affirms the enhanced functionalization with successful insertion of sulfur and amine groups on the GO sheets using cysteamine.[39]

XPS analysis was performed in order to gain further insight on the chemical composition and chemical states of the synthesized adsorbent. A survey scan of Cyst-prGO (SI, Figure S4) revealed the elemental composition of C, O, S, and N at 78.13%, 18.62%, 1.66%, and 1.59%, respectively, in Cyst-prGO. The nearly identical atomic percentage achieved by both N and S atoms in this quantitative data suggests that the GO surface effectively functionalized via the thiol−ene click reaction using cysteamine. The slight discrepancy of 0.07% between S and N atomic composition could be due to the presence of residual sulfate (use of sulfuric acid) during the oxidation of graphite.[9] It should be noted that the evidence of thiol−ene click reaction in Cyst-prGO is also well supported by the selected high resolution C 1s, S 2p, and N 1s spectra (Figure 3D−F). Deconvolution of C 1s spectrum for bare GO (Figure 3D) shows a few characteristic peaks centered at 284.3, 285, 287.2, 288.9, and 290.8 eV, which can be assigned to C=C, C−C, C−O, O−C=O, and O−CO−O bonds, respectively.[40−43] It is noteworthy to find that all the aforementioned peaks in GO appear on the C 1s narrow scan of Cyst-prGO except the peak at 284.3 eV (C=C) which diminished after functionalization with cysteamine. This suggests that the oxygen functional groups are still present in Cyst-prGO and the click reaction took place between the sp^2 carbon on GO with the thiol group on cysteamine. This result is also well correlated with the FTIR analysis in which the band at 1620 cm^{-1} (C=C) diminished in Cyst-prGO after the functionalization reaction as mentioned previously in this paper. On top of that, the fitting of the experimental data of C 1s in Cyst-prGO demonstrates two new peaks arise at 285.5 and 287.1 eV which can be allotted to C−S bond are consistent with the peaks (C−S bond) found in FTIR analysis of Cyst-prGO.[40,44,45] On the other hand, the narrow spectra of S 2p and N 1s of Cyst-prGO (Figure 3E and F) evidently confirmed that thiol−ene click reaction has occurred between the -SH group on cysteamine with C=C on GO. The deconvolution of S 2p peak into a doublet positioned at 163.6 and 165 eV can be attributed to S $2p_{3/2}$ and S $2p_{1/2}$ of C−S bond, respectively.[46,47] Meanwhile, a peak at 168.8 eV associated with the oxidized S is visible on the high resolution S 2p spectrum.[47] This is in good agreement with the discrepancy found in the atomic quantification data of S and N. In addition, the detailed scan of N 1s indicates the presence of three types of nitrogen species in Cyst-prGO with the peaks centered at 401.1 and 401.7 eV for N−H, 398.9 eV for C−N−C and near 400 eV for C-NH_2 bonds.[28,48−50] It is apparent that the chemical states of the species present in Cyst-prGO probed using XPS analysis are very well correlated to the FTIR results discussed in the previous section. The combination of the characterization results including XRD, Raman, FTIR, TGA, and XPS analyses offer strong evidence on the formation of Cyst-prGO by thiol−ene click reaction involving −SH group from cysteamine and C=C on GO.

3.2. Adsorption Kinetics. Figure 4 shows the rate of Hg(II) adsorption for the three different adsorbent dosages (1, 10, and 100 mg L^{-1}) of Cyst-prGO. The steep upward Hg(II) uptake pattern visibly shows an exceptionally rapid initial adsorption rate of Hg(II). About 96% Hg(II) was removed for 10 and 100 mg L^{-1} of Cyst-prGO and the Hg(II) uptake was leveled out with approximate 98% at equilibrium for all the adsorbent dosages, whereas nearly 70% mercury was removed when 1 mg L^{-1} of Cyst-prGO was used within the first 10 min. In terms of the adsorption kinetics, the performance achieved by Cyst-prGO (10 min) in lesser sorbent dosage is outstanding in relative to the adsorbents prepared in our previous studies,

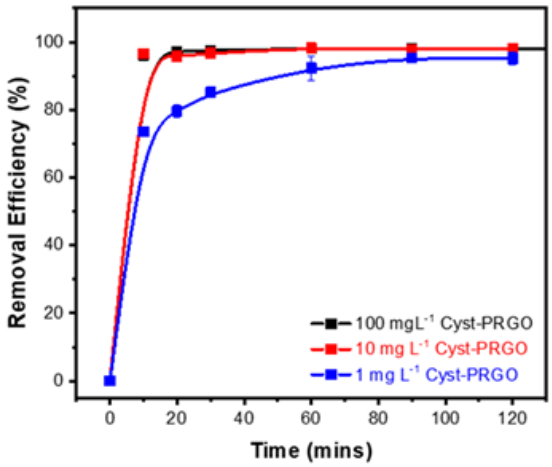

Figure 4. Time dependence study of Hg(II) adsorption on different sorbent dosage of Cyst-prGO. Conditions: pH 5.3, $[Hg^{2+}]_i$ = ~1.5 mg L^{-1}, T = 23.0 °C.

DOI: 10.1021/acsami.8b17131
ACS Appl. Mater. Interfaces 2019, 11, 6350−6362

graphene-diatom silica aerogels (30 min) and functionalized graphene hybrid (20 min) to attain the adsorption equilibrium.[6,9] Moreover, in comparison to graphene oxide/Fe−Mn hybrid (GO/Fe−Mn) prepared by J. Tang et al., about 25 min (10 min for Cyst-prGO) were required to achieve the adsorption equilibrium when almost similar initial mercury(II) concentration but higher sorbent dosage (120 mg L^{-1}) was used in their studies.[51] On top of that, the adsorption rate of Cyst-prGO also superseded 3DGON reported by Henrique et al. when lower initial mercury(II) concentration, 0.05 mg L^{-1} (~1.5 mg L^{-1} for Cyst-prGO) was applied, yet 24 h (10 min for Cyst-prGO) was needed to achieve about 90% removal at pH 5.[10]

In order to gain further insight about the adsorption mechanism of Hg(II) onto Cyst-prGO, these outstanding kinetic results were fitted into the linearized form of two kinetic models (pseudo first- and pseudo second-) as depicted in (SI, Figure S5). From the fitting analysis using the aforementioned sorption kinetic profiles, pseudo-second order kinetic model provides the best fit with the highest linear correlation coefficient (R^2 = 1.000) compared to the pseudo first model (R^2 = 0.473). This suggests that chemisorption is the rate-controlling step for Hg(II) uptake on Cyst-prGO. Pseudo-second order model has been commonly applied to describe the sorption of contaminants from aqueous solution in wastewater treatment which undertakes that chemisorption process with respect to the number of adsorption site available for the exchange process at the solid-solution interface. This model also presumes the bimolecular interaction by sharing and exchange of electrons between the adsorbate and adsorbent which can be correlated to the electron-donating groups present on Cyst-prGO adsorbent.[52]

3.3. Influence of Solution pH. The effect of solution pH toward Hg(II) removal by Cyst-prGO was studied over the pH range of 3−10 (Figure 5) with other parameters kept at constant. The pH studies indicate that this material exhibited different stages of sorption with the highest Hg(II) removal efficiency (above 95%) recorded at around pH 5. This observation is well supported by the highly negative zeta potential value of Cyst-prGO measured at the same pH, which accounted for the strong electrostatic attraction between the negative surface charge of Cyst-prGO and the positively charged divalent mercury ion. At this optimum pH, mercury exists as a divalent form, which readily coordinates with sulfur, oxygen and nitrogen atoms on the binding sites of Cyst-prGO via surface complexation. In addition, the electron rich surface of the adsorbent which is less protonated at this pH makes the bond formation between Hg (II) ion and the negatively charged surface more facile via lone pair electron sharing.[13]

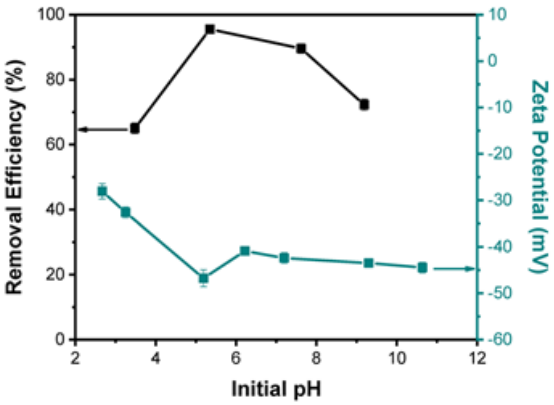

Figure 5. Effect of pH on Hg(II) removal efficiency and zeta potential of 10 mg L^{-1}Cyst-prGO measured at different pH. Conditions: $[Hg^{2+}]_i$ = ~1.5 mg L^{-1}, T = 23.0 °C.

A significant drop of about 30% Hg(II) uptake was observed at approximately pH 3. This unfavorable adsorption phenomenon could be attributed to the competition for binding sites between Hg(II) and H^+ ions as well as the protonation of the functional groups on the surface of Cyst-prGO. Moreover, functional groups such as hydroxyl, carboxyl and amine groups on the surface of Cyst-prGO tend to be protonated, which are positively charged at low pH. This leads to the electrostatic repulsion between the binding site and Hg(II) ions, resulting in low mercury uptake.[12,13,53] Interestingly, although Cyst-prGO exhibited almost similar negative zeta potential magnitude at pH 7−10, a lower sorption of Hg(II) ions was detected at about pH 9 compared to pH 7. This slight drop of mercury uptake might be attributed to the formation of $Hg(OH)^{3-}$ due to the increase of OH^- ions as pH increases, which are likely to repel the negatively charged surface of Cyst-prGO.[6,12] It is also noteworthy that the zeta potential measurement shows that Cyst-prGO has a negative surface charge (<−28 mV) which implies that the adsorption of Hg(II) onto this material is feasible as evidenced by >60% Hg(II) uptake regardless of the pH applied. Remarkably, this material was found to be well dispersed in the solution above pH 5, which is advantageous for mercury removal as the pH of most natural water systems fall in this pH region. This further affirmed the potential application of this material as an effective adsorbent to remove Hg(II) due to its great affinity toward the positively charged toxic metal ion based on electrostatic attraction at different aqueous media. Since most heavy metals, particularly mercury, tend to precipitate in their hydroxides form when pH is greater than 6, hence pH in the range of 5.0−5.5 was chosen to conduct all the mercury adsorption experiments, unless otherwise stated.[28,54,55]

3.4. Adsorption Isotherms. The study of adsorption isotherm of Cyst-prGO toward Hg(II) removal is crucial to evaluate the interactions between adsorbate and adsorbent so that the use of the adsorbent into real applications can be optimized. As presented in Figure 6, an adsorption capacity of 169 ± 19 mg Hg(II) per g of adsorbent was achieved in the study. Further fitting of the experimental data into the Langmuir and Freundlich isotherm models shows that the adsorption behavior of Cyst-prGO correlates better with Langmuir isotherm with correlation coefficient, R^2 = 0.9901 in relative to Freundlich isotherm (R^2 = 0.0089) as shown in (SI, Figure S6A and B). Thus, it can be assumed that the adsorption process that takes place between Cyst-prGO and Hg(II) is homogeneous with all the binding sites equivalent, which results in uniform and monolayer surface coverage.[56] Furthermore, the estimated maximum sorption capacity, q_{max} from Langmuir model is found to be 169.5 mg Hg(II) per g of adsorbent which agrees well with the obtained experimental data, q_e value (172.4 mg g^{-1}) determined from the estimation of pseudo-second order equation when 10 mg L^{-1} of Cyst-prGO was used for Hg(II) adsorption. All the calculated K_R values exhibit positive values which fall in the range of 0−1 (SI, Figure S6C), signifying favorable adsorption of Hg(II) on

DOI: 10.1021/acsami.8b17131
ACS Appl. Mater. Interfaces 2019, 11, 6350−6362

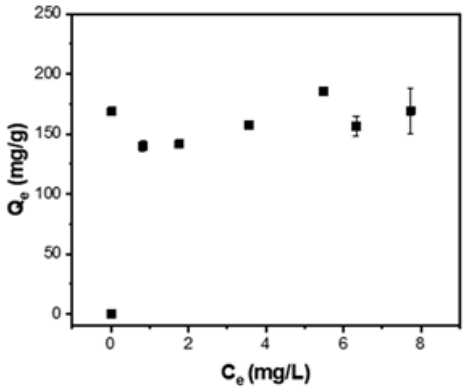

Figure 6. Experimental data of Hg(II) adsorption isotherm for Hg(II) adsorption on Cyst-prGO. Conditions: pH 5.3, $[Hg^{2+}]_i$ = 0−10 mg L^{-1}, adsorbent dosage = 10 mg L^{-1}, T = 20.6 °C.

Cyst-prGO under the conducted adsorption conditions. The K_R values were found to decline as the initial Hg(II) concentration increased which indicated that the sorption of Hg(II) onto Cyst-prGO became more favorable.[57,58]

It should be highlighted that it is challenging to make an impartial comparison between the adsorbent investigated in this work and other adsorbents studied previously due to different experimental conditions such as amount of sorbent used, volume of Hg (II) solutions, range of initial Hg(II) concentration, equilibration time, pH and temperature used in the performance assessment of adsorbents. These varied adsorption parameters could greatly affect the adsorption capacity achieved by the adsorbents. Moreover, it was found that some experiments were conducted at unrealistic adsorption conditions such as extremely high initial mercury concentration and 10−500 times higher adsorbent dosage compared to our current study which do not reflect the practicability of the adsorbents in real applications therefore may leave behind severe environmental impact with amass of toxic spent adsorbents generated. As tabulated in Table 1, a more pertinent comparison was made between GO adsorbents in the literature with the adsorbent investigated in this work. By applying similar sorbent dosage (10 mg L^{-1}) and lower initial Hg(II) concentration (0.050 mg L^{-1}), Henriques et al. showed that the maximum sorption capacity of 3DGON is 35 mg g^{-1} (about 4 times lesser than Cyst-prGO).[10] Almost identical maximum sorption capacity (32.9 mg g^{-1}) was reported by J. Tang et al. for graphene oxide/Fe−Mn hybrid using an initial Hg(II) concentration between 0.1 and 5 mg L^{-1} and 120 mg of sorbent per liter of Hg(II) solution (12 times higher sorbent dose compared to the current study).[51] Similarly, lower maximum sorption capacity was found with some adsorbents reported in the literature including amino functionalized graphene hybrid (Fe_3O_4-GS, q_e = 23.03 mg g^{-1}, $[Hg(II)]_i$ = 5 mg L^{-1}),[59] L-cysteine functionalized exfoliated graphene oxide (q_e = 79.36 mg g^{-1}, $[Hg(II)]_i$ = 10 mg L^{-1}),[12] and mercaptobenzothiazole functionalized graphene oxide (q_e = 107.52 mg g^{-1}, $[Hg(II)]_i$ = 80 mg L^{-1}).[13] It could be discerned that the sorbent dosage employed in their studies was more than 20 times higher compared to the present study. Although Cyst-prGO exhibited lower maximum sorption capacity (169 mg g^{-1}) than other adsorbents (528 mg g^{-1} for graphene-diatom silica aerogels[6] and 881 mg g^{-1} for functionalized 3D graphene hybrid[9]) reported in our previous work, Cyst-prGO was found to have a faster adsorption rate (10 min) compared to graphene-diatom silica aerogels (30 min) and functionalized graphene hybrid (20 min) to reach equilibrium. Moreover, the sorbent dosage in this work was four times lesser than our previously reported studies.[6,9] Taking into account of the efficiency of adsorbents in terms of dosage, time, cost, and environmental footprint, Cyst-prGO is found to be a more promising adsorbent although its adsorption capacity is lower than IT-PRGO (624 mg g^{-1})[28] and Fe_3O_4−polypyrrole-GO (400 mg g^{-1})[60] adsorbents due to its lower sorbent dosage (5−10 times lesser dosage) and outstanding adsorption rate (10 min). Unlike the multistepped preparation required in some of the aforementioned adsorbents, the thiol−ene click functionalization involved only one-pot synthesis at mild reaction conditions which is more economically viable. Overall, Cyst-prGO is found more environmentally friendly, time-saving, and cost-effective in terms of its low dosage required to effectively remove mercury from waters with lower amount of final residue generated.

Table 1. Comparison of Adsorption Capacity with Experimental Conditions of Various Adsorbents for Hg(II)

type of Hg adsorbent	initial Hg(II) conc.(mg L^{-1})	sorbent dosage (mg L^{-1})	temp. (°C)	pH	specific surface area(m^2 g^{-1})	max. sorption capacity(mg g^{-1})	ref
3DGON	0.05(=50 μg L^{-1})	1−20	21.0	4.5	400[a]	35	10
graphene oxide/Fe−Mn hybrid (GO/Fe−Mn)	0.1−5	120	25.0	7.0	153.43[a]	32.9	51
2-imino-4-thiobiuret-partially reduced graphene oxide (IT-PRGO)	0−900	100 (0.005 g in 5 mL)	25.0	5	NA	624	28
MBT-functionalized Graphene Oxide	80	500−5000 (0.01−0.10 g in 20 mL)	25.0	5.4−6.9	NA	107.52	13
L-cysteine functionalized EGO	10	1667− 5000 (0.05−0.25 g in 30 mL)	NA	5.5−7.0	NA	79.36	12
amino functionalized graphene hybrids (Fe_3O_4-GS)	5	200 (10 mg in 50 mL)	25.0	NA	62.43[a]	23.03	59
graphene-diatom silica aerogel (GN-DE-FeOOH)	50−400	40 (10 mg in 250 mL)	25.0	6.5	368[b]	528	6
graphene hybrid (GN-DE-FeOOH-SH)	10−500	40 (10 mg in 250 mL)	25.0	6.5	340.8[b]	881	9
cyst-prGO	**0−10**	**10**	**20.6**	**5.3**	**672[b]**	**169**	**this work**

[a]refers to Brunauer−Emmett−Teller (BET). [b]Refers to methylene blue method of specific surface area measurement.

DOI: 10.1021/acsami.8b17131
ACS Appl. Mater. Interfaces 2019, 11, 6350−6362

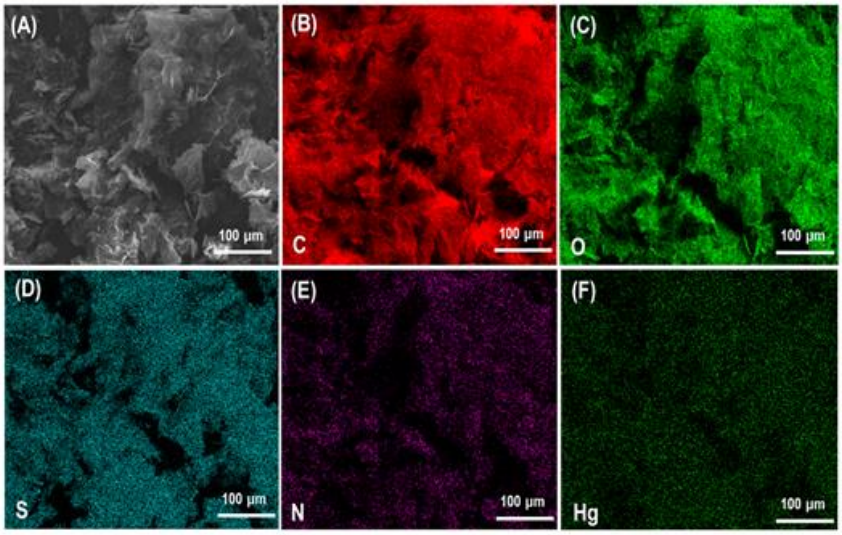

Figure 7. (A) SEM image of Cyst-prGO, (B–F) corresponding EDS mapping of Cyst-prGO containing C, O, S, N, and Hg elements after Hg(II) adsorption.

3.5. Adsorption Mechanism of Hg(II). Elemental mapping, FTIR, and XPS analyses were employed to confirm Hg adsorption on Cyst-prGO. Prior to freeze-drying, the spent Hg(II) solid sample was rinsed with copious amount of water to remove the physically and loosely bound Hg(II) on the surface of the adsorbent. Elemental mapping of Cyst-prGO as displayed in Figure 7 further authenticated the presence of elements including carbon (C) and oxygen (O) related to GO structure as well as sulfur (S) and nitrogen (N) related to the presence of cysteamine on Cyst-prGO due to the successful grafting of these functional groups on the GO sheet (Figure 7A–E). Apart from that, the uniform distribution of mercury (Figure 7F) discloses that it may react with elements such as N, O, or S found on the surface of the adsorbent during the adsorption process.

FTIR analysis was employed to further identify the chemical changes happening on Cyst-prGO before and after mercury adsorption. Three major changes were observed on the vibration pattern of Cyst-prGO as displayed in (SI, Figure S7A). Notably, vibrations at 1513 cm^{-1} ($NH-C-(S)-NH_2$), 1410 and 1435 cm^{-1} (C–S), 1384 cm^{-1} (–C–O), 1247 cm^{-1} ($-CH_2-S$), as well as 660 cm^{-1} (C–S) diminished after reacting with mercury. Interestingly, the peak at 1644 cm^{-1} (N–H) was also missing on the Cyst-prGO after reaction with mercury but this peak was shifted to 1616 cm^{-1}, closer to the peak at 1620 cm^{-1} (C=C) detected on the GO spectrum. Furthermore, the less intense peak at 3236 cm^{-1} corresponding to N–H was found shifted from 3205 cm^{-1}. A similar pattern was also observed on the peak at 1714 cm^{-1}(C=O stretching of COOH) in addition of a slight shift from 1717 cm^{-1} as well as the band at 1234 cm^{-1} which can be ascribed to the slight displacement of the C–O bond from 1229 cm^{-1} before mercury adsorption.[61−63]

In addition, a more surface-sensitive tool, XPS was applied to study the mechanism of the uptake of Hg(II) ions on the adsorbent after mercury adsorption. As illustrated in (SI, Figure S7B), the survey scan of Cyst-prGO obtained after Hg(II) adsorption with the inset of the Hg 4f narrow spectrum denotes the presence of mercury species. An obvious doublet peak was observed around 101 and 105 eV which can be assigned to Hg $4f_{7/2}$ and Hg $4f_{5/2}$,respectively.[10] Significant changes after mercury adsorption can be evidenced by their respective deconvoluted peaks of C 1s, S 2p, N 1s, and O 1s as depicted in (SI, Figure S8). The high resolution C 1s spectra (SI, Figure S8A) suggest the interaction between mercury and S atom following by the disappearance of a peak at 287.1 eV and a shift of the peak at 285.5 eV corresponding to the C–S bond in Cyst-prGO. This finding is well supported by a slight shift observed for the doublet at 163.6 eV (S $2p_{3/2}$) and 165 eV (S $2p_{1/2}$) to 163.7 and 164.9 eV, respectively, after mercury adsorption in (SI, Figure S8B). On the other hand, it can be seen that the peak positioned at 287.3 eV (C–O) was shifted to 287.1 eV after Hg(II) adsorption. This observation can be well correlated to the narrow scan of O 1s with the minor shift occurred at 532.9 eV (C–O/O–H) to 532.8 eV after Hg(II) adsorption, implying the involvement of oxygen functional groups in the complexation with mercury. A substantial change was found on the high resolution spectra of N 1s with the peak missing at 401.1 eV corresponding to N–H bond and a shift of about 0.2 eV was detected for C–N–C bond from 398.9 to 399.1 eV after mercury adsorption.

From the FTIR and XPS results, we can infer that three primary heteroatoms (S, N, and O) in Cyst-prGO significantly play their roles in Hg(II) adsorption. Based on *Hard Soft Acid Base (HSAB)* theory, Hg(II), a soft acid, can be strongly bound to the ligands (soft bases) including sulfur, amine, and oxygen-containing functionalities on Cyst-prGO via electron pair sharing which led to the formation of covalent bonds. A metal–chelate complex could be resulted from the interaction between the ligands which donate their lone electron pairs to metal ion which serves as an electron pair acceptor due to the availability of vacant orbitals in the divalent mercury ion.[53,64] Moreover, the adsorption mechanism of Hg(II) onto Cyst-prGO can also be discussed in terms of the electronegativity of the heteroatoms on the adsorbent surface. Typically, the electronegativity of the electron donors increases in the order

DOI: 10.1021/acsami.8b17131
ACS Appl. Mater. Interfaces 2019, 11, 6350–6362

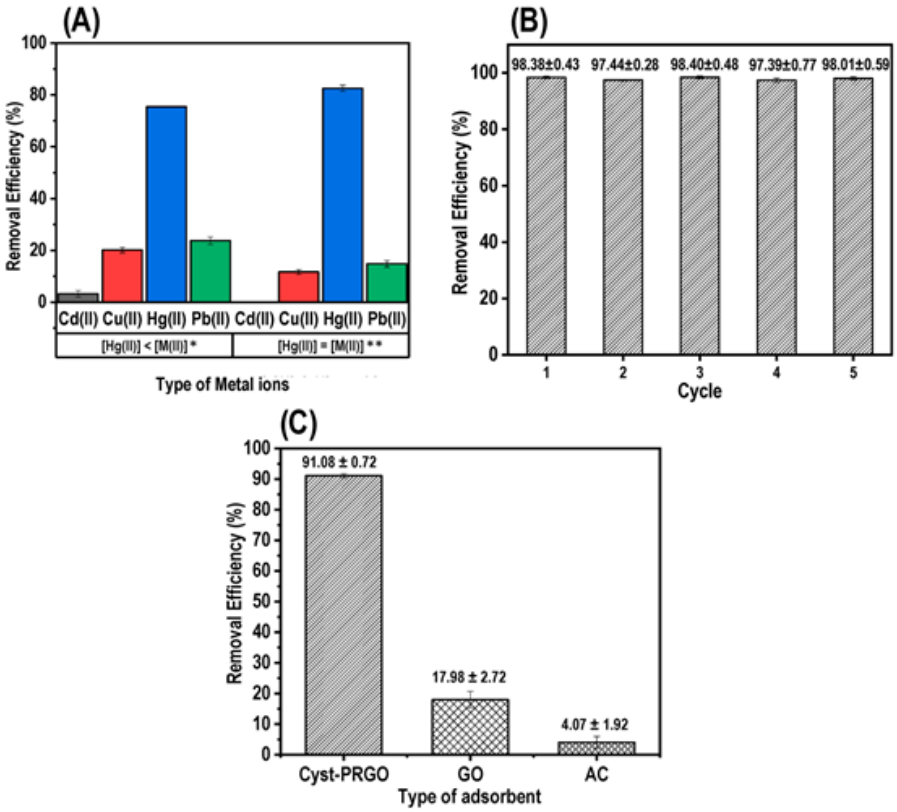

Figure 8. (A) Influence of co-ions on Hg(II) adsorption by Cyst-prGO (*[Hg(II)] = 30 μg L^{-1}, [M(II)] = 1000 μg L^{-1}; **[Hg(II) = [M (II)] = 1000 μg L^{-1}), (B) regeneration of Cyst-prGO and (C) Hg(II) removal efficiency using Hg(II) spiked river water on different adsorbents.

of S < N < O which results in stronger attraction of lone pair electrons to their respective nucleus in O than N than S. Therefore, it can be assumed that the tendency to share the lone pair electron is more facile in S compared to N and O in forming bond with mercury. In comparison to S atom which is strongly attached to C (C−S bond) via the thiol−ene click reaction, the complexation of Hg(II) with N and O atoms in this case could be more spontaneous due to the presence of labile−NH_2 and −COOH groups on Cyst-prGO as evidenced by the visible changes from FTIR and XPS analyses. Nevertheless, despite the difference in the electronegativity magnitude of the heteroatoms on Cyst-prGO which affects the strength of the bond between the heteroatoms and Hg(II), we surmised that a stronger Hg−chelate complex could be formed due to the pronounced chelating effect from multiple ligands (S, N, and O) on Cyst-prGO which provide rich electron pair binding sites to form Hg(II) complex via electrostatic attraction and chemical adsorption. Additionally, we found that the reserve of bountiful oxygen-containing functional groups such as carboxyl, hydroxyl, and epoxy groups on the surface of the partially reduced adsorbent due to the improved functionalization step has rendered good dispersion of this material in water. This could be explained by the formation of hydrogen bonds between the oxygen containing groups on the hydrated Cyst-prGO with the water molecules which enhanced the interaction between Hg(II) in water with Cyst-prGO.[65]

3.6. Influence of Competing Ions. It is essential to investigate the influence of co-ions such as Cd (II), Cu (II), and Pb (II) on Cyst-prGO toward Hg(II) uptake since they commonly coexist and create competitive adsorption with Hg(II) in surface water sources.[66] The preferential affinity of Cyst-prGO is found to be in the order of Hg(II) > Pb(II) > Cu(II) > Cd(II) under the two experimental approaches conducted in this study. As displayed in Figure 8A, the removal efficiency of Hg(II), Pb(II), Cu(II), and Cd(II) by Cyst-prGO is 83%, 15%, 12%, and 0%, respectively, when equal concentration of Hg(II) and tripartite co-ions was used in the experiment. The affinity of Cyst-prGO toward Hg(II) is only slightly affected despite the strong competition between Hg(II) and the three analyzed metal ions. It is noteworthy that when initial concentration of 30 μg L^{-1} Hg(II) in the presence of 1000 μg L^{-1} of each of the three co-ions was used in the adsorption study, 75.4% Hg(II) removal was achieved with 7.6 ppb mercury remaining in the final solution using merely 10 mg L^{-1} of Cyst-prGO after 2 h equilibrium time. It should be emphasized that Cyst-prGO was able to show remarkable selectivity toward Hg(II) removal to meet the acceptance limit of mercury (10 ppb) in wastewater despite the strong competition from about 30 times higher concentration of the three coexisting metal ions.[67] This finding further manifests the potential applicability of this adsorbent toward Hg(II) removal in real wastewater systems.

DOI: 10.1021/acsami.8b17131
ACS Appl. Mater. Interfaces 2019, 11, 6350−6362

3.7. Regeneration of Adsorbent. The reusability of the adsorbent after Hg(II) uptake is an important aspect to be examined as it significantly leaves an impact on the effective cost of mercury treatment apart from the generation of contaminated wastes. A mixture of 2% (w/v) thiourea in 0.1 M HCl was chosen as the eluent in this work due to its high desorption efficiency of mercury that also prevented the overdissolution of the adsorbent by HCl, the common eluent used in mercury desorption study.[68] Remarkably, this material was able to maintain its performance efficiency (>97%) with negligible decline of mercury uptake even after the fifth cycle of repeated adsorption−desorption process as displayed in Figure 8B. This could be due to the recovery of plethora of binding sites available for mercury complexation after each desorption step with the use of suitable eluent which leads to high recyclability of this material. This outstanding result reveals that Cyst-prGO has good stability and reusability which can help to reduce the amount of spent adsorbent generated. From an economic and environmental perspective, Cyst-prGO supersedes several existing mercury adsorbents studied in the past (SI, Table S1) which promises a low cost solution for mercury remediation technology in the long run.

3.8. The Application Study using Real Water Samples. In order to assess the efficiency of Cyst-prGO in real application conditions, adsorption studies were performed using local river water spiked with Hg(II) and compared with GO and commercial activated carbon (AC) as the controls (Figure 8C). River water is a complex matrix comprising of various ions which can compete for available binding sites on the sorbent. Moreover, the presence of organic matters in this natural system restricts the mobility of mercuric ions and complicates the adsorption of Hg(II) onto the sorbent.[10,69] Nevertheless, the experimental results revealed that the adsorption efficiency of Cyst-prGO was only slightly affected under this complex natural aquatic system. In spite of the lower specific surface area of Cyst-prGO (672 ± 1.0 m^2 g^{-1}) compared to GO(900 ± 1.0 m^2 g^{-1}), a great removal efficiency of 91% was achieved in relation to GO (18%) in this real application study. Furthermore, the efficiency of AC (23 ± 0.9 m^2 g^{-1}, < 5%) was worse with hardly any affinity to mercury. Owing to the availability of the active functional groups such as sulfur and amine groups on the surface of Cyst-prGO, the decreased surface area in Cyst-prGO due to the insertion of additional functional groups and the blocking of some pores during thiol functionalization using cysteamine does not seem to affect the outstanding performance of the prepared adsorbent. It was also noticed that the results from the real application study using river water (pH ~7) is in good agreement with the pH study where the mercury removal efficiency is about 90% at pH 7. This reveals that the mercury removal efficiency of this material is highly dependent on pH. This outstanding result further promises the potentiality of this material to trap mercury in real water systems.

4. CONCLUSIONS

In this study, a graphene composite functionalized with multiple binding functionalities including sulfur, amine, and oxygen groups was successfully synthesized by covalently bonding cysteamine on GO via the thiol−ene click reaction and used as a high performing mercury adsorbent. Characterization results confirmed that the prepared Cyst-prGO adsorbent has tailored multiple surface chemistry with a high density of active sites for specific binding and high surface area that are critical for designing high performance absorbents. The results from the adsorption studies showed very high adsorption rate, stability and selectivity toward removal of low concentration of Hg(II) (~1.5 mg L^{-1}) with only a low amount of adsorbent (10 mg L^{-1}) used with a maximum sorption capacity of 169 mg g^{-1} at pH 5. Cyst-prGO fitted the pseudo-second order and Langmuir isotherm models toward Hg(II) removal. With only a low dosage (10 mg L^{-1}) used, the merits of this adsorbent are unreservedly manifested in its remarkable adsorption rate (~96% removal in 10 min), outstanding regeneration ability (>97% Hg(II) after 5 adsorption−desorption cycles), high selectivity despite the strong competition from 30 times higher the concentration of the mixture of competing ions (Pb (II), Cu (II), and Cd (II)). In the final experiment, the performance of the adsorbent using real river water samples for removal of Hg ions was successfully demonstrated. Based on these performances including eco-friendly and scalable synthesis, high adsorption capacity for low concentration of mercury using low dosages, very-high selectivity and recyclability, the developed Cyst-prGO hybrid can be considered as a promising candidate for solving concerning problems of mercury removal from environmental and drinking waters. This innovative approach to engineer graphene composites with multifunctional chemistry is generic, versatile, low-cost, eco-friendly and scalable that can be adapted for broad applications.

■ ASSOCIATED CONTENT

Supporting Information

The Supporting Information is available free of charge on the ACS Publications website at DOI: 10.1021/acsami.8b17131.

FTIR spectra of samples prepared with GO: cysteamine and control samples (without cysteamine); photographs of Cyst-prGO after washing and freeze-drying; Characterization techniques of samples; TGA and mass derivatives of graphite, GO and Cyst-prGO; XRD of graphite, GO and Cyst-prGO; XPS survey spectra of GO and Cyst-prGO; fitting of experimental data of Hg(II) adsorption for pseudo-first order and pseudo-second order kinetic models; fitting of experimental data of Hg(II) adsorption for Langmuir and Freundlich isotherm models and plot of K_R as a function of initial Hg(II) concentration; XPS survey and FTIR spectra of Cyst-prGO before and after mercury adsorption; XPS high resolution spectra of Cyst-prGO before and after mercury adsorption; table of comparison of regeneration cycle of various adsorbents for Hg(II) (PDF)

■ AUTHOR INFORMATION

Corresponding Author

*E-mail: dusan.losic@adelaide.edu.au.

ORCID

Diana N. H. Tran: 0000-0002-4023-3373

Dusan Losic: 0000-0002-1930-072X

Author Contributions

The manuscript was written through contributions of all authors. All authors have given approval to the final version of the manuscript.

Funding

The Australian Research Council (ARC IH150100003) for Graphene Enabled Industry Transformation Hub

DOI: 10.1021/acsami.8b17131
ACS Appl. Mater. Interfaces 2019, 11, 6350−6362

Notes

The authors declare no competing financial interest.

■ ACKNOWLEDGMENTS

We acknowledge the funding by the ARC Research for Graphene Enabled Industry Transformation Hub, (IH150100003) and thank The University of Adelaide, School of Chemical Engineering and Dr Sarah Gilbert (Adelaide Microscopy) for her technical support for ICP−MS measurements.

■ ABBREVIATIONS

GO = graphene oxide
graphene-DE-αFeOOH = graphene hybrids decorated with iron nanoparticles interconnected with diatoms
graphene-DE-αFeOOH-SH = thiol modified with 3-mercaptopropyltrimethoxysilane graphene hybrids decorated with iron nanoparticles interconnected with diatoms
Cyst-prGO = cysteamine modified partially reduced graphene oxide
Hg = mercury
H_2SO_4 = sulfuric acid
H_3PO_4 = phosphoric acid
H_2O_2 = hydrogen peroxide
HCl = hydrochloric acid
HNO_3 = nitric acid
NaOH = sodium hydroxide
C_2H_7NS = cysteamine
$HgCl_2$ = mercury(II) chloride
CH_4N_2S = thiourea
DMF = N,N-dimethylforamide
$C_8H_{12}N_4$/AIBN = 2,2-azobis-2-methylpropionitrile
SEM = scanning electron microscopy
TEM = transmission electron microscopy
FTIR = Fourier Transform Infrared spectroscopy
TGA = thermogravimetric analysis
XRD = X-ray diffraction
XPS = X-ray photoelectron spectroscopy
SSA = specific surface area
MB = methylene blue
UV−vis = UV−vis spectroscopy
ICP−MS = inductively coupled plasma-mass spectroscopy
C_0 and C_t = initial and mercury concentration at time (t)
V = volume of solution
m = mass of adsorbent
R_t = removal efficiency at time (t)
I_D/I_G = intensity ratio of D and G bands
GO/Fe−Mn = graphene oxide/Fe−Mn hybrids
IT-PRGO = 2-Imino-4-thiobiuret-Partially reduced graphene oxide
Fe_3O_4-Polypyrrole-GO = Fe_3O_4-Polypyrrole-graphene oxide
EGO = exfoliated graphene oxide
conc = concentration
temp = temperature
max = maximum
ref = reference
C = carbon
O = oxygen
S = sulfur
N = nitrogen
AC = activated carbon

■ REFERENCES

(1) Sadegh, H.; Ali, G. A. M.; Gupta, V. K.; Makhlouf, A. S. H.; Shahryari-ghoshekandi, R.; Nadagouda, M. N.; Sillanpää, M.; Megiel, E. The Role of Nanomaterials as Effective Adsorbents and Their Applications in Wastewater Treatment. *J. Nanostructure Chem.* **2017**, *7*, 1−14.
(2) Theron, J.; Walker, J. A.; Cloete, T. E. Nanotechnology and Water Treatment: Applications and Emerging Opportunities. *Crit. Rev. Microbiol.* **2008**, *34*, 43−69.
(3) Sweetman, M.; May, S.; Mebberson, N.; Pendleton, P.; Vasilev, K.; Plush, S.; Hayball, J. Activated Carbon, Carbon Nanotubes and Graphene: Materials and Composites for Advanced Water Purification. *C* **2017**, *3*, 18.
(4) Li, G.; Zhao, Z.; Liu, J.; Jiang, G. Effective Heavy Metal Removal from Aqueous Systems by Thiol Functionalized Magnetic Mesoporous Silica. *J. Hazard. Mater.* **2011**, *192*, 277−283.
(5) Walcarius, A.; Mercier, L. Mesoporous Organosilica Adsorbents: Nanoengineered Materials for Removal of Organic and Inorganic Pollutants. *J. Mater. Chem.* **2010**, *20*, 4478−4511.
(6) Kabiri, S.; Tran, D. N. H.; Azari, S.; Losic, D. Graphene-Diatom Silica Aerogels for Efficient Removal of Mercury Ions from Water. *ACS Appl. Mater. Interfaces* **2015**, *7*, 11815−11823.
(7) Gadipelli, S.; Guo, Z. X. Graphene-based Materials: Synthesis and Gas Sorption, Storage and Separation. *Prog. Mater. Sci.* **2015**, *69*, 1−60.
(8) Kemp, K. C.; Seema, H.; Saleh, M.; Le, N. H.; Mahesh, K.; Chandra, V.; Kim, K. S. Environmental Applications Using Graphene Composites: Water Remediation and Gas Adsorption. *Nanoscale* **2013**, *5*, 3149−3171.
(9) Kabiri, S.; Tran, D. N.; Cole, M. A.; Losic, D. Functionalized Three-Dimensional (3D) Graphene Composite for High Efficiency Removal of Mercury. *Environ. Sci.: Water Res. Technol.* **2016**, *2*, 390−402.
(10) Henriques, B.; Gonçalves, G.; Emami, N.; Pereira, E.; Vila, M.; Marques, P. A. A. P. Optimized Graphene Oxide Foam with Enhanced Performance and High Selectivity for Mercury Removal from Water. *J. Hazard. Mater.* **2016**, *301*, 453−461.
(11) Gao, W.; Majumder, M.; Alemany, L. B.; Narayanan, T. N.; Ibarra, M. A.; Pradhan, B. K.; Ajayan, P. M. Engineered Graphite Oxide Materials for Application in Water Purification. *ACS Appl. Mater. Interfaces* **2011**, *3*, 1821−1826.
(12) Kumar, A. S. K.; Jiang, S.-J. Preparation and Characterization of Exfoliated Graphene Oxide-L-cystine as an Effective Adsorbent of Hg (II) Adsorption. *RSC Adv.* **2015**, *5*, 6294−6304.
(13) Krishna Kumar, A. S.; Jiang, S.-J.; Tseng, W.-L. Facile Synthesis and Characterization of Thiol-Functionalized Graphene Oxide as Effective Adsorbent for Hg(II). *J. Environ. Chem. Eng.* **2016**, *4*, 2052−2065.
(14) Aghdam, K.; Panahi, H. A.; Alaei, E.; Hasani, A. H.; Moniri, E. Preparation of Functionalized Graphene Oxide and its Application as a Nanoadsorbent for Hg^{2+} Removal from Aqueous Solution. *Environ. Monit. Assess.* **2016**, *188*, 223.
(15) Hosseinzadeh, H.; Ramin, S. Fast and Enhanced Removal of Mercury from Aqueous Solutions by Magnetic Starch-g-poly(acrylamide)/Graphene Oxide Nanocomposite Superabsorbents. *Polym. Sci., Ser. B* **2016**, *58*, 457−473.
(16) Salavagione, H. J. Promising Alternative Routes for Graphene Production and Functionalization. *J. Mater. Chem. A* **2014**, *2*, 7138−7146.
(17) Hoyle, C. E.; Bowman, C. N. Thiol−Ene Click Chemistry. *Angew. Chem., Int. Ed.* **2010**, *49*, 1540−1573.
(18) Marcano, D. C.; Kosynkin, D. V.; Berlin, J. M.; Sinitskii, A.; Sun, Z.; Slesarev, A.; Alemany, L. B.; Lu, W.; Tour, J. M. Improved Synthesis of Graphene Oxide. *ACS Nano* **2010**, *4*, 4806−4814.
(19) Luong, N. D.; Sinh, L. H.; Johansson, L. S.; Campell, J.; Seppälä, J. Functional Graphene by Thiol-ene Click Chemistry. *Chem. - Eur. J.* **2015**, *21*, 3183−3186.

DOI: 10.1021/acsami.8b17131
ACS Appl. Mater. Interfaces 2019, 11, 6350−6362

(20) Tran, D. N.; Kabiri, S.; Wang, L.; Losic, D. Engineered Graphene−Nanoparticle Aerogel Composites for Efficient Removal of Phosphate from Water. *J. Mater. Chem. A* **2015**, *3*, 6844−6852.
(21) Lagergren, S. K. About the Theory of So-Called Adsorption of Soluble Substances. *Sven. Vetenskapsakad. Handingarl* **1898**, *24*, 1−39.
(22) Ho, Y. S.; McKay, G. Pseudo-Second Order Model for Sorption Processes. *Process Biochem.* **1999**, *34*, 451−465.
(23) Langmuir, I. The Constitution and Fundamental Properties of Solids and Liquids. II. Liquids. *J. Am. Chem. Soc.* **1917**, *39*, 1848−1906.
(24) Freundlich, H. Over the Adsorption in Solution. *Z. Phys. Chem.* **1906**, 385−470.
(25) Su, S.; Chen, B.; He, M.; Hu, B. Graphene Oxide−Silica Composite Coating Hollow Fiber Solid Phase Microextraction Online Coupled with Inductively Coupled Plasma Mass Spectrometry for the Determination of Trace Heavy Metals in Environmental Water Samples. *Talanta* **2014**, *123*, 1−9.
(26) Yari, M.; Norouzi, M.; Mahvi, A. H.; Rajabi, M.; Yari, A.; Moradi, O.; Tyagi, I.; Gupta, V. K. Removal of Pb(II) Ion from Aqueous Solution by Graphene Oxide and Functionalized Graphene Oxide-Thiol: Effect of Cysteamine Concentration on the Bonding Constant. *Desalin. Water Treat.* **2016**, *57*, 11195−11210.
(27) Khalil, E. S.; Saad, B.; Negim, E.-S. M.; Saleh, M. I. Novel Water-Soluble Chitosan Derivative Prepared by Graft Polymerization of Dicyandiamide: Synthesis, Characterisation, and Its Antibacterial Property. *J. Polym. Res.* **2015**, *22*, 116.
(28) Awad, F. S.; AbouZeid, K. M.; El-Maaty, W. M. A.; El-Wakil, A. M.; El-Shall, M. S. Efficient Removal of Heavy Metals from Polluted Water with High Selectivity for Mercury(II) by 2-Imino-4-thiobiuret−Partially Reduced Graphene Oxide (IT-PRGO). *ACS Appl. Mater. Interfaces* **2017**, *9*, 34230−34242.
(29) Deng, M.; Huang, Y.; Zhang, X.; Feng, Z.; Gou, J.; Sun, B. Preparation of a Novel Chelating Resin Bearing amidinothiourea Moieties and its Removal Properties for Hg(II) Ions in Aqueous Solution. *Sep. Sci. Technol.* **2016**, *51*, 1499−1508.
(30) Aina, V.; Ghigo, D.; Marchis, T.; Cerrato, G.; Laurenti, E.; Morterra, C.; Malavasi, G.; Lusvardi, G.; Menabue, L.; Bergandi, L. Novel Bio-Conjugate Materials: Soybean Peroxidase Immobilized on Bioactive Glasses Containing Au Nanoparticles. *J. Mater. Chem.* **2011**, *21*, 10970−10981.
(31) Fleissner, G.; Kozlowski, P. M.; Vargek, M.; Bryson, J. W.; O'Halloran, T. V.; Spiro, T. G. UVRR Spectroscopy and Vibrational Analysis of Mercury Thiolate Compounds Resembling d10 Metal Binding Sites in Proteins. *Inorg. Chem.* **1999**, *38*, 3523−3528.
(32) Orth, E. S.; Fonsaca, J. E. S.; Domingues, S. H.; Mehl, H.; Oliveira, M. M.; Zarbin, A. J. G. Targeted Thiolation of Graphene Oxide and its Utilization as Precursor for Graphene/Silver Nanoparticles Composites. *Carbon* **2013**, *61*, 543−550.
(33) El-Khodary, S. A.; El-Enany, G. M.; El-Okr, M.; Ibrahim, M. Preparation and Characterization of Microwave Reduced Graphite Oxide for High-Performance Supercapacitors. *Electrochim. Acta* **2014**, *150*, 269−278.
(34) Wojtoniszak, M.; Chen, X.; Kalenczuk, R. J.; Wajda, A.; Łapczuk, J.; Kurzewski, M.; Drozdzik, M.; Chu, P. K.; Borowiak-Palen, E. Synthesis, Dispersion, and Cytocompatibility of Graphene Oxide and Reduced Graphene Oxide. *Colloids Surf., B* **2012**, *89*, 79−85.
(35) Tran, D. N. H.; Kabiri, S.; Losic, D. A Green Approach for the Reduction of Graphene Oxide Nanosheets Using Non-Aromatic Amino Acids. *Carbon* **2014**, *76*, 193−202.
(36) Navaee, A.; Salimi, A. Efficient Amine Functionalization of Graphene Oxide through the Bucherer Reaction: an Extraordinary Metal-Free Electrocatalyst for the Oxygen Reduction Reaction. *RSC Adv.* **2015**, *5*, 59874−59880.
(37) Jiayang, Z.; Chubei, W.; Jianwei, Z. Ethylenediamine-Functionalized Reduced Graphene Oxide for Enhanced Methylene Blue Removal. *Environ. Eng. Sci.* **2017**, *34*, 394−400.
(38) Liu, D.; Wang, Y.; Zhao, G. Preparation of Graphene Aerogel for Determining Oxalic Acid. *Int. J. Electrochem. Sci.* **2015**, *10*, 6794−6802.
(39) Kudelski, A.; Hill, W. Raman Study on the Structure of Cysteamine Monolayers on Silver. *Langmuir* **1999**, *15*, 3162−3168.
(40) Liu, J.; Zhu, K.; Jiao, T.; Xing, R.; Hong, W.; Zhang, L.; Zhang, Q.; Peng, Q. Preparation of Graphene Oxide-Polymer Composite Hydrogels via Thiol-ene Photopolymerization as Efficient Dye Adsorbents for Wastewater Treatment. *Colloids Surf., A* **2017**, *529*, 668−676.
(41) Baskoro, F.; Wong, C.-B.; Kumar, S. R.; Chang, C.-W.; Chen, C.-H.; Chen, D. W.; Lue, S. J. Graphene Oxide-Cation Interaction: Inter-Layer Spacing and Zeta Potential Changes in Response to Various Salt Solutions. *J. Membr. Sci.* **2018**, *554*, 253−263.
(42) Yu, H.; Xie, K.; Hu, J.; Shen, C.; Wang, J.-G.; Wei, B. The Importance of Raw Graphite Size to the Capacitive Properties of Graphene Oxide. *RSC Adv.* **2016**, *6*, 17023−17028.
(43) Han, F.; Yang, S.; Jing, W.; Jiang, K.; Jiang, Z.; Liu, H.; Li, L. A Highly Efficient Synthetic Process of Graphene Films with Tunable Optical Properties. *Appl. Surf. Sci.* **2014**, *314*, 71−77.
(44) Tian, Z.; Li, J.; Zhu, G.; Lu, J.; Wang, Y.; Shi, Z.; Xu, C. Facile Synthesis of Highly Conductive Sulfur-Doped Reduced Graphene Oxide Sheets. *Phys. Chem. Chem. Phys.* **2016**, *18*, 1125−1130.
(45) Tadjarodi, A.; Ferdowsi, S. M.; Zare-Dorabei, R.; Barzin, A. Highly Efficient Ultrasonic-Assisted Removal of Hg(II) Ions on Graphene Oxide Modified with 2-Pyridinecarboxaldehyde Thiosemicarbazone: Adsorption Isotherms and Kinetics Studies. *Ultrason. Sonochem.* **2016**, *33*, 118−128.
(46) Fu, Y.; Yang, Y.; Tuersun, T.; Yu, Y.; Zhi, J. Simple Preparation and Highly Selective Detection of Silver Ions Using an Electrochemical Sensor Based on Sulfur-Doped Graphene and a 3,3′,5,5′-Tetramethylbenzidine Composite Modified Electrode. *Analyst* **2018**, *143*, 2076−2082.
(47) Chang, Y.; Hong, F.; He, C.; Zhang, Q.; Liu, J. Nitrogen and Sulfur Dual-Doped Non-Noble Catalyst Using Fluidic Acrylonitrile Telomer as Precursor for Efficient Oxygen Reduction. *Adv. Mater.* **2013**, *25*, 4794−4799.
(48) Xu, J.; He, S.; Zhang, H.; Huang, J.; Lin, H.; Wang, X.; Long, J. Layered Metal-Organic Framework/Graphene Nanoarchitectures for Organic Photosynthesis under Visible Light. *J. Mater. Chem. A* **2015**, *3*, 24261−24271.
(49) Yang, L.; Qin, A.; Chen, S.; Liao, L.; Qin, J.; Zhang, K. Manganese (II) Enhanced Fluorescent Nitrogen-Doped Graphene Quantum Dots: A Facile and Efficient Synthesis and Their Applications for Bioimaging and Detection of Hg^{2+} Ions. *RSC Adv.* **2018**, *8*, 5902−5911.
(50) Jalani, G.; Cerruti, M. Nano Graphene Oxide-Wrapped Gold Nanostars as Ultrasensitive and Stable SERS Nanoprobes. *Nanoscale* **2015**, *7*, 9990−9997.
(51) Tang, J.; Huang, Y.; Gong, Y.; Lyu, H.; Wang, Q.; Ma, J. Preparation of a Novel Graphene Oxide/Fe-Mn Composite and Its Application for Aqueous Hg(II) Removal. *J. Hazard. Mater.* **2016**, *316*, 151−158.
(52) Liu, T.; Yang, M.; Wang, T.; Yuan, Q. Prediction Strategy of Adsorption Equilibrium Time Based on Equilibrium and Kinetic Results To Isolate Taxifolin. *Ind. Eng. Chem. Res.* **2012**, *51*, 454−463.
(53) Kushwaha, S.; Sreedhar, B.; Padmaja, P. Sorption of Phenyl Mercury, Methyl Mercury, and Inorganic Mercury onto Chitosan and Barbital Immobilized Chitosan: Spectroscopic, Potentiometric, Kinetic, Equilibrium, and Selective Desorption Studies. *J. Chem. Eng. Data* **2010**, *55*, 4691−4698.
(54) Navarro, A. Review of Characteristics of Mercury Speciation and Mobility from Areas of Mercury Mining in Semi-Arid Environments. *Rev. Environ. Sci. Bio/Technol.* **2008**, *7*, 287−306.
(55) Puigdomenech, I. Make Equilibrium using Sophisticated Algorithms (MEDUSA) program. *Inorganic Chemistry Department. Royal Institute of Technology* **2004**, *100*, 44.
(56) Langmuir, I. The Adsorption of Gases on Plane Surfaces of Glass, Mica and Platinum. *J. Am. Chem. Soc.* **1918**, *40*, 1361−1403.

DOI: 10.1021/acsami.8b17131
ACS Appl. Mater. Interfaces 2019, 11, 6350−6362

(57) Poots, V. J. P.; McKay, G.; Healy, J. J. Removal of Basic Dye from Effluent Using Wood as an Adsorbent. *J. Water Pollut. Control Fed.* **1978**, *50*, 926−935.
(58) Hall, K. R.; Eagleton, L. C.; Acrivos, A.; Vermeulen, T. Pore- and Solid-Diffusion Kinetics in Fixed-Bed Adsorption under Constant-Pattern Conditions. *Ind. Eng. Chem. Fundam.* **1966**, *5*, 212−223.
(59) Guo, X.; Du, B.; Wei, Q.; Yang, J.; Hu, L.; Yan, L.; Xu, W. Synthesis of Amino Functionalized Magnetic Graphenes Composite Material and its Application to Remove Cr(VI), Pb(II), Hg(II), Cd(II) and Ni(II) from Contaminated Water. *J. Hazard. Mater.* **2014**, *278*, 211−220.
(60) Zhou, C.; Zhu, H.; Wang, Q.; Wang, J. X.; Cheng, J.; Guo, Y. F.; Zhou, X. J.; Bai, R. B. Adsorption of Mercury (II) with an Fe_3O_4 Magnetic Polypyrrole-Graphene Oxide Nanocomposite. *RSC Adv.* **2017**, *7*, 18466−18479.
(61) Ahmed, S.; Brockgreitens, J.; Xu, K.; Abbas, A. A Nanoselenium Sponge for Instantaneous Mercury Removal to Undetectable Levels. *Adv. Funct. Mater.* **2017**, *27*.
(62) Ke, J.; Li, X.; Zhao, Q.; Hou, Y.; Chen, J. Ultrasensitive Quantum Dot Fluorescence Quenching Assay for Selective Detection of mercury Ions in Drinking Water. *Sci. Rep.* **2015**, *4*, 5624.
(63) Wang, X. Q.; Wang, P.; Ning, P.; Ma, Y. X.; Wang, F.; Guo, X. L.; Lan, Y. Adsorption of Gaseous Elemental Mercury with Activated Carbon Impregnated with Ferric Chloride. *RSC Adv.* **2015**, *5*, 24899−24907.
(64) Xu, H.; Xu, D. C.; Wang, Y. Natural Indices for the Chemical Hardness/Softness of Metal Cations and Ligands. *ACS Omega* **2017**, *2*, 7185−7193.
(65) Medhekar, N. V.; Ramasubramaniam, A.; Ruoff, R. S.; Shenoy, V. B. Hydrogen Bond Networks in Graphene Oxide Composite Paper: Structure and Mechanical Properties. *ACS Nano* **2010**, *4*, 2300−2306.
(66) Chowdhury, S.; Mazumder, M. A. J.; Al-Attas, O.; Husain, T. Heavy Metals in Drinking Water: Occurrences, Implications, and Future Needs in Developing Countries. *Sci. Total Environ.* **2016**, *569*−*570*, 476−488.
(67) Ritter, J. A.; Bibler, J. P. Removal of Mercury from Waste Water: Large-Scale Performance of an Ion Exchange Process. *Water Sci. Technol.* **1992**, *25*, 165−172.
(68) Ziaei, E.; Mehdinia, A.; Jabbari, A. A Novel Hierarchical Nanobiocomposite of Graphene Oxide−Magnetic Chitosan Grafted with Mercapto as a Solid Phase Extraction Sorbent for the Determination of Mercury Ions in Environmental Water Samples. *Anal. Chim. Acta* **2014**, *850*, 49−56.
(69) Rocha, L. S.; Lopes, C. B.; Henriques, B.; Tavares, D. S.; Borges, J. A.; Duarte, A. C.; Pereira, E. Competitive Effects on Mercury Removal by an Agricultural Waste: Application to Synthetic and Natural Spiked Waters. *Environ. Technol.* **2014**, *35*, 661−673.

DOI: 10.1021/acsami.8b17131
ACS Appl. Mater. Interfaces 2019, 11, 6350−6362

Supporting Information

Multifunctional Binding Chemistry on Modified Graphene Composite for Selective and Highly Efficient Adsorption of Mercury

Pei Lay Yap[†,‡], *Shervin Kabiri*[†,‡], *Diana, N.H. Tran*[†,‡] *and Dusan Losic*[*†,‡]

[†]School of Chemical Engineering, The University of Adelaide, Adelaide, SA 5005, Australia

[‡]ARC Hub for Graphene Enabled Industry Transformation, The University of Adelaide, Adelaide, SA 5005, Australia

Corresponding author: dusan.losic@adelaide.edu.au

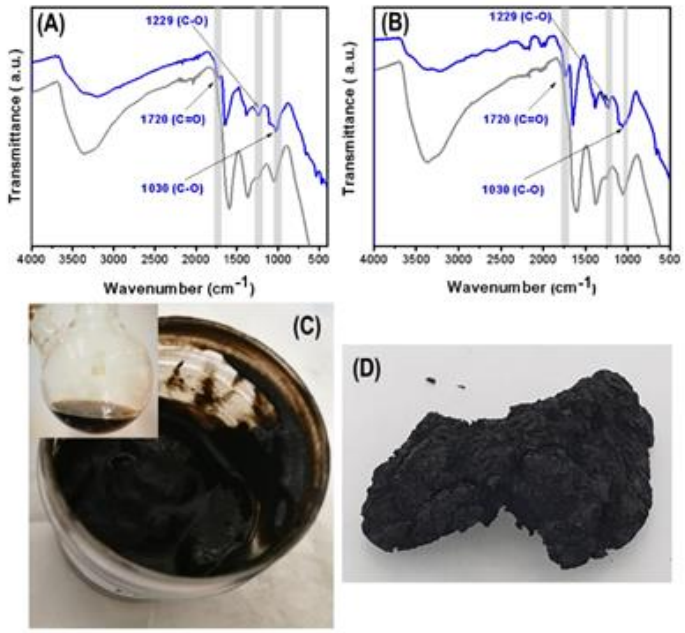

Figure S1. (A) FTIR spectra of samples prepared with GO: cysteamine =10: 5, 70 ˚C, 12 hours and (B) FTIR spectra of control samples (without cysteamine) at 70 ˚C, 12 hours. Blue line represents washing step using hexane, ethyl acetate and ethanol. Grey line represents washing step using NaOH and ethanol and grey shaded area represents significant changes on IR bands. Photographs of Cyst-prGO (C) after sequential washing steps using hexane, ethyl acetate, ethanol and water with the inset displaying the final product before washing steps and (D) after freeze-drying.

The significant changes in FTIR graphs during washing steps are evidenced by the presence of various bands attributed to the oxygen functional groups including peaks at around 1720 cm^{-1} (C=O of COOH), 1030 cm^{-1} and 1229 cm^{-1} (C-O) on the FTIR spectra (Figure S1A) using our modified washing step[1-4]. To further verify this result, we synthesized two control samples (without cysteamine) at the same functionalization condition with two different washing steps. As displayed in Figure S1B, the disappearance of the aforementioned peaks on the FTIR spectrum on the control

sample when NaOH was used in the washing step further affirmed the loss of the oxygen functionalities during the washing step. This shows that NaOH has greatly reduced the GO by removing several oxygen functionalities due to the neutralisation reaction between acid and base in the washing step. Hence, the modified washing step using hexane and ethyl acetate was found to successfully produce the functionalized adsorbent without compensating the oxygen functional groups attached on GO.

Characterizations.

The prepared solid materials were characterized by several techniques including scanning electron microscopy equipped with EDX Silicon Drift Detectors (FE-SEM, Quanta 450 FEG, FEI, USA; EDX, Ultim Max 170mm SDD, Oxford Instruments, UK) and transmission electron microscopy (TEM, Tecnai G2 Spirit) to characterize the morphology of the materials. Fourier Transform Infrared spectroscopy (FTIR, Nicolet 6700, Thermo Fisher) recorded in the range of 500-4000 cm^{-1} was used to identify the functional groups present in the materials. Raman spectroscopy (LabRAM HR Evolution, Horiba Jvon Yvon Technology, Japan) with a 532 nm laser (mpc 3000) as excitation source was employed to determine the vibrational characteristics of the materials. All the spectra were collected with an integration time of 10 seconds each on 3 different spots. The X-ray diffraction (600 Miniflex, Rigaco, Japan) was used to unveil the composition of the materials in the range of 2θ = 5-80° at 40 kV and 15 mA with the scan speed of $10^{\circ}min^{-1}$. Thermal decomposition of the materials was studied using thermogravimetric analysis (TGA, Q500, TA Instruments, USA) under air atmosphere with the samples heated to 900 °C at a heating rate of 10 °C min^{-1}. The zeta potential of the prepared adsorbent was measured as a function of pH in triplicate using a Malvern Zetasizer (Nanoseries, Australia). The adsorbent was

dispersed in Milli-Q water with the pH of the mixture adjusted using HCl or NaOH in the range of 3-10. The elemental composition and chemical state of the materials were determined using X-ray photoelectron spectrometer, AXIS Ultra_DLD (Kratos, UK) equipped with a monochromatic Al Kα radiation source (hv =1486.7 eV) at 225 W, 15 kVand 15 mA. Survey scans were performed at 0.5 eV step size over -10-1100 eV at the pass energy of 160 eV while high resolution data were acquired with a 0.1 eV step size and pass energy of 20 eV. The fitting of curves and data processing were performed using Casa XPS™ software. Solution ICP-MS (QQQ 8900, Agilent) was used to measure the remaining concentration of Hg (II) solution after the adsorption experiments. The specific surface area (SSA) of the materials was determined by methylene blue (MB) adsorption method using UV-Vis spectroscopy (Shimadzu UV-1601, Japan) as reported in our previous work.[2]

Adsorption kinetics.

The pseudo-first order equation:[5]

$$\log(q_e - q_t) = \log q_e - \frac{k_1}{2.303} t$$

The pseudo-second order equation:[6]

$$\frac{t}{q_t} = \frac{1}{k_2 q_e^2} + \frac{t}{q_e}$$

where q_e and q_t represent the amount of mercury (II) ions adsorbed (mg g^{-1}) at equilibrium and at time t respectively; k_1, *and* k_2 are the rate constants for the pseudo-first order and pseudo-second order kinetic models respectively.

Adsorption isotherms.

Langmuir isotherm is used to describe the monolayer coverage of sorption of molecule onto homogeneous active sites on adsorbents while Freundlich isotherm is based on the adsorption on the heterogeneous surface with uniform energy and it is not confined to the formation of monolayer.[7] The collected experimental data were fitted into the corresponding linearized equations as displayed below:

The Langmuir equation:[8]

$$\frac{C_e}{q_e} = \frac{1}{bq_{max}} + \frac{C_e}{q_{max}}$$

where q_e is the adsorption capacity (mg g^{-1}), C_e denotes the concentration of mercury (II) ions at equilibrium (mg L^{-1}); b and q_{max} are the Langmuir constants derived from the intercept and slope of the linear plot of C_e/q against C_e respectively. On another hand, the favourableness of a sorption process in a batch adsorption system can also be predicted using isotherm shape factor analysis with a dimensionless constant, separation factor, K_R as defined in the following relationship:[9-10]

$$K_R = \frac{1}{1 + bC_0}$$

where K_R is the dimensionless separation factor, C_0 is the initial Hg (II) concentration and b is the Langmuir constant. The value of K_R indicates the favourableness of a sorption process with $K_R > 1$ for unfavourable process, $0 < K_R < 1$ being favourable, $K_R = 1$ being linear and $K_R = 0$ for irreversible process.

The Freundlich equation:[11]

$$\log q_e = \frac{1}{n}\log C_e + \log K$$

where K signifies the Freundlich adsorption constant (L mg^{-1}) and $1/n$ is the adsorption intensity which can be determined from the intercept and slope of the plot of log q_e versus $log\ C_e$.

Materials characterizations.

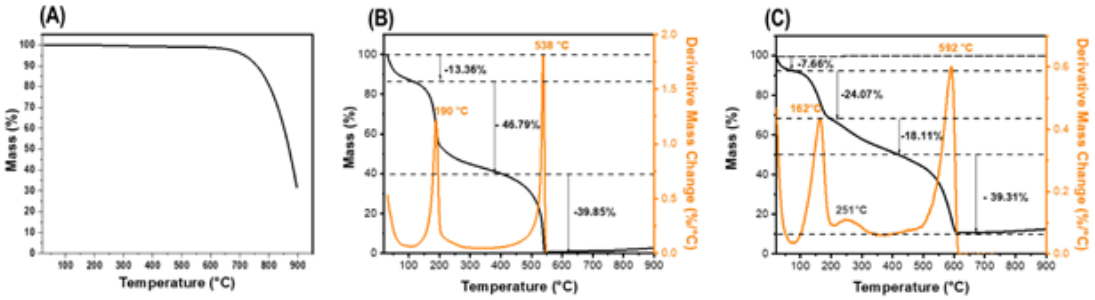

Figure S2. TGA of (A) graphite, TGA and derivative mass change of (B) GO and (C) Cyst-prGO showing stages of mass loss.

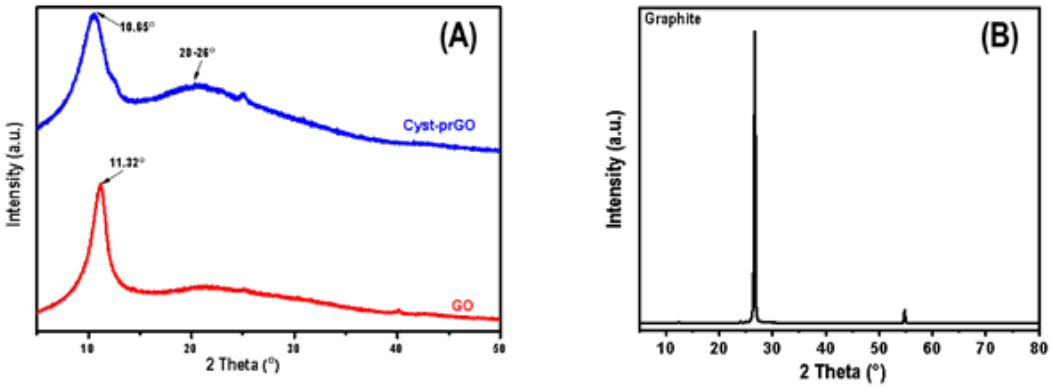

Figure S3. XRD patterns of (A) GO, Cyst-prGO and (B) graphite.

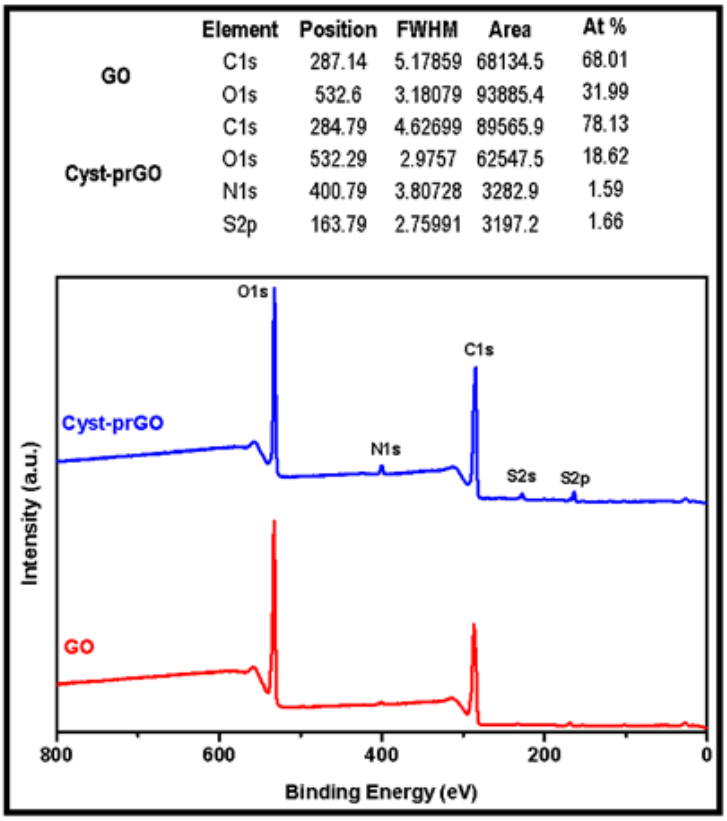

Figure S4. XPS survey spectra of GO, Cyst-prGO and their respective normalized atomic quantification.

Adsorption kinetics and isotherms.

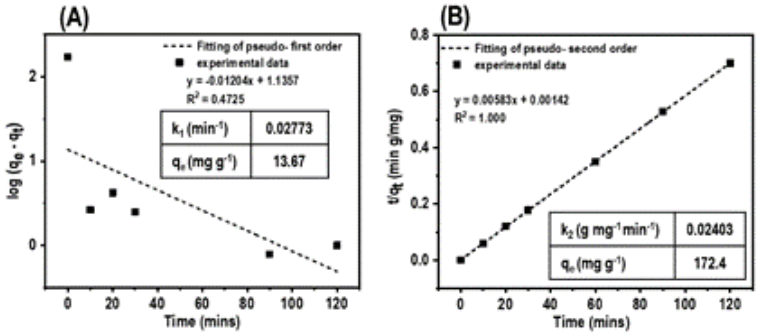

Figure S5. Fitting of experimental data of Hg (II) adsorption on 10 mg/L of Cyst-prGO for (A) pseudo-first order and (B) pseudo-second order kinetic models. Conditions: pH = 5.3, $[Hg^{2+}]_i$ = ~1.5 mg L^{-1}, T= 23.0 °C.

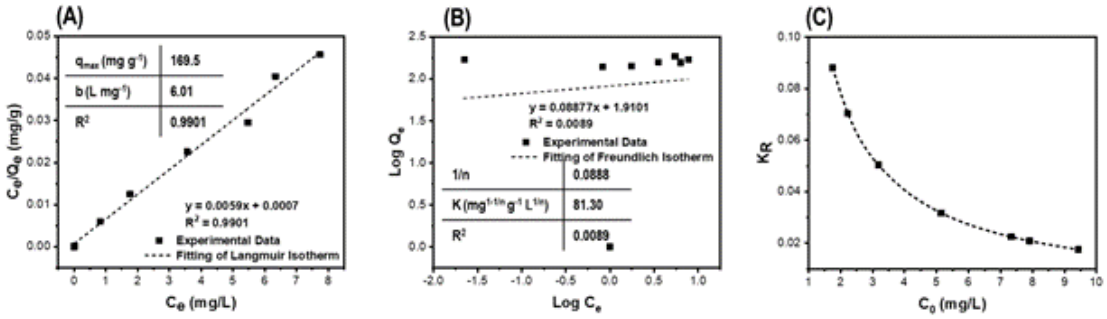

Figure S6. Fitting of experimental data of Hg (II) adsorption on Cyst-prGO for (A) Langmuir (B) Freundlich isotherm models and (C) plot of K_R against initial Hg (II) concentration for Hg (II) adsorption on Cyst-prGO. Conditions: pH = 5.3, $[Hg^{2+}]_i$ = 0- 10 mg L^{-1}, adsorbent dosage =10 mg L^{-1}, T= 20.6 °C.

Adsorption mechanism.

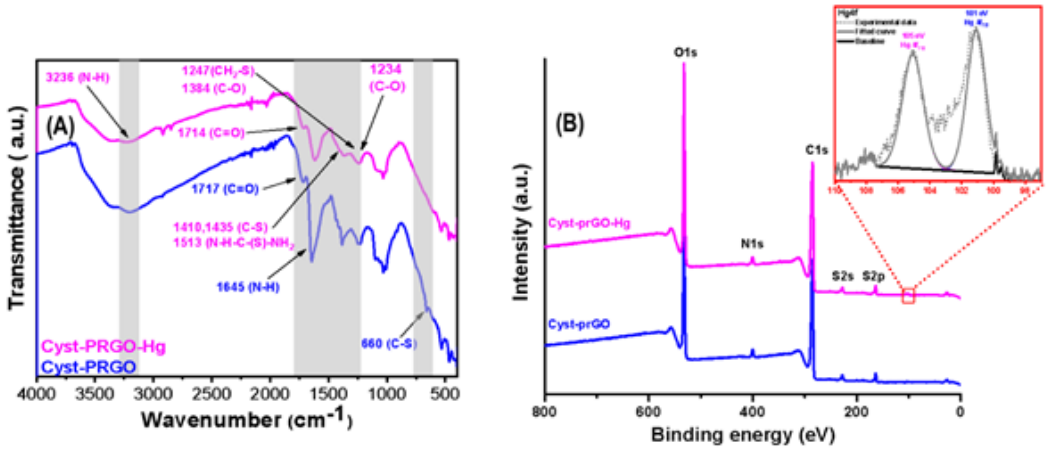

Figure S7. (A) FTIR of Cyst-prGO before and after Hg (II) adsorption (Grey shaded area represents changes after Hg (II) adsorption) and (B) XPS survey spectra of Cyst-prGO before and after Hg (II) adsorption with inset of high resolution spectrum Hg4f.

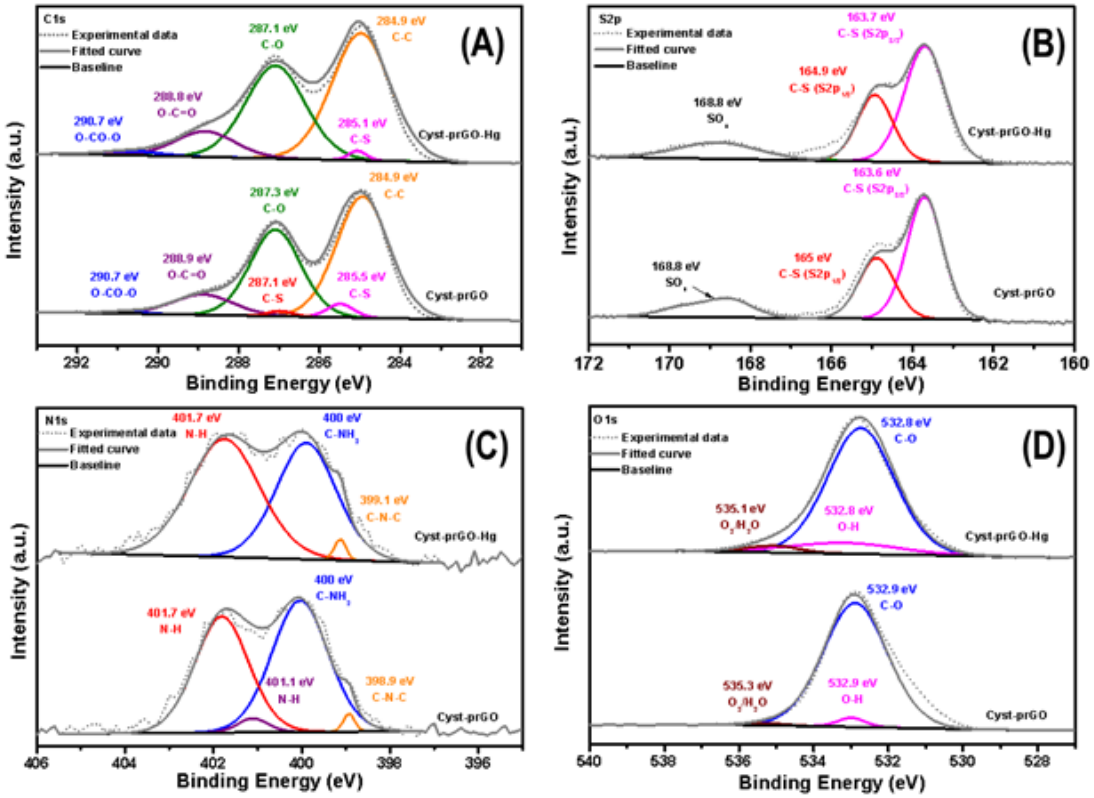

Figure S8. XPS high resolution spectra of (A) C1s (B) S2p (C) N1s and (D) O1s of Cyst-prGO before and after mercury adsorption.

Regeneration of adsorbent.

Table S1. Comparison of regeneration cycle of various adsorbents for Hg (II).

Type of Hg Adsorbent	Regeneration cycles with > 95% removal efficiency	Reference
Graphene oxide modified with 2-pyridinecarboxaldehyde thiosemicarbazone	0 cycle	12
Sulfur / reduced graphene oxide nanohybrid (SRGO) by lemon juice	2 cycles	13
Thiol-functionalized graphene oxide by mercapto benzothiazole	3 cycles	14
Exfoliated graphene oxide-L-cystine	4 cycles	15
Cyst-prGO	**5 cycles**	**This work**

References:

(1) Kabiri, S.; Tran, D. N.; Cole, M. A.; Losic, D. Functionalized three-dimensional (3D) graphene composite for high efficiency removal of mercury. *Environ. Sci.: Water Res. Technol* **2016,** *2*, 390-402.

(2) Tran, D. N.; Kabiri, S.; Wang, L.; Losic, D. Engineered Graphene–Nanoparticle Aerogel Composites for Efficient Removal of Phosphate from Water. *J. Mater. Chem. A* **2015,** *3*, 6844-6852.

(3) Kabiri, S.; Tran, D. N. H.; Azari, S.; Losic, D. Graphene-Diatom Silica Aerogels for Efficient Removal of Mercury Ions from Water. *ACS Appl. Mater. Interfaces* **2015,** *7*, 11815-11823.

(4) Su, S.; Chen, B.; He, M.; Hu, B. Graphene Oxide–Silica Composite Coating Hollow Fiber Solid Phase Microextraction Online Coupled with Inductively Coupled Plasma Mass Spectrometry for the Determination of Trace Heavy Metals in Environmental Water Samples. *Talanta* **2014,** *123*, 1-9.

(5) Lagergren, S. K. About the Theory of So-Called Adsorption of Soluble Substances. *Sven. Vetenskapsakad. Handingarl* **1898,** *24*, 1-39.

(6) Ho, Y. S.; McKay, G. Pseudo-Second Order Model for Sorption Processes. *Process Biochem.* **1999,** *34*, 451-465.

(7) Bera, R.; Kundu, S.; Patra, A. 2D Hybrid Nanostructure of Reduced Graphene Oxide–CdS Nanosheet for Enhanced Photocatalysis. *ACS Appl. Mater. Interfaces* **2015,** *7*, 13251-13259.

(8) Langmuir, I. The Constitution and Fundamental Properties of Solids and Liquids. II. Liquids. *J. Am. Chem. Soc.* **1917,** *39*, 1848-1906.

(9) Poots, V. J. P.; McKay, G.; Healy, J. J. Removal of Basic Dye from Effluent Using Wood as an Adsorbent. *J. Water Pollut. Control Fed.* **1978,** *50*, 926-935.

(10) Hall, K. R.; Eagleton, L. C.; Acrivos, A.; Vermeulen, T. Pore- and Solid-Diffusion Kinetics in Fixed-Bed Adsorption under Constant-Pattern Conditions. *Ind. Eng. Chem. Fundam.* **1966,** *5*, 212-223.

(11) Freundlich, H. Over the Adsorption in Solution. *Z. Phys.Chem.* **1906,** 385-470.

(12) Tadjarodi, A.; Moazen Ferdowsi, S.; Zare-Dorabei, R.; Barzin, A. Highly Efficient Ultrasonic-Assisted Removal of Hg(II) Ions on Graphene Oxide Modified with 2-Pyridinecarboxaldehyde Thiosemicarbazone: Adsorption Isotherms and Kinetics Studies. *Ultrason. Sonochem.* **2016,** *33*, 118-128.

(13) Thakur, S.; Das, G.; Raul, P. K.; Karak, N. Green One-Step Approach to Prepare Sulfur/Reduced Graphene Oxide Nanohybrid for Effective Mercury Ions Removal. *The Journal of Physical Chemistry C* **2013,** *117*, 7636-7642.

(14) Krishna Kumar, A. S.; Jiang, S.-J.; Tseng, W.-L. Facile Synthesis and Characterization of Thiol-Functionalized Graphene Oxide as Effective Adsorbent for Hg(II). *J. Environ. Chem. Eng.* **2016,** *4*, 2052-2065.

(15) Kumar, A. S. K.; Jiang, S.-J. Preparation and Characterization of Exfoliated Graphene Oxide-L-cystine as an Effective Adsorbent of Hg (II) Adsorption. *RSC Adv.* **2015,** *5*, 6294-6304.

CHAPTER 6

FUNCTIONALIZED GRAPHENE COMPOSITES VIA PHOTOINITIATED THIOL-ENE CLICK APPROACH FOR WATER PURIFICATION

6. FUNCTIONALIZED GRAPHENE COMPOSITES VIA PHOTOINITIATED THIOL-ENE CLICK APPROACH FOR WATER PURIFICATION

6.1. Overview and Significance of Work

Efficient and sustainable water purification technologies are still highly sought-after due to uncontrollable widespread of multi-pollutants in water bodies. This section describes the design of three-dimentional (3D) sulfur-functionalized porous graphene aerogels through a green and scalable UV thiol-ene click approach. This work aims to:

- devise an energy-efficient, environmentally friendly, and scalable modification method for preparing robust graphene sorbents
- design robust bio-polymer sorbents with strong affinity and high regenerability to tackle multi water pollutants

Outcomes from this work fulfilled Objectives 3 and 4, which are consolidated in two published peer-reviewed research articles.

6.2. Statement of Authorship

Statement of Authorship

Title of Paper	Multithiol functionalized graphene bio-sponge via photoinitiated thiol-ene click chemistry for efficient heavy metal ions adsorption.
Publication Status	☒ Published ☐ Accepted for Publication ☐ Submitted for Publication ☐ Unpublished and Unsubmitted work written in manuscript style
Publication Details	Yap, P. L., Auyoong, Y. L., Hassan, K., Farivar, F., Tran, D. N. H., Ma, J., & Losic, D. (2020). Multithiol functionalized graphene bio-sponge via photoinitiated thiol-ene click chemistry for efficient heavy metal ions adsorption. Chemical Engineering Journal, 395, 124965.

Principal Author

Name of Principal Author (Candidate)	Pei Lay Yap		
Contribution to the Paper	Prepared, characterized and conducted performance testing on all the samples, interpreted data as well as wrote the manuscript.		
Overall percentage (%)	85%		
Certification:	This paper reports on original research I conducted during the period of my Higher Degree by Research candidature and is not subject to any obligations or contractual agreements with a third party that would constrain its inclusion in this thesis. I am the primary author of this paper.		
Signature		Date	01/09/20

Co-Author Contributions

By signing the Statement of Authorship, each author certifies that:

i. the candidate's stated contribution to the publication is accurate (as detailed above);

ii. permission is granted for the candidate in include the publication in the thesis; and

iii. the sum of all co-author contributions is equal to 100% less the candidate's stated contribution.

Name of Co-Author	Yow Loo Au Yoong		
Contribution to the Paper	Helped in sample characterization and revised manuscript.		
Signature		Date	02/10/20

Name of Co-Author	Kamrul Hassan		
Contribution to the Paper	Helped in sample characterization and revised manuscript.		
Signature		Date	02/10/20

Please cut and paste additional co-author panels here as required.

Statement of Authorship

Title of Paper	Multithiol functionalized graphene bio-sponge via photoinitiated thiol-ene click chemistry for efficient heavy metal ions adsorption.
Publication Status	☒ Published ☐ Accepted for Publication ☐ Submitted for Publication ☐ Unpublished and Unsubmitted w ork w ritten in manuscript style
Publication Details	Yap, P. L., Auyoong, Y. L., Hassan, K., Farivar, F., Tran, D. N. H., Ma, J., & Losic, D. (2020). Multithiol functionalized graphene bio-sponge via photoinitiated thiol-ene click chemistry for efficient heavy metal ions adsorption. Chemical Engineering Journal, 395, 124965.

Principal Author

Name of Principal Author (Candidate)	Pei Lay Yap		
Contribution to the Paper	Prepared, characterized and conducted performance testing on all the samples, interpreted data as well as wrote the manuscript.		
Overall percentage (%)	85%		
Certification:	This paper reports on original research I conducted during the period of my Higher Degree by Research candidature and is not subject to any obligations or contractual agreements with a third party that would constrain its inclusion in this thesis. I am the primary author of this paper.		
Signature		Date	01/09/20

Co-Author Contributions

By signing the Statement of Authorship, each author certifies that:

i. the candidate's stated contribution to the publication is accurate (as detailed above);

ii. permission is granted for the candidate in include the publication in the thesis; and

iii. the sum of all co-author contributions is equal to 100% less the candidate's stated contribution.

Name of Co-Author	Farzaneh Farivar		
Contribution to the Paper	Helped in sample characterization.		
Signature		Date	02/10/20

Name of Co-Author	Diana N.H. Tran		
Contribution to the Paper	Co-supervised and revised manuscript.		
Signature		Date	02/10/20

Please cut and paste additional co-author panels here as required.

Statement of Authorship

Title of Paper	Multithiol functionalized graphene bio-sponge via photoinitiated thiol-ene click chemistry for efficient heavy metal ions adsorption.
Publication Status	☒ Published ☐ Accepted for Publication ☐ Submitted for Publication ☐ Unpublished and Unsubmitted work written in manuscript style
Publication Details	Yap, P. L., Auyoong, Y. L., Hassan, K., Farivar, F., Tran, D. N. H., Ma, J., & Losic, D. (2020). Multithiol functionalized graphene bio-sponge via photoinitiated thiol-ene click chemistry for efficient heavy metal ions adsorption. Chemical Engineering Journal, 395, 124965.

Principal Author

Name of Principal Author (Candidate)	Pei Lay Yap		
Contribution to the Paper	Prepared, characterized and conducted performance testing on all the samples, interpreted data as well as wrote the manuscript.		
Overall percentage (%)	85%		
Certification:	This paper reports on original research I conducted during the period of my Higher Degree by Research candidature and is not subject to any obligations or contractual agreements with a third party that would constrain its inclusion in this thesis. I am the primary author of this paper.		
Signature		Date	01/09/20

Co-Author Contributions

By signing the Statement of Authorship, each author certifies that:

i. the candidate's stated contribution to the publication is accurate (as detailed above);

ii. permission is granted for the candidate in include the publication in the thesis; and

iii. the sum of all co-author contributions is equal to 100% less the candidate's stated contribution.

Name of Co-Author	Jun Ma		
Contribution to the Paper	Edited and revised manuscript.		
Signature	Jun Ma Digitally signed by Jun Ma Date: 2020.09.21 09:11:23 +09'30'	Date	21/09/20

Name of Co-Author	Dusan Losic		
Contribution to the Paper	Supervised the development of work, edited, revised the manuscript and acted as the corresponding author.		
Signature		Date	02/10/20

Please cut and paste additional co-author panels here as required.

6.3. Published work

This section is presented as a published peer-reviewed article:

1. ***Yap, P. L.***, *Auyoong, Y. L., Hassan, K., Farivar, F., Tran, D. N. H., Ma, J., & Losic, D. (2020). Multithiol functionalized graphene bio-sponge via photoinitiated thiol-ene click chemistry for efficient heavy metal ions adsorption. Chemical Engineering Journal, 395, 124965.* Reproduced with permission.[19] Copyright (2020) Elsevier.

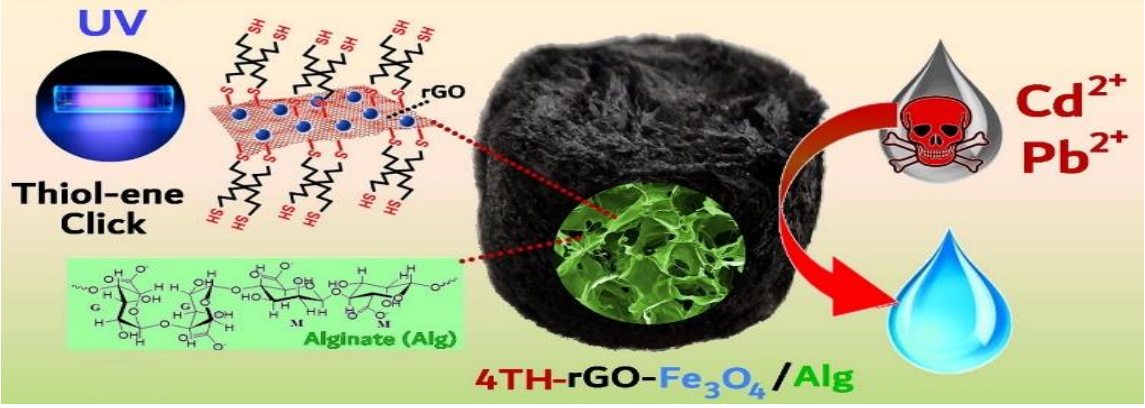

Figure 15. Graphical abstract of "*Multithiol functionalized graphene bio-sponge via photoinitiated thiol-ene click chemistry for efficient heavy metal ions adsorption*". *Reproduced with permission.[19] Copyright (2020) Elsevier.*

Chemical Engineering Journal 395 (2020) 124965

Contents lists available at ScienceDirect

Chemical Engineering Journal

journal homepage: www.elsevier.com/locate/cej

Multithiol functionalized graphene bio-sponge via photoinitiated thiol-ene click chemistry for efficient heavy metal ions adsorption

Pei Lay Yap[a,b], Yow Loo Auyoong[c], Kamrul Hassan[a,b], Farzaneh Farivar[a,b], Diana N.H. Tran[a,b], Jun Ma[b,d,e], Dusan Losic[a,b,*]

[a] School of Chemical Engineering and Advanced Materials, The University of Adelaide, Adelaide, SA 5005, Australia
[b] ARC Hub for Graphene Enabled Industry Transformation, The University of Adelaide, Adelaide, SA 5005, Australia
[c] Innovation and Commercial Partnerships, The University of Adelaide, Adelaide, SA 5000, Australia
[d] Future Industries Institute, University of South Australia, Mawson Lakes, SA 5095, Australia
[e] School of Engineering, University of South Australia, Mawson Lakes, SA 5095, Australia

HIGHLIGHTS

- Multithiol-functionalized graphene bio-sponge was prepared by UV thiol-ene click method.
- High density (> 10%) and controllable level of S-containing groups were achieved by this process.
- Outstanding selectivity towards Pb (II) and Cd (II) surpassed commercial adsorbents.
- Remarkable regeneration ability after five cycles meeting US EPA limits for Pb.
- A promising adsorbent for heavy metals removal from waste waters is demonstrated.

GRAPHICAL ABSTRACT

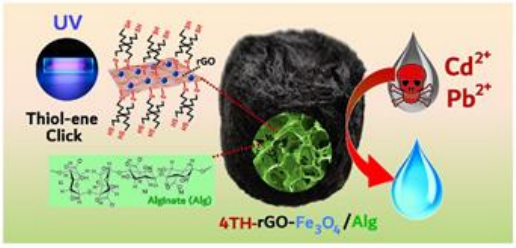

ARTICLE INFO

Keywords:
Multithiol functionalized graphene composites
Photoinitiated
Thiol-ene click
Green chemistry
Water treatment
Heavy metals removal

ABSTRACT

Heavy metals contamination in the natural waters remains an unresolved environmental challenge pressing for the development of purification technologies. This paper presents the green engineering of a new bio-sponge for heavy metals adsorption composed of alginate bio-polymeric network encapsulated with reduced graphene oxide (rGO) modified with iron oxide nanoparticles and covalently attached multithiol (pentaerythritol tetrakis-mercaptopropionate) molecules using photoinitiated thiol-ene click chemistry. The multithiol functionalized graphene bio-sponge (SH-Graphene bio-sponge) is designed to enhance adsorption performances of heavy metals including structural approach combined with oxygen functionalities and high density of sulfur-containing groups (10.2 at % S, confirmed by X-ray Photoelectron Spectroscopy, XPS) with high binding affinity towards specific heavy metals (Cd and Pb). It was shown that the level of thiol functionalization on the graphene structure within the bio-sponge can be controlled by tuning the Ultraviolet (UV) irradiation time without adjusting the concentration of the precursors. SH-functionalized graphene bio-sponge showed outstanding adsorption capacity for Pb (II): 101.01 mg/g and Cd (II): 102.99 mg/g, outperformed commercial and literature reported adsorbents in highly competitive selectivity studies using co-existing heavy metal ions (Cu, Co, Pb and Cd) spiked- sea water. The multithiol modified bio-sponge also showcased an excellent stability and reusability feature with only 0.015 mg/L Pb (II) detected, conforming the strict United States Environmental Protection Agency (US EPA) maximum contaminant level (MCL) for lead, after five recurring cycles using mixed heavy metal ions solution

* Corresponding author at: School of Chemical Engineering and Advanced Materials, The University of Adelaide, Adelaide, SA 5005, Australia.
E-mail address: dusan.losic@adelaide.edu.au (D. Losic).

https://doi.org/10.1016/j.cej.2020.124965
Received 21 February 2020; Received in revised form 1 April 2020; Accepted 2 April 2020
Available online 05 April 2020
1385-8947/

and acidic eluent. The outcomes from this work present valuable and promising contribution towards the development of a scalable and sustainable adsorbents for efficient remediation of heavy metals from waters.

1. Introduction

The deterioration of clean water regardless it is in the context of quantity or quality has been an alarming global challenge, leading to the global water scarcity and water stress these days. According to a recent statistics by World Resources Institute, 17 countries (about a quarter of the world's population) are identified as the regions with extremely high water stress [1]. Unpredictable climate change, growing freshwater demand due to increased population, and worsening water pollution are the prime factors contributing to the current water crisis. Water pollution particularly related to heavy metal ions such as lead, cadmium, mercury and chromium has been a major concern due to their bio-accumulative, toxic and carcinogenic properties, which adversely poses hazards to human health and environmental sustainability [2]. Due to the long range transport and high mobility of heavy metals in aquatic ecosystems which eventually magnify in the food chain, the urge to remove these noxious contaminants from our precious yet overexploited resource, water, is mandatory [3].

Existing water purification technologies including precipitation, membrane separation, reduction, ion exchange, electrochemical treatment and adsorption have been broadly applied to remove heavy metals from contaminated water. Adsorption, a mass transfer process to transport the pollutant substances from the liquid phase to the surface of a solid, which the adsorbates are then bound to the adsorbent network by physical or chemical interaction, is still the most desirable approach owing to its cost-effectiveness, flexibility in field operation, less energy- and labor- intensive in relative to the rest of the water treatment methods [4–6]. Although conventional adsorbent materials such as activated carbon, biochar, clay and cellulose are relatively low cost and possess high surface area, the binding affinity and adsorption performance of these materials towards the targeted contaminants (heavy metal ions) are unsatisfactory with poor sorbent recyclability due to the lack of chemical functionalities on the sorbent surface with high binding affinity to selectively remove specific metal ions from waters. To address these drawbacks, specific functional groups particularly sulfur-containing groups are crucial to modify the surface of the adsorbents in achieving higher sorption capacity and better selectivity for heavy metals [7]. To date, myriads of chemically modified adsorbents such as metal oxides, metal-based nanomaterials, metal organic frameworks, and carbon nanomaterials such as graphene oxide, graphene, functionalized graphene and their composites have been explored with improved adsorption performance towards heavy metals removal [8–11]. One of the key barriers being commonly overlooked in these developed adsorbents is their formulations in the forms of powder or suspension which may trigger concerns regarding the risk of nanomaterials for water security, separation and recovery limitations after adsorption process. These limitations undoubtedly restrict the advancement of nanomaterial-based adsorbents within the vicinity of lab-scale research, which hampers its implementation for real water remediation in field operations.

Natural biopolymers such as cellulose, chitosan, pectin and alginate on the other hand are green alternatives for the development of sustainable sorbent materials in the long run due to their non-toxicity, high biocompatibility, low cost, and high abundance [12]. Among the biopolymers, alginate, a polyanionic polymer, is one of the preferred candidates owing to its high hydrophilicity and high density of negatively charged oxygen-containing groups which can feasibly attract positively charged heavy metal ions. Apparently, the integration of anionic alginate with nanomaterials laden with desired functional groups to form crosslinked 3D polymeric networks can be used to overcome the barriers associated with water security due to the use of nanomaterials in water, sorbent-sorbate separation and recovery of spent sorbent after adsorption process. Previous studies have shown success of the use of 3D alginate-based sorbent and their modifications for targeted heavy metals adsorption including the fabrication of 3D porous graphene/lignin/alginate (PG/L/SA) via hydrothermal method for capturing Cd (II) and Pb (II) in the aqueous system [13]. Meanwhile, Z-j Shao et al. post-modified the alginate beads by mixing 2-acrylamido-2-methylpropane-1-sulfonic acid, N,N'-methylenebis(acrylamide) and ammonium persulfate for 12 h, followed by soaking the mixture under the ice-bath for 12 h before reacting the mixture in the oven for 3 h at 75 °C. The post-modified alginate beads exhibited promising adsorption capacity for heavy metal ions and methylene blue [14]. As reported by Kolodyriska et al., titania-silica modified with alginate was used to adsorb various heavy metal ions in water. The adsorbent was first prepared by heating titanium isopropoxide in 2-propanolinitially at

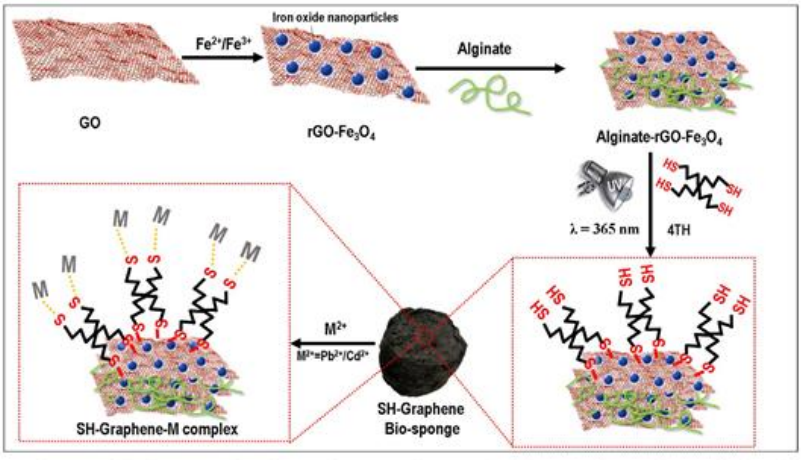

Fig. 1. Schematic diagram of the fabrication of Graphene-SH bio-sponge for removal of heavy metal ions, Pb (II) and Cd (II), from the water.

200 °C for two hours followed by calcination at 800 °C in air for one hour [15]. It is worth stating that despite substantial work on combining biopolymer (alginate) with nanomaterials have been reported, few work has been focused on the grafting of specific functional groups to enhance the adsorption performance towards heavy metal ions. Although some alginate-based sorbents possess high sorption capacity, the selectivity and the reusability of the sorbents are often neglected which may not reflect the sustainability and economic feasibility in the long term. Moreover, majority of the fabrication or modification step for the adsorbents reported are complicated, energy-intensive and time consuming apart from utilizing harmful chemicals at high temperature which potentially triggers laboratory hazards.

Inspired by the advantages and proven capabilities of alginate based bio-adsorbents, we proposed to develop a highly-engineered hybrid composites with the aims to further enhance their adsorption performance and selectivity towards heavy metals. To achieve that, we presented the use of alginate bio-sponge as porous scaffold modified with reduced graphene oxide (rGO) which is specifically functionalized to achieve these aims in creating a stable and robust adsorbent in the bio-sponge form. Firstly, the GO sheets were decorated with magnetic iron oxide nanoparticles to encapsulate within the GO network to provide an enhanced heavy metal ions uptake, stabilization of graphene- alginate network and magnetic separation capability by magnetic field after the adsorption process. Secondly, the functionalization of GO sheets embedded in the alginate network is performed by covalent attachment of multithiol (pentaerythritol tetrakis-mercaptopropionate) (4TH) molecules using photoinitiated thiol-ene click chemistry approach to achieve high density of sulfur-containing groups for targeting efficient removal of heavy metal ions in the water. The significance of this functionalization approach is given that this method is generic, environmentally-friendly and scalable with the ability to provide controllable surface modification. The proposed concept of SH-graphene bio-sponge adsorbent and its application for removal of selected heavy metals such as Pb and Cd is illustrated in Fig. 1. Via the optimized control of the UV irradiation time, we proposed that the surface of Graphene bio-sponge can be tailored with desired functional groups including free thiol group and thioether without changing the concentration ratio of the thiol and -ene precursors. Unlike the thermal thiol-ene click reaction as described in our previous work, the photoclick modification approach developed hereby, apart from giving rise to a more effective functionalization, can also be regarded as highly energy efficient as this reaction can be conducted at room temperature without the need to raise the reaction temperature. In comparison to our previous reported thermal thiol-ene click approach, the merits of this alternative green UV-click reaction also lie on the use of non-toxic solvent, shorter reaction time with no emission of harmful organic compounds which greatly emphasize on the concept of 12 principles of Green Chemistry developed by Paul Anastas and John Warner [16–18]. The surface, thermal and chemical properties of this new and eco-friendly multithiol modified 3D graphene bio-sponge were elucidated using a series of characterization techniques. The heavy metal ions uptake performance of the developed adsorbent was evaluated in view of the sorption kinetics, capacity, effect of pH, competing ions and in real water sample system. The outcomes of this study suggest that the alginate biopolymer sponge combined with multithiol functionalized graphene is a promising and realistic solution in designing a new generation adsorbent for efficient water purification.

2. Experimental

2.1. Materials and characterization

The details of the chemicals and instruments used in this work are provided in the Supplementary Material. All the chemicals and instruments were used as received unless otherwise stated.

2.2. Graphene bio-sponge and SH-Graphene bio-sponge fabrication

GO was synthesized using improved Hummer's method as published previously [18,19] while magnetic Fe_3O_4-rGO was prepared according to the modification of methodology stated in the literature [20]. For the fabrication of Graphene bio-sponge, first, $FeSO_4{\cdot}7H_2O$ (0.8340 g) and $FeCl_3{\cdot}6H_2O$ (0.8109 g) were added in 60 mL milli-Q water, heated at 50 °C under continuous magnetic stirring and nitrogen gas purge for 10 min. 120 mL of well-dispersed GO (2 mg/mL) was added slowly into Fe^{2+}/Fe^{3+} solution with continuous stirring under nitrogen blanket for 15 min. 15 mL ammonium hydroxide was added dropwise into the mixture and stirred in nitrogen gas at 50 °C for 1.5 h. After 1.5 h, the temperature was further increased to 70 °C for 1 h and allowed to cool to room temperature prior washing with milli Q water using centrifuge. In a separate beaker, about 2 g sodium alginate was dissolved in 60 mL water under continuous stirring until a well-mixed gel formed. 60 mL of well-dispersed Fe_3O_4-rGO solution (2 mg/mL) was added into the alginate gel with stirring until a homogeneous hydrogel formed and the hydrogel was lyophilized at −20 °C for 72 h. The freeze-dried gel was soaked in 1 M calcium chloride solution for 2 h, washed with milli-Q water and lyophilized again at −20 °C for 72 h to make Graphene bio-sponge (Alginate/rGO/Fe_3O_4 composite). For SH-Graphene bio-sponge synthesis, about 17.5 mg 2,2-dimethoxy-2-phenylacetophenone (DMPA) and 1.5 mL 4TH were first mixed in 120 mL ethanol and sonicated for 30 min at 45 °C to obtain a homogeneous mixture. The Graphene bio-sponge was then added into the mixture and brought under UV irradiation at 365 nm with about 5 cm distance from the UV light source (Luyor-3405, 20 mW/cm^2, Luyor Corporation) for 180 min. After UV irradiation, the as-formed product was washed thoroughly with ethanol and milli-Q water until a clear filtrate was observed before loading it into the freeze dryer at −20 °C for 72 h to obtain SH-Graphene bio-sponge.

2.3. Heavy metal ions adsorption

In this study, Cd (II) and Pb (II) were chosen as the representatives of heavy metal ions and were used to perform all the adsorption experiments. The uptake of heavy metal ions using solid adsorbent with known mass was conducted via batch study in triplicate by oscillating the contained adsorbent in their respective metal ion solution at 200 rpm on an orbital mixer (Ratek, Model OM7) with a control (without adsorbent) running in parallel. The pH of the solutions was adjusted with diluted HCl or NaOH and measured using a pH meter FiveGO FG2, (Mettler Toledo) at ambient temperature. Liquid samples were withdrawn at particular time intervals and diluted with acidified 2% HNO_3 prior to ICP-MS analysis to determine the metal ions concentration. The amount of heavy metal ions adsorbed per unit of adsorbent mass at a given time, t (q_t, mg g^{-1}) was calculated using the following equation [16]:

$$q_t = \frac{(C_0 - C_t)V}{m} \quad (1)$$

where C_0 and C_t are initial and metal ion concentration at time t (mg L^{-1}), while V is the volume of solution (L) and m is the mass of adsorbent (g). The removal efficiency (R_t, %) at a given time, t, was calculated based on Eq. (2) [16]:

$$R_t = \frac{(C_0 - C_t)}{C_0} \times 100 \quad (2)$$

2.3.1. Effect of solution pH

For the effect of solution pH, approximately 20 mg sample was added into the 20 mL metal ion solution (3 and 5 ppm for Cd (II) for Pb (II), respectively) at 21 °C for 5 h.

2.3.2. Effect of contact time

For effect of contact time, about 20 mg sample was added into individual metal ion solution containing 70 mL of 10 ppm Cd (II) for Pb (II) each at 21 °C pH around 5. The obtained kinetics data was fitted into Lagergren pseudo-first-order [21] and Ho's pseudo-second–order [22] kinetic models in their linear forms as represented by Eqs. (3) and (4):

The pseudo-first order equation:

$$\log(q_e - q_t) = \log q_e - \frac{k_1}{2.303} t \quad (3)$$

The pseudo-second order equation:

$$\frac{t}{q_t} = \frac{1}{k_2 q_e^2} + \frac{t}{q_e} \quad (4)$$

where q_e and q_t are the amount of heavy metal ions adsorbed (mg g^{-1}) at equilibrium and at time t respectively; k_1, and k_2 are the rate constants for the pseudo-first order and pseudo-second order kinetic models respectively; C is the intercept.

2.3.3. Effect of initial metal ion concentration

The effect of initial metal ion concentration (C_0) was performed by adding about 20 mg sample into 20 mL metal ion solution (C_0 = 10–110 ppm) at pH around 5 under 24 h equilibration time. The collected data was fitted into the linearized Langmuir [23] and Freundlich [24] isotherm models to study the adsorption behaviour of SH-Graphene bio-sponge. The Langmuir relationship is provided in Eq. (5) while the feasibility of a sorption process in a batch adsorption system can be predicted using isotherm shape factor analysis with a dimensionless constant, separation factor, K_R as defined in Eq. (6).

$$\frac{C_e}{q_e} = \frac{1}{bq_{max}} + \frac{C_e}{q_{max}} \quad (5)$$

$$K_R = \frac{1}{1 + bC_0} \quad (6)$$

where q_e and q_m denote the adsorption capacity at equilibrium and maximum monolayer coverage capacity respectively (mg g^{-1}), C_e represents the concentration of heavy metal ions at equilibrium (mg L^{-1}) and b is the Langmuir constant.

Meanwhile, the Freundlich equation can be described in the following relationship:

$$\log q_e = \frac{1}{n} \log C_e + logK \quad (7)$$

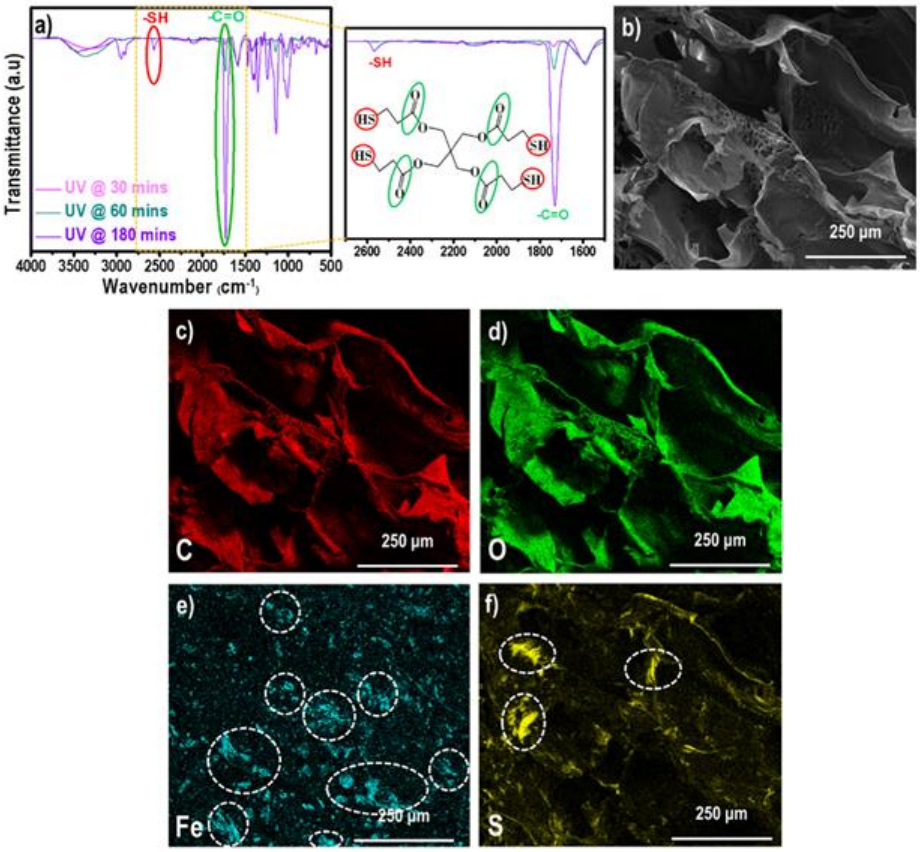

Fig. 2. (a) Baseline corrected FTIR spectra of thiol-modified Graphene bio-sponge under UV irradiation at different time interval (30, 60 and 180 min) with magnified FTIR spectra at the right embedded with an inset showing the chemical structure of pentaerythritol tetrakis (3-mercaptopropionate), 4TH. (b) SEM image and (c-f) selected EDX map of SH-Graphene bio-sponge consisting of C, O, Fe and S elements. Particular element (Fe and S) concentric area is circled in white dotted line in its respective EDX map.

where K is the Freundlich adsorption constant (L mg^{-1}) and $1/n$ is the adsorption intensity determined from the intercept and slope of the plot of log q_e versus log C_e.

2.3.4. Effect of competing ions in spiked milli-Q water and sea water

The effect of competing ions (selectivity) of the adsorbent was performed by adding separately about 20 mg adsorbent into a container consisting of 20 mL milli-Q water and spiked sea water with mixed metal ions containing Cd (II), Pb (II), Cu (II) and Co (II) ions (~5 ppm for each metal ion) at around pH 5 for 5 h. Commercial activated carbon (AC) was used as a benchmark adsorbent and alginate sponge as a control. The sea water (Henley Beach, Adelaide, South Australia, 34°54′51.1″S 138°29′ 30.0″E) was used without pre-treatment and pH adjustment to simulate real natural water sample.

2.3.5. Effect of recyclability

The regeneration capability of the fabricated adsorbent was studied under adsorption condition of 20 mL mixed metal ions solution (2 ppm for each metal ion, Pb (II) and Cd (II)), stirring at 200 rpm at pH ~5.5 for 6 h. The spent adsorbent was then desorbed using 30 mL eluent (2% w/v thiourea in 0.1 M HCl), stirring at 250 rpm for 1 h. The desorbed adsorbent was then washed to pH above 5 with large amount of milli-Q water and was left to dry for one day at ambient conditions before the next adsorption-desorption cycle. The adsorption-desorption cycles were repeated for five times and the remaining metal ion concentration in each cycle was determined by ICP-MS analysis.

3. Results and discussion

3.1. Optimization towards the formation of SH-Graphene bio-sponge

With the aim to synthesize SH-Graphene bio-sponge functionalized with high density of thiol group to maximise its adsorption capacity and selectivity, the click-chemistry process was optimized by exploring different UV irradiation time (30–180 min). Successful modification was monitored by FTIR with the presence of functional groups, -SH and –C = O, of neat 4TH around 2556 and 1730 cm^{-1}, respectively [25]. The time dependence study monitored by FTIR (Fig. 2A) showed that shorter irradiation time (30 and 60 min) was not enough to allow successful grafting of -SH group within the network of Graphene bio-sponge. The appearance of one of the main functional groups, –C = O band, on the FTIR spectra for irradiation time 30 and 60 min with no sign of thiol group, indicates that longer time (180 min) is required to achieve free –SH group on graphene surface via thiol-ene click reaction. This tetrafunctional thiol agent is well-recognized in polymer science as an active polythiol coupling agent which is commonly used to react with the alkene group via photoinitiated thiol-ene click reactions [26]. In principle, thiol-ene photoinitiated reaction is governed by a step growth radical polymerization mechanism by reacting an active thiol group with -ene group of a molecule. A photoinitiator, once activated by light, abstracts the hydrogen atom from thiol group, generating a thiyl radical which then propagates by attacking the alkene group [27]. Our results suggest that UV irradiation time prolonged to 180 min is needed to allow remaining free thiol groups to dangle on the graphene

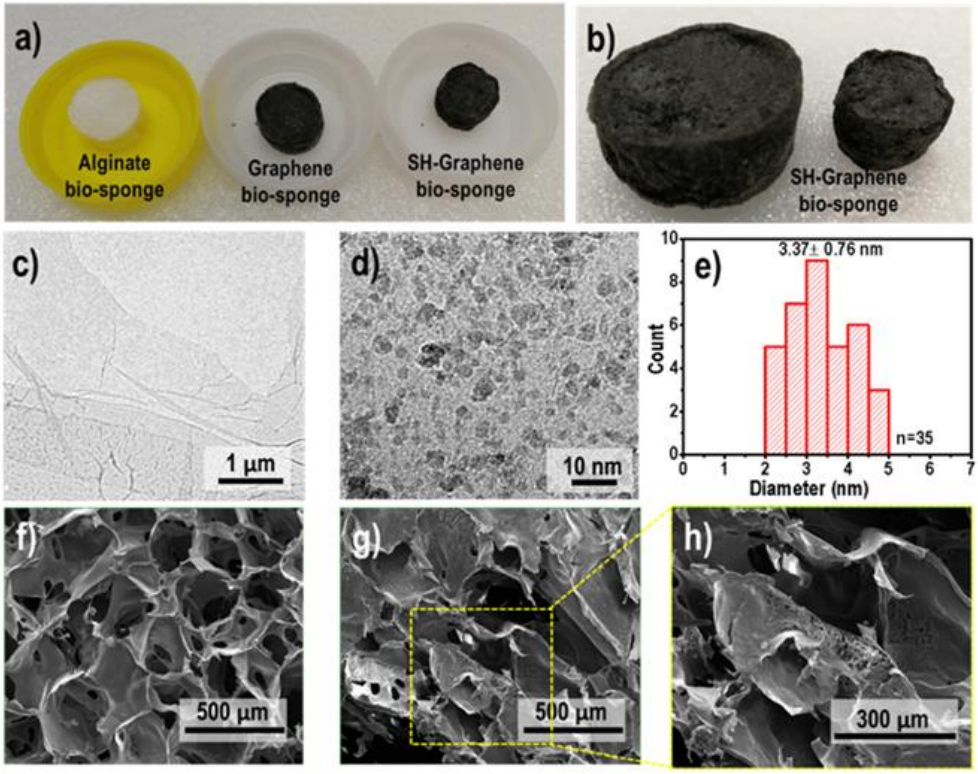

Fig. 3. (a) Photographs of Alginate, Graphene and SH-Graphene bio-sponges after freeze- drying process. (b) SH-Graphene bio-sponge moulded in different sizes. TEM image of (c) GO, (d) Fe_3O_4 nanoparticles on rGO sheet. (e) Size distribution plot of Fe_3O_4 nanoparticles determined from the diameter of Fe_3O_4 nanoparticles with reference to Fig. 3d. SEM images of (f) bare alginate sponge and (g-h) SH-Graphene bio-sponge at different magnifications.

structure when available sp^2 carbon binding sites within the graphene structure was saturated after photoinitiated click reaction. Since there are four thiol groups per molecule of 4TH, we surmised that only certain number of the thiol groups have successfully coupled to the graphene structure, while some remain as free thiol. This outcome was also corroborated with stronger –C = O band (1730 cm^{-1}) recorded on the FTIR spectrum of the product treated at 180 min compared to the products obtained at 30 and 60 min as depicted in the magnified image of Fig. 2a.

On the other hand, it is also possible that the active thiol group may have reacted with iron which is present as iron oxide in the polymeric network of SH-Graphene sponge. To confirm this deduction, elemental mapping of SH-Graphene bio-sponge was performed as presented in Fig. 2b–f. Based on the concentration of the spatial elemental distribution, carbon and oxygen were found to dominantly make up majority of the framework of SH-Graphene bio-sponge. This was because alginate and GO mainly consist of carbon and oxygen elements in their polymeric structure. The individual elemental distribution map of iron and sulfur (Fig. 2e and f) showed that both of the highly concentrated regions did not overlap with one another, implying that no interaction or covalent bond was formed between iron and sulfur elements. This result precludes the possibility of the reaction between the iron with the active thiol group.

Few key findings can be inferred from the coupling of the systematically-devised experiments and characterization results: First, the intensified C = O band collected on the sample treated for 180 min showed that this functional group does not involve in the new bond formation during the photoinitiated reaction. Second, the reaction site on the graphene structure was not completely saturated with available sp^2 carbon on graphene structure at 30–60 min. Nevertheless, prolonging the UV irradiation time promotes the maximum extent of covalent attachment of thiol group on the graphene structure. Unlike most of the reported work which typically showed the manipulation of the ratio of ene: thiol precursor to achieve the desired functional groups, here, we demonstrated that the control of UV irradiation time can be used as a more efficient controlling parameter to tailor the surface functionality without changing the precursor concentration [28,29]. This result is significant, unveiling that a very simple, eco-friendly UV-directed click-chemistry modification approach can be used to create desired surface functional groups in materials design which is highly advantageous for numerous applications. In order to demonstrate the application of this novel engineered and designed material, SH-Graphene bio-sponge (UV irradiation under 180 min) was chosen to conduct the heavy metal ions adsorption experiments in this work. The surface and structural properties of this thiol-modified graphene sponge was further confirmed using a series of characterization techniques as discussed in the next section.

3.2. Characterization of SH-Graphene bio-sponge

Fig. 3a shows the physical appearance of the 3D alginate-, Graphene- and SH-Graphene bio-sponges. The colour of the Graphene bio-sponge changed immediately from white to black after the incorporation of iron oxide nanoparticles and GO sheets. Both the alginate and Graphene bio-sponges exhibit soft and slightly elastic structure after freeze-drying process. Meanwhile, SH-Graphene sponge, appearing in black, shows harder and more robust structure after the UV modification process using 4TH precursor. As evidenced in Fig. 3b, the shape of SH-Graphene bio-sponge can be controlled depending on the mould and can be made into any size and form including tubes, cylinders, pads and membranes which makes the large scale fabrication highly feasible. Characterization results of initial materials used for the preparation of SH-Graphene bio-sponge such as alginate, GO, magnetic oxide nanoparticles (NPs) decorated on rGO are summarized in Figs. S1 and 3 c-f. The microstructure of these sponge structure was investigated using scanning electron microscopy (SEM) and transmission electron microscopy (TEM) techniques. Fig. 3c depicts the TEM image of GO which clearly revealed the successful exfoliated GO sheet, showing the presence of single layer GO nanosheet produced from the graphite flakes. The existence of Fe_3O_4 nanoparticles was evident with the TEM image (Fig. 3d) showing the spherical nanoparticles decorated on the exfoliated rGO sheet with the histogram (Fig. 3e) indicating the diameter distribution of Fe_3O_4 nanoparticles in the range of 2–5 nm with an average size of 3.37 ± 0.76 nm. The SEM images, of the control alginate sponge (Fig. 3f) illustrates a highly porous architecture in micron-size range with well-defined and interconnected pores within its framework. While, the porous structure of the thiol-modified sponge was slightly different from its control with less-defined and uneven pores observed after the photoinitiated reaction as depicted in Fig. 3g. The magnified area as displayed in Fig. 3h (dotted box in Fig. 3g) shows the presence of a mass of micro-pores (pore size in few micron-size range) on the wall of the alginate-rGO network which are vital to enhance the surface area of the sorbent material for better heavy metal ions removal.

More details about the chemical identity of GO, intermediates and functionalized Graphene bio-sponge can be unravelled from the FTIR graphs (Fig. S1) to collect the information on their chemical bonds in order to understand their chemical properties related to their adsorption performances. Typically, the FTIR spectrum of GO (Fig. S1a) shows characteristic functional groups of bare GO including −OH stretching (~3400 cm^{-1}), –C = O stretching of COOH (1720 cm^{-1}), C = C (1622 cm^{-1}) and C-O-C (1030 cm^{-1}) groups. With reference to the

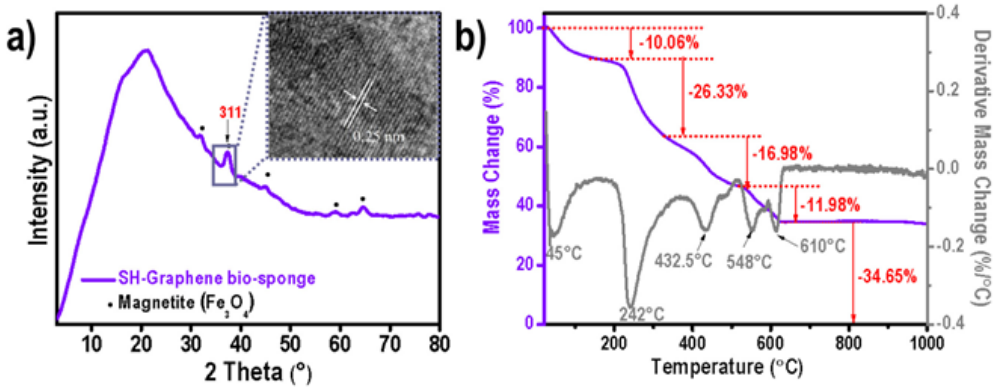

Fig. 4. (a) XRD diffractogram with the inset showing the corresponding lattice fringe of Fe_3O_4 nanoparticles and (b) TGA-DTG plot of SH-Graphene bio-sponge.

chemical structure of alginate (Fig. S1b), the common peaks such as −OH (~3400 cm^{-1}), –COO^- (1590 cm^{-1} and 1420 cm^{-1}) and C-O-C (1020 cm^{-1}) groups were detected on the FTIR spectrum of bare alginate sponge (Fig. S1a) which were also found on the FTIR spectrum of SH-Graphene bio-sponge [16,30]. This reveals that the highly negative –COO^- groups of alginate still remain as active species in the final product. As evidenced from the FTIR analysis (Fig. 2a with UV exposure at 180 min), several indicative bands of successful functionalization using 4TH precursor including peaks at 2569 cm^{-1} (–SH) and 1730 cm^{-1} (–C = O) could be observed [25]. The –C = O peak was found initially on the FTIR spectrum of GO but was absent from the alginate and Graphene bio-sponges. This particular functional group (–C = O) which is part of the chemical structure of the 4TH precursor arose again after the photoinitiated reaction, confirming the successful modification of the SH-Graphene bio-sponge. Meanwhile, the key peak, -SH, did not appear on the FTIR spectra of all the control samples prepared in this work but appear on the FTIR plot of SH-Graphene bio-sponge treated under UV irradiation of 180 min.

The XRD diffractogram of SH-Graphene bio-sponge (Fig. 4a) exhibits a strong and broad peak at around 21° after the photoinitiated reaction. In comparison to its control, GO (Fig. S1c), a typical sharp peak was found at ~10.8°, indicating the successful insertion of oxygen functional groups after the harsh oxidation reaction of graphite flakes. The diffraction peaks of iron oxide (Fe_3O_4) nanoparticles with its corresponding planes of (2 2 0), (3 1 1), (4 0 0), (5 1 1) and (4 4 0) were identified on the XRD diffractogram of the SH-Graphene bio-sponge (Fig. 4a). The interlayer spacing (3 1 1) plane identified on the XRD diffractogram was in good agreement with the lattice fringe determined on the HRTEM image, verifying the existence of magnetite nanoparticles in the SH-Graphene bio-sponge. The peak broadening effect observed on the XRD diffractogram was because of the nano-sized iron particles as verified by TEM analysis in the previous section (Fig. 3d and e) [31,32].

The thermal behaviour and stability of the SH-Graphene sponge were characterized using thermogravimetric technique under air atmosphere with its corresponding thermogram depicted in Fig. 4b. As displayed in Fig. 4b, the thermal decomposition pattern of the multithiol-modified graphene sponge is distinctly different from GO and slightly dissimilar to the rest of the controls (Fig. S1d and e). From the thermograms, GO can be considered as the most thermal unstable material which started to lose its mass at temperature below 100 °C due to the elimination of interstitial water and decomposed completely at around 570 °C. The major mass loss occurred between 150 and 300 °C can be associated with the loss of oxygen-functional groups including hydroxyl and epoxy moieties. In comparison to the thermogram of the controls (Fig. S1d), SH-Graphene bio-sponge is relatively more stable with its first mass loss (10.06 %) took place below 100 °C owing to the removal of adsorbed water (Fig. 4b). Similar to GO, the main mass decomposition event in the range of 150–300 °C can be linked to the loss of oxygen functional groups attached in the alginate and GO polymeric network. The additional peak maximum at 432.5 °C detected only on the DTG curve of SH-Graphene bio-sponge in relative to its controls (Fig. S1e) can be correlated to the detachment of thiol moiety from 4TH molecules in the GO-alginate matrix. The lower char residue remained (34.65 %) for SH-Graphene bio-sponge at 626 °C in comparison to the control sponges suggests the successful modification of the graphene sponge [16,33].

Fig. 5a illustrates the XPS survey scan of SH-Graphene bio-sponge with four characteristic peaks which can be assigned to C1s, O1s, S2p and Ca2p at around 284.5, 531.5, 163 and 346.5 eV, respectively, are identified on its survey spectrum, confirming the presence of these elements on the surface of SH-Graphene bio-sponge. Notably, results (Table S1) showed that the surface of SH-Graphene bio-sponge consists of extraordinarily high sulfur content (10.20 at %) apart from other expected elements including carbon (63.46 at %), oxygen (25.77 at %) and Ca (0.57 at %), suggesting that its surface was successfully decorated with S-containing groups. This observation was well-supported by the absence of S2p peak on the survey spectra of all the controls (Fig. S1f). From Table S1, both the controls, alginate and GO recorded high O at % (35.85 and 28.89 at %, respectively), indicating that these two materials are enriched with oxygen functional groups. Meanwhile, Graphene bio-sponge exhibited 33.54 at % O with its C/O atomic ratio of 1.83, between GO (2.46) and alginate (1.68). Interestingly, the multithiol-modified bio-foam showed the same C/O atomic ratio of GO (2.46), implying that the combination of the precursors used in this hybrid did not lead to oxygen compensation in relative to GO due to the presence of rich oxygen functionalities in alginate matrix although multithiol precursor, commonly used as a mild reducing agent tends to reduce oxygen groups [34]. Given that majority of the functionalization agents are likely to reduce the oxygen content of GO after the modification process, the use of alginate which is rich in oxygen groups to prepare the adsorbent hereby is strategically advantageous for heavy metals adsorption because oxygen is one of the major chelating agents for metal complexation. Calcium element on the other hand detected in alginate (3.95 at %) and Graphene (4.93 at %) bio-sponge was originated from calcium chloride solution which was used as the ionic crosslinking agent to interact with the carboxylate groups in the aerofoam matrix. Nevertheless, the corresponding peak of Ca2p was ambiguously detected on the spectrum of SH-Graphene bio-sponge with only 0.57 at % calcium (Table S1), suggesting that the initial Ca^{2+} ion crosslinking agent in the aerofoam matrix could be displaced by the multithiol crosslinker during the UV initiated reaction. The peak fitting of the high resolution scans for the C1s and S2p core levels of SH-Graphene bio-sponge as depicted in Fig. 5b and c was performed to understand the formation chemistry of the thiol modified bio-sponge. As illustrated in Fig. 5b, five peaks positioned at 284.3, 284.8, 285.9,

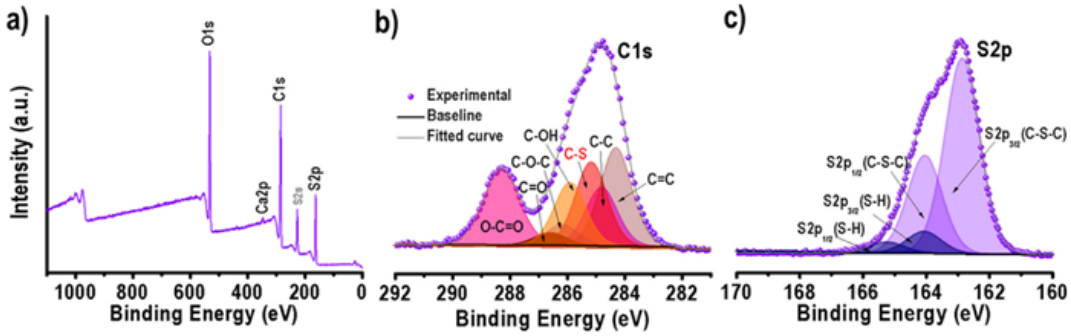

Fig. 5. XPS (a) survey spectrum, high resolution spectra (b) C1s and (c) S2p of SH-Graphene bio-sponge.

286.2, 286.6 and 288.3 eV corresponding to C = C, C–C, C-OH, C-O-C, C = O and O-C = O, respectively, were resolved for the detailed C1s core peak of SH-Graphene bio-sponge. Additionally, the peak at 285.2 eV which can be assigned to C-S bond is visible on the C1s spectrum of SH-Graphene bio-sponge [35,36]. Interestingly, no iron peak was identified from the XPS spectra of all the samples from XPS analysis although its presence was verified from XRD and elemental mapping analyses discussed in the previous section. This could be due to its non-homogeneous distribution in the alginate-GO matrix. To confirm this deduction, a more detailed EDX analysis was performed on the SH-Graphene sample as demonstrated in Fig. S2. The localized elemental composition analysis clearly corroborated the deduction on the uneven distribution of Fe element based on different spots captured with a broad range of relative atomic concentration determined including 0.10 at %, 0.21 at%, 6.20 at % and 7.39 at % of Fe element on Spot 1, 2, 3 and 4 respectively. Remarkably, higher Fe at % was recorded on the bulges microstructure (spots 3 and 4) appeared on the surface of alginate-GO matrix (Fig. S2), indicating the encapsulation of iron oxide nanoparticles which can be distinguishably observed from the smooth surface found on spots (1) and (2). Since the depth profiling of XPS analysis is approximately 10–15 nm while it is 1000–2000 nm for EDX analysis, the absence of Fe peak on the XPS spectrum can be justified with that the iron oxide nanoparticles were embedded underneath the surface of the modified sponge which is beyond the detectable limit of XPS technique.

Primarily, further deconvolution analysis of the core S2p peak (Fig. 5c) for SH-Graphene bio-sponge verified successful photoninitiated click reaction of multithiol precursor onto the alginate-GO matrix with resolved peaks detected at 162.9 and 164.0 eV, which could be referenced to $S2p_{3/2}$ and $S2p_{½}$ respectively for C-S-C bond while another doublet peak positioned at 164.2 and 165.4 eV, responsible for $S2p_{3/2}$ and $S2p_{½}$, respectively, of unbound -SH species. Remarkably, the thiol-modified bio-sponge does not record any peak with binding energy > 166 eV (high binding energy for S-O peak), suggesting that the immobilized sulfur species is highly stable within the polymeric network without any oxidized sulfur species including sulfonates or sulfates formed despite the exposure of the material to readily oxidized conditions [37,38]. This prominent information also suggests that the reactive thiol group does not react with the bountiful oxygen groups in the alginate-GO matrix, confirming the thiol-ene click chemistry between thiol and C = C groups. Based on the combined outcomes collected from FTIR, XPS, EDX and its mapping analyses, it can be further ascertained that the multithiol precursor has successfully clicked onto the GO-alginate network via the UV-directed reaction.

3.3. Heavy metal ions adsorption

The evaluation of the multithiol-modified sponge (SH-Graphene) was conducted under the effect of several factors including pH, initial concentration, contact time, recyclability, co-existing ions and attested for its application in real sample assessment using activated carbon as benchmark.

3.3.1. Effect of solution pH

Initially, the surface charge of the SH-Graphene bio-sponge was determined using zeta potential measurement prior to the study of the effect of pH towards the adsorption efficiency of Pb^{2+} and Cd^{2+}. Results indicated that the surface of the modified SH-Graphene bio-sponge was negatively charged ranging from −20 to −10 mV over pH 4–9 (Fig. 6a). Coupled with the information on the surface charge of the

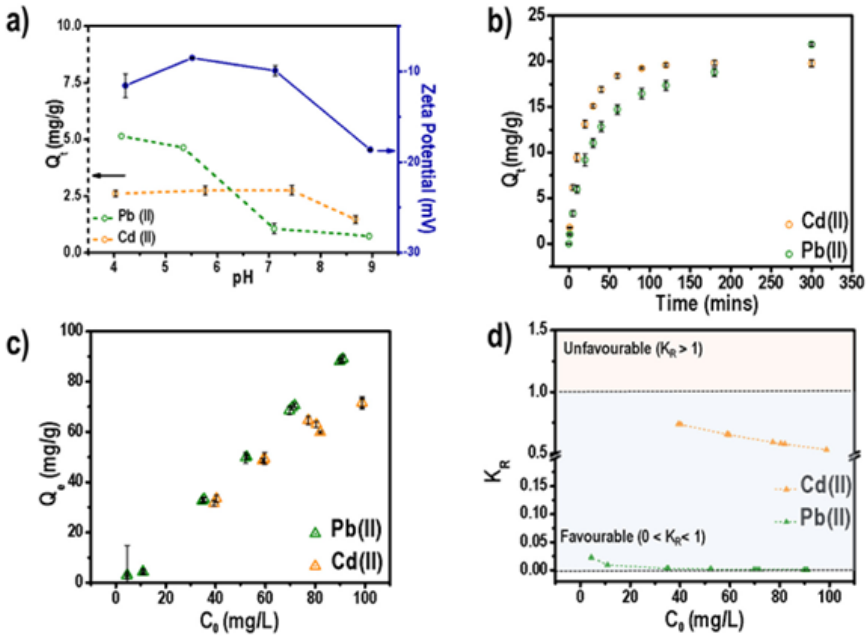

Fig. 6. Effect of (a) solution pH for adsorption of Pb (II) and Cd (II) using SH-Graphene bio-sponge; zeta potential as a function of pH measurment of SH-Graphene bio-sponge, [Conditions: C_0 = ~5 ppm for Pb (II), C_0 = ~3 ppm for Cd (II), temperature = 21.0 °C, mass of sorbent = ~20 mg, volume of metal ion solution = 20 mL, equilibration time: 5 h], (b) contact time [Conditions: C_0 = ~10 ppm, pH ~5, temperature = 21.0 °C, mass of sorbent = ~20 mg, volume of metal ion solution = 70 mL] and (c) initial concentration of heavy metal ions [Conditions: C_0 = 10–110 ppm, pH ~5, temperature = 21.0 °C, mass of sorbent = ~20 mg, volume of metal ion solution = 20 mL, equilibration time: 24 h]. (d) Plot of dimensionless separation factor (K_R) over initial metal ion concentration of SH-Graphene bio-sponge.

adsorbent system and the speciation diagrams (Fig. S3) constructed based on the possible species present in the adsorbent-adsorbate system, the interaction involved can be elucidated over the pH investigated. It can be clearly observed that the adsorption behaviour of SH-Graphene bio-sponge was entirely different for Pb (II) and Cd (II) ions. For Pb (II) ion, higher metal ion removal trend was detected at region pH 4–5.5. The high uptake could be due to the strong electrostatic attraction between the negatively-charged surface of the adsorbent and the presence of positively charged Pb^{2+} ions (Pb^{2+} and $PbCl^{+}$) at this pH region. A drastic drop of the sorption capacity was detected at pH 7–9 which could be due to the unfavourable binding affinity of the neutral species such as $Pb(OH)_2$ present at this pH on the charged surface of the modified graphene bio-sponge which affected its adsorption efficiency towards Pb (II) in the water. On the other hand, the Cd (II) uptake pattern by the SH-Graphene bio-sponge was relatively stable over the pH studied. Almost similar removal efficiency was achieved over the acidic to neutral pH. This could be attributed to the strong electrostatic interaction between Cd^{2+} and $CdCl^{+}$ ions as evidenced from the cadmium speciation diagram (Fig. S3b) with the negative charged adsorbent surface. At alkaline pH, a slight drop of Cd^{2+} uptake was observed which could be related to the absence of positive charged Cd^{2+} species with the formation of $Cd(OH)_2$ due to the presence of excessive OH^{-} ions. In summary, the adsorption of heavy metal ions from aqueous solution at alkaline pH leads to precipitation of created metal ion hydroxide complexes on the active sites of the adsorbent that could potentially block the binding sites of the adsorbent, thus affecting the mass transport of the heavy metal ions to the adsorbent. As a result, the adsorption of Pb (II) and Cd (II) ions was affected at alkaline pH [10,39].

3.3.2. Effect of contact time and adsorption kinetics

The kinetics aspect of an adsorbent towards metal ions uptake is also crucial to understand the mechanism and the rate of metal ions uptake of the modified sponge. From Fig. 6b, a gradual and steep inclination could be observed with the equilibrium achieved within the first hour for both Cd (II) and Pb (II) ions, indicating a steady uptake of heavy metal ions into the porous structure of SH-Graphene bio-sponge. Interestingly, the uptake of Cd (II) ions surpassed Pb (II) ions initially but with Pb (II) ions overtook Cd (II) eventually. Furthermore, the kinetics data was fitted into two linearized kinetic models (pseudo-first and pseudo-second) to unveil their respective adsorption mechanisms. The kinetics fitting analysis (Fig. S4, Table S2) clearly indicated that the adsorption of both metal ions follows pseudo-second-order kinetic model with high correlation coefficients ($R^2 > 0.99$) attained, suggesting that chemisorption is the rate controlling step for the adsorption of both the metal ions studied using the SH-Graphene bio-sponge. Pseudo-second-order model has been broadly adopted to describe the adsorption behaviour of water pollutants, particularly heavy metal ions on the adsorbent by taking the assumption that the interaction between the adsorbent and adsorbate is by electron sharing and exchange. Owing to the presence of rich oxygen and thiol groups on the surface of the modified graphene bio-sponge which readily share or donate their electrons with Pb (II) and Cd (II) ions, the primary adsorption mechanism could be associated to the electron sharing or exchange process between the adsorbent-adsorbate system. [16,40]

3.3.3. Effect of initial concentration of metal ions and adsorption isotherms

The effect of initial concentration of metal ions was investigated to determine the adsorption capacity of Pb (II) and Cd (II) onto the multithiol-functionalized bio-sponge. Higher initial concentration of metal ions resulting in greater sorption capacity due to stronger driving force to compensate the mass transfer resistance for the transport of adsorbates (metal ions) from the water system to the binding sites of the adsorbent. The fitting of the equilibrium data for Cd (II) and Pb (II) into the linearized isotherm models, Langmuir and Freundlich isotherm models, (Fig. S5) showed that adsorption of both Cd (II) and Pb (II) ions correlates well with Langmuir isotherm model with high correlation coefficient, R^2, > 0.97 achieved. According to the described model, we can surmise that monolayer coverage of Cd (II) and Pb (II) over the homogeneous binding sites occurred on the SH-Graphene bio-sponge [16]. The calculated maximum sorption capacity, 101.01 mg g^{-1} and 102.99 mg g^{-1}, for Pb (II) and Cd (II), respectively also disclosed strong binding affinity between the metal ions and the modified graphene bio-sponge. This could be well-evidenced by all the dimensionless separation factor, K_R, accomplished in both metal ions which fall within $0 < K_R < 1$, the favourable region as depicted in Fig. 6d. This outcome strongly suggests that the adsorption of Cd (II) and Pb (II) is favourably driven to the binding sites of the modified bio-sponge [41].

It is critical to highlight that several experimental parameters such as the sorbent form, sorbent dosage, initial concentration of metal ions, pH and the temperature applied in the adsorption studies should be carefully considered when making comparison across the adsorbents in the literature. A more relevant evaluation was made among the previous investigated alginate-based adsorbents with the green surface-modified SH-Graphene bio-sponge fabricated as tabulated in Table 1. It could be seen that the developed SH-Graphene bio-sponge outperformed several alginate-based sponge reported in the literature for Pb (II) and Cd (II) ions removal. Taking silica modified calcium alginate-xanthan gum hybrid bead composites as example, although it possessed high regeneration ability (> 25 times), its ~5 times lower

Table 1
Comparison of adsorption capacity with experimental conditions of alginate-based adsorbents for Pb (II) and Cd (II) ions removal.

Adsorbent	SSA (m^2 g^{-1})	Metal ions uptake Conditions	Max. sorption capacity (mg g^{-1})	Regeneration cycles with > 90% removal efficiency	Ref.
Silica modified calcium alginate-xanthan gum hybrid bead composites	196.47[a]	C_0: 5–100 mgL^{-1}, sorbent dosage: 3750 mgL^{-1}, 25 °C, pH 6	Pb (II): 18.9	25 cycles in Pb (II) single system	[42]
Carboxymethyl chitosan-sodium/graphene oxide (CMCNa/GO) hydrogel	NA	C_0: 100 mgL^{-1}, sorbent dosage: 1200 mgL^{-1}, 20 °C, pH 6	Pb (II): 19.19 Cd (II): 27.01	NA	[43]
Iron oxide modified clay activated carbon composite beads	433 [a]	C_0: 12–350 mgL^{-1} (Pb^{2+}); 10–300 mgL^{-1}(Cd^{2+}), sorbent dosage: 2000 mgL^{-1}, 21.0 °C, pH 4.5	Pb (II): 74.2 Cd (II): 41.3	NA	[44]
Titania-coated silica modified sodium alginate (ST20-ALG)	42 [a]	C_0: 50–250 mgL^{-1}, sorbent dosage: 1000 mgL^{-1}, 20.0 °C, pH: 5	Pb (II): 32.49 Cd (II): 18.85	NA	[15]
SH- Graphene bio-sponge	115 ± 0.27[b]	C_0: 10–110 mg/L, sorbent dosage: 1000 mg/L, 21.0 °C, pH 5.3	Pb (II): 101.01 Cd (II): 102.99	5 cycles in binary metal ions (Pb and Cd) system	This work

SSA: Specific Surface Area, NA: Not Available. a refers to Brunauer–Emmett–Teller (BET) and b refers to methylene blue method of specific surface area measurement.

maximum sorption capacity (18.9 mgg^{-1} for Pb (II) ions) using 3.75 times higher sorbent dosage (3750 mgL^{-1}) compared to SH-Graphene bio-sponge (101.01 mgg^{-1}, 1000 mgL^{-1}) simply did not reflect the adsorption efficiency and economic feasibility of the adsorbent [42]. Furthermore, despite the complicated synthesis method, carboxymethyl chitosan-sodium/graphene oxide (CMCNa/GO) hydrogel could only achieve the maximum sorption capacity of 19.19 mgg^{-1} and 27.01 mgg^{-1} for Pb (II) and Cd (II) ions, respectively, by using = 1200 mgL^{-1} in their adsorption studies. The performance was considered less efficient because higher maximum sorption capacity (Pb^{2+}: 101.01 mgg^{-1}, Cd^{2+}: 102.99 mgg^{-1}) with lower sorbent dosage (1000 mgL^{-1}) could be achieved by SH-Graphene bio-sponge to immobilize these noxious ions in the water system [43]. The outstanding uptake of Pb (II) and Cd (II) ions from the water is unreservedly manifested by the SH-Graphene bio-sponge (maximum sorption capacity:101.01 mgg^{-1} (Pb^{2+}), 102.99 mgg^{-1}(Cd^{2+}); sorbent dosage = 1000 mgL^{-1}) compared to the work published by Pawar et al., on iron oxide modified clay activated carbon composite beads (74.2 mg g^{-1}(Pb^{2+}), 41.3 mg g^{-1}(Cd^{2+}); sorbent dosage = 2000 mgL^{-1}). Despite the double amount of sorbent dosage applied in their metal ions sorption studies as well as many different types of precursors introduced to modify the adsorbent, the lower maximum sorption capacity simply reflected the incompetence of their adsorbent. It is also surprising to find out that activated carbon which has been commercially used as the adsorbent for removing various types of pollutants was unable to meet the performance expectation even after multiple stepwise modifications [44]. Moreover, Kołodyńska et al. also reported the synthesis of titania-coated silica sorbent modified by sodium alginate for the adsorption of heavy metal ions including Pb (II) and Cd (II) ions. Apart from the complex synthesis process as well as huge energy consumption (calcination in air at 800 °C), the maximum sorption capacity accomplished by their modified sorbent (32.49 mgg^{-1} for Pb^{2+}, 18.85 mgg^{-1} for Cd^{2+}) was approximately 3–5 times lesser than SH-Graphene sponge (101.01 mgg^{-1} for Pb^{2+}, 102.99 mgg^{-1} for Cd^{2+}) with the same sorbent dosage applied in the metal ions removal experiments [15]. Overall, it is paramount to emphasize that the sorbent dosage used and the performance efficiency are highly correlated to the economic viability and practicability of an adsorbent to be introduced for water purification process in the industry scale. Taking into account of all the aspects (cost, performance efficiency and sustainability), SH-Graphene bio-sponge engineered via an environmentally-friendly modification approach (UV at 365 nm) clearly exhibited its potential in wastewater management due to its energy-efficiency, cost-effectiveness and performance competency in relative to majority of the sorbent materials reported in the literature.

3.3.4. Effect of recycling times

The regeneration and recovery of an adsorbent are one of the chief criteria to evaluate its feasibility for long term adsorption–desorption cycle performance to accomplish the cost efficiency and sustainability of an adsorbent. Fig. 7a shows the removal efficiency of Pb (II) and Cd (II) uptake in their co-existing metal ion mixture for five consecutive adsorption–desorption cycles using 2% w/v thiourea in 0.1 M HCl as eluent. In general, the removal efficiency of metal ions, during recycling of adsorbent, decreases with each cycle. This is mainly influenced by lack of full recovery of adsorbed metals during desorption process and by potential damaging of structure or binding chemistry of adsorbent in this process. We observed a slight increase of the metal ion adsorption after the first cycling for < 7%, but no further increase with expected slight decrease after third and fifth cycle. We assumed that the increased efficiency after the first desorption cycle could be attributed to the use of acidic diluent that removes the impurities in the alginate matrix (from the commercial manufacturer) which could be trapped within the pores of the adsorbent, thus exposing larger binding sites for adsorption to take place [45] SH-Graphene bio-sponge showed excellent results for the reusability of the sorbent material with > 85% and 90% removal efficiency achieved for Cd (II) and Pb (II) ions, respectively, even after five adsorption–desorption cycles. With merely 0.247 mgL^{-1} Cd (II) and 0.015 mgL^{-1} Pb (II) ions detected after the fifth metal ions uptake, SH-Graphene bio-sponge can be regarded as a highly stable material with bountiful of binding sites for water pollutants. This is because not only that this material can persistently withstand the co-existence of both heavy metal ions, but also the harsh eluent used as well as the multiple washing steps throughout the continuous regeneration experiments. It should also be highlighted that the remaining concentration of Pb (II) in the water after the continuous regeneration cycles meets the stringent maximum contaminant level (MCL) for lead (0.015 mg/L) as regulated by US EPA [46]. This again affirms the reusability of the SH-Graphene bio-sponge developed as a promising futuristic adsorbent for water decontamination.

3.3.5. Effect of competing ions in spiked milli-Q water and spiked-sea water

In order to investigate the effect of co-existing ions in real water sample, special designed adsorption experiments were performed using the SH-Graphene bio-sponge, commercial adsorbent (activated carbon) as benchmark and alginate sponge as control adsorbent in multiple mixed metal ions solution containing Cu (II), Cd (II), Pb (II) and Co (II) ions. Similar selectivity test in mixed metal ions-spiked local sea water was also conducted to probe the performance of SH-Graphene bio-sponge in natural water matrix. Fig. 7b shows that the selectivity of the SH-Graphene bio-sponge achieved in milli-Q water was extraordinarily good with > 90% removal efficiency for nearly all the metal ions investigated except for Co (II). Remarkably, the best selectivity performance was achieved for Pb (II) with only 0.058 ppm (58 ppb) of Pb (II) detected using the SH-Graphene bio-sponge, reaching 98.8% removal efficiency despite the strong competition with the co-existing heavy metal ions in the water. Meanwhile, 0.47 ppm Cd (II) with 90.2%

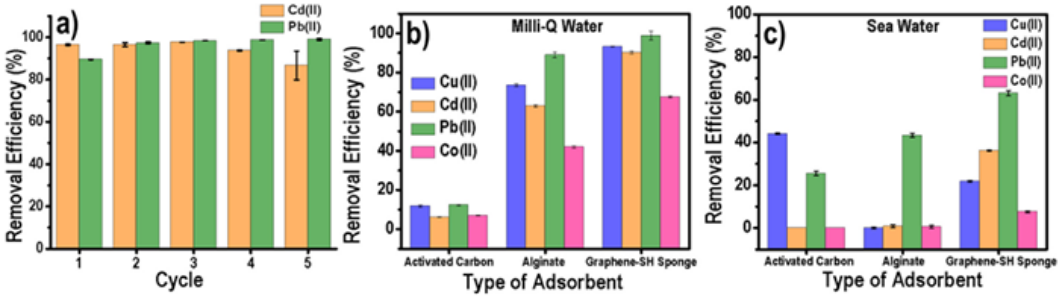

Fig. 7. Effect of (a) recyclability of SH-Graphene bio-sponge towards Cd (II) and Pb (II) ions, selectivity of multiple metal ions in (b) milli-Q water and (c) spiked sea water for Graphene-SH bio-sponge in comparison with activated carbon and alginate sponge.

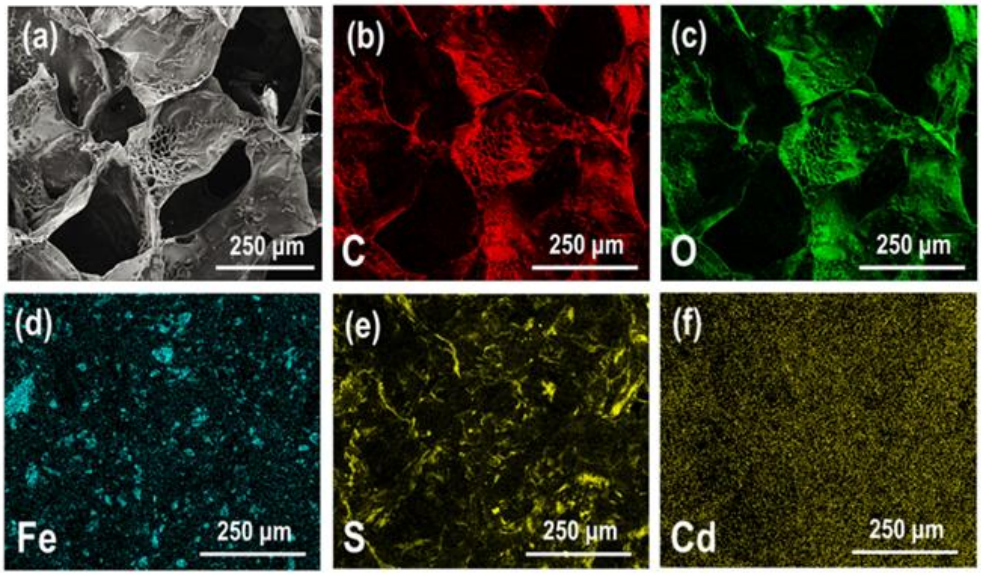

Fig. 8. (a) SEM image of Cd-SH-Graphene bio- sponge after Cd (II) adsorption, (b-f) corresponding EDX map with selected elements (C, O, Fe, S and Cd) after adsorption process.

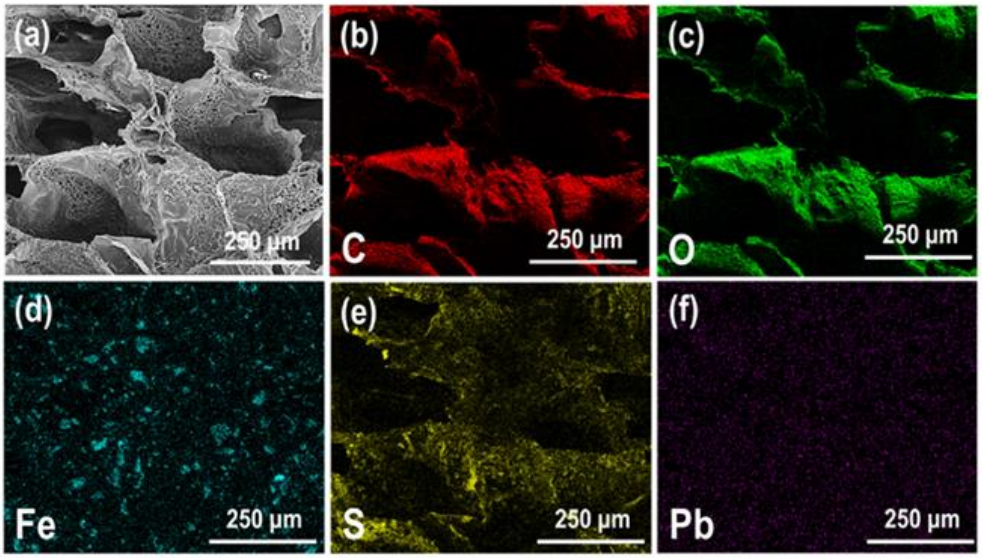

Fig. 9. (a) SEM image of Pb-SH-Graphene bio-sponge after Pb (II) adsorption, (b-f) corresponding EDX map with selected elements (C, O, Fe, S and Pb) after adsorption process.

removal efficiency recorded in the same selectivity test using SH-Graphene bio-sponge. On the other hand, when SH-Graphene bio-sponge was investigated in the similar mixed metal ions in spiked sea water, the removal efficiency was reduced to 63.1% and 36.1% for Pb (II) and Cd (II) ions, respectively. Although the heavy metal ions removal efficiency of SH-Graphene bio-sponge was decreased in sea water, the modified sponge still outperformed activated carbon (25.5% for Pb^{2+}; 0% for Cd^{2+}) and alginate sponge (43.3% for Pb^{2+}; 0.79% for Cd^{2+}) in real water sample assessment. It is noteworthy to state that sea water is a complex natural water comprising of various kinds of inorganics and organics which compete for sorption sites of an adsorbent. The organics present in the sea water tend to block the pores of the adsorbent which may greatly affect the metal ions uptake performance of an adsorbent. Among all the tested sorbents, it should be emphasized that SH-Graphene bio-sponge still demonstrated the highest removal efficiency for Pb (II), Cd (II) and Co (II) in comparison to activated carbon and

alginate sponge regardless of the type of water matrix despite the stiff competition for active sites from the huge flux of inorganics and organic matters in the natural water sample, as well as the co-existing spiked metal ions. Given the high tolerance ability as well as strong binding affinity for Pb (II) and Cd (II) ions compared to the commercial adsorbent, SH-Graphene bio-sponge meets the requirements and expectation as a potential adsorbent in real water purification application.

3.4. Establishing the structural and chemical properties of SH-Graphene bio-sponge with metal ions removal performance

The presence of functional groups including the oxygen and thiol groups in the polymeric matrix of the SH-Graphene bio-sponge are primarily accountable for good binding affinity towards Pb (II) and Cd (II) ions in the water system. From the detailed pH studies in this work, electrostatic attraction is the dominant mechanism resulting from the presence of rich carboxylate groups on alginate as well as the deprotonation of the thiol and oxygen functionalities of the SH-Graphene bio-sponge in water. This is well-evidenced by the zeta potential measurement of the thiol-modified graphene sponge at different pH which confirmed the highly negative charged surface of the fabricated adsorbent that resulted in strong attraction with the positively charged Pb (II) and Cd (II) species.

On the other hand, according to *Hard Soft Acid Base (HSAB)* theory, a metal–ligand complex could be formed between the metals (Lewis acids with vacant orbital) and the ligands (Lewis bases with readily shared valence electron pair) via covalent bonding [47]. Considering that SH-Graphene bio-sponge is enriched with Lewis bases including thiol and oxygen-containing groups as evinced from the FTIR analysis discussed in the previous section, a metal-chelate complex could be resulted from the valence electron pair donated to the electron-deficient metal ions (Pb^{2+} and Cd^{2+}). Due to the fact that Cd (II) falls under the soft acids category while Pb (II) is a borderline Lewis acid, a more favourable chelation process could be expected between the SH-Graphene bio-sponge with Cd (II) ions according to the rule of thumb in *HSAB* concept: "Hard acids prefer to bind to hard bases and soft acids prefer to bind to soft bases" [47]. In relative to Pb (II) ions, a more stable metal-chelate complex and more feasible adsorption process is expected between Cd^{2+} (soft acid) and the thiol groups (soft base) on the modified graphene sponge as supported by the dimensionless K_R plot discussed in the section above. As reported in the literature, the existence of a myriad type of oxygen functional groups including carbonyl, carboxylate and epoxide groups in the adsorbent framework also act as electron-donor which led to surface complexation with the Cd^{2+} and Pb^{2+}, contributing to the uptake of metal ions. In addition, the magnetic iron oxide nanoparticles encapsulated in the alginate-GO matrix also improved the removal efficiency of the heavy metal pollutants besides facilitating in adsorbent-adsorbate separation after adsorption process. As described in the literature, the surface oxygen groups from the iron oxide particles as well as its nano-size particles give rise to higher surface area, leading to better uptake of the heavy metal ions [31,48,49].

We also found that the porous matrix with opened and interconnected pores found within the SH-Graphene bio-sponge as verified from the SEM imaging technique also helps in the metal ions uptake by providing more rooms to immobilize and trap the water pollutants within the micropores for adsorption process to take place. This is well-supported by the elemental mapping of the spent adsorbents (Figs. 8 and 9) which evidently showed that the studied water pollutants, lead and cadmium metal ions, were scattered within the large and tiny pores of the SH-Graphene bio-sponge, indicating that the opened and interconnected pores allowed the pollutants to penetrate through easily for adsorption to take place. Unlike activated carbon, this observation also implies that the mass transport of the metal ions throughout the polymeric matrix of SH-Graphene bio-sponge is highly accessible and not limited by internal diffusion. For activated carbon, the interaction of pollutant with activated carbon requires diffusion into its porous structure and may often experience pore blockage [50]. Another important highlight as shown in Fig. 8a and 9a revealed that the pore structure of the modified graphene sponge did not collapse which can be considered robust with its 3D porous structure retained even after oscillating in water for 24 h in the presence of heavy metal ions, washing with highly acidic conditions and drying steps. This again ascertained its potential application for water purification purpose.

4. Conclusions

In summary, SH-Graphene bio-sponge grafted with high density of S-containing groups (10.2 at %) was successfully synthesized via photoinduced thiol-ene click approach. The successful surface engineered graphene bio-sponge using multithiol was confirmed using XPS, FTIR, elemental mapping and TGA-DTG techniques. Assessment of adsorption performance of the multithiol modified Graphene bio-sponge showed satisfactorily high adsorption capacity, best fitted into Langmuir isotherm models ($R^2 > 0.97$) at ~103 mg/g and ~101 mg/g for Cd (II) and Pb (II) ions, respectively. Kinetics evaluation of the developed adsorbent revealed that this modified adsorbent followed pseudo-second order model for both Cd (II) and Pb (II) ions with $R^2 > 0.99$ attained. Adsorption studies suggested that the multithiol functionalized graphene bio-sponge showed exceptionally good selectivity towards Cd (II) and Pb (II) in both milli-Q and sea water. This novel surface-engineered graphene bio-sponge also demonstrated extraordinarily high recyclability (> 90 %) with only 15 ppb Pb (II) and 470 ppb Cd (II) detected after five consecutive adsorption–desorption cycles. The highly sustainable, selective and regenerative SH-Graphene bio-sponge provides a cutting-edge water purification solution with its promising results surpassing commercial adsorbent and control in real water sample assessment. The green and sustainable UV-directed thiol-ene click surface modification by combining biopolymers and functionalized graphene presented hereby paves a promising strategy to design advanced adsorbents for removal heavy metals from waters contributing to address global environmental problems.

Acknowledgements

The authors acknowledge the funding by the ARC Research Hub for Graphene Enabled Industry Transformation, (IH150100003). We thank Australian Microscopy and Microanalysis Research Facility (AMMRF) for the access of SEM and TEM facilities, Dr. Sarah Gilbert and Chris Bassell for their technical support on ICP-MS and XPS measurements, respectively. The XPS analysis was carried out at the Microscopy Australia facilities located at the University of South Australia, infrastructure co-funded by the University of South Australia, the South Australian State Government, and the Australian Federal Governments NCRIS scheme.

Appendix A. Supplementary data

Supplementary data to this article can be found online at https://doi.org/10.1016/j.cej.2020.124965.

References

[1] W.H. Rutger, R. Paul, S. Leah, 17 Countries, Home to One-Quarter of the World's Population, Face Extremely High Water Stress, World Resources Institute, USA, 2019.
[2] Y. Zou, X. Wang, A. Khan, P. Wang, Y. Liu, A. Alsaedi, T. Hayat, X. Wang, Environmental remediation and application of nanoscale zero-valent iron and its composites for the removal of heavy metal ions: a review, Environ. Sci. Technol. 50 (2016) 7290–7304.
[3] J. Potapowicz, D. Szumińska, M. Szopińska, Ż. Polkowska, The influence of global climate change on the environmental fate of anthropogenic pollution released from the permafrost: Part I. Case study of Antarctica, Sci. Total Environ. 651 (2019) 1534–1548.

[4] J. Xu, Z. Cao, Y. Zhang, Z. Yuan, Z. Lou, X. Xu, X. Wang, A review of functionalized carbon nanotubes and graphene for heavy metal adsorption from water: preparation, application, and mechanism, Chemosphere 195 (2018) 351–364.

[5] S. Kim, C.M. Park, M. Jang, A. Son, N. Her, M. Yu, S. Snyder, D.-H. Kim, Y. Yoon, Aqueous removal of inorganic and organic contaminants by graphene-based nanoadsorbents: a review, Chemosphere 212 (2018) 1104–1124.

[6] K.C. Khulbe, T. Matsuura, Removal of heavy metals and pollutants by membrane adsorption techniques, Appl. Water Sci. 8 (2018) 19.

[7] Z. Wang, A. Sim, J.J. Urban, B. Mi, Removal and recovery of heavy metal ions by two-dimensional MoS_2 nanosheets: performance and mechanisms, Environ. Sci. Technol. 52 (2018) 9741–9748.

[8] H. Zhu, J. Yuan, X. Tan, W. Zhang, M. Fang, X. Wang, Efficient removal of Pb^{2+} by Tb-MOFs: identifying the adsorption mechanism through experimental and theoretical investigations, Environ. Sci. Nano 6 (2019) 261–272.

[9] Y. Wang, G. Ye, H. Chen, X. Hu, Z. Niu, S. Ma, Functionalized metal–organic framework as a new platform for efficient and selective removal of cadmium(II) from aqueous solution, J. Mater. Chem. A 3 (2015) 15292–15298.

[10] G. Zhao, J. Li, X. Ren, C. Chen, X. Wang, Few-layered graphene oxide nanosheets as superior sorbents for heavy metal ion pollution management, Environ. Sci. Technol. 45 (2011) 10454–10462.

[11] P.L. Yap, T.T. Tung, S. Kabiri, N. Matulick, D.N.H. Tran, D. Losic, Polyamine-modified reduced graphene oxide: a new and cost-effective adsorbent for efficient removal of mercury in waters, Sep. Purif. Technol. 238 (2020) 116441.

[12] G.A. Martău, M. Mihai, D.C. Vodnar, The use of chitosan, alginate, and pectin in the biomedical and food sector—biocompatibility, bioadhesiveness, and biodegradability, Polymers 11 (2019) 1837.

[13] F. Zhou, X. Feng, J. Yu, X. Jiang, High performance of 3D porous graphene/lignin/sodium alginate composite for adsorption of Cd(II) and Pb(II), Environ Sci. Pollut. R. 25 (2018) 15651–15661.

[14] Z.-J. Shao, X.-L. Huang, F. Yang, W.-F. Zhao, X.-Z. Zhou, C.-S. Zhao, Engineering sodium alginate-based cross-linked beads with high removal ability of toxic metal ions and cationic dyes, Carbohydr. Polym. 187 (2018) 85–93.

[15] D. Kołodyńska, M. Gęca, E. Skwarek, O. Goncharuk, Titania-coated silica alone and modified by sodium alginate as sorbents for heavy metal ions, Nanoscale Res. Lett. 13 (2018) 96.

[16] P.L. Yap, S. Kabiri, D.N.H. Tran, D. Losic, Multifunctional binding chemistry on modified graphene composite for selective and highly efficient adsorption of mercury, ACS Appl. Mater. Interfaces 11 (2019) 6350–6362.

[17] P.T. Anastas, J.C. Warner, Principles of green chemistry, Green chemistry: theory and practice (1998) 29-56.

[18] P.L. Yap, S. Kabiri, Y.L. Auyoong, D.N.H. Tran, D. Losic, Tuning the multifunctional surface chemistry of reduced graphene oxide via combined elemental doping and chemical modifications, ACS Omega 4 (2019) 19787–19798.

[19] D.C. Marcano, D.V. Kosynkin, J.M. Berlin, A. Sinitskii, Z. Sun, A. Slesarev, L.B. Alemany, W. Lu, J.M. Tour, Improved synthesis of graphene oxide, ACS Nano 4 (2010) 4806–4814.

[20] Z. Wu, W. Deng, W. Zhou, J. Luo, Novel magnetic polysaccharide/graphene oxide @Fe_3O_4 gel beads for adsorbing heavy metal ions, Carbohydr. Polym. 216 (2019) 119–128.

[21] S.K. Lagergren, About the theory of so-called adsorption of soluble substances, Sven. Vetenskapsakad. Handingarl 24 (1898) 1–39.

[22] Y.S. Ho, G. McKay, Pseudo-second order model for Sorption processes, Process Biochem. 34 (1999) 451–465.

[23] I. Langmuir, The adsorption of gases on plane surfaces of glass, mica and platinum, J. Am. Chem. Soc. 40 (1918) 1361–1403.

[24] H. Freundlich, Over the adsorption in solution, Z. Phys. Chem. 385–470 (1906).

[25] S. Kuypers, S.K. Pramanik, L. D'Olieslaeger, G. Reekmans, M. Peters, J. D'Haen, D. Vanderzande, T. Junkers, P. Adriaensens, A. Ethirajan, Interfacial thiol–isocyanate reactions for functional nanocarriers: a facile route towards tunable morphologies and hydrophilic payload encapsulation, Chem. Commun. 51 (2015) 15858–15861.

[26] S. Huang, M. Podgórski, X. Zhang, J. Sinha, M. Claudino, J.W. Stansbury, C.N. Bowman, Dental Restorative Materials Based on Thiol-Michael Photopolymerization, J. Dent. Res. 97 (2018) 530–536.

[27] K. Shanmuganathan, R.K. Sankhagowit, P. Iyer, C.J. Ellison, Thiol-ene chemistry: a greener approach to making chemically and thermally stable fibers, Chem. Mater. 23 (2011) 4726–4732.

[28] B.T. Michal, W.A. Brenn, B.N. Nguyen, L.S. McCorkle, M.A.B. Meador, S.J. Rowan, Thermoresponsive shape-memory aerogels from thiol-ene networks, Chem. Mater. 28 (2016) 2341–2347.

[29] A.C. Levine, G.W. Heberlig, C.T. Nomura, Use of thiol-ene click chemistry to modify mechanical and thermal properties of polyhydroxyalkanoates (PHAs), Int. J. Biol. Macromol. 83 (2016) 358–365.

[30] G. Lawrie, I. Keen, B. Drew, A. Chandler-Temple, L. Rintoul, P. Fredericks, L. Grøndahl, Interactions between Alginate and Chitosan Biopolymers Characterized Using FTIR and XPS, Biomacromolecules 8 (2007) 2533–2541.

[31] J. Sun, Y. Chen, H. Yu, L. Yan, B. Du, Z. Pei, Removal of Cu^{2+}, Cd^{2+} and Pb^{2+} from aqueous solutions by magnetic alginate microsphere based on Fe_3O_4/MgAl-layered double hydroxide, J. Colloid Interface Sci. 532 (2018) 474–484.

[32] Z. Schnepp, S.C. Wimbush, M. Antonietti, C. Giordano, Synthesis of Highly Magnetic Iron Carbide Nanoparticles via a Biopolymer Route, Chem. Mater. 22 (2010) 5340–5344.

[33] B. Yu, X. Wang, W. Xing, H. Yang, X. Wang, L. Song, Y. Hu, S. Lo, Enhanced thermal and mechanical properties of functionalized graphene/thiol-ene systems by photopolymerization technology, Chem. Eng. J. 228 (2013) 318–326.

[34] J. Zhu, Q. Lu, C. Chen, J. Hu, J. Liu, One-step synthesis and self-assembly of a luminescent sponge-like network of gold nanoparticles with high absorption capacity, J. Mater. Chem. C 5 (2017) 6917–6922.

[35] D.G. Matei, N.-E. Weber, S. Kurasch, S. Wundrack, M. Woszczyna, M. Grothe, T. Weimann, F. Ahlers, R. Stosch, U. Kaiser, A. Turchanin, Functional Single-Layer Graphene Sheets from Aromatic Monolayers, Adv. Mater. 25 (2013) 4146–4151.

[36] B. Lesiak, L. Kövér, J. Tóth, J. Zemek, P. Jiricek, A. Kromka, N. Rangam, C sp^2/sp^3 hybridisations in carbon nanomaterials – XPS and (X)AES study, Appl. Surf. Sci. 452 (2018) 223–231.

[37] Q. Zhang, J. Teng, G. Zou, Q. Peng, Q. Du, T. Jiao, J. Xiang, Efficient phosphate sequestration for water purification by unique sandwich-like MXene/magnetic iron oxide nanocomposites, Nanoscale 8 (2016) 7085–7093.

[38] C.-Y. Lee, H.E. Canavan, L.J. Gamble, D.G. Castner, Evidence of Impurities in Thiolated Single-Stranded DNA Oligomers and Their Effect on DNA Self-Assembly on Gold, Langmuir 21 (2005) 5134–5141.

[39] J. Perić, M. Trgo, N. Vukojević Medvidović, Removal of zinc, copper and lead by natural zeolite—a comparison of adsorption isotherms, Water Res. 38 (2004) 1893–1899.

[40] F.S. Awad, K.M. AbouZeid, W.M.A. El-Maaty, A.M. El-Wakil, M.S. El-Shall, Efficient removal of heavy metals from polluted water with high selectivity for mercury(II) by 2-Imino-4-thiobiuret–partially reduced graphene oxide (IT-PRGO), ACS Appl. Mater. Interfaces 9 (2017) 34230–34242.

[41] A. Khan, J. Xing, A.M. Elseman, P. Gu, K. Gul, Y. Ai, R. Jehan, A. Alsaedi, T. Hayat, X. Wang, A novel magnetite nanorod-decorated Si-Schiff base complex for efficient immobilization of U(vi) and Pb(ii) from water solutions, Dalton T. 47 (2018) 11327–11336.

[42] S. Zhang, F. Xu, Y. Wang, W. Zhang, X. Peng, F. Pepe, Silica modified calcium alginate–xanthan gum hybrid bead composites for the removal and recovery of Pb (II) from aqueous solution, Chem. Eng. J. 234 (2013) 33–42.

[43] J. Liu, H. Chu, H. Wei, H. Zhu, G. Wang, J. Zhu, J. He, Facile fabrication of carboxymethyl cellulose sodium/graphene oxide hydrogel microparticles for water purification, RSC Adv. 6 (2016) 50061–50069.

[44] R.R. Pawar, M. Lalhmunsiama, J.-G. Kim, S.-M. Kim, S.Y. Hong, S.M. Sawant, Lee, Efficient removal of hazardous lead, cadmium, and arsenic from aqueous environment by iron oxide modified clay-activated carbon composite beads, Appl. Clay Sci. 162 (2018) 339–350.

[45] B.H. Rehm, M.F. Moradali, Alginates and their biomedical applications, Springer2018.

[46] M. US EPA, National primary drinking water regulations, EPA-816-F-09–004 Search PubMed, 2009.

[47] R.G. Pearson, Hard and soft acids and bases, HSAB, part 1: Fundamental principles, J. Chem. Educ. 45 (1968) 581.

[48] M. Jain, M. Yadav, T. Kohout, M. Lahtinen, V.K. Garg, M. Sillanpää, Development of iron oxide/activated carbon nanoparticle composite for the removal of Cr(VI), Cu (II) and Cd(II) ions from aqueous solution, Water Resour. Ind. 20 (2018) 54–74.

[49] J.-H. Deng, X.-R. Zhang, G.-M. Zeng, J.-L. Gong, Q.-Y. Niu, J. Liang, Simultaneous removal of Cd(II) and ionic dyes from aqueous solution using magnetic graphene oxide nanocomposite as an adsorbent, Chem. Eng. J. 226 (2013) 189–200.

[50] M. Sweetman, S. May, N. Mebberson, P. Pendleton, K. Vasilev, S. Plush, J. Hayball, Activated carbon, carbon nanotubes and graphene: materials and composites for advanced water purification, C 3 (2017) 18.

Supplementary Material

Multithiol Functionalized Graphene Bio-Sponge via Photoinitiated Thiol-ene Click Chemistry for Efficient Heavy Metal Ions Adsorption

Pei Lay Yap,[a,b] *Yow Loo Auyoong,*[c] *Kamrul Hassan,*[a,b] *Farzaneh Farivar,*[a,b] *Diana, N.H. Tran*[a,b] *Jun Ma*[b,d,e] *and Dusan Losic*[*a,b]

[a] School of Chemical Engineering and Advanced Materials, [b]ARC Hub for Graphene Enabled Industry Transformation, The University of Adelaide, Adelaide, SA 5005, Australia

[c] Innovation and Commercial Partnerships, The University of Adelaide, Adelaide, SA 5000, Australia

[d] Future Industries Institute, [e] School of Engineering, University of South Australia, Mawson Lakes, SA 5095, Australia

*Corresponding author: dusan.losic@adelaide.edu.au

Materials

Natural graphite rocks (Uley, Eyre Peninsula, South Australia, Australia) were crushed into powder using a benchtop ring mill (Rocklabs) and sifted through 25 µm sieve. 85 % w/w phosphoric acid (Chem-Supply), 98 % sulfuric acid (Chem-Supply), potassium permanganate (Sigma Aldrich), 30 % hydrogen peroxide (Chem-Supply), 36 % hydrochloric acid (Chem-Supply), sodium hydroxide (Chem-Supply), ethanol (Chem-Supply), sodium alginate (Chem-Supply), calcium chloride (Chem-Supply), 2,2-dimethoxy-2-phenylacetophenone (DMPA, Sigma-Aldrich), iron(III) chloride (Chem-Supply), iron (II) sulfate (Chem-Supply), ammonium hydroxide (Sigma Aldrich), pentaerythritol tetrakis(3-mercaptopropionate) (4TH, Sigma Aldrich), cadmium nitrate (Mallinckrodt), copper nitrate (Chem-Supply), lead nitrate(Univar), cobalt nitrate (Ajax), and thiourea (Sigma Aldrich) were used directly without prior purification.

Materials Characterization

The morphology, mapping and EDX analysis of the materials were studied using scanning electron microscope equipped with EDX Silicon Drift Detectors (FE-SEM, Quanta 450 FEG, FEI, USA, EDX, Ultim Max 170 mm SDD, Oxford Instruments, UK) at 10-15 kV (operating voltage). The functional groups in the samples were identified by FTIR (Nicolet 6700, Thermo Fisher) in the range of 500-4000 cm^{-1}. High-resolution transmission electron microscope (HRTEM, Philips CM200, Japan) was used to capture the sample image at 200 kV. The sample preparation involved the dispersion of sample in ethanol via bath sonication to form a homogeneous dispersion on a Cu grid. XRD with Cu X-ray tube (600 Miniflex, Rigaku, Japan) was performed under 40 kV and 15 mA with 10° min^{-1} scan speed at 2θ = 5- 80° to probe the bulk phase identification. Thermal stability and properties of the materials were investigated using TGA/DSC 2, STARe System

(Mettler Toledo, Switzerland) under air atmosphere with the samples heated in alumina crucible to 1000 ˚C at 10 ˚C min^{-1} heating rate. The surface elemental composition and chemical species of the materials were studied using X-ray Photoelectron Spectroscopy (XPS, AXIS Ultra_DLD, Kratos, UK) equipped with a monochromatic Al Kα radiation source (hv =1486.7 eV) at 225 W, 15 kV and 15 mA. XPS wide scans were recorded at 0.5 eV step size over -10-1100 eV at the pass energy of 160 eV while the narrow scans were collected at a 0.1 eV step size and pass energy of 20 eV. The peak fitting and deconvolution were analysed using Casa XPS™ software with the core-level spectra involved calibrated to the primary peak (C-C/C-H peak) of adventitious carbon at 284.8 eV. The full width at half maximum (fwhm) for all corresponding components were constrained within the difference of 0.2 eV. For the curve fitting of S2p high resolution peak, the peak was resolved into $S2p_{3/2}$ and $S2p_{1/2}$ components at a peak area ratio of 2: 1 with 1.18 eV energy separation. The specific surface area measurement was determined using methylene blue adsorption approach using UV-Vis spectroscopy (Shimadzu, UV 1601, Japan) as described in our previous work [1, 2]. The surface charge of the materials was determined as a function of pH with the average zeta potential repeated three times using a Malvern Zetasizer (Nanoseries, Australia). The sample was dispersed in milli-Q water and bubbled in nitrogen gas to drive off the dissolved CO_2 gas and allowed to stand for a week before zeta potential measurement using HCl or NaOH solution adjusted between pH 3-10. Solution ICP-MS (QQQ 8900, Agilent) was applied to measure the concentration of metal ions remained after the adsorption experiments. Specific surface area of the material was analysed according to the method reported in our previous work[1].

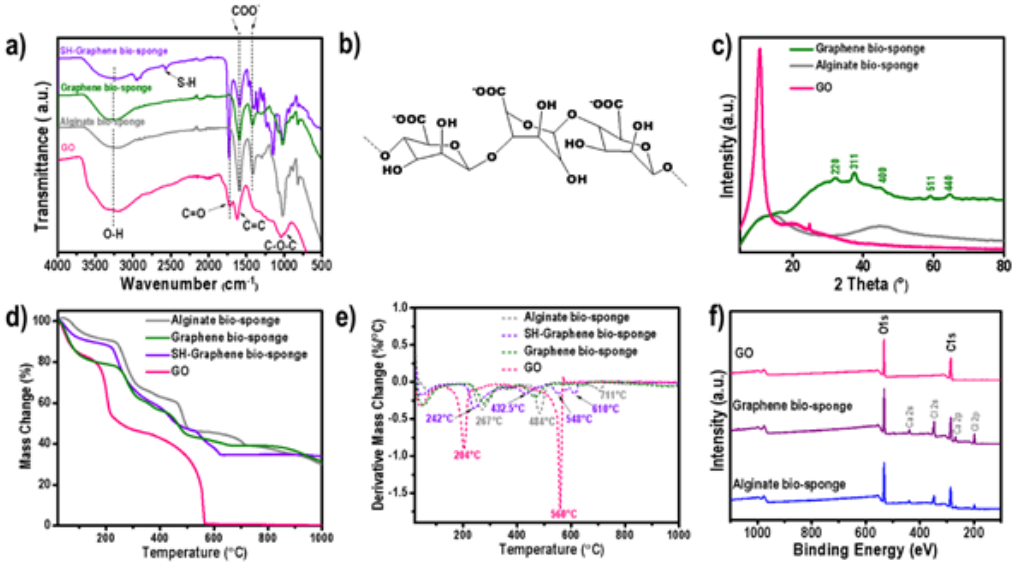

Fig. S1 (a) FTIR spectra of the synthesized materials. (b) Chemical structure of alginate. (c) XRD, (d) TGA, (e) DTG plots and (f) XPS survey spectra of the products prepared.

Table S1 Normalized chemical composition of samples determined from their respective XPS survey plots.

Element	Atomic %				C/O atomic ratio
	C	O	Ca	S	
GO	71.11	28.89	-	-	2.46
Alginate bio-sponge	60.20	35.85	3.95	-	1.68
(Graphene bio-sponge) Alginate/rGO/Fe_3O_4	61.54	33.54	4.93	-	1.83
SH-Graphene bio-sponge	63.46	25.77	0.57	10.20	2.46

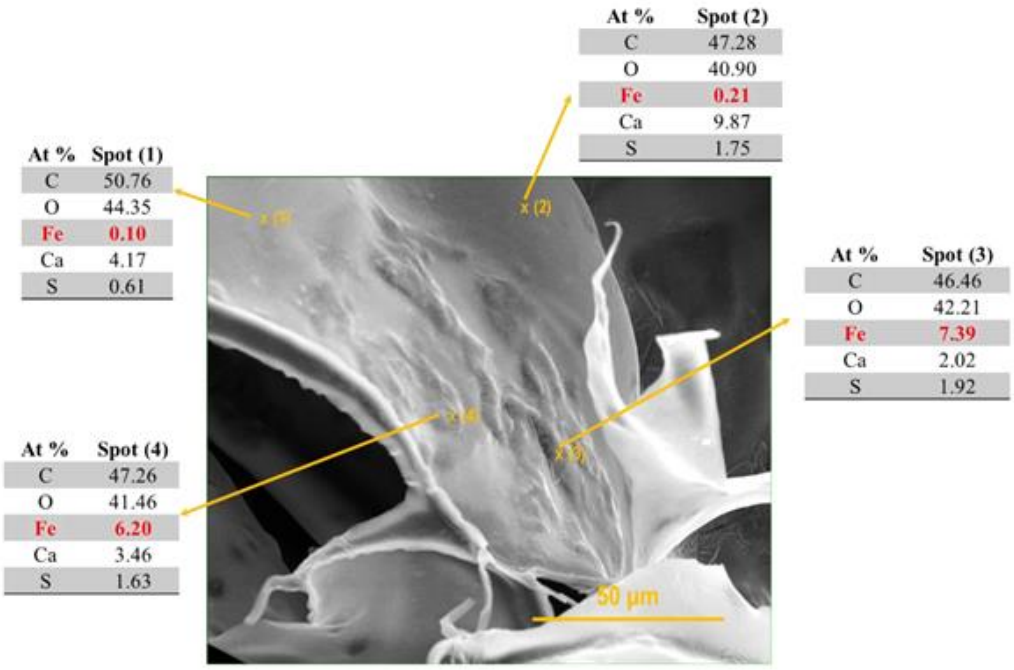

Fig. S2 EDX analysis performed on four different spots with SEM image, showing the normalized elemental composition of SH-Graphene bio-sponge.

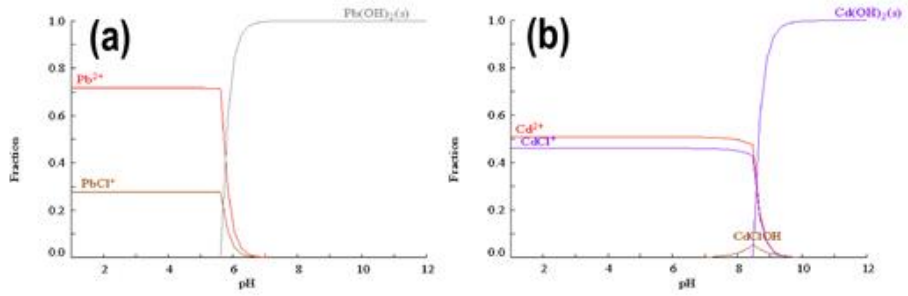

Fig. S3 Metal species distribution diagram plotted as a function of pH (total metal concentration 1.0×10^{-4} M) for (a) lead and (b) cadmium calculated using the computer programs HYDRA and MEDUSA[3].

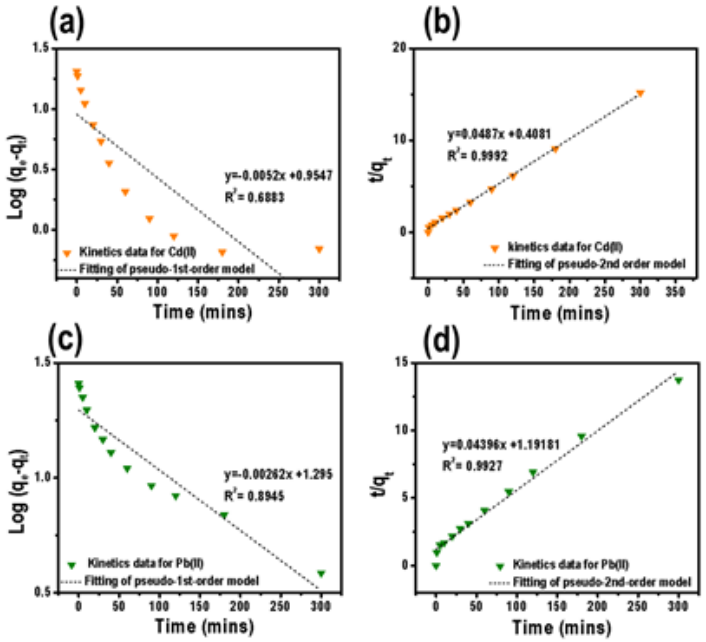

Fig. S4 Kinetic modelling plots of pseudo-first order and pseudo-second order, respectively, for the experimental data extracted from the sorption process of SH-Graphene bio-sponge for (a and b) Cd (II), (c and d) Pb (II) ions.

Table S2 Adsorption kinetics parameters of pseudo-first order and pseudo-second order kinetic models for Cd (II) and Pb (II) ions on SH-Graphene bio-sponge.

Kinetic Model	Parameter	Metal ion	
		Cd (II)	Pb (II)
Pseudo-first order	k_1 (min^{-1})	2.258×10^{-3}	1.1376×10^{-3}
	q_e ($mg\ g^{-1}$)	9.01	19.71
	R^2	0.6883	0.8945
Pseudo-second order	k_2 ($g\ mg^{-1}\ min^{-1}$)	5.814×10^{-3}	1.621×10^{-3}
	q_e ($mg\ g^{-1}$)	20.53	22.75
	R^2	0.9992	0.9927

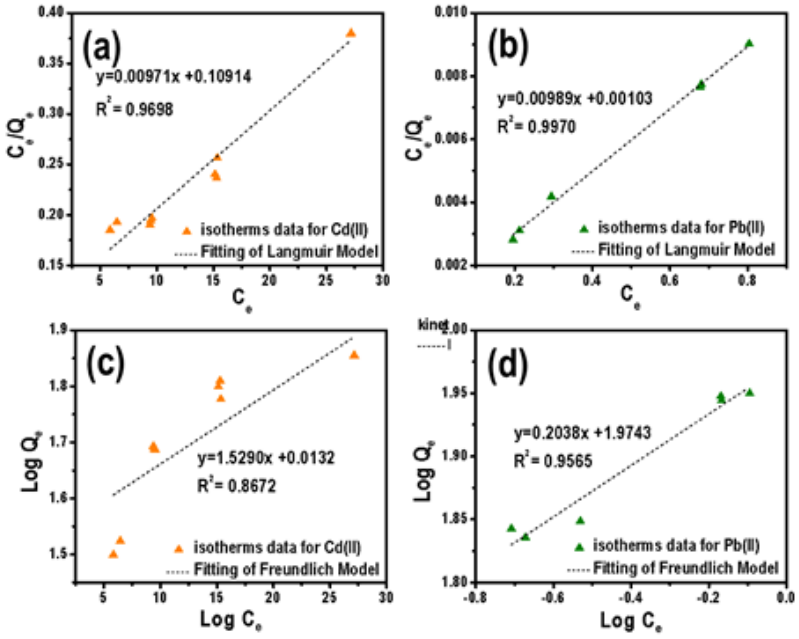

Fig. S5 Equilibrium plots of Langmuir isotherm model for (a) Cd (II) and (b) Pb (II) ions on SH-Graphene bio-sponge. Equilibrium plots of Freundlich isotherm model for (c) Cd (II) and (d) Pb (II) ions on SH-Graphene bio-sponge. [Conditions: sorbent dosage= 1000 mgL^{-1}, initial metal ion concentration=20-110 mgL^{-1}, pH ~5 at 21.0 °C.]

Table S3 Adsorption isotherm parameters of Langmuir and Freundlich models for Cd (II) and Pb (II) ions on SH-Graphene bio-sponge.

Isotherm Model	Parameter	Metal ion	
		Cd(II)	Pb(II)
Langmuir	q_{max} (mg g^{-1})	102.99	101.01
	b (L mg^{-1})	0.0089	9.61
	R^2	0.9698	0.9970
Freundlich	1/n	0.0132	0.2038
	K ($mg^{1-1/n}$ g^{-1} $L^{1/n}$)	33.81	94.25
	R^2	0.8672	0.9565

References:

[1] P.L. Yap, S. Kabiri, D.N.H. Tran, D. Losic, Multifunctional binding chemistry on modified graphene composite for selective and highly efficient adsorption of mercury, ACS Appl. Mater. Interfaces 11 (2019) 6350-6362.

[2] D.N. Tran, S. Kabiri, L. Wang, D. Losic, Engineered graphene–nanoparticle aerogel composites for efficient removal of phosphate from water, J. Mater. Chem. A 3 (2015) 6844-6852.

[3] I. Puigdomenech, Make Equilibrium using Sophisticated Algorithms (MEDUSA) program, Inorganic Chemistry Department. Royal Institute of Technology, 2004, pp. 44.

6.4. Statement of Authorship

Statement of Authorship

Title of Paper	All-in-One Bioinspired Multifunctional Graphene Biopolymer Foam for Simultaneous Removal of Multiple Water Pollutants.
Publication Status	☒ Published ☐ Accepted for Publication ☐ Submitted for Publication ☐ Unpublished and Unsubmitted w ork w ritten in manuscript style
Publication Details	Yap, P. L., Hassan, K., Auyoong, Y. L., Mansouri, N., Farivar, F., Tran, D. N., & Losic, D. (2020). All-in-One Bioinspired Multifunctional Graphene Biopolymer Foam for Simultaneous Removal of Multiple Water Pollutants. Advanced Materials Interfaces, 2000664.

Principal Author

Name of Principal Author (Candidate)	Pei Lay Yap		
Contribution to the Paper	Prepared, characterized and conducted performance testing on all the samples, interpreted data as well as wrote the manuscript.		
Overall percentage (%)	85%		
Certification:	This paper reports on original research I conducted during the period of my Higher Degree by Research candidature and is not subject to any obligations or contractual agreements with a third party that would constrain its inclusion in this thesis. I am the primary author of this paper.		
Signature		Date	01/10/20

Co-Author Contributions

By signing the Statement of Authorship, each author certifies that:

i. the candidate's stated contribution to the publication is accurate (as detailed above);

ii. permission is granted for the candidate in include the publication in the thesis; and

iii. the sum of all co-author contributions is equal to 100% less the candidate's stated contribution.

Name of Co-Author	Yow Loo Au Yoong		
Contribution to the Paper	Helped in sample characterization and revised manuscript.		
Signature		Date	02/10/20

Name of Co-Author	Kamrul Hassan		
Contribution to the Paper	Helped in sample characterization and revised manuscript.		
Signature		Date	02/10/20

Please cut and paste additional co-author panels here as required.

Statement of Authorship

Title of Paper	All-in-One Bioinspired Multifunctional Graphene Biopolymer Foam for Simultaneous Removal of Multiple Water Pollutants.
Publication Status	☒ Published ☐ Accepted for Publication ☐ Submitted for Publication ☐ Unpublished and Unsubmitted w ork w ritten in manuscript style
Publication Details	Yap, P. L., Hassan, K., Auyoong, Y. L., Mansouri, N., Farivar, F., Tran, D. N., & Losic, D. (2020). All-in-One Bioinspired Multifunctional Graphene Biopolymer Foam for Simultaneous Removal of Multiple Water Pollutants. Advanced Materials Interfaces, 2000664.

Principal Author

Name of Principal Author (Candidate)	Pei Lay Yap		
Contribution to the Paper	Prepared, characterized and conducted performance testing on all the samples, interpreted data as well as wrote the manuscript.		
Overall percentage (%)	85%		
Certification:	This paper reports on original research I conducted during the period of my Higher Degree by Research candidature and is not subject to any obligations or contractual agreements with a third party that would constrain its inclusion in this thesis. I am the primary author of this paper.		
Signature		Date	21/10/20

Co-Author Contributions

By signing the Statement of Authorship, each author certifies that:

i. the candidate's stated contribution to the publication is accurate (as detailed above);

ii. permission is granted for the candidate in include the publication in the thesis; and

iii. the sum of all co-author contributions is equal to 100% less the candidate's stated contribution.

Name of Co-Author	Negar Mansouri		
Contribution to the Paper	Helped in sample characterization.		
Signature		Date	22/10/20

Name of Co-Author	Farzaneh Farivar		
Contribution to the Paper	Helped in sample characterization.		
Signature		Date	22/10/20

Please cut and paste additional co-author panels here as required.

Statement of Authorship

Title of Paper	All-in-One Bioinspired Multifunctional Graphene Biopolymer Foam for Simultaneous Removal of Multiple Water Pollutants.
Publication Status	☒ Published ☐ Accepted for Publication ☐ Submitted for Publication ☐ Unpublished and Unsubmitted work written in manuscript style
Publication Details	Yap, P. L., Hassan, K., Auyoong, Y. L., Mansouri, N., Farivar, F., Tran, D. N., & Losic, D. (2020). All-in-One Bioinspired Multifunctional Graphene Biopolymer Foam for Simultaneous Removal of Multiple Water Pollutants. Advanced Materials Interfaces, 2000664.

Principal Author

Name of Principal Author (Candidate)	Pei Lay Yap		
Contribution to the Paper	Prepared, characterized and conducted performance testing on all the samples, interpreted data as well as wrote the manuscript.		
Overall percentage (%)	85%		
Certification:	This paper reports on original research I conducted during the period of my Higher Degree by Research candidature and is not subject to any obligations or contractual agreements with a third party that would constrain its inclusion in this thesis. I am the primary author of this paper.		
Signature		Date	01/10/20

Co-Author Contributions

By signing the Statement of Authorship, each author certifies that:

i. the candidate's stated contribution to the publication is accurate (as detailed above);

ii. permission is granted for the candidate in include the publication in the thesis; and

iii. the sum of all co-author contributions is equal to 100% less the candidate's stated contribution.

Name of Co-Author	Diana N.H. Tran		
Contribution to the Paper	Co-supervised and revised manuscript.		
Signature		Date	02/10/20

Name of Co-Author	Dusan Losic		
Contribution to the Paper	Supervised the development of work, edited, revised the manuscript and acted as the corresponding author.		
Signature		Date	02/10/20

Please cut and paste additional co-author panels here as required.

6.5. Published work

This section is presented as a published peer-reviewed article:

2. ***Yap, P. L.***, *Hassan, K., Auyoong, Y. L., Mansouri, N., Farivar, F., Tran, D. N., & Losic, D. (2020). All-in-one bioinspired multifunctional graphene biopolymer foam for simultaneous removal of multiple water pollutants. Advanced Materials Interfaces, 2000664.* Reproduced with permission.[24] Copyright (2020) Wiley-VCH.

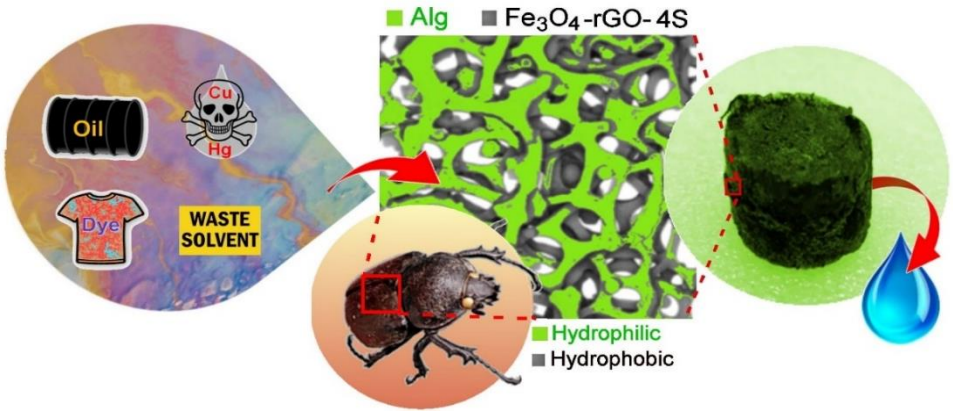

Figure 16. Graphical abstract of "*All-in-one bioinspired multifunctional graphene-biopolymer foam for simultaneous removal of multiple water pollutants*". *Reproduced with permission.[24] Copyright (2020) Wiley-VCH.*

FULL PAPER

ADVANCED MATERIALS INTERFACES
www.advmatinterfaces.de

All-in-One Bioinspired Multifunctional Graphene Biopolymer Foam for Simultaneous Removal of Multiple Water Pollutants

*Pei Lay Yap, Kamrul Hassan, Yow Loo Auyoong, Negar Mansouri, Farzaneh Farivar, Diana N. H. Tran, and Dusan Losic**

Polluted waters are complex systems with many different co-existing contaminants that make their simultaneous removal a very challenging task. To address this problem, all-in-one ad/ab-sorbent with unique combination of interfacial properties and multiple surface chemistry is developed to simultaneously and efficiently remove several pollutants including heavy metals, dyes, oils, and organic solvents. By mimicking the wetting micro-topology of a darkling beetle with a combined hydrophilic-hydrophobic surface, a new bioinspired adsorbent, graphene biopolymer foam (Alg-Fe_3O_4-rGO-4S) for removal of multiple water pollutants is engineered by combining alginate (Alg) and reduced graphene oxide (rGO) functionalized with tetrathiol that is also decorated with iron oxide nanoparticles (Fe_3O_4). This concept is first proved by single pollutant removal, showing adsorption capacity of 789.7 ± 36 mg/g for methylene blue (MB), 107.0 ± 2.1 mg/g for Hg (II), 73.5 ± 0.7 mg/g for Cu (II), and rapid oil-water separation with high sorption capacity (11–18 g/g). A remarkable performance for simultaneous removal of their mixtures in milli-Q, river, and sea water is demonstrated with efficiency for MB (≈90%), Cu (II) (>99.99%) and Hg (II) (100%) and rapid (≈30 s) uptake of organic solvents and oils. The obtained results indicate a valuable potential of proposed concept for simultaneous removal of co-existing water pollutants.

1. Introduction

With the rapid industrial and agricultural development, the water pollution caused by the discharge of wastewater from broad range of industries such as chemical, metallurgy, mining, oil and petrol, papermaking, printing, dying, food and agriculture become one of the most serious global challenges faced by the humanity. The pollutants in contaminated water system become more diverse with thousands of different hazardous compounds, making the search for universal water purification technology a very challenging task.[1] Various separation and treatment technologies including precipitation, separation membranes filtration, reduction, ion-exchange, adsorption, and photocatalytic degradation have been introduced.[2] Among them, adsorption using adsorbents is well accepted as a water purification method to remove inorganic and organic pollutants from water owing to its low operational cost, high efficiency, simplicity, and high flexibility to be applied in different water systems.[2b] Many adsorbents have been explored and practically used in the last decades including activated carbon (AC), different types of porous carbon and their composites, natural or synthetic clays and silica, metal oxides, metal organic frameworks, natural and synthetic porous polymers.[3] AC produced from waste material is one of the most frequently and commercially-used adsorbents due to its high porosity, large surface area, low-cost, and good sorption capacity. However, AC has many disadvantages such as pore blockage, lack of selectivity especially for heavy metals that limits its applications to be used as a universal adsorbent.[4]

Graphene has recently emerged as an excellent choice for designing a new generation of multifunctional sorbent materials attributed to its desirable physicochemical properties including its opened-up layer structure, large surface area, high mechanical strength, and tailorable surface chemistry.[4,5] Numerous studies based on different forms of graphene, GO and their composites have been performed showing an excellent performance for removal of single type pollutant from water. Surprisingly, although graphene is renowned for its highly tailorable surface that enables decoration of a

P. L. Yap, K. Hassan, Dr. F. Farivar, Dr. D. N. H. Tran, Prof. D. Losic
School of Chemical Engineering and Advanced Materials
The University of Adelaide
Adelaide, SA 5005, Australia
E-mail: dusan.losic@adelaide.edu.au
P. L. Yap, K. Hassan, N. Mansouri, Dr. F. Farivar, Dr. D. N. H. Tran, Prof. D. Losic
ARC Hub for Graphene Enabled Industry Transformation
The University of Adelaide
Adelaide, SA 5005, Australia
Dr. Y. L. Auyoong
Innovation and Commercial Partnerships
The University of Adelaide
Adelaide, SA 5000, Australia
N. Mansouri
School of Electrical and Electronic Engineering
The University of Adelaide
Adelaide, SA 5005, Australia
The ORCID identification number(s) for the author(s) of this article can be found under https://doi.org/10.1002/admi.202000664.

DOI: 10.1002/admi.202000664

ADVANCED SCIENCE NEWS
www.advancedsciencenews.com

ADVANCED MATERIALS INTERFACES
www.advmatinterfaces.de

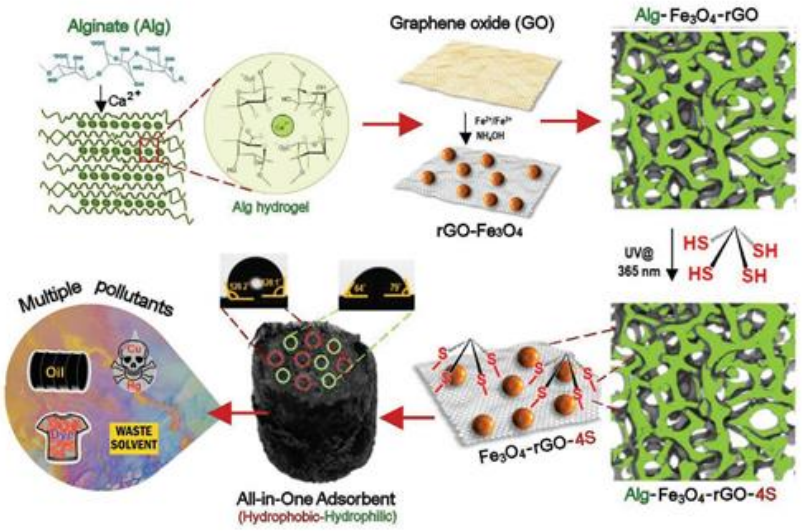

Figure 1. Schematic diagram showing the formation of multifunctional graphene biopolymer (Alg-Fe_3O_4-rGO-4S) foam with a combined hydrophilic-hydrophobic microstructure and specific surface chemistry functionalized for efficient and simultaneous removal of co-existing water pollutants including heavy metals, organic dyes, solvents, and oils in water.

wide range of functional groups to target for different class of water pollutants, very limited research has been reported on their application for simultaneous removal of co-existing water contaminants. One of the examples included highly porous and superhydrophobic graphene reported by Tabish et al. that exhibited high selectivity, good recyclability, and excellent adsorption capacities for arsenic, fluoride, nitrate, MB, rhodamine B, and oil from water performed on single pollutant but not on their simultaneous removal.[6] The study with sulfonated graphene adsorbent was shown to effectively remove the water pollutants such as phenanthrene, MB, and Cd^{2+} from water.[7] In another work, Cheng et al. have demonstrated the efficient removal ability of polydopamine assembled graphene aerogel to remove multiple type of oils, organic solvents, and dyes from contaminated water.[8] However, one of the disadvantages of this composite is the use of styrene which is a carcinogen and mutagen that is not acceptable for water purification systems.

Majority of the reported adsorbents were explored to remove pollutants individually from single or binary models of water pollutants with no consideration to target on simultaneous uptake of co-existing pollutants from complex water pollution systems. Realistically, contaminated waters consist of not only a single type of pollutant, but a broad spectrum of pollutants such as oil, dyes, and heavy metals that occur simultaneously resulting from residential, agricultural, and industrial sources, which impose a very challenging task of designing universal adsorbents for their remediation[2b] This phenomenon is further accentuated by the recent call for multi-pollutant modeling approach instead of the conventional single pollutant modeling method for comprehensive water quality assessment at a global scale.[9] The key challenge to address these requirements is to design sorbents that can integrate multifunctional surface chemistry with the dual-surface-bulk wettability, which is able to meet the ad/ab-sorption criteria for both hydrophilic heavy metal ions and organic substances (dyes) as well as hydrophobic organic pollutants (oil and solvents). Despite the synthesis of these multifunctional composites have been reported for different purposes, there are still many remaining gaps on practical studies to confirm their applicability for simultaneous adsorption of multiple contaminants.[2b] There is a lack of better understanding on the relationship between their structural-physiochemical surface properties and properties of contaminants during simultaneous and competitive adsorption process.

Motivated by this challenging problem to design an all-in-one and "universal" sorbent toward achieving comprehensive remediation of multiple pollutants, in this paper, we present our biomimetic approach on specially-engineered multifunctional graphene-biopolymer foam with unique combination of interfacial properties and multiple surface chemistry to simultaneously and efficiently remove a broad spectrum of pollutants including heavy metals, organic dyes, oils, and organic solvents. The concept is inspired by the asymmetric wetting micro-topology of a darkling beetle that possesses combined hydrophobic-hydrophilic surface, which is able to attract/retract both type hydrophilic (water) hydrophobic (oil) compounds. To mimic these properties, we engineered a new adsorbent consisting of alginate (Alg) polymer foam with embedment of reduced graphene oxide (rGO) sheets decorated with iron oxide nanoparticles (Fe_3O_4) and functionalized with tetrathiol using a photoinitiated thiol–ene click chemistry as presented in **Figure 1**. In this approach, the graphene-biopolymer (Alg-Fe_3O_4-rGO-4S) with chemically functionalized hydrophobic and hydrophilic porous patterns can be generated in hundreds of micron meters dimensions that are randomly organized and interconnected across the foam structure. The

ADVANCED SCIENCE NEWS
www.advancedsciencenews.com

ADVANCED MATERIALS INTERFACES
www.advmatinterfaces.de

second important feature proposed is its highly porous network in the foam which serves as a depot to store contaminant molecules apart from allowing a continuous passage of water carrying pollutants to the binding sites of the sorbent. Unlike the use of majority commercial foams such as melamine and polyurethane, in this work, sodium alginate (Alg) biopolymer was selected as the basic structural scaffold owing to its low-cost, non-toxicity with hydrophilic surface, high density of hydroxyl and carboxylate groups, which are beneficial for attracting hydrophilic and cationic pollutants. While, reduced graphene (rGO) is used in the design of this sorbent material for several reasons. First, it improves mechanical strength and robustness of the foam in the foam matrix. Second, rGO is decorated with magnetic iron oxide nanoparticles (NPs), which also have binding affinity for many pollutants (phosphates, arsenic, etc.) that can provide magnetic property to the foam.[10] Finally, rGO structure is used as a functionalization platform for attachment of specific binding chemistry that can be tailored by selection of functional groups for uptake of specific contaminants. In this work, UV photoinitiated thiol–ene click reaction was used to covalently attach tetrathiol molecules with four thiol groups on sp^2 carbon on the basal plane of graphene to enhance the adsorption of heavy metals.[2a,11,13] The UV thiol–ene click modification is regarded as a mild, environmentally friendly, and sustainable approach with low energy (room temperature) consumption compared to the conventional thermal click chemistry process demonstrated in our previous work.[2a] The structural, thermal, chemical, and mechanical properties of the developed graphene-biopolymer foam (Alg-Fe_3O_4-rGO-4S) were elucidated using a series of characterization techniques including scanning electron microscopy-energy dispersive X-ray (SEM-EDX), high resolution transmission electron microscopy (HRTEM), powder X-ray diffraction (XRD), thermogravimetry analysis (TGA), Fourier transform infrared (FTIR), X-ray photoelectron spectroscopy (XPS), contact angle, dynamic mechanical, and mercury porosimetry analyses to understand their interfacial and adsorption properties for simultaneous removal of multiple water pollutants. Adsorption performances and recyclability of prepared graphene-biopolymer foams were explored by series of experiments using single and mixed pollutants scenarios (milli-Q, river, and sea water) such as MB, Hg (II), Cu (II), oil, and series of organic solvents. These removal experiments were also benchmarked and compared with AC as commercial adsorbent to confirm their application for simultaneous removal of broad range of co-existing pollutants.

2. Results and Discussion

2.1. Characterization of Multifunctional Graphene-Biopolymer Foam (Alg-Fe_3O_4-rGO-4S)

Structural and chemical composition characterizations of the fabricated graphene-biopolymer foam (Alg-Fe_3O_4-rGO-4S) during different stages of preparation were elucidated using SEM and EDAX as summarized in **Figure 2**. The GO material before and after the decoration with iron oxide nanoparticles (NPs) are presented in Figure 2a,b showing typical few layered GO sheets with randomly dispersed NPs. Higher magnification of the HRTEM image (Figure 2c) confirmed the presence of randomly dispersed Fe_3O_4 NPs with average particle size of 3.40 ± 0.77 nm on rGO surface (Figure S1a, Supporting Information). The inset image depicts the refined lattice fringes and the selected area electron diffraction (SAED) patterns of Fe_3O_4 NPs with an interplanar distance of 0.25 nm, corresponding to the (311) diffraction plane of magnetite, Fe_3O_4. This result clearly shows that the desired size of highly crystalline Fe_3O_4 NPs was achieved and well-dispersed on the GO sheets.[12] SEM image of cross-sectional structure of functionalized graphene-biopolymer foam (Figure 2d) with highly porous architecture after tetrathiol modification showed similar morphology resembling the control, alginate foam (Figure S1c–e, Supporting Information) before thiol modification. The foam structure is composed of intersected micropores networks with dimensions of 5–13 µm (Figure 2e) embedded in the large few hundreds micrometers pore structures. These special architectural micropores are beneficial for water penetration to readily trap the water contaminants with different sizes.

Elemental mapping on the tetrathiol modified foam confirmed the distribution of elements within the foam microstructure through thiol–ene click chemistry (Figure 2g–k). A noticeable observation from the micrographs of Figure 2h,i revealed the uniform distribution of carbon and oxygen within the foam network, authenticating the existence of carbon and oxygen in the pristine framework of alginate and rGO. Meanwhile, the iron elemental distribution map (Figure 2j) shows that the iron element is randomly located within the foam matrix based on its concentric spots detected (white arrows). Sulfur element is found throughout the analyzed region (Figure 2k) with intense S regions identified (white arrows). Under the same analyzed region, the high concentric sulfur region does not coincide with the region rich with iron, indicating that S does not bound to or react with iron to form Fe_xS, which ruled out the possibility of the chemical reaction between tetrathiol with iron oxides during the photoinitiated reaction.

XPS results of different stage of prepared functionalized graphene-biopolymer foam are summarized in **Figure 3**a showing survey spectra of three prominent peaks (C1s, O1s, and Ca2p at around 285, 532, and 347 eV, respectively). From Table S1, Supporting Information, both the controls, alginate and GO, recorded high oxygen at% (35.85 and 28.89 at%, respectively) as expected, indicating that these two materials are enriched with oxygen functional groups which are beneficial for metal complexation in the water purification process. Peak fitting analysis of the C1s narrow scan (Figure 3b) showed that five peaks deconvoluted at 284.7, 286.2, 286.9, 288.1, and 288.9 eV can be assigned to C−C, C−OH, C−O−C, C= O, and O−C= O, respectively. A noticeable shift of binding energy could be observed on the C1s high resolution spectra of Alg-Fe_3O_4-rGO and Alg-Fe_3O_4-rGO-4S after the incorporation of GO sheets into the alginate matrix with additional C= C peak deconvoluted at 284.7 and 284.1 eV for Alg-Fe_3O_4-rGO and Alg-Fe_3O_4-rGO-4S, respectively. Assignment of C−S peak at around 285.4 eV on the C1s high resolution spectrum of Alg-Fe_3O_4-rGO-4S showed successful grafting of the tetrathiol molecule on the alginate-graphene network.[13] Deconvolution of the high resolution S2p peak of Alg-Fe_3O_4-rGO-4S foam into 163.0 and 164.2 eV ($S2p_{3/2}$ and $S2p_{1/2}$) can be assigned to C−S−C species while additional doublet

ADVANCED SCIENCE NEWS
www.advancedsciencenews.com

ADVANCED MATERIALS INTERFACES
www.advmatinterfaces.de

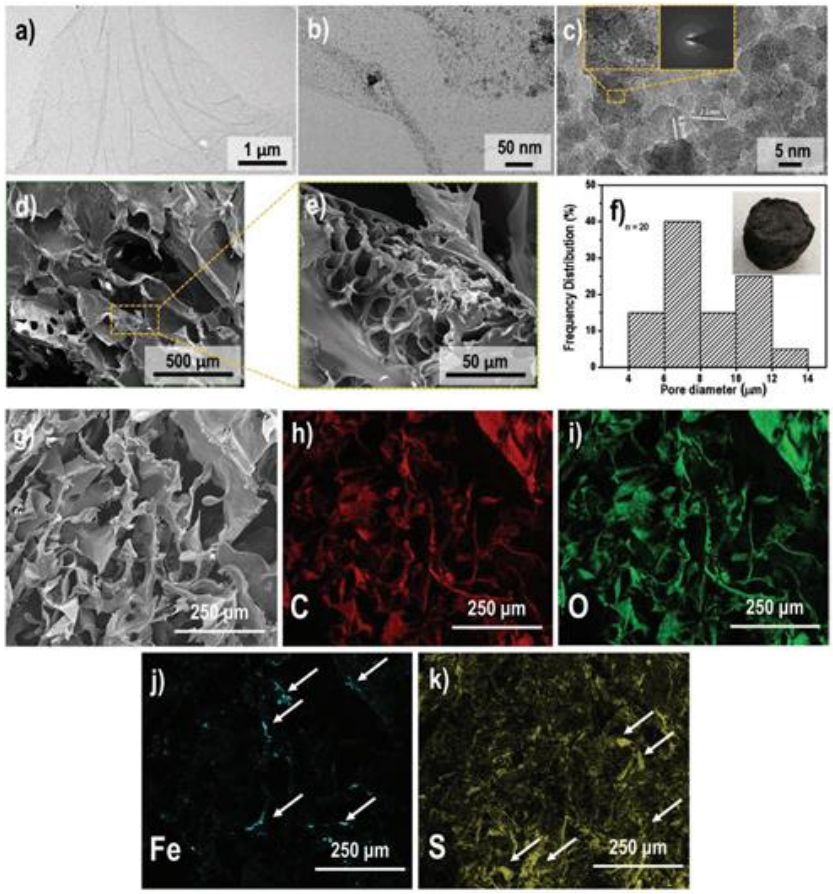

Figure 2. TEM image of a) GO, b) Fe_3O_4 nanoparticles on rGO sheet, and c) HRTEM micrographs of Fe_3O_4 nanoparticles on rGO sheet with the inset of lattice fringes and SAED pattern of Fe_3O_4 nanoparticles. d,e) SEM images of functionalized graphene-biopolymer (Alg-Fe_3O_4-rGO-4S) under different magnifications and f) pore size distribution plot of functionalized graphene-biopolymer foam with the inset showing the photograph of Alg-Fe_3O_4-rGO-4S foam. g) SEM image and h–k) selected EDS map of Alg-Fe_3O_4-rGO-4S foam consisting of C, O, Fe, and S elements. White arrows indicate the concentric area of the particular element found in the sample.

peak centered at 163.5 and 164.6 eV could be allotted to $S2p_{3/2}$ and $S2p_{1/2}$ of C−S peak.[14] No sign of S−O peak (>166 eV) was observed, suggesting that sulfonates or sulfates did not form despite the exposure of the material to readily oxidized conditions and the active thiol group did not react with the oxygen groups in the alginate-rGO matrix. This result strongly suggests that the photo-click modification approach is highly resistant to oxidation.[15]

The prominent appearance of the peak around 1733 cm^{-1} attributed to the strong −C= O stretch of ester group in the tetrathiol molecule and the disappearance of the peak at 2564 cm^{-1} corresponding to the reactive thiol group (−SH) on the infrared spectroscopic (IR) spectra of functionalized graphene-biopolymer foam (Figure 3d). These results clearly indicate that tetrathiol molecules were covalently attached to graphene surface via the photoinitiated reaction providing chemical functionalization of the Alg-Fe_3O_4-rGO matrix. It could be observed that the C= O vibration band at 1720 cm^{-1} of GO disappeared after grafting of Fe−O particles on the GO sheets, however, the C= O peak was observed again on the Alg-Fe_3O_4-rGO-4S foam after the functionalization reaction. While, the existence of alginate was evinced by the two strong and common bands at 1593 cm^{-1} and 1421 cm^{-1} due to the asymmetric and symmetric stretching vibrations, respectively of $-COO^-$ group on the IR spectra of all alginate composites.[16] The strong and broad peak between 3000 and 3500 cm^{-1} resulted from the stretching vibration of −OH group was found in all the IR spectra of the samples, revealing the abundance of −OH groups in the developed samples.

As shown in Figure 3e, the phase and the crystallinity of the samples prepared were confirmed by powder XRD technique. Typically, GO shows a strong and sharp peak at 10.76° (interlayer distance = 8.22 Å) which reveals its enhanced interlayer spacing after the incorporation of oxygen functional groups

ADVANCED SCIENCE NEWS
www.advancedsciencenews.com

ADVANCED MATERIALS INTERFACES
www.advmatinterfaces.de

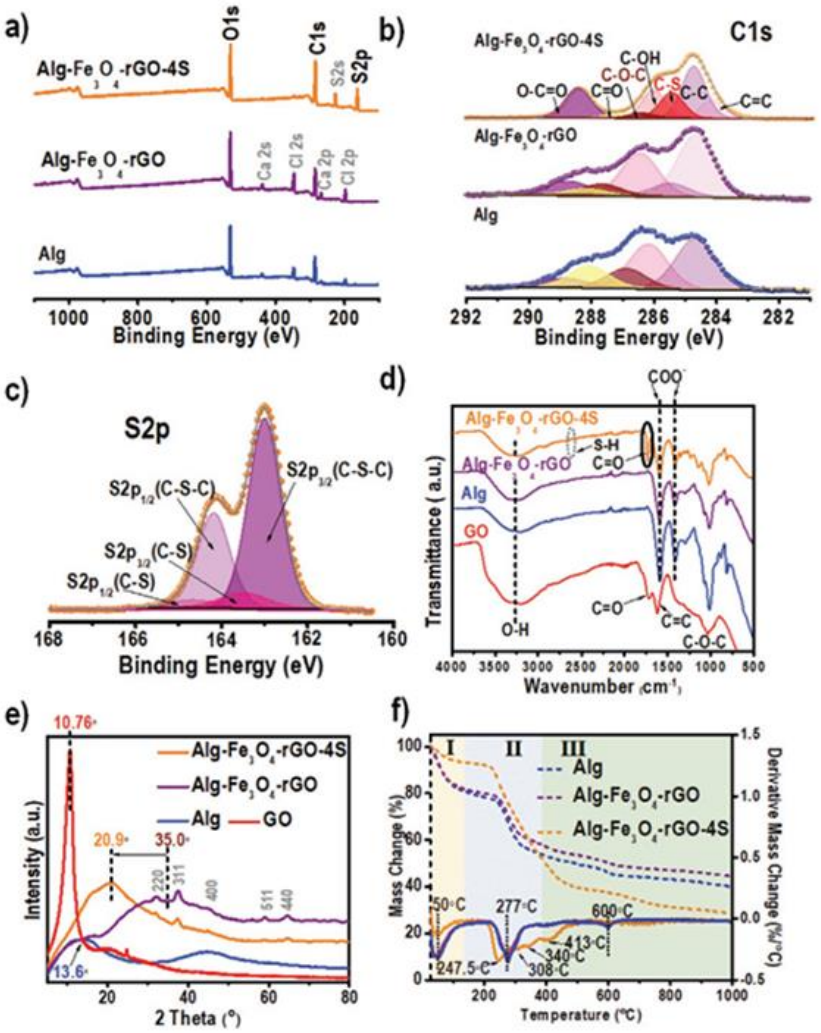

Figure 3. XPS a) survey, b) C1s high resolution, c) S2p high resolution spectra, d) FTIR spectra, e) XRD diffractograms, and f) TGA-DTG plots of samples prepared in this work.

resulting from the complete oxidation of graphite with its characteristic peak positioned at 26.62° (3.34 Å).[2a] The XRD plot of alginate is distinguished with a broad peak recorded at 13.6° (6.50 Å), signifying the amorphous state of alginate foam.[17] Additionally, broad diffraction peaks of Fe_3O_4 NPs with its indexed planes, (220), (311), (400), (511), and (440) as confirmed by bare Fe_3O_4 NPs in Figure S1b, Supporting Information, were observed on the XRD diffractograms of both the unmodified and modified Fe_3O_4-Alg-rGO foams. This result agrees well with the interlayer spacing of (311) plane determined from the HRTEM analysis in the previous section, which verified the incorporation of Fe_3O_4 NPs in the Alg-GO matrix. The obvious broadening peaks recorded for the encapsulated Fe_3O_4 particles could be due to the nano-sized of the iron particles as manifested in the HRTEM image (Figure 2c).[18] On the other hand, the shift of the apparent diffraction peak at ≈20.9° (4.25 Å) for the UV-modified sample from the broadened peak of Alg-Fe_3O_4-rGO centered around 35° (2.56 Å) could be due to the effective insertion of the tetrathiol moieties through photoinitiated thiol–ene click reaction.

The fabrication of Alg-Fe_3O_4-rGO-4S foam was also confirmed by TGA-DTG analysis with its distinctive thermal decomposition profile compared to the controls, alginate and Fe_3O_4-Alg-rGO foams, as illustrated in Figure 3f. The first derivative of the TGA curve, DTG, of the foams, (solid line, Figure 3f) clearly corroborated the grafting of the thiol molecule with prominent peaks observed at around 308, 340 and 413 °C which could be due to the degradation of tetrathiol

ADVANCED SCIENCE NEWS
www.advancedsciencenews.com

ADVANCED MATERIALS INTERFACES
www.advmatinterfaces.de

moieties covalently attached in the alginate–GO matrix in relative to the thermal degradation of the controls. The mass loss of the foams can be generally divided into three main steps with the first mass loss that occurred below 120 °C, attributed to the removal of physisorbed and interstitial moisture trapped within the foam.[19] This was followed by the thermal degradation from 120 to 400 °C due to the elimination of oxygen functional groups of the alginate–GO matrix. Finally, the foams showed an insignificant mass loss after 370 °C with a minor shoulder peak traced at 600 °C on their DTG curves which could be due to the pyrolysis of carbon network and their TGA curves remained almost unchanged after 650 °C.[20] Consistent with the collective outcomes from TGA-DTG, XRD, FTIR, XPS, EDX and its mapping analyses, we can infer that the tetrathiol precursor has been successfully clicked onto the rGO-alginate network via the photoinitiated thiol–ene click reaction. Further discussion on the mechanical and pore properties of the functionalized graphene-biopolymer foam are discussed in Supporting Information S1.

2.2. Adsorption Performance of Heavy Metal Ions

The adsorption performance of the tetrathiol-functionalized graphene-biopolymer foam (Alg-Fe_3O_4-rGO-4S) on selected heavy metals was first evaluated under the influence of initial solution pH (pH 4–9) and presented in **Figure 4**a. As evident from Figure 4a, almost similar metal ion adsorption trend could be observed with optimum metal ion removal efficiency recorded around pH 5 for Hg (II) and Cu (II). This was followed by a drop in the performance at pH around 9 for the two metal ions studied. To better understand the metal sorption mechanism at different pH the zeta potential and surface charge of the adsorbent at different pH correlated with the created metal species distribution diagrams are presented in Figure S4, Supporting Information. The sorption process between an adsorbent and the metal ions at different pH is a complex process by taking into account that metal ions do not solely exist as a cation but feasibly complex with other ligands exist in the aqueous system. More details on the existence of different ionic species for Hg and Cu and their impact on adsorption process at different pH is provided in Figure S4, Supporting Information. Overall, the good performance of functionalized graphene-biopolymer foam to maintain its optimum performance over a broad range of pH is highly advantageous to be used in different contaminated water systems.

Figure 4b demonstrates the heavy metal ions adsorption efficiency of Alg-Fe_3O_4-rGO-4S foam under the influence of contact time at a steady uptake trend with their corresponding plateaus reaching at around 200 min for Hg (II) and Cu (II) ions. Further fitting of the kinetics data into the non-linearized kinetic models (pseudo-first and pseudo-second) was performed to understand their adsorption mechanism toward Hg (II) and Cu (II) ions. The kinetics fitting outcomes (Table S4, Supporting Information) visibly showed higher correlation coefficients ($R^2 > 0.998$) for pseudo-second-order kinetic model for both investigated ions, implying that the adsorption kinetics of

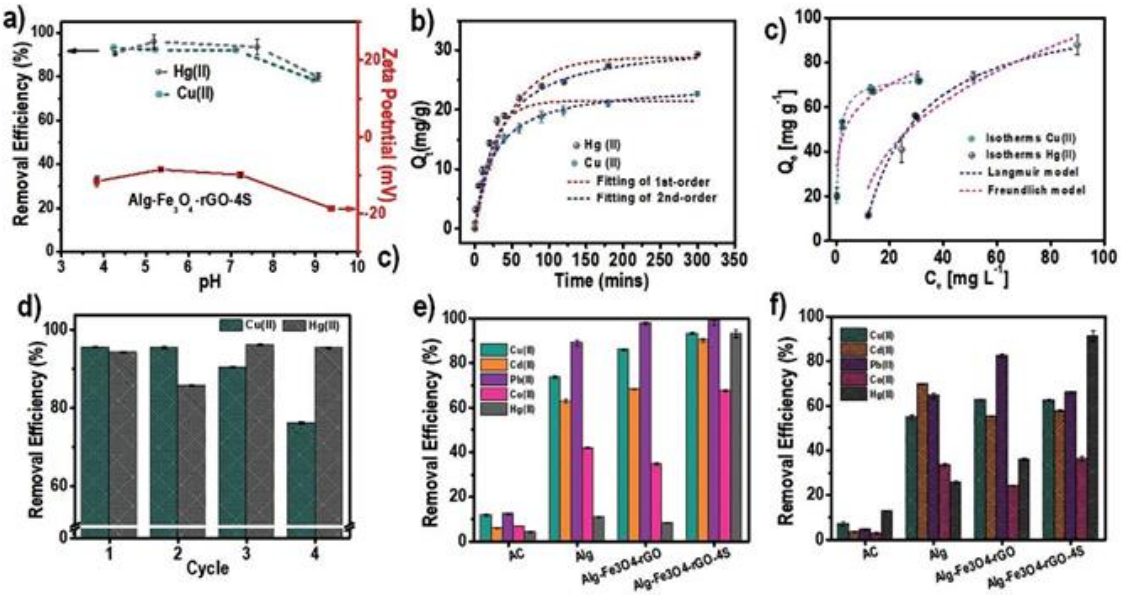

Figure 4. a) Influence of solution pH of Hg (II) and Cu (II) ions on multifunctional graphene biopolymer (Alg-Fe_3O_4-rGO-4S) foam (conditions: C_0 ≈5 ppm, temperature = 21.0 °C, mass of sorbent ≈20mg, volume of metal ion solution = 20 mL, equilibration time: 5 h). b) Influence of contact time with fitted kinetic models (conditions: C_0 ≈10 ppm, pH ≈5, temperature = 21.0 °C, mass of sorbent ≈20mg, volume of metal ion solution = 70 mL). c) Adsorption isotherms with fitted isotherm models for Hg (II) and Cu (II) ions (conditions: C_0 = 20–110 ppm, pH ≈5, temperature = 21.0 °C, mass of sorbent ≈20mg, volume of metal ion solution = 20 mL, equilibration time: 24 h). Influence of d) adsorption-desorption cycle of multifunctional graphene biopolymer foam toward Hg (II) and Cu (II) ions, competing ions in e) milli-Q and f) river water.

Alg-Fe_3O_4-rGO-4S foam can be well-described using the pseudo-second-order model. This signifies that chemisorption is the rate controlling step for the uptake of the studied metal ions (Cu, Hg) on Alg-Fe_3O_4-rGO-4S foam. In fact, pseudo-second-order model has been widely adopted to relate the adsorption of water pollutants, particularly heavy metal ions, on the adsorbent by assuming that the interaction between the adsorbent and adsorbate is by electron sharing and exchange. This phenomenon can be associated to the interaction between the electron-rich donor, Alg-Fe_3O_4-rGO-4S adsorbent, with the electron-deficient acceptors, Hg (II) and Cu (II) ions.[2a,21]

Influence of initial concentration of metal ions was explored to probe the adsorption capacity of tetrathiol-functionalized graphene biopolymer foam toward Hg (II) and Cu (II) ions. The equilibrium isotherm profiles of the metal ions studied were simulated using non-linear Langmuir and Freundlich isotherm models to establish the equilibrium relationship between the adsorbent and the adsorbates. According to the fitting analysis of non-linear isotherm models (Table S5, Supporting information), the high correlation coefficient ($R^2 > 0.9$) achieved for both the investigated metal ions clearly disclosed that its adsorption behavior can be well-correlated with the Langmuir isotherm model. This suggests that the adsorption of the Hg (II) and Cu (II), adsorbates, took place by homogeneous and uniform monolayer coverage over the binding sites within the functionalized graphene-biopolymer foam (adsorbent).[2a] Furthermore, the maximum sorption capacity, q_{max}, was determined as 107.0 and 73.5 mg/g for Hg (II) and Cu (II), respectively, implying high affinity of these ions toward the binding sites of functionalized graphene-biopolymer foam.

Comparison of adsorption capacity with experimental conditions of various adsorbents for Cu (II) and Hg (II) ions reported in literature is presented in Table S6, Supporting information.[18a,22–26] In comparison, the tetrathiol modified graphene biopolymer foam presented in this work showed very good performance for heavy metal ions removal in terms of its adsorption capacity and uptake efficiency at different pH range considering the adsorbent dosage required. More details about previous studies are provided in Supporting Information.

One of the main criteria to assess the cost efficiency and sustainability of an adsorbent is its long-term adsorption-desorption cycle performance in pollutants removal. With the use of 2% w/v thiourea in 0.1 M HCl as eluent, good removal efficiency up to fourth cycle of recurring adsorption–desorption process (Figure 4d) was attained when the fabricated adsorbent was oscillated in a dual-mixed metal ion (Hg and Cu) system. Notably, the residual concentration (0.38 mg L^{-1}) of Cu (II) detected in the water after the fourth continuous adsorption-desorption cycle was below the maximum contaminant level (MCL) of drinking water for copper (1.3 mg L^{-1}) as regulated by United States Environmental Protection Agency (US EPA).[27] This again affirms the high stability and reusability of the functionalized graphene biopolymer foam despite the use of binary metal ions and corrosive eluent, portraying it as a promising futuristic adsorbent for water decontamination.

Since presence of inorganic ions in water can compete for binding sites of the adsorbent, the influence of co-existing ions was explored in milli-Q water as well as natural water (river water) to evaluate the potential practical applications of multifunctional graphene biopolymer foam. Apart from the control adsorbents (Alg and Alg-Fe_3O_4-rGO foams), a commercial adsorbent, AC, was also characterized to benchmark the metal ions removal efficiency using multiple metal ions (Cu, Cd, Pb, Co, and Hg)-spiked water samples. In the milli-Q water system, the outstanding performance of multifunctional graphene biopolymer foam was unreservedly manifested by its highest removal efficiency (>90% for Cu^{2+}, Cd^{2+}, Pb^{2+}, and Hg^{2+} ions; ≈65% for Co^{2+} ion), superseded the performance of the controls and AC. Particularly, in the presence of multiple ions that co-existed in the water, the measured concentration (0.33 mg L^{-1}) of Cu (II) was lower than the MCL of drinking water for copper (1.3 mg L^{-1}) regulated by US EPA.[27] Despite the strong competition among the co-existing spiked metal ions, large flux of inorganics and organic matters present in the river water, the functionalized graphene biopolymer foam outperformed the control and commercial adsorbents for majority of the studied metal ions, particularly for Hg (II) ions in the river water assessment. This strongly suggests that it has exceptionally strong binding affinity toward Hg (II), followed by Pb (II), Cd (II), Cu (II), and Co (II) ions regardless in pure water or complicated water system (river water), reflecting excellent binding affinity and high tolerance ability of the tailored foam for potential real water purification application.

2.3. Adsorption Performance of Organic Dyes

In order to evaluate the multiple pollutant removal ability of the prepared Alg-Fe_3O_4-rGO-4S foam, the adsorption study was extended to include organic dyes, where MB was selected as the model organic dye, which is a common water pollutant in textile industry. Under the influence of initial concentration of MB (**Figure 5**a), the foam shows exceptional good removal efficiency (>85% removal efficiency) over 1–500 ppm MB as evidenced by the significant decolorization of MB (Figure 5b). The strong affinity of MB is caused by multiple factors including the high porosity of the foam structure, the strong electrostatic interaction between the positively-charged MB molecule and the negatively charged oxygen groups in alginate matrix and iron oxide NPs.[28] The fitting of the isotherm data into non-linear Langmuir and Freundlich isotherm models (Table S5, Supporting Information) showed that the adsorption behavior of Alg-Fe_3O_4-rGO-4S foam conforms well with Langmuir isotherm, achieving 789.70 ± 36 mg/g maximum sorption capacity with high correlation coefficient, ($R^2 = 0.9982$) compared to Freundlich isotherm ($R^2 = 0.9895$).

Comparative studies of several alginate-based adsorbents reported in literature are summarized in Table S7, Supporting Information. Previous reports using different type of graphene alginate adsorbents such as GO/alginate gel, GO/calcium alginate, and tannic acid-poly(vinyl alcohol)/sodium alginate exhibited significantly lower maximum sorption capacities of 357.14, 181.81, and 147.06 mg/g, compared to functionalized graphene biopolymer foam (789.70 mg/g).[29] Based on this outstanding maximum sorption capacity accomplished, functionalized graphene biopolymer foam can be successfully used for removal of toxic dyes from contaminated waters.

ADVANCED SCIENCE NEWS
www.advancedsciencenews.com

ADVANCED MATERIALS INTERFACES
www.advmatinterfaces.de

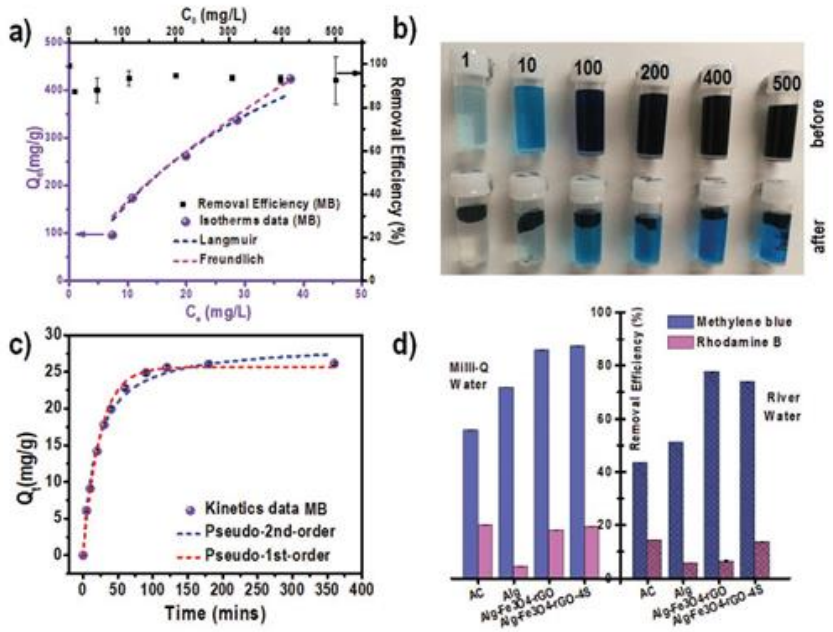

Figure 5. a) Influence of initial concentration and isotherm study of MB on Alg-Fe_3O_4-rGO-4S foam (conditions: C_0 = 1–500 ppm, pH ≈5.3, temperature = 21.0 °C, mass of adsorbent ≈20 mg, volume of metal ion solution = 20 mL), b) photographs of MB solutions before and after adsorption on functionalized graphene biopolymer foam at different initial concentration (1–500 ppm) of MB, c) Influence of contact time and kinetics study of MB on functionalized graphene biopolymer foam (conditions: C_0 ≈10 ppm, pH 5.5, temperature = 21.0 °C, mass of adsorbent ≈20 mg, volume of metal ion solution = 70 mL). d) Comparison of removal efficiency of MB and rhodamine B using AC, Alg, Alg-Fe_3O_4-rGO, and functionalized graphene biopolymer foam in milli-Q and river water (conditions: C_0 ≈10 ppm, pH = 5.5 (MB); pH 4.6 (rhodamine B); pH 8.1 (binary system in river water), temperature = 21.0 °C, mass of adsorbent ≈20 mg, volume of metal ion solution = 20 mL).

In terms of the kinetics toward MB adsorption, a gradual uptake trend of MB could be observed until a plateau was reached at around 120 min, signifying that the sorption equilibrium was achieved. Similar to the uptake of heavy metal ions, further fitting analysis performed on the kinetics data (Table S4, Supporting Information) confirmed that it follows pseudo-second-order with $R^2 > 0.99$ accomplished. In order to reflect the practicability of the modified sorbent for MB removal, selectivity adsorption experiments were first conducted independently over two single systems (MB and rhodamine B) in milli-Q water, followed by a binary system (mixed MB and rhodamine B) in river water using the controls (Alg and Alg-Fe_3O_4-rGO foams), AC and functionalized graphene biopolymer foam. As depicted in Figure 5d, preferential binding affinity was shown toward MB (≈90%) in relative to rhodamine B (≈20%). Over the tested adsorbents, functionalized graphene biopolymer foam (≈90%) performed slightly better than Alg-Fe_3O_4-rGO foam (≈86%), showing better MB removal performance than the commercial adsorbent (≈56%) and alginate foam (≈72%). Remarkably, the uptake performance of the modeled organic dye was not significantly affected when the functionalized foam was tested in the binary system in the river water compared to the experiment conducted in milli-Q water despite the fact that river water is a complex entity containing high flux of ions and organic species which tend to compete for binding sites of the adsorbent. These results again confirm that the functionalized graphene biopolymer foam can be excellent adsorbent to be applied for MB removal in real water system.

2.4. Absorption Performance of Organic Solvents and Oils

Furthermore, the potential application of the Alg-Fe_3O_4-rGO-4S foam is finally investigated for removal of organic solvents and oil pollutants in waters. Prior to the assessment of organics removal, water contact angle measurement was performed to determine the wettability of the materials at the solid–water interface. It is noteworthy to state that the surface of both the controls (Alg and Alg-Fe_3O_4-rGO foams) is superhydrophilic (<90° for hydrophilic, >90° for hydrophobic, and ≥145° for superhydrophobic) with water contact angle ≈0° as the water droplet completely spread out and instantaneously absorbed from their solid surface (Movies S1 and S2, Supporting Information). While, the water droplet still remains spherical and static on the surface of the functionalized graphene biopolymer as evidenced in Movie S3, Supporting Information.[30] **Figure 6**a,b shows the water contact angle measurements performed on randomly selected spots on the top and cross-sectional surface of the prepared graphene biopolymer foam. These results showed that the foam have both the hydrophilic and hydrophobic properties with contact angles spanning between 50° and 130° at different spots confirming similar interfacial

ADVANCED SCIENCE NEWS
www.advancedsciencenews.com

ADVANCED MATERIALS INTERFACES
www.advmatinterfaces.de

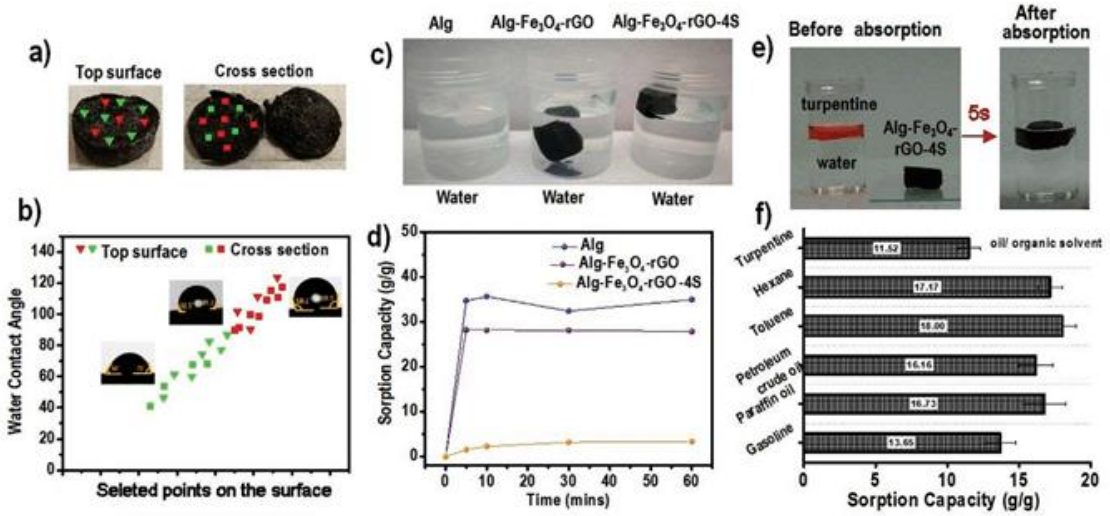

Figure 6. a) Photographs of Alg-Fe_3O_4-rGO-4S graphene biopolymer foam (diameter: 2.5 cm, thickness: 1.0 cm) before and after cutting using a blade exposing its surface and cross section before water contact angle (WCA) measurement. b) Water contact angle measurement performed on several spots of the top surface and cross section of functionalized graphene biopolymer foam with photographs of selected water contact angle droplets. c) Photograph of water absorption experiment using Alg, Alg-Fe_3O_4-rGO and Alg-Fe_3O_4-rGO-4S foams. d) Plot of water absorption capacity over residence time. e) Photograph of an example of experiment showing before and after absorption using functionalized graphene biopolymer foam in dyed turpentine-water system. f) Plot of sorption capacity of functionalized graphene biopolymer foam using different type of oils and organic solvents.

properties of a darkling beetle as evidenced by the measured contact angles (47.5°–109.1°) on the elytral surface of various adult beetles in the literature.[31] These findings implied that the wettability of the modified material has been extended to the hydrophobicity spectrum compared to its highly superhydrophilic controls throughout the surface and the bulk structure of the functionalized graphene biopolymer foam.

To confirm this postulation, a couple of experiments including water absorption test over a period of time was conducted using the controls and the functionalized graphene-biopolymer foam (Figure 6c,d). The results clearly showed that the uptake of water of both the controls (completely sink in the water in less than 5 min) was almost 6–7 times higher than the functionalized graphene biopolymer foam (partially submerged in the water). Meanwhile, contact angle on the surface of the functionalized graphene-biopolymer foam was also measured using petroleum crude oil. The tested oil was absorbed entirely and instantly into the foam (Movie S4, Supporting Information), indicating the oleophilicity feature of the tetrathiol modified graphene-biopolymer foam. This promising result was also well-supported by the rapid absorption of dyed turpentine (within 5 s) as presented in Figure 6e and Movie S5, Supporting Information. As depicted in Figure 6f, excellent absorption capacity was also achieved using several examined organic solvents (hexane-17.17 g/g, toluene-18.00 g/g) and oils (petroleum crude oil-16.16 g/g, paraffin oil-16.73 g/g, gasoline-13.65 g/g and turpentine-11.52 g/g) with the oils and organic solvents characteristic detailed in Table S8, Supporting Information. Despite the combined hydrophilic and hydrophobic wettability exhibited by the functionalized graphene biopolymer foam, its sorption performance toward organic pollutant was found to overperform many composite materials reported in literature which are deemed as strongly hydrophobic (Table S9, Supporting Information). This outstanding result could be attributed to the unique porous architecture that can concentrate oil pollutants within the pores to facilitate the transport, storage, and separation of oil from water. The interconnected porous network with micrometer size as evident by its SEM images and pore size distribution plot of the functionalized foam can provide a larger room for organics including oil storage which enhanced the organics absorption to take place.

2.5. Simultaneous Ad/Ab-Sorption Performance of Multiple Water Pollutants

The most important and final experiment with simultaneous water pollutants removal using Alg-Fe_3O_4-rGO-4S graphene biopolymer foam was explored using mixture of all water pollutants from different classes including heavy metal ions (Cu^{2+} and Hg^{2+}), organic dye (MB), solvents (hexane and toluene), and oils (turpentine, paraffin and petroleum crude oil) in three different water systems (milli-Q, river, and sea water). Results are summarized in **Figure 7**a–c in order to confirm the multifaceted application of functionalized graphene biopolymer foam for practical water purification purpose. Notably, instantaneous removal of mixed organic phase water pollutants which initially appeared on the top layer of aqueous phase was observed for the first 30 s after loading the functionalized graphene biopolymer foam into the water pollutants mixture (Movie S6, Supporting Information). The rapid absorption of the organic pollutants with complete disappearance of the dyed

ADVANCED SCIENCE NEWS
www.advancedsciencenews.com

ADVANCED MATERIALS INTERFACES
www.advmatinterfaces.de

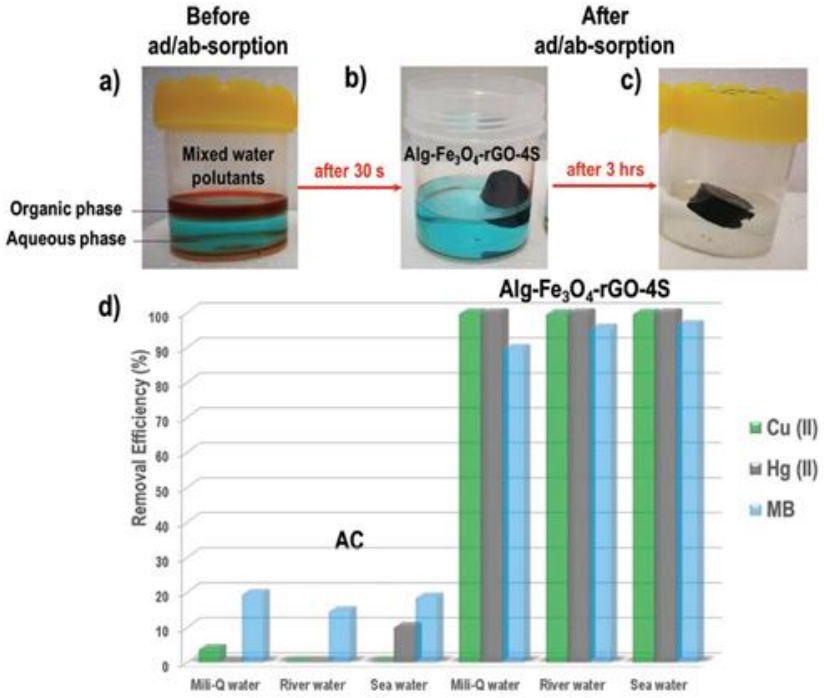

Figure 7. Characterization of performance of Alg-Fe_3O_4-rGO-4S foam for simultaneous removal of multiple contaminants. a) Photo of water pollutants mixture containing aqueous phase (Cu^{2+}, Hg^{2+} and MB) and organic phase (dyed turpentine, paraffin oil, petroleum crude oil, hexane and toluene) before ad/ab-sorption, b) photo of ad/ab-sorption after 30 s, showing complete removal of organic pollutants after ad/ab-sorption, c) photo showing adsorption after 3 h showing decolorization of aqueous phase from blue to colorless confirming removal MB and Cu^{2+}, and d) comparative performance of Alg-Fe_3O_4-rGO-4S foam and activated carbon (AC) for simultaneous removal of water pollutants including Cu(II), Hg (II), MB, oils, and organic solvents in milli-Q water (pH = 5.10 at 23.4 °C), river water (pH = 8.00 at 21.9 °C), and sea water (pH 7.38 at 22.1 °C).

organic pollutants by the functionalized graphene biopolymer foam significantly outperformed AC with no apparent removal spotted even after three hours (Movie S7 and Figure S5, Supporting Information). The outstanding organics uptake results of functionalized graphene-biopolymer foam can be attributed to its highly porous structure, the π–π interaction, and hydrophobic effect of the sp^2 carbon in the graphene framework. Meanwhile, functionalized graphene-biopolymer foam also demonstrated remarkable removal efficiency for aqueous pollutants including MB (≈90%), Cu^{2+} (>99.99%), and Hg^{2+} (100%) in the three investigated water systems (milli-Q, river, and sea water). Remarkably, undetectable Hg^{2+} (<3.3 µg L^{-1} recorded, detection limit of inorganic mercury by ICP-MS), which is below the maximum acceptable limit of drinking water recommended by WHO, 6 µg L^{-1}, was found in the remaining solution for all the investigated water systems of functionalized graphene biopolymer foam after three hours of simultaneous ad/ab-sorption.[32] Meanwhile, only 1.4 µg L^{-1} Cu^{2+} was detected in the sea water sample using functionalized graphene-biopolymer foam, which was far beyond the MCL of drinking water for copper (1.3 mg L^{-1}) as enforced by US EPA.[27] Excellent MB uptake was also recorded by functionalized graphene biopolymer foam with only 0.05 mg L^{-1} MB remaining in the sea water sample after the simultaneous water pollutants removal experiment. It should also be highlighted that the volume of aqueous solution remained was almost 20 mL with no significant withdrawal of water uptake by the functionalized graphene biopolymer foam. The outstanding performance for simultaneous uptake of multiple classes of water pollutants including heavy metal ions, organic dyes, solvents, and oils achieved by the functionalized graphene biopolymer foam evidently confirmed its feasibility and efficiency for multi-pollutant control in targeting the co-existing of pollutants in water which could be hardly achieved by any reported ad/ab-sorbent.

2.6. Unraveling the Relationship between the Structural-Physicochemical Properties and Ad/Ab-Sorption Efficiency of Functionalized Graphene Biopolymer Foam

It is well accepted that the ad/ab-sorption efficiency toward pollutants is highly directed by the combination of structural and physicochemical properties of an ad/ab-sorbent. The observed outstanding performance of the functionalized graphene biopolymer foams toward broad range of different classes of co-existing pollutants could be explained as a result of their unique structure, combined hydrophobic-hydrophilic properties, and thiol–ene chemical functionalization. First, as it

was proposed, their wettability was successfully tailored from its superhydrophilic controls (Alg and Alg-Fe_3O_4-rGO) to an asymmetric hydrophilic-hydrophobic structure after a photoinitiated reaction using a tetrathiol modifier. Hydrogen bonds formed between the water molecules and the −OH groups (alginate and rGO sheets) as well as the same remaining −COOH group at the edges of rGO sheets are the key contributors to the hydrophilicity of the foams as supported in the contact angle measurement and water absorption studies. Based on the measured contact angle and the ad/ab-sorption experiments using different solvents, we surmise that the grafting of the tetrathiol precursor to the Alg-rGO matrix with the introduced −S group has rendered hydrophobic domains to the modified foam. The unique wetting feature, combined hydrophobicity, and hydrophilicity, created on both surface and bulk structure of the modified foam endows a good passage and flow of water for efficient penetration of both inorganic and organic pollutants, allowing sufficient exposure of water pollutants within the porous network of the modified adsorbent.

Second, the formation of a porous network with interconnected pores in general aids in entrapping organic pollutants, resulting in enhanced ad/ab-sorption removal efficiency.[33] The opened and interconnected pores found in the tetrathiol modified foam network clearly divulged that the highly porous and interconnected structure with the creation of pores allows a greater capacity for oil storage in the porous material. Moreover, our preliminary metal ions and organic dyes adsorption studies applying both the beads and foam forms (detailed discussion in Supporting Information S3) also verified that the highly porous structure induced within the thin layers in the modified foam matrix demonstrated up to four times better removal efficiency than the beads form due to the presence of increased active ad/ab-sorption sites for the enhanced pollutants uptake.

Third, the presence of high-density functional groups grafted on the sp^3 carbon of rGO (S-bearing groups) and the alginate (hydroxyl and carboxylate groups) framework are active for pollutants adsorption. We surmised that electrostatic interaction (coulombic attraction) is the dominant adsorption mechanism for the cationic pollutants owing to the strong attraction between the negatively charged surface resulting from the ionization of densely-packed oxygen functional groups such as hydroxyls and carboxylate groups with the cationic pollutants (mercury, copper, and MB as presented). The poor sorption efficiency of rhodamine B could be ascribed to the repulsion of the deprotonated oxygen groups in the rhodamine B molecule owing to the existence of its zwitterionic form (N^+ and COO^-) at pH >3. At pH >3, the positive charge density of the molecule decreased as a result of the aggregation of RhB molecule due to interaction between the zwitterions in RhB moelcue. This reduced the interaction of the RhB moclecule with the negatively charged surface on the modified foam, thereby resulting in low uptake of rhodamine B from the water.[34] The removal outcomes clearly manifested that the engineered functionalized graphene biopolymer foam works chiefly based on the electrostatic attraction to remove the pollutants from the aqueous systems.

Furthermore, the high removal efficiency achieved by functionalized graphene biopolymer foam could be explained based on hard soft acid base concept which expounded on the contribution of covalent and electrostatic interactions stemming from the existence of soft acids and soft bases in this work. The high atomic % of −S groups detected on the functionalized graphene biopolymer foam can be accounted for the high uptake of the cationic pollutants. Conceptually, soft bases including the electron-rich aromatics, C=C, CO, and C−S−C groups found in the modified graphene-biopolymer can readily donate their electrons to the electron-deficient soft acid such as Hg (II) to result in a stable metal-chelate complex via covalent bonds. This could be reflected by the high sorption capacity, 107 mg/g for Hg (II). Meanwhile, the lower sorption capacity, 73.5 mg/g, achieved for Cu (II) may be due to the borderline nature of Cu (II) to complex with the soft ligands found on the surface of the modified sorbent, leading to less favorable affinity toward the binding sites of the sorbent compared to Hg (II).[35] The decoration of iron oxide NPs on the rGO sheets also aids in enhancing the removal efficiency of the heavy metal pollutants as supported in the reported work that the adsorption of Cu (II) primarily occurred through the complexation with the surface oxygen groups from iron oxide particles, leading to an enhanced removal efficiency of the heavy metals.[11,18a]

Additionally, the absorption affinity of Alg-Fe_3O_4-rGO-4S foam toward the organic pollutants including rhodamine B, MB, hexane, toluene, and hydrocarbons found in the oils could be due to the presence of π–π interaction and hydrophobic effect with the planar sp^2 hybridized rGO surface present in the absorbent framework. This increased the propensity of the same kind attraction (π–π interaction) and hydrophobic effect, making this modified absorbent highly desirable for decontamination of organic pollutants after the recovery of the sp^2 hybridized graphene structure.[7,28b]

3. Conclusion

In summary, a highly porous functionalized graphene/alginate biopolymer foam (Alg-Fe_3O_4-rGO-4S) with unique combination of mixed hydrophilic-hydrophobic feature, functionalized with polythiol surface chemistry and iron oxide NPs is successfully fabricated and demonstrated for simultaneous and efficient removal of several co-existing pollutants including heavy metal ions, cationic dyes, organic solvents, and oils in water. Detailed structural and compositional characterization of prepared foam confirmed the microporous structure of rGO and alginate network, high porosity and pore volume, good mechanical strength with mixed hydrophilic-hydrophobic feature, negative surface charge at pH 4–9, and specific surface chemistry with high density of sulfur and oxygen as well as presence of iron oxide NPs. Single adsorption experiments confirmed very high maximum sorption capacity for heavy metals $Hg^{2+}$and Cu^{2+} (107.0 ± 2.1 and 73.5 ± 0.7 mg/g, respectively), MB (789.7 ± 36 mg/g) with high regeneration ability up to 90% and 75% removal efficiency for Hg (II) and Cu (II) even after fourth consecutive adsorption-desorption cycles in their mixed metal ion solution. Very rapid and good maximum absorption efficiency of oil and organic solvent (13–18 g/g) is achieved for the oils and organic solvents. Finally outstanding results are achieved in targeting simultaneous removal of multiple co-existing water pollutants in real and sea water conditions to undetectable concentration for Hg

ADVANCED SCIENCE NEWS
www.advancedsciencenews.com

ADVANCED MATERIALS INTERFACES
www.advmatinterfaces.de

(II), 1.4 µg L^{-1} for Cu (II), 0.5 mg L^{-1} for MB and rapid (≈30 s) uptake of organic solvents and oils.

These results showed that the performance of prepared Alg-Fe_3O_4-rGO-4S foam surpassed the reported adsorbents in the literature and more significantly commercial adsorbent (AC) in the spiked river water assessment despite the co-existing ions and organic matters in the mixed metal ions-spiked river water. Unlike the majority research on environmental adsorbent that focused on single pollutant removal, this presented multifunctional graphene/alginate foam addressed the challenging issues as a promising new generation adsorbent in targeting simultaneous removal of multiple co-existing water pollutants and provides valuable contribution to this field.

4. Experimental Section

Fabrication of Functionalized Graphene Biopolymer Foam (Alg-Fe_3O_4-rGO-4S): GO was prepared according to the improved Hummer's method as reported in the authors' previous work.[36] Fe_3O_4-rGO composite was synthesized based on the adapted methodology in the literature.[19] Briefly, $FeCl_3{\cdot}6H_2O$ (0.8109 g) and $FeSO_4{\cdot}7H_2O$ (0.8340 g) were dissolved in ultrapure water (60 mL, 50 °C) under continuous magnetic stirring and nitrogen gas purge for 10 min. The well-dispersed GO in milli-Q water (2 mg mL^{-1}, 120 mL) was added into Fe^{2+}/Fe^{3+} solution with continuous stirring under nitrogen gas purge for 15 min. Ammonium hydroxide (15 mL) was added dropwise into the mixture and stirring was continued under nitrogen blanket (50 °C, 1.5 h) with heating extended to 70 °C for 1 h. Subsequently, the obtained Fe_3O_4-rGO solution was cooled to room temperature and washed with milli-Q water using centrifuge. Separately, sodium alginate (1.9367 g) was dissolved in water under continuous stirring (60 mL, 45 °C) until a homogeneous gel formed. Ultrasonically dispersed Fe_3O_4-rGO solution (2 mg mL^{-1}, 60 mL) was added into the alginate gel with stirring until a well-mixed hydrogel was formed and transferred into the well plates. The hydrogel was freeze dried (–20 °C, 72 h) to retain its porous structure. For crosslinking process, the freeze-dried gel was immersed in calcium chloride solution (1 M, 2 h), washed with milli-Q water a couple of times and freeze dried (–20 °C, 72 h) to form Fe_3O_4-Alg-rGO foam. For the photoinitiated functionalization of Fe_3O_4-Alg-rGO, DMPA (17.5 mg), tetrathiol (1.5 mL), and ethanol (120 mL) were first mixed and sonicated (30 min). The freeze-dried Alg-Fe_3O_4-rGO foam was then added into the mixture and brought under UV irradiation at about 5 cm distance from the UV light source (Luyor-3405, 365 nm, 30 min). The as-formed product was washed with ethanol and copious amount of milli-Q water until the filtrate turned clear before loading it into the freeze dryer (–20 °C, 72 h) to obtain Alg-Fe_3O_4-rGO-4S foam (detailed information on materials and materials characterization are described in Supporting Information S4 and S5).

Metal Ions Uptake Studies: Removal of water pollutants using solid adsorbent with known mass was carried out via batch study in triplicate by oscillating the adsorbent in their respective solution on an orbital mixer (Ratek, Model OM7) at 200 rpm with a blank (without adsorbent) running in parallel. The pH of the solutions was measured using a pH meter FiveGO FG2, (Mettler Toledo) and adjusted using diluted HCl or NaOH in a series of pollutant concentrations at ambient temperature. The condition for adsorption experiments to investigate the influence of solution pH, contact time and initial concentration of heavy metal ions was detailed in the caption of Figure 4. For selectivity experiment, liquid samples were withdrawn at particular time intervals and diluted with acidified with 2% HCl (for Hg^{2+} ion) or 2% HNO_3 (for the rest of the metal ions) prior to ICP-MS analysis to determine the residual metal ions concentration from their respective standard calibration curves. The selectivity experiment was performed by adding ≈20 mg adsorbent into a 20 mL mixed metal ion solution containing Cu (II), Cd (II), Pb (II), Hg (II), and Co (II) at around pH 5 for 5 h using commercial AC as benchmark, alginate (Alg) and Fe_3O_4-Alg-rGO foams as controls. For real sample assessment, ≈20 mg of each adsorbent was loaded into ≈5 ppm mixed metal ions-spiked river (Torrens River, Adelaide, South Australia, 34°55′02.7″S 138°36′ 14.6″E) water without pre-treatment and pH adjustment to simulate real natural water sample. The regeneration experiments (adsorption cycle) were conducted using 20 mL mixed metal ions (2 ppm of each mercury and copper) solution for each metal ion, stirring at 200 rpm at pH ≈5.5 for 6 h. For the desorption cycle, the spent adsorbent was desorbed using 30 mL eluent (2% w/v thiourea in 0.1 M HCl), stirring at 250 rpm for 1 h. The desorbed adsorbent was washed to pH above 5 with large amount of milli-Q water and was left to dry for 1 day at ambient conditions before the following adsorption cycle. The adsorption-desorption cycles were repeated for four times and the remaining metal ion concentration in each cycle was determined by ICP-MS.

Organic Dyes Uptake Studies: The selectivity performance of the functionalized graphene-biopolymer foam toward organic dyes removal was carried out by oscillating ≈20 mg adsorbent in individual ≈10 ppm MB and rhodamine B (without pH adjustment) at 200 rpm for 3 h on the orbital shaker. The real sample evaluation of the adsorbents was performed by loading ≈20 mg of each adsorbent into ≈10 ppm mixed organic dyes-spiked river (Torrens River, Adelaide, South Australia, 34°55′02.7″S 138°36′ 14.6″E) without filtration and pH adjustment to simulate real natural water condition. The concentration of the remaining dyes after adsorption experiment was analyzed by measuring their corresponding maximum absorbance (MB at 664 nm and rhodamine B at 555 nm) determined from their standard calibration curves respectively using UV–vis spectrometer (Shimadzu, UV-1601).

Performance Analysis of Pollutants: The amount of pollutants adsorbed per unit of adsorbent mass at a given time, t (q_t, mg/g) was quantified using the following equation:[2a]

$$q_t = \frac{(C_0 - C_t)V}{m} \tag{1}$$

where C_0 and C_t are initial and pollutant concentrations at time t (mg L^{-1}), while V is the volume of solution (L) and m is the mass of adsorbent (g). The removal efficiency (R_t, %) at a given time, t, was calculated based on the following equation:[2a]

$$R_t = \frac{(C_0 - C_t)}{C_0} \times 100 \tag{2}$$

Kinetic Models: The uptake rate of the pollutants by the adsorbent was studied by fitting the kinetics data into Lagergren pseudo-first-order[37] and the Ho's pseudo-second-order[38] models in their non-linear forms:

The pseudo-first-order equation:

$$q_t = q_e\left(1 - e^{-k_1 t}\right) \tag{3}$$

The pseudo-second-order equation:

$$q_t = (q_e^2 k_2 t)/(1 + q_e k_2 t) \tag{4}$$

where q_e and q_t represent the amount of pollutant adsorbed (mg/g) at equilibrium and at time t respectively; k_1 and k_2 are the rate constants for the pseudo-first-order and pseudo-second-order kinetic models respectively; t is the time.

Isotherm Models: The interaction between the adsorbent and the pollutants was investigated using the two-parameter isotherm models in their non-linear forms, that is, Langmuir[39] and Freundlich[40] isotherms:

The Langmuir equation:

$$q_e = \frac{q_m b_L C_e}{1 + b_L C_e} \tag{5}$$

where q_e and q_m are the adsorption capacity at equilibrium and maximum monolayer coverage capacity respectively (mg/g), C_e denotes the concentration of pollutant at equilibrium (mg L^{-1}) and b_L is the Langmuir constant.

The Freundlich equation:

$$q_e = K_F C_e^{1/n} \quad (6)$$

where K_F represents the Freundlich adsorption constant ($mg^{1-1/n}\ L^{1/n}\ g^{-1}$), C_e signifies the concentration of pollutant at equilibrium (mg L^{-1}) and $1/n$ is the adsorption intensity.

Uptake of Oils and Organic Solvents: The oil and organic solvent absorption experiments were conducted using ≈20 mg solid sorbent and placed in a saturated oil system for an h as adapted from ASTMF726-99 (Standard Test Method for Sorbent Performance of Adsorbents) and the authors' previous work.[41] The weight of the absorbent before and after absorption experiments was recorded using a mass balance (Mettler Toledo, Model XSE105). All the experiments were performed in triplicate and the oils (gasoline, petroleum crude oil, and paraffin oil) as well as the organic solvents (hexane and toluene) were stained with Sudan red III (except for petroleum crude oil) prior to absorption experiments to improve the visibility by naked eyes. The water absorption test was conducted by placing the adsorbent into a container filled with water and the interim weight at a particular time interval was recorded over 60 min. The weight of the adsorbent before (w_i) and after (w_f) water absorption was recorded using the mass balance. The absorption capacity (Q, g/g) for both water and organics was determined by the weight gain after the absorption experiments divided by the initial weight of the adsorbent as stated in the following:

$$Q = \frac{w_f - w_i}{w_i} \quad (7)$$

Simultaneous Ad/Ab-Sorption Performance of Water Pollutants: Simultaneous water pollutants removal experiments were carried out using three different water systems (milli-Q, river, and sea water). Same river water as described in the previous section was used while sea water was collected from Henley Beach, Adelaide, South Australia, 34°54′51.1″S 138°29′ 30.0″E. About 100 mg samples (Alg-Fe_3O_4-rGO-4S and AC) was separately loaded into three pre-mixed water systems containing an aqueous phase (20 mL of ≈1.5 mg L^{-1} each Cu (II), Hg (II), and MB) and an organic phase (2 mL of mixed and dyed turpentine, paraffin oil, petroleum crude oil, toluene, and hexane), oscillated at 200 rpm with a blank (without ad/ab-sorbent) running in parallel for 3 h. The pH of the pre-mixed milli-Q water system was adjusted to ≈5.5 while both river and sea water were used without pre-treatment to simulate real natural water samples. After 3 h, aliquot of solution from each water system was withdrawn and separated into three different vials to determine the remaining concentration of metal ions and MB. Two portions of the withdrawn aliquots were diluted using 2% HNO_3 and 2% HCl for Cu (II) and Hg (II) ions, respectively, prior analysis by ICP-MS. Meanwhile, concentration of remaining MB in the final portion was analyzed with maximum absorbance at 664 nm by UV–vis measurement.

Supporting Information

Supporting Information is available from the Wiley Online Library or from the author.

Acknowledgements

This study was supported by the ARC Research Hub for Graphene Enabled Industry Transformation, (IH150100003). The authors thank Australian Microscopy and Microanalysis Research Facility (AMMRF) for the access of SEM and TEM facilities, Dr. Sarah Gilbert, Chris Bassell and Dr. Ulrike Schacht for their technical support on ICP-MS, XPS, and mercury porosimetry measurements, respectively. The XPS analysis was carried out at the Microscopy Australia facilities located at the University of South Australia, infrastructure co-funded by the University of South Australia, the South Australian State Government, and the Australian Federal Governments NCRIS scheme.

Conflict of Interest

The authors declare no conflict of interest.

Keywords

alginate, graphene, heavy metals, oils removal, organic dyes

Received: April 15, 2020
Revised: July 1, 2020
Published online:

[1] a) World Health Organization (WHO), Geneva: World Health Organization, **2008**, https://www.who.int/water_sanitation_health/publications/gdwq3rev/en/ (accessed: March 2020); b) S. Bolisetty, M. Peydayesh, R. Mezzenga, *Chem. Soc. Rev.* **2019**, *48*, 463.
[2] a) P. L. Yap, S. Kabiri, D. N. H. Tran, D. Losic, *ACS Appl. Mater. Interfaces* **2019**, *11*, 6350; b) G. N. Hlongwane, P. T. Sekoai, M. Meyyappan, K. Moothi, *Sci. Total Environ.* **2019**, *656*, 808.
[3] a) D. Wang, J. Song, S. Lin, J. Wen, C. Ma, Y. Yuan, M. Lei, X. Wang, N. Wang, H. Wu, *Adv. Funct. Mater.* **2019**, *29*, 1901009; b) M. Sarcletti, D. Vivod, T. Luchs, T. Rejek, L. Portilla, L. Müller, H. Dietrich, A. Hirsch, D. Zahn, M. Halik, *Adv. Funct. Mater.* **2019**, *29*, 1805742; c) D. Kim, D. W. Kim, O. Buyukcakir, M.-K. Kim, K. Polychronopoulou, A. Coskun, *Adv. Funct. Mater.* **2017**, *27*, 1700706; d) S. Ahmed, J. Brockgreitens, K. Xu, A. Abbas, *Adv. Funct. Mater.* **2017**, *27*, 1606572; e) X. Zhang, Z. Li, K. Liu, L. Jiang, *Adv. Funct. Mater.* **2013**, *23*, 2881; f) G. McKay, M. J. Bino, A. R. Altamemi, *Water Res.* **1985**, *19*, 491; g) S. Kabiri, D. N. H. Tran, S. Azari, D. Losic, *ACS Appl. Mater. Interfaces* **2015**, *7*, 11815.
[4] M. Sweetman, S. May, N. Mebberson, P. Pendleton, K. Vasilev, S. Plush, J. Hayball, *C* **2017**, *3*, 18.
[5] Y. Shen, Q. Fang, B. Chen, *Environ. Sci. Technol.* **2015**, *49*, 67.
[6] T. A. Tabish, F. A. Memon, D. E. Gomez, D. W. Horsell, S. Zhang, *Sci. Rep.* **2018**, *8*, 1817.
[7] Y. Shen, B. Chen, *Environ. Sci. Technol.* **2015**, *49*, 7364.
[8] C. Cheng, S. Li, J. Zhao, X. Li, Z. Liu, L. Ma, X. Zhang, S. Sun, C. Zhao, *Chem. Eng. J.* **2013**, *228*, 468.
[9] M. Strokal, J. E. Spanier, C. Kroeze, A. A. Koelmans, M. Flörke, W. Franssen, N. Hofstra, S. Langan, T. Tang, M. T. H. van Vliet, Y. Wada, M. Wang, J. van Wijnen, R. Williams, *Curr. Opin. Environ. Sustainability* **2019**, *36*, 116.
[10] a) D. N. Tran, S. Kabiri, L. Wang, D. Losic, *J. Mater. Chem. A* **2015**, *3*, 6844; b) I. Andjelkovic, D. N. H. Tran, S. Kabiri, S. Azari, M. Markovic, D. Losic, *ACS Appl. Mater. Interfaces* **2015**, *7*, 9758.
[11] M. Jain, M. Yadav, T. Kohout, M. Lahtinen, V. K. Garg, M. Sillanpää, *Water Resour. Ind.* **2018**, *20*, 54.
[12] N. A. Zubir, C. Yacou, J. Motuzas, X. Zhang, J. C. Diniz da Costa, *Sci. Rep.* **2015**, *4*, 4594.
[13] a) D. G. Matei, N.-E. Weber, S. Kurasch, S. Wundrack, M. Woszczyna, M. Grothe, T. Weimann, F. Ahlers, R. Stosch, U. Kaiser, A. Turchanin, *Adv. Mater.* **2013**, *25*, 4146; b) B. Lesiak, L. Kövér, J. Tóth, J. Zemek, P. Jiricek, A. Kromka, N. Rangam, *Appl. Surf. Sci.* **2018**, *452*, 223.
[14] S. K. Brauman, *J. Polym. Sci., Part A: Polym. Chem.* **1989**, *27*, 3285.
[15] D. G. Castner, K. Hinds, D. W. Grainger, *Langmuir* **1996**, *12*, 5083.
[16] G. Lawrie, I. Keen, B. Drew, A. Chandler-Temple, L. Rintoul, P. Fredericks, L. Grøndahl, *Biomacromolecules* **2007**, *8*, 2533.

[17] C. Jiao, J. Xiong, J. Tao, S. Xu, D. Zhang, H. Lin, Y. Chen, *Int. J. Biol. Macromol.* **2016**, *83*, 133.
[18] a) J. Sun, Y. Chen, H. Yu, L. Yan, B. Du, Z. Pei, *J. Colloid Interface Sci.* **2018**, *532*, 474; b) Z. Schnepp, S. C. Wimbush, M. Antonietti, C. Giordano, *Chem. Mater.* **2010**, *22*, 5340.
[19] Z. Wu, W. Deng, W. Zhou, J. Luo, *Carbohydr. Polym.* **2019**, *216*, 119.
[20] J. L. Shamshina, G. Gurau, L. E. Block, L. K. Hansen, C. Dingee, A. Walters, R. D. Rogers, *J. Mater. Chem. B* **2014**, *2*, 3924.
[21] F. S. Awad, K. M. AbouZeid, W. M. A. El-Maaty, A. M. El-Wakil, M. S. El-Shall, *ACS Appl. Mater. Interfaces* **2017**, *9*, 34230.
[22] N. Mohammed, A. Baidya, V. Murugesan, A. A. Kumar, M. A. Ganayee, J. S. Mohanty, K. C. Tam, T. Pradeep, *ACS Sustainable Chem. Eng.* **2016**, *4*, 6167.
[23] Y. Zhang, D. Kogelnig, C. Morgenbesser, A. Stojanovic, F. Jirsa, I. Lichtscheidl-Schultz, R. Krachler, Y. Li, B. K. Keppler, *J. Hazard. Mater.* **2011**, *196*, 201.
[24] H. Dogan, *Toxicol. Environ. Chem.* **2012**, *94*, 482.
[25] J. Liu, H. Chu, H. Wei, H. Zhu, G. Wang, J. Zhu, J. He, *RSC Adv.* **2016**, *6*, 50061.
[26] O.-H. Kwon, J.-O. Kim, D.-W. Cho, R. Kumar, S. H. Baek, M. B. Kurade, B.-H. Jeon, *Chemosphere* **2016**, *160*, 126.
[27] US EPA, EPA-816-F-09–004, https://www.nrc.gov/docs/ML1307/ML13078A040.pdf (accessed: May 2020).
[28] a) A. Mohammadi, A. H. Doctorsafaei, K. M. Zia, *Int. J. Biol. Macromol.* **2018**, *120*, 1353; b) J. Xiao, W. Lv, Z. Xie, Y. Tan, Y. Song, Q. Zheng, *J. Mater. Chem. A* **2016**, *4*, 12126.
[29] X. Liu, B. Cui, S. Liu, Q. Ma, *Fibers Polym.* **2019**, *20*, 1666.
[30] K.-Y. Law, *J. Phys. Chem. Lett.* **2014**, *5*, 686.
[31] M. Sun, A. Liang, G. S. Watson, J. A. Watson, Y. Zheng, L. Jiang, *PLoS One* **2012**, *7*, e46710.
[32] J. Xu, Z. Cao, Y. Zhang, Z. Yuan, Z. Lou, X. Xu, X. Wang, *Chemosphere* **2018**, *195*, 351.
[33] A. Turco, C. Malitesta, G. Barillaro, A. Greco, A. Maffezzoli, E. Mazzotta, *J. Mater. Chem. A* **2015**, *3*, 17685.
[34] J. Liu, J. Shi, C. Qian, Y. Zhao, L. Chen, L. Huang, X. Luo, *BioResources* **2017**, *12*, 8612.
[35] R. G. Pearson, *J. Chem. Educ.* **1968**, *45*, 581.
[36] a) P. L. Yap, S. Kabiri, Y. L. Auyoong, D. N. H. Tran, D. Losic, *ACS Omega* **2019**, *4*, 19787; b) D. C. Marcano, D. V. Kosynkin, J. M. Berlin, A. Sinitskii, Z. Sun, A. Slesarev, L. B. Alemany, W. Lu, J. M. Tour, *ACS Nano* **2010**, *4*, 4806.
[37] S. Lagergren, K. Sven, *Vetenskapsakad. Handl.* **1898**, *24*, 1.
[38] Y. S. Ho, G. McKay, *Process Biochem.* **1999**, *34*, 451.
[39] I. Langmuir, *J. Am. Chem. Soc.* **1918**, *40*, 1361.
[40] H. Freundlich, *Z. Phys.Chem.* **1906**, *57*, 385.
[41] S. Kabiri, D. N. H. Tran, T. Altalhi, D. Losic, *Carbon* **2014**, *80*, 523.

ADVANCED MATERIALS INTERFACES

Supporting Information

for *Adv. Mater. Interfaces,* DOI: 10.1002/admi.202000664

All-in-One Bioinspired Multifunctional Graphene Biopolymer Foam for Simultaneous Removal of Multiple Water Pollutants

*Pei Lay Yap, Kamrul Hassan, Yow Loo Auyoong, Negar Mansouri, Farzaneh Farivar, Diana N. H. Tran, and Dusan Losic**

Supporting Information

All-in-One Bioinspired Multifunctional Graphene Biopolymer Foam for Simultaneous Removal of Multiple Water Pollutants

Pei Lay Yap, Kamrul Hassan, Yow Loo Auyoong, Negar Mansouri, Farzaneh Farivar, Diana, N.H. Tran and Dusan Losic*

P.L. Yap, K. Hassan, Dr. F. Farivar, Dr. D.N.H. Tran, Prof. D. Losic
School of Chemical Engineering and Advanced Materials, The University of Adelaide, Adelaide, SA 5005, Australia
E-mail: dusan.losic@adelaide.edu.au

P.L. Yap, K. Hassan, N. Mansouri, Dr. F. Farivar, Dr. Diana, N.H. Tran, Prof. D. Losic
ARC Hub for Graphene Enabled Industry Transformation, The University of Adelaide, Adelaide, SA 5005, Australia

Dr. Y. L. Auyoong
Innovation and Commercial Partnerships, The University of Adelaide, Adelaide, SA 5000, Australia

N. Mansouri
School of Electrical and Electronic Engineering, The University of Adelaide, Adelaide, SA 5005, Australia

Keywords: alginate, graphene, heavy metals, organic dyes, oils removal

S1. Characterization of Multifunctional Graphene-Biopolymer Foam (Alg-Fe_3O_4-rGO-4S)

Structural Characterizations

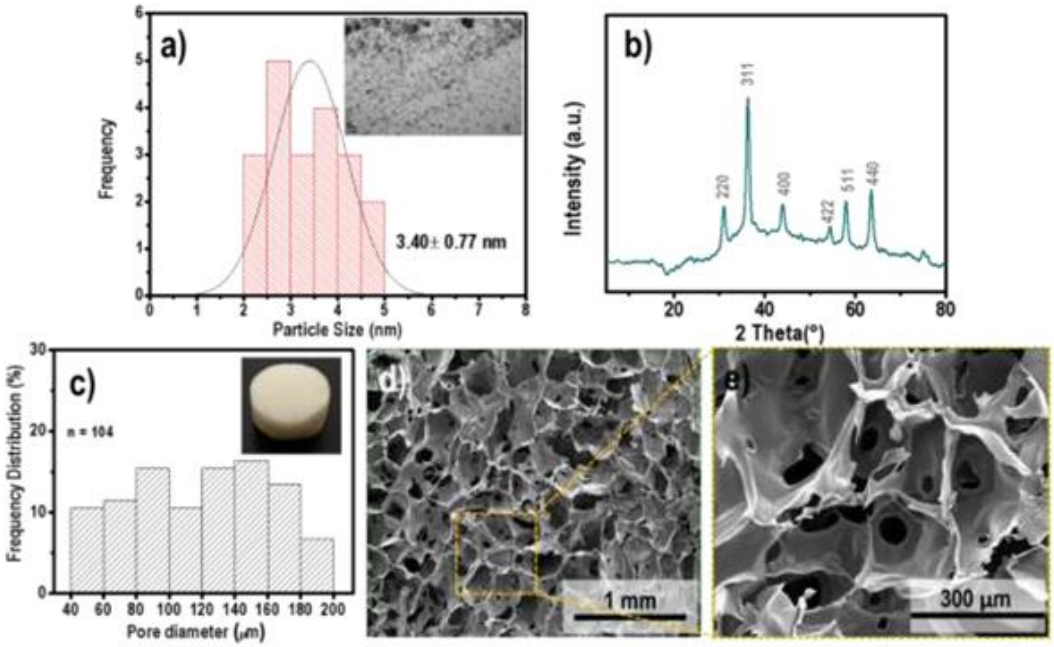

Figure S1. (a) Particle size distribution with inset of TEM image of Fe_3O_4 nanoparticles, (b) XRD diffractogram of Fe_3O_4 nanoparticles, (c) Pore size distribution plot determined from the pore size measurement of **Figure S1d** with the inset displaying freeze-dried alginate (Alg) foam, (d-e) SEM images under different magnifications. Meanwhile, the alginate foam exhibits highly porous polymeric network (Figure S1d). A higher resolution image (Figure S1e) indicates the formation of interconnected pores in the polymeric matrix with wide range of pore size ranging from 25 to 325 μm as visualized from the pore size distribution plot (Figure S1c).

Table S1. Normalized chemical composition of samples determined from their respective XPS survey plots in atomic %.

Element	Atomic %			
	C	O	Ca	S
GO	71.11	28.89	-	-
Alg foam	60.20	35.85	3.95	-
Alg-Fe_3O_4-rGO foam	61.54	33.54	4.93	-
Alg-Fe_3O_4-rGO-4S foam	63.03	27.59	0.51	8.86

EDX analysis of Functionalized Graphene Biopolymer Foam. Since the expected iron peak could not be detected from the XPS analysis although its presence was confirmed using XRD and elemental mapping techniques as discussed in the previous section, backscattered electron (BSE) technique was used to verify the existence of iron oxide (Figure S2c). As shown in Figure S2c, the brighter region (Spot A) compared to Spot B, clearly divulged the formation of a bulge particles embedded within the polymeric matrix. EDX results on Spot A and B (Table S2) showed a huge difference of Fe content (16.6 at% and 8.0 at%) which corroborated with the EDX mapping analysis that iron oxide was non-homogeneously distributed across the polymeric matrix. Furthermore, Figure S2b imaged under secondary electron microscopy showed obvious dark and bright contrast, indicating the depth difference of the topography of the material studied. Under secondary electron microscopy technique, a darker region shows a deeper or inner side of a material while brighter region indicates an upper surface. The darker region of Spot A which is rich with iron oxide nanoparticles indicated that the iron oxide nanoparticles was embedded in the inner layer of the polymeric matrix which justified the undetectable iron by ~10 atoms thickness depth detection limit of surface sensitive XPS analysis.

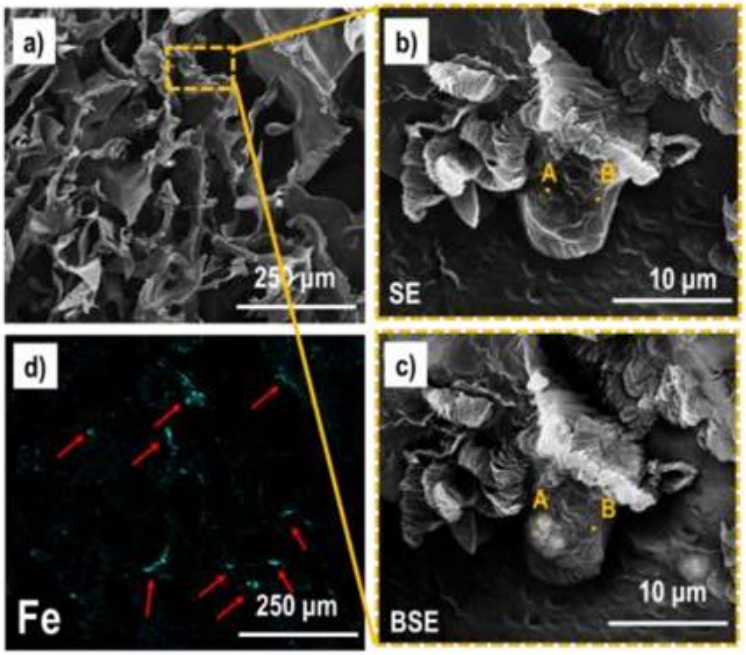

Figure S2. (a) SEM micrograph of Alg-Fe_3O_4-rGO-4S foam at detailed (b) secondary electron (SE) and (c) backscattered electron (BSE) showing the concentric region of Fe with the relative chemical composition analysis tabulated in Table S2. (d) EDS map of Fe with red arrows showing the distribution of iron in the Alg-Fe_3O_4-rGO-4S foam.

Table S2. Normalized EDX chemical composition of Alg-Fe_3O_4-rGO-4S for Spot A and B as outlined in Figure S2.

Element	Normalized at %	
	Spot A	Spot B
C	48.3	47.8
O	24.5	23.8
Fe	**16.6**	**8.0**
Ca	9.3	16.0
S	1.3	4.4

Mechanical and pore porosity analysis of Functionalized Graphene Biopolymer Foam. The mechanical strength is also a pivotal aspect for designing a sorbent given that the sorbent for water purification is subjected to withstand stress and strain resulting from the water flow which may affect its practical application in water treatment.[1] Representative compressive stress–strain curves (Figure S3a) demonstrated the mechanical behaviour of Alg, Alg-Fe_3O_4-rGO and Alg-Fe_3O_4-rGO-4S foams. It could be clearly observed that the mechanical strength of the tetrathiol modified foam (Alg-Fe_3O_4-rGO-4S) has been enhanced with compressive modulus of 16.039±0.756 kPa recorded after thiol-ene click functionalization compared to its controls (9.107±0.756 kPa and 12.425±0.685 kPa for Alg and Alg-Fe_3O_4-rGO, respectively). However, due to the hydrated condition of the mechanical analysis, the samples' strength could be notably reduced as water deteriorates the structure's resistance to the external force. The enhanced mechanical performance of the functionalized foam could be due to the reinforcement of the covalent bond formed between the thiol groups (tetrathiol) with the sp^2 carbons on rGO sheets, which is highly beneficial for the practical application of this material in water treatment.

The porograms (mercury intruded and extruded volumes against pressure) of the foams were converted into pore diameter distribution against cumulative and pore volume (Figure S3b and c) plot according to the Washburn equation.[2] Both the controls, alginate and Alg-Fe_3O_4-rGO foams, (Figure S3b) exhibit similar intrusion-extrusion pattern with only a single step observed on the intrusion curve, clearly denoting the unimodal pore size distribution for their unmodified structure as also evidenced by a distinct and sharp peak detected in the order of hundred micrometer range. This result is in good agreement with the pore size distribution plot of alginate foam determined from the SEM imaging technique (Figure S1a) which showed that the pore size of alginate foam falls between 40-200 µm. Unlike the unimodal trend exhibited by

the control samples, the stepped-intrusion curve of tetrathiol modified graphene foam indicates bimodal distribution of pore size as verified by the presence of multiple peaks found in few micrometers and in the order of hundreds micrometers range, indicating the effect of the insertion of tetrathiol moieties using photoinitiated reaction.[2-3] It should also be noted that the mercury injection and ejection curves for both the control samples were consistent without a hysteresis loop, implying that the sample network consists of mainly closed pores. In contrast with the control samples, a significant hysteresis loop (Figure S3c) identified on the mercury intrusion-extrusion curve for tetrathiol functionalized graphene foam which may indicate the presence of closed and open pores in its structure resulted from the photoinitiated reaction.[4] More details on the porosity characteristics of the analysed samples can be found in Table S3.

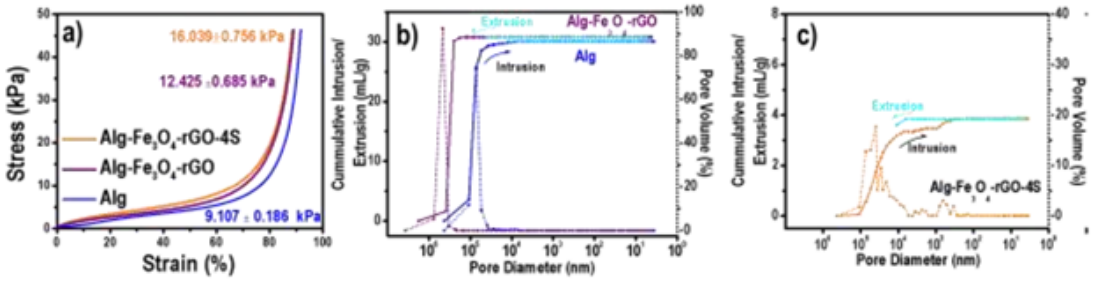

Figure S3. (a) Average stress-strain curve of Alg, Alg-Fe_3O_4-rGO and Alg-Fe_3O_4-rGO-4S foams immersed in water before performing the dynamic mechanical analysis. Pore size distribution analysis derived from mercury intrusion porosimetry plotted as functions of cumulative intrusions/extrusions (left axis) and percentage of pore volume (right axis) for (b) Alg and Alg-Fe_3O_4-rGO control samples and (c) Alg-Fe_3O_4-rGO-4S foam.

Table S3. Summary of porosity characteristics of foams analysed using Mercury Intrusion Porosimetry technique.

Foam	Mean pore diameter (µm)	Total pore volume (mL/g)	Porosity (%)	Grain Density (g/cm^3)	Bulk Density (g/cm^3)
Alg	227.7	20.4	98.3	2.8591	0.0483
Alg-Fe_3O_4-rGO	206.9	14.4	70.9	0.1700	0.0494
Alg-Fe_3O_4-rGO-4S	63.1	4.1	83.3	1.2100	0.2018

S2. Sorption Performance of Alg-Fe_3O_4-rGO-4S

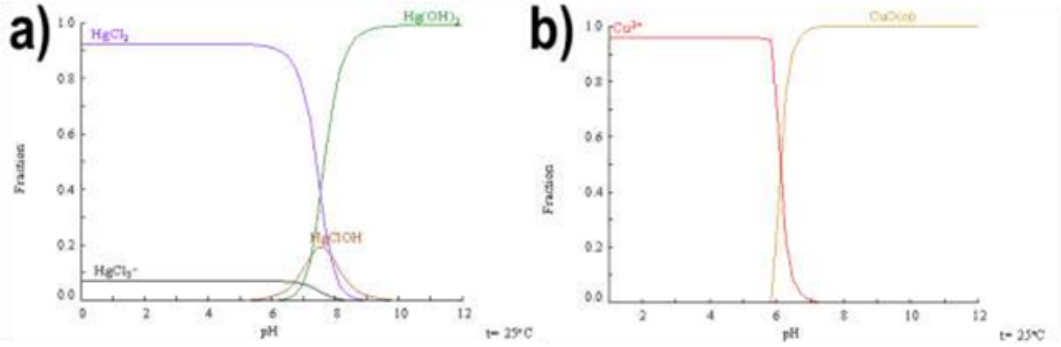

Figure S4. Metal species distribution diagram as a function of pH (total metal concentration 1.0×10^{-4} M) for (a) mercury and (b) copper calculated by using the computer programs HYDRA and MEDUSA[5].

For the studied metal ions (Hg and Cu), they predominantly exist as soluble divalent metal ions up to pH 6.5 for Hg (II) and around pH 6 for Cu (II). The negatively charged surface of the functionalized graphene-biopolymer as evident from the negative zeta potential values (Figure 4a) strongly suggests that electrostatic interaction is the primary adsorption mechanism accounted for the excellent uptake of metal ions from pH 4 to 7. At acidic pH, the uptake performance of mercury is slightly reduced (~90%) which could be attributed to the competition with H^+ ions for binding sites on the adsorbent surface. Significantly, the removal efficiency of all the tested metal ions decreased at basic pH which could be due to the dramatic reduction of

positively charged metal ion species (Hg^{2+}, Cu^{2+}) and the presence of excessive hydroxide ions (OH^-) which potentially react with the investigated metal ions to form $Hg(OH)_2$, HgClOH and CuO precipitates as evidenced from their respective speciation diagrams (Figure S4). These neutral species may not feasibly adsorb on the highly negatively charged surface of the functionalized graphene biopolymer foam as compared to their highly positive charged species in the water, thereby reducing the metal ions uptake at this pH region.

Table S4. Adsorption parameters of pseudo-first and pseudo-second order kinetic models for Hg (II), Cu (II) ions and methylene blue on Alg-Fe_3O_4-rGO-4S foam.

Kinetic Model	Parameter	Water Pollutants		
		Hg (II)	Cu (II)	Methylene Blue
Pseudo-first order	k_1 (min^{-1})	0.023±0.0036	0.044±0.0017	0.042±0.0024
	q_e (mg g^{-1})	28.80±0.52	21.51±0.58	25.66±0.40
	R^2	0.9956	0.9926	0.9983
Pseudo-second order	k_2 (g mg^{-1} min^{-1})	0.0010±0.00018	0.0016 ±0.000022	0.0018 ±0.000016
	q_e (mg g^{-1})	31.69±0.72	24.29± 0.13	28.83± 0.55
	R^2	0.9981	0.9997	0.9984

Table S5. Adsorption isotherm parameters of Langmuir and Freundlich models for Hg (II), Cu (II) ion and methylene blue on Alg-Fe_3O_4-rGO-4S foam.

Isotherm Model	Parameter	Water Pollutants		
		Hg (II)	Cu (II)	Methylene Blue
Langmuir	q_{max} (mg g^{-1})	107.0±2.1	73.5±0.7	789.7±36
	b (L mg^{-1})	0.23±0.01	1.01±0.04	0.026±0.0019

	R^2	0.9952	0.9950	0.9982
Freundlich	**n**	2.77±0.33	5.38±0.87	1.44±0.078
	K ($mg^{1-1/n}$ g^{-1} $L^{1/n}$)	31.33±3.26	40.18±3.03	34.00±3.95
	R^2	0.9747	0.8055	0.9895

Table S6. Comparison of adsorption capacity with experimental conditions of various adsorbents for Cu (II) and Hg (II) ions.

Adsorbent	Surface area (m^2g^{-1})	Metal ions uptake conditions	Maximum sorption capacity ($mg\ g^{-1}$)	Ref
Bovine serum albumin-protected nanocluster-loaded cellulose nanocrystal-alginate hydrogel beads (Au@BSA NCs)	**N.A.**	C_0: 20-100 mg/L, sorbent dosage: $100x10^3$ mg/L, 25 °C, pH 7	Hg (II): 26	[6]
Tricapryylmethylammoniu m 2-(methylthio)benzoate(A336) (MTBA) PVA-alginate beads	**N.A.**	C_0: 10-50 mg/L, sorbent dosage: 1000 mg/L, 24.9 °C, pH 5.8	Hg (II): 49.89	[7]
Alginate-entrapped humic acid (AL/HA)	**N.A.**	C_0: 50 mg/L, sorbent dosage: 2000 mg/L, 25 °C, pH 3-4	Hg (II): 74	[8]
Carboxymethyl chitosan-sodium /graphene oxide (CMCNa/GO) hydrogel	**N.A.**	C_0: 100 mg/L, sorbent dosage: 1200 mg/L, 20 °C, pH 6	Cu (II): 28.41	[9]
Zirconium oxide immobilized alginate beads (ZOAB)	**13.2**[a]	C_0: 48.5 mg/L, sorbent dosage: 1000 mg/L, 25 °C, pH 5	Cu (II): 69.9	[10]
Mg alginate/MgAl-layered double hydroxide (Fe_3O_4/LDH-AM)	**3.42**[a]	C_0: 80 mg/L, sorbent dosage: 2500 mg/L, 25.0 °C, pH NA	Cu (II): 64.66	[11]
Alg-Fe_3O_4-rGO-4S Foam	**125.10±0.07**[b]	**C_0: 20-110 mg/L, sorbent dosage: 1000 mg/L, 21.0 °C, pH 5.3**	**Hg (II): 107.0 Cu (II): 73.5**	**This work**

NA: Not Available. [a] *refers to Brunauer–Emmett–Teller (BET) method and* [b] *refers to methylene blue method.*

For Hg (II) ions, Mohammed et al. demonstrated that the maximum sorption capacity achieved by the bovine serum albumin-protected nanocluster-loaded cellulose nanocrystal-alginate hydrogel beads (Au@BSA NCs) was 26 mg g^{-1}(nearly 4 times lesser than Alg-Fe_3O_4-rGO-4S foam) using 100 times higher sorbent dosage compared to our present study.[6] In another study conducted by Zhang et al., chemically modified alginate beads, tricapryylmethylammonium 2-(methylthio)benzoate(A336) (MTBA) PVA-alginate (PVA/IL([A336][MTBA]) achieved 49.89 mg/g of maximum sorption capacity (2 times lower than Alg-Fe_3O_4-rGO-4S foam) when same sorbent dosage was adopted in the Hg (II) ion removal study.[7] Almost 1.4 times lower maximum sorption capacity (74 mg g^{-1}) was recorded for alginate-entrapped humic acid (AL/HA) adsorbent in relative to functionalized graphene biopolymer foam (107 mg g^{-1}) when 2 times higher sorbent dosage was used in their work.[8] Excellent Cu (II) ion removal performance also showcased by functionalized graphene biopolymer foam (maximum sorption capacity =73.5 mg g^{-1}; sorbent dosage =1000 mg/L) compared to the work reported by Liu et al., on carboxymethyl chitosan-sodium/graphene oxide (CMCNa/GO) hydrogel (maximum sorption capacity =28.41 mg g^{-1} ; sorbent dosage =1200 mg/L).[9] Similarly, when same sorbent dosage and pH were applied in Cu (II) removal study, zirconium oxide immobilized alginate beads (ZOAB) reached lower maximum sorption capacity (69.9 mg/g).[10] Higher Cu (II) sorption capacity (73.5 mg/g) compared to alginate/MgAl-layered double hydroxide (Fe_3O_4/LDH-AM) which showed 64.66 mg/g maximum sorption capacity using 2.5 times higher sorbent dosage in relative to our material.[11] In brief, the tetrathiol modified foam is evidently an economical-efficient and

environmentally-friendly sorbent given that the amount of spent sorbent generated with regard to the sorbent dosage required to achieve similar or higher uptake performance.

Table S7. Comparison of adsorption capacity with experimental conditions of selected alginate-based adsorbents for methylene blue (organic dye).

Adsorbent	Surface area (m^2g^{-1})	Organic dyes uptake conditions	Maximum sorption capacity ($mg\ g^{-1}$)	Ref
GO/alginate gel	N.A.	C_0: 50-250 mg/L, sorbent dosage: 1000 mg/L, 24.9 °C, pH NA	357.14	[12]
GO/calcium alginate composites	N.A.	C_0: 20-70 mg/L, sorbent dosage: 500 mg/L, 25 °C, pH 5.4	181.81	[13]
Tannic acid-poly(vinyl alcohol)/sodium alginate hydrogel	N.A.	C_0: 20-160 mg/L, sorbent dosage: 500 mg/L, 30 °C, pH 9	147.06	[8]
Alg-Fe_3O_4-rGO-4S Foam	**125.10±0.07[b]**	**C_0: 100-500 mg/L, sorbent dosage: 1000 mg/L, 21.0 °C, pH 5.3**	**789.70**	**This work**

NA: Not Available. [a] refers to Brunauer–Emmett–Teller (BET) method and [b] refers to methylene blue method.

Table S8. Viscosity and density values of the studied organic solvents and oils.

Organics	Viscocity (cP)	Density (g/cm^3)
Hexane	0.31	0.66
Toluene	0.58	0.87
Petroleum crude oil	-	0.88
Paraffin oil	32	0.93
Gasoline	0.6	0.75

Table S9. Comparison of sorption capacity with material property of various adsorbents for organics pollutants removal.

Sorbent	Surface area (m^2g^{-1})	Water Contact Angle (°)	Type of Organics	Max. sorption capacity ($g\ g^{-1}$)	Ref.
Swellable porous polydimethylsiloxane / multiwalled carbon nanotubes (PDMS/MWNTs)	N.A.	153.4	Hexane Toluene Gasoline	15.05 12.04 11.1	[14]
Swellable porous polydimethylsiloxane (PDMS)	N.A.	144	Toluene Crude oil Gasoline	18.7 9.0 22.0	[15]
PDMS sponge	N.A.	120-130	Toluene	5	[16]
Polyurethane-CNT-PDMS	N.A.	162	Hexane Gasoline	15 18	[17]
MTMS-DMDMS gels	N.A.	153	Hexane Petroleum ether Toluene	6 6 8	[18]
Alg-Fe_3O_4-rGO-4S foam	**125.10±0.07[b]**	**50-130**	**Hexane Toluene Petroleum Crude oil Paraffin oil Gasoline**	**17.17 18.00 16.16 16.73 13.65**	**This work**

NA: Not Available. [a] refers to Brunauer–Emmett–Teller (BET) method and [b] refers to methylene blue method.

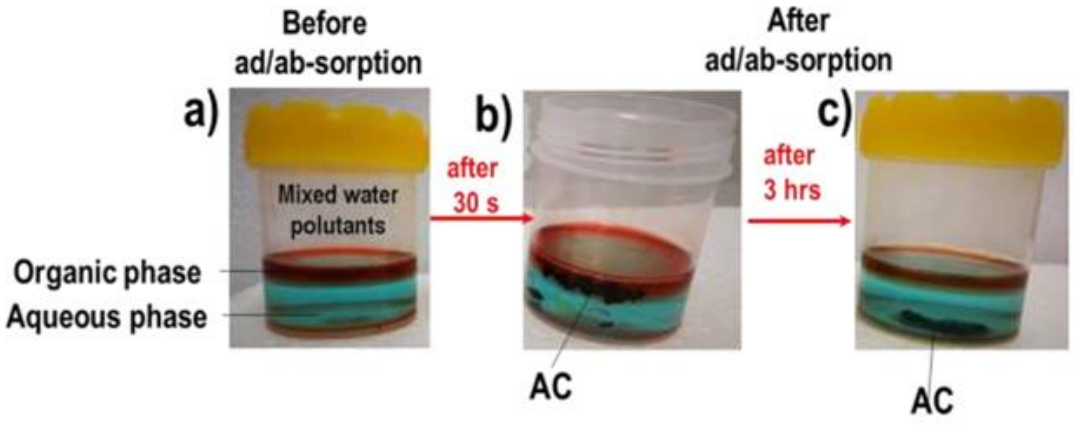

Figure S5. Photographs of (a) water pollutants mixture containing aqueous phase (Cu^{2+}, $Hg^{2+}$and methylene blue) and organic phase (dyed turpentine, paraffin oil, petroleum crude oil, hexane and toluene) before sorption, Activated carbon (AC) in water pollutants mixture after ad/ab-sorption of (b) 30 seconds, showing no significant removal of organic phase pollutants and (c) 3 hours, showing no significant visual change of pollutant mixture compared to blank sample in (a).

S3. Optimization of ad/ab-sorbent form for enhanced pollutants uptake efficiency

The effect of concentration or wt % of Fe_3O_4-rGO towards the robustness and strength of the final sorbent material was studied. Figure S6a shows that as the concentration (wt %) of Fe_3O_4-rGO increases, the robustness of the foam decreases, resulting in the deformation of the foam structure. Hence, 6.2 wt % (2 mg/mL) of Fe_3O_4-rGO was used to perform the water pollutants removal studies due to its optimum strength to maintain its structure. Alg-Fe_3O_4-rGO-4S composite was also fabricated in two different forms, i.e. bubble beads and foam as illustrated in Figure S6b to explore the effect of sorbent form towards sorption of water pollutants. Notably, we found that the removal efficiency of Alg-Fe_3O_4-rGO-4S in foam form was up to four times better compared to its beads form in the preliminary metal ion adsorption study (Figure S6c and d). These results clearly confirmed that material of the same chemical composition but different forms could significantly affect the adsorption performance. Hence, the adsorbent material in foam was applied for all the sorption investigations in this work.

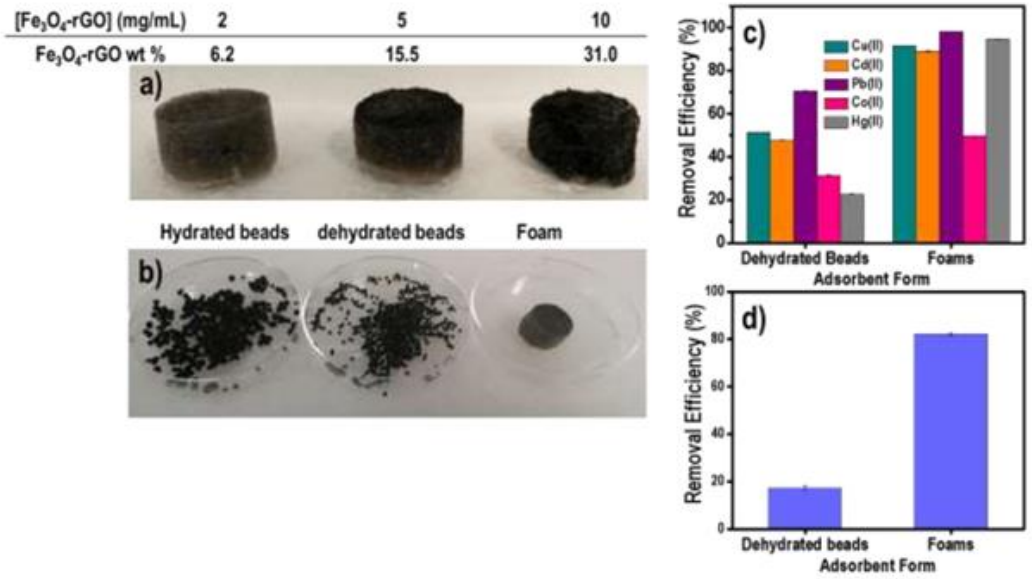

Figure S6. (a) Photograph of Alg-Fe_3O_4-rGO-4S foams in different wt % showing that as the concentration or wt % of Fe_3O_4-rGO increases, the foam becomes less robust and difficult to hold its structure. (b) Photograph of Alg-Fe_3O_4-rGO-4S in different forms. (c) Preliminary selectivity adsorption study in a multi-metallic ion solution containing Cu (II), Cd (II), Pb (II), Co (II) and Hg (II) ions using Alg-Fe_3O_4-rGO-4S in dehydrated beads and foams forms [Conditions: C_0= ~10 ppm, pH~5, temperature=21.0˚C, mass of sorbent= ~20mg, volume of metal ion solution = 20 mL]. (d) Preliminary adsorption study of methylene blue using Alg-Fe_3O_4-rGO-4S in dehydrated beads and foams forms [Conditions: C_0= ~25 ppm, pH~5.5, temperature=21.0˚C, mass of sorbent= ~20mg, volume of metal ion solution = 20 mL].

S4. Materials

Natural graphite rocks were obtained from a local mining site (Uley, Eyre Peninsula, South Australia, Australia), crushed into powder using a benchtop ring mill (Rocklabs) and sifted using

a 25 µm sieve. Potassium permanganate (Sigma Aldrich), 85 % w/w phosphoric acid (Chem-Supply), 98 % sulfuric acid (Chem-Supply), 30 % hydrogen peroxide (Chem-Supply), 36 % hydrochloric acid (Chem-Supply), sodium hydroxide (Chem-Supply), ethanol (Chem-Supply), sodium alginate (Chem-Supply), calcium chloride (Chem-Supply), 2,2-dimethoxy-2-phenylacetophenone (DMPA, Sigma-Aldrich), iron (II) sulfate (Chem-Supply), iron (III) chloride (Chem-Supply), ammonium hydroxide (Sigma Aldrich), pentaerythritol tetrakis(3-mercaptopropionate) (tetrathiol, Sigma Aldrich), cadmium nitrate (Mallinckrodt), copper nitrate (Chem-Supply), lead nitrate (Univar), mercury chloride (Chem-Supply), cobalt nitrate (Ajax), and thiourea (Sigma Aldrich) were used directly without prior purification.

S5. Material Characterization

Surface topography, elemental composition and mapping of materials were investigated by scanning electron microscope equipped with EDX Silicon Drift Detectors (FE-SEM, Quanta 450 FEG, FEI, USA, EDX, Ultim Max 170 mm SDD, Oxford Instruments, UK) at operating voltage of 10 kV. A high-resolution Philips CM200 transmission electron microscope (TEM, Japan) was used to image the sample at 200 kV. The sample was prepared by dispersing it in ethanol to form a homogeneous dispersion on a Cu grid. FTIR (Nicolet 6700, Thermo Fisher) in the range of 500-4000 cm^{-1} was recorded to identify the chemical functional groups in the materials. XRD equipped with Cu X-ray tube (600 Miniflex, Rigaku, Japan) in the range of 2θ = 5- 80° at 40 kV and 15 mA with 10° min^{-1} scan speed was primarily used for bulk phase identification. Thermal stability and decomposition of the materials were studied using TGA/DSC 2, STAR^e System (Mettler Toledo, Switzerland) under nitrogen atmosphere with the samples heated to 1000 °C at a heating rate of 10 °C min^{-1}. The surface chemical composition and species of the materials were

determined using XPS (AXIS Ultra_DLD (Kratos, UK) equipped with a monochromatic Al Kα radiation source (hv =1486.7 eV) at 225 W, 15 kV and 15 mA. XPS wide scans were acquired at 0.5 eV step size over -10-1100 eV at the pass energy of 160 eV while the narrow scans were obtained at a 0.1 eV step size and pass energy of 20 eV. The deconvolution and fitting of peaks were performed using Casa XPS^{TM} software. All the core-level spectra involved in this work were calibrated to the primary peak (C-C/C-H peak) of adventitious carbon at 284.8 eV with their respective full width at half maximum (fwhm) for all components were constrained within the difference of 0.2 eV. The contact angle measurement was performed at ambient conditions with Attension Theta Optical Tensiometer system (KSV instruments, Finland) using sessile drop method. Sample (Diameter: 2.5 cm, thickness: 1.0 cm) was first cut to the top and cross-sectional surfaces using a blade. 1 µL of milli-Q water was auto-dropped on several spots of the sample. The static contact angle was recorded after 60s (when droplet achieves stability on the sample surface) and average of the contact angle was analysed accordingly. The mechanical properties of prepared samples were tested with TA Q800 DMA instrument with parallel-plate compression clamps in the controlled force mode at the rate of 1 N/min. All the samples were immersed in distilled water for 24 hours prior to the test with two replicates performed at room temperature. The compressive modulus of the samples was calculated according to the stress-strain curves and up to 10 % of strain before the pores completely collapsed. The porosity characteristics and density of the foams were determined via mercury intrusion porosimeter (Micromeritics, Autopore 9600) using a known weight. Low pressure mercury intrusion (0-60 psia) was used to measure the interconnected pore diameter distributions. Surface area measurement was determined by methylene blue adsorption method using UV-Vis spectroscopy (Shimadzu, UV 1601, Japan) as described in our previous work.[19] The zeta potential of the sample was

measured as a function of pH in triplicate using a Malvern Zetasizer (Nanoseries, Australia). The sample was dispersed in milli Q water and bubbled by nitrogen gas to drive off the dissolved CO_2 gas before pH adjustment using HCl or NaOH solution between pH 3-10, followed by standing for a week before zeta potential measurement. UV-Vis spectrometer (UV -1601, Shimadzu) in the range of 200-800 cm^{-1} was used to probe the residual of methylene blue concentration (λ_{max} = 665 nm). Solution ICP-MS (QQQ 8900, Agilent) was used to measure the remaining concentration of metal ions after the adsorption experiments.

References

[1] Y. Yue, X. Wang, Q. Wu, J. Han, J. Jiang, *Polymers* **2019**, 11, 1239.
[2] M. A. Ramos, M. H. Gil, E. Schacht, G. Matthys, W. Mondelaers, M. M. Figueiredo, *Powder Technol.* **1998**, 99, 79.
[3] M. Alshaaer, M. H. Kailani, N. Ababneh, S. A. A. Mallouh, B. Sweileh, A. Awidi, *Processing and Application of Ceramics* **2017**, 11, 13.
[4] P. Wei, Y. Liang, S. Zhao, S. Peng, X. Li, R. Meng, *Processes* **2018**, 7, 13.
[5] I. Puigdomenech, Make Equilibrium using Sophisticated Algorithms (MEDUSA) program, http://www.kemi.kth.se/medusa, accessed: 100.
[6] N. Mohammed, A. Baidya, V. Murugesan, A. A. Kumar, M. A. Ganayee, J. S. Mohanty, K. C. Tam, T. Pradeep, *ACS Sustainable Chemistry & Engineering* **2016**, 4, 6167.
[7] Y. Zhang, D. Kogelnig, C. Morgenbesser, A. Stojanovic, F. Jirsa, I. Lichtscheidl-Schultz, R. Krachler, Y. Li, B. K. Keppler, *J. Hazard. Mater.* **2011**, 196, 201.
[8] H. Dogan, *Toxicol. Environ. Chem.* **2012**, 94, 482.
[9] J. Liu, H. Chu, H. Wei, H. Zhu, G. Wang, J. Zhu, J. He, *RSC Adv.* **2016**, 6, 50061.
[10] O.-H. Kwon, J.-O. Kim, D.-W. Cho, R. Kumar, S. H. Baek, M. B. Kurade, B.-H. Jeon, *Chemosphere* **2016**, 160, 126.
[11] J. Sun, Y. Chen, H. Yu, L. Yan, B. Du, Z. Pei, *J. Colloid Interface Sci.* **2018**, 532, 474.
[12] X. Liu, B. Cui, S. Liu, Q. Ma, *Fibers and Polymers* **2019**, 20, 1666.
[13] Y. Li, Q. Du, T. Liu, J. Sun, Y. Wang, S. Wu, Z. Wang, Y. Xia, L. Xia, *Carbohydr. Polym.* **2013**, 95, 501.
[14] A. Turco, C. Malitesta, G. Barillaro, A. Greco, A. Maffezzoli, E. Mazzotta, *J. Mater. Chem. A* **2015**, 3, 17685.
[15] A. Zhang, M. Chen, C. Du, H. Guo, H. Bai, L. Li, *ACS Appl. Mater. Interfaces* **2013**, 5, 10201.
[16] S.-J. Choi, T.-H. Kwon, H. Im, D.-I. Moon, D. J. Baek, M.-L. Seol, J. P. Duarte, Y.-K. Choi, *ACS Appl. Mater. Interfaces* **2011**, 3, 4552.
[17] C.-F. Wang, S.-J. Lin, *ACS Appl. Mater. Interfaces* **2013**, 5, 8861.
[18] G. Hayase, K. Kanamori, M. Fukuchi, H. Kaji, K. Nakanishi, *Angew. Chem. Int. Ed.* **2013**, 52, 1986.

[19] a) P. L. Yap, S. Kabiri, D. N. H. Tran, D. Losic, *ACS Appl. Mater. Interfaces* **2019**, 11, 6350; b) D. N. Tran, S. Kabiri, L. Wang, D. Losic, *J. Mater. Chem. A* **2015**, 3, 6844.

List of videos:

Video S1: Water contact angle of Alg foam **[Click for online hyperlink]**

Video S2: Water contact angle of Alg-Fe_3O_4-rGO foam **[Click for online hyperlink]**

Video S3: Water contact angle of Alg-Fe_3O_4-rGO-4S foam **[Click for online hyperlink]**

Video S4: Oil contact angle of Alg-Fe_3O_4-rGO-4S foam **[Click for online hyperlink]**

Video S5: Removal of oil by Alg-Fe_3O_4-rGO-4S foam **[Click for online hyperlink]**

Video S6: Removal of oils, solvent, dye, Cu (II) and Hg (II) mixture by Alg-Fe_3O_4-rGO-4S foam **[Click for online hyperlink]**

Video S7: Comparative removal of oils, solvent, dye, Cu (II) and Hg (II) mixture by activated carbon **[Click for online hyperlink]**

CHAPTER 7

CONCLUSIONS AND PERSPECTIVES

7. CONCLUSIONS AND PERSPECTIVES

7.1. Conclusions

This thesis contributes to the development of advanced graphene-based composites using novel functionalization methodologies towards providing technological solutions for water purification and addressing the rising water pollution issues worldwide. This comprehensive study aims to address specific challenges faced by the conventional adsorbent (AC) for remediation of water pollutants. In essence, this thesis is devoted to the development of new generation water purification technologies based on the surface and structural engineering of graphene derivatives with exploration on different modification approaches using several functionalization agents. Three main concepts can be summarized based on the research outcomes in this thesis:

1. **Fundamental insights on surface engineering and structural design of advanced graphene composites (Objective 2):** Controllable modulation of surface functionalities on graphene composites was achieved through simultaneous chemical reduction and nitrogen doping of GO, followed by a thermal thiol-ene click reaction. By varying the amount of reducing agent, a series of N-doped rGO with different levels of oxygen groups were prepared for subsequent attachment of amino-terminated thiol molecules through the thiol-ene click reaction. A correlation was established between different reduction degree of N doped-GO with new tunable functionalities including

nitrogen (-NH_2) and sulfur (C-S-C, C=S, S-O) groups on functionalized graphene composites. Fundamental insights on the structural, chemical and thermal properties of functionalized graphene materials with tailorable doping levels, functional groups and interfacial properties at varied oxidation levels were acquired. Outcomes from this research study provide basic understanding on the structural, chemical and thermal properties of doped- and thiol-ene functionalized graphene materials for subsequent studies in this thesis. Resulting graphene derivatives from this combined modification paves a practical design pathway for novel advanced graphene materials with potential applications in polymer composites, supercapacitors, electrocatalysts, adsorbents and sensors.

2. **Design and engineering of advanced graphene composites (Objective 3):** Four novel modification strategies were explored to engineer graphene in addressing the key challenges faced by AC including its energy-intensive preparation approach and less effective immobilization of residual heavy metal ions at low concentrations detected in effluents after a typical water treatment process. Essentially, the surface and interface of graphene were tailored to graft multifunctional groups to achieve better dispersibility, material robustness and stability in water for trapping myriads of pollutants in water. Structural, chemical and thermal properties of the advanced graphene composites fabricated herein, were prudently investigated to understand their corresponding formation mechanisms. To target for a low cost, low energy, environmentally friendly and scalable modification approach, hydrothermal and chemical reduction were adopted to covalently graft polyamine precursor

on the epoxides and carboxyls groups on GO. Formation of rich and multiple type of nitrogen containing groups on rGO through ring opening nucleophilic and amidation was proposed based on detailed XPS and FTIR analyses. Both polyamine modified rGO exhibited 8.28 and 5.74 atomic % nitrogen content with high surface area (270 ±10 m^2/g and 63 ±8 m^2/g) respectively, achieved from the chemical reduction and hydrothermal approaches.

Meanwhile, engineering of multifunctional graphene-based composite was explored to introduce cysteamine, a precursor bearing sulfur and amino functional groups onto GO through a thermal thiol-ene click method. Benefited from the advantages of a modular, catalysts-free and mild reaction condition, this multifunctional graphene composite was successfully functionalized with thiol groups (cysteamine) attached to the sp^2 carbon (GO). The high surface area (672 m^2/g), multifunctional partially reduced GO composite was confirmed with almost equal amount of nitrogen (1.59 atomic %) and sulfur (1.66 atomic %) detected on its surface.

On the other hand, a facile, energy-efficient, and environmentally friendly (use of non-toxic solvent with no emission of harmful organic compounds) photoinitiated thiol-ene click approach was applied to design multithiol functionalized graphene-based aerogels. By varying the UV irradiation time using pentaerythritol tetrakis-mercaptopropionate as a thiol-precursor, optimization of this UV-directed modification strategy successfully created multifunctional graphene aerogels with two different types of sulfur chemistry. Both SH-graphene bio-sponge and Alg-Fe_3O_4-rGO-4S bio-polymer foam exhibited high surface area and high density of sulfur-containing groups

(115.0 and 125.1 m^2/g; 10.2 atomic % S and 8.86 atomic % S, respectively). In these graphene-based composites, alginate biopolymer was added to mechanically strengthen the graphene aerogel, while magnetic nanoparticles (Fe_3O_4) were introduced to facilitate separation after the sorption process besides enhancing the uptake of water pollutants.

3. **Sorption performance of advanced graphene composites (Objective 4):** Evaluation of pollutant sorption using the developed advanced graphene-based composites was performed on different types of water pollutants including heavy metal ions, organic dyes, organic solvents and oil. Heavy metal ions are the most studied pollutant in this work owing to their inherent properties including their toxicity even exposure at very low concentration, almost invisible and persistence in water that make them difficult to be removed compared to other contaminants. Interaction mechanisms between the developed adsorbents and pollutants were investigated through pH, kinetics and isotherms studies, which were fitted into kinetics models (pseudo-first- and pseudo-second-order models) as well as isotherms models (Langmuir and Freundlich models). Performance testings on the aspects of selectivity, regeneration, real sample analysis and simultaneous pollutants removal were also explored to assess the potential application of the developed adsorbents in real water systems. In summary, the adsorbents developed through green, scalable, cost-, and energy- efficient methods hereby exhibit excellent activity, outstanding selectivity and good regenerability than the commercial adsorbent towards water purification.

7.2. Future Work Recommendations

This research study marked an exciting journey with novel discovery that underpinned the mastery on functionalization of graphene derivatives through different chemical modification strategies, engineering of new graphene-based composites and advancing their performance for sorption of broad range of pollutants that open many new frontiers that require further explorations. For future direction, several key aspects highlighted as the following are recommended to fully unlock the potential of functionalized graphene-based materials in advanced water purification technology:

1. **Extension of thiol-ene click concept to pristine graphene, other 2D materials and their hybrids:** Although several examples of graphene-based composites with remarkable water purfication performance have been successfully demonstrated to functionalize GO through thiol-ene click approach in this thesis, this modification approach is still at its infancy especially with its great potential to modify pristine graphene directly. Owing to the abundance of sp^2 carbon ('ene') in the graphene newtwork, the thiol-ene click modification approach is expected to give rise to extraordinary properties such as high electrical conductivity with enhanced dispersion in water if this modification strategy is systematically studied to functionalize pristine graphene. Thorough understanding of this concept at the atomic level of the fabricated materials is necessary because it is beneficial not only for environmental applications (e.g. environmental sensors), but also for other promising applications such as energy storage and biomedical devices.

2. **Optimization of the robustness and structural properties of functionalized graphene-based materials:** Exploration on the optimization of the functionalization parameters for fine-tuning the mechanical and structural properties of graphene-based composites to achieve robust, flexible, free-standing nanoporous graphene in different forms (paper, films, sponge and membrane) is still highly desirable. These properties are critical to improve the durability, recyclability and sustainability of the functionalized graphene materials for enhanced removal of water pollutants. In fact, majority solutions to global challenges are just around us. By exploring biomimetic design, desirable nanostructural properties of materials can be achieved to create nature-inspiring technology for water purification. For example, water repellency property of a material can be developed by biomimicking the structure of the superhydrophobic leaves of a lotus flower to achieve enhanced removal of spilled oils in water.

3. **Design of less hazardous and sustainable synthesis:** It is recommended that the synthetic methods should be devised to use chemicals that pose little or no toxicity to human health and the environment as emphasized in *The Twelve Principles of Green Chemistry.*[26] Alternative of biodegradable and sustainable raw materials should be considered to substitute the use of hazardous synthetic feedstock. For example, natural bacterial iron-oxide with magnetic property recovered from the biofilm waste in the groundwater pumping system can be used as an alternative of raw material to replace corrosive chemicals including base (ammonia solution) as well as iron (II) and (III) salts required to synthesize magnetic iron oxide nanoparticles in the

future work. Apart from achieving the sustainability goal by using the natural recycled raw materials, this strategy can give rise to magnetic separation after the sorption process and reduce the cost of production of graphene-based materials for removal of water pollutants.

4. **Expansion of pollutants removal studies to emerging water contaminants (micro- and nanoplastics) using advanced graphene-based materials**: Emergence of highly persistent micro- and nanoplastics contaminants (per-and polyfluoroalkyl substances e.g. perfluorooctanoic acid-PFOA and polyfluoroalkyl substances-PFAS) from consumer products (e.g. non-stick coatings on cookware, food packaging, electronics, fuel additives and fire retardants) since the 1940s has recently stirred environmental and human health concerns. These emerging contaminants are associated with cancer, reproductive, liver and immune systems failures that trigger public urgency to contain them from entering our water supply and food chain. Owing to the hydrophobic interactions between the micro- and nanoplastics structure with the conjugated systems of neat graphene, graphene-based materials can potentially be a solution to tackle this environmental crisis. Therefore, future research work should be expanded to cover specific tailoring surface chemistry for efficient removal of these non-degradable plastic debris by applying advanced graphene-based composites.

5. **Cost reduction of graphene-based composites for full-scale water purification:** Development of cost-effective, scalable and sustainable graphene functionalization strategies is still highly in demand to meet the competitive low-cost AC for remediation of water pollutants. As demonstrated

in this thesis, performance of numerous functionalized graphene composites surpassed AC in all the testing aspects, yet nearly none of them has been fully adopted in water treatment processes at a commercial level. This is because cost is the major constraint given that the market price of graphene at present is *ca.* USD $ 100 per kilogram, which is still far away from the ideal price of *ca.* USD $ 6.81 per kilogram for AC (buyactivatedcharcoal.com) in the market. With the emerging of graphene producers in the market and the ever rapid-growing graphene research, it is optimistic that the market price of graphene can achieve that of AC. More research focus should be given to the development of economical-viable large-scale processing of graphene methods since graphene is derived from a cheap raw source, graphite, *ca.* USD $ 7.70 per kilogram (Saint Jean Carbon, Inc.). Furthermore, the material cost can also be lowered by using natural recycled raw materials (e.g. magnetic biofilm waste as discussed above) for enhanced contaminants removal from water.

6. **Integration of advanced graphene-based sorbents with other water purification and water generation technologies:** Apart from using graphene-based materials in the adsorption process, assimilation of the developed graphene-based materials into other water purification techniques (filtration, photocatalysis, capacitive deionization, etc.) and water generation technologies (solar steam generation, fog harvesting, desalination, etc.) are also critical to effectively address the clean water shortage worldwide.
7. **Translation of laboratory innovations into graphene-enabled commercialization products:** graphene-based materials developed herein

which are proven to successfully remove various water pollutants can be turned into real advanced water purification system. For instance, by integrating 3D printing technology in the future work, these graphene-based materials can be potentially printed into water filtration catridges that can be prospectively used in the water purification system.

8. **Investigating the safety and environmental risk of developed graphene-based composites:** Concern arises on the use of nanomaterials including graphene and its derivatives in water treatment due to possible remaining nanomaterials still trapped in the water that may trigger water security issue. Cytotoxicity experiments on the material stability and degradation (i.e. shelf-life) should be performed on the developed graphene-based composites in water to understand its long-term effect to the aquatic life and its presence in the water supply.

Despite various challenges associated with the use of graphene-related materials, their prospect in water purification is still optimistic provided that there is continuous injection of research funding to support the research development in this area for sustainable global supply of clean water. Inputs and advice on the feasibility of the developed materials from industry experts are important to ensure the successful translation of the lab scale water purification technology into field operations. Furthermore, this implementation will not be possible without the continuous support from the policy makers to set out comprehensive environmental regulations and guidelines over the water quality besides creating public awareness about the global water crisis. In summary, active collaborative engagement among the policy makers, industry experts and researchers is critical to optimize the socio-techno-economic

assessment of the developed graphene-based technological solutions in addressing the global water crisis.

BIBLIOGRAPHY

(1) UNEP, Half the World to Face Severe Water Stress by 2030 unless Water Use is "Decoupled" from Economic Growth, Says International Resource Panel. Paris/Nairobi, 2016.

(2) United States Geological Survey (USGS) The distribution of water on, in, and above the Earth. https://www.usgs.gov/media/images/distribution-water-and-above-earth-0.

(3) Gleick, P. H. Water in crisis. *Pacific Institute for Studies in Dev., Environment & Security. Stockholm Env. Institute, Oxford Univ. Press. 473p* **1993,** *9*.

(4) Food and Water Watch *Desalination: An Ocean of Problems*; 2009; p 20.

(5) Hlongwane, G. N.; Sekoai, P. T.; Meyyappan, M.; Moothi, K. Simultaneous removal of pollutants from water using nanoparticles: A shift from single pollutant control to multiple pollutant control. *Sci. Total Environ.* **2019,** *656*, 808-833.

(6) Cimboláková, I.; Uher, I.; Laktičová, K. V.; Vargová, M.; Kimáková, T.; Papajová, I. Heavy metals and the environment. In *Environmental Factors Affecting Human Health*; IntechOpen: 2019.

(7) Strokal, M.; Spanier, J. E.; Kroeze, C.; Koelmans, A. A.; Flörke, M.; Franssen, W.; Hofstra, N.; Langan, S.; Tang, T.; van Vliet, M. T. H.; Wada, Y.; Wang, M.; van Wijnen, J.; Williams, R. Global multi-pollutant modelling of water quality: scientific challenges and future directions. *Curr. Opin. Environ. Sustain.* **2019,** *36*, 116-125.

(8) Alvarez, P. J. J.; Chan, C. K.; Elimelech, M.; Halas, N. J.; Villagrán, D. Emerging opportunities for nanotechnology to enhance water security. *Nat Nanotechnol.* **2018,** *13*, 634-641.

(9) Tchounwou, P. B.; Yedjou, C. G.; Patlolla, A. K.; Sutton, D. J. Heavy metal toxicity and the environment. In *Molecular, Clinical and Environmental Toxicology: Volume 3: Environmental Toxicology*; Luch, A., Ed.; Springer Basel: Basel, 2012; pp 133-164.

(10) Gusain, R.; Kumar, N.; Ray, S. S. Recent advances in carbon nanomaterial-based adsorbents for water purification. *Coord. Chem. Rev.* **2020,** *405*, 213111.

(11) Jaishankar, M.; Tseten, T.; Anbalagan, N.; Mathew, B. B.; Beeregowda, K. N. Toxicity, mechanism and health effects of some heavy metals. *Interdiscip. Toxicol.* **2014,** *7*, 60-72.

(12) Xu, J.; Cao, Z.; Zhang, Y.; Yuan, Z.; Lou, Z.; Xu, X.; Wang, X. A review of functionalized carbon nanotubes and graphene for heavy metal adsorption from water: preparation, application, and mechanism. *Chemosphere* **2018,** *195*, 351-364.

(13) Bolisetty, S.; Peydayesh, M.; Mezzenga, R. Sustainable technologies for water purification from heavy metals: review and analysis. *Chem. Soc. Rev.* **2019,** *48*, 463-487.

(14) Yap, P. L.; Kabiri, S.; Tran, D. N. H.; Losic, D. Multifunctional binding chemistry on modified graphene composite for selective and highly efficient adsorption of mercury. *ACS Appl. Mater. Interfaces* **2019,** *11*, 6350-6362.

(15) Wang, L.; Shi, C.; Wang, L.; Pan, L.; Zhang, X.; Zou, J.-J. Rational design, synthesis, adsorption principles and applications of metal oxide adsorbents: a review. *Nanoscale* **2020,** *12*, 4790-4815.

(16) Sweetman, M.; May, S.; Mebberson, N.; Pendleton, P.; Vasilev, K.; Plush, S.; Hayball, J. Activated carbon, carbon nanotubes and graphene: materials and composites for advanced water purification. *C* **2017,** *3*, 18.

(17) De Gisi, S.; Lofrano, G.; Grassi, M.; Notarnicola, M. Characteristics and adsorption capacities of low-cost sorbents for wastewater treatment: a review. *SM&T* **2016,** *9*, 10-40.

(18) Wang, H.; Mi, X.; Li, Y.; Zhan, S. 3D graphene-based macrostructures for water treatment. *Adv. Mater.* **2020,** *32*, 1806843.

(19) Yap, P. L.; Auyoong, Y. L.; Hassan, K.; Farivar, F.; Tran, D. N. H.; Ma, J.; Losic, D. Multithiol functionalized graphene bio-sponge via photoinitiated thiol-ene click chemistry for efficient heavy metal ions adsorption. *Chem. Eng. J.* **2020,** *395*, 124965.

(20) Shen, Y.; Chen, B. Sulfonated graphene nanosheets as a superb adsorbent for various environmental pollutants in water. *Environ. Sci. Technol.* **2015,** *49*, 7364-7372.

(21) Yousefi, N.; Lu, X.; Elimelech, M.; Tufenkji, N. Environmental performance of graphene-based 3D macrostructures. *Nat Nanotechnol.* **2019,** *14*, 107-119.

(22) Yap, P. L.; Kabiri, S.; Auyoong, Y. L.; Tran, D. N. H.; Losic, D. Tuning the multifunctional surface chemistry of reduced graphene oxide via combined elemental doping and chemical modifications. *ACS Omega* **2019,** *4*, 19787-19798.

(23) Yap, P. L.; Tung, T. T.; Kabiri, S.; Matulick, N.; Tran, D. N. H.; Losic, D. Polyamine-modified reduced graphene oxide: A new and cost-effective adsorbent for efficient removal of mercury in waters. *Sep. Purif. Technol.* **2020,** *238*, 116441.

(24) Yap, P. L.; Hassan, K.; Auyoong, Y. L.; Mansouri, N.; Farivar, F.; Tran, D. N.; Losic, D. All-in-one bioinspired multifunctional graphene biopolymer foam for simultaneous removal of multiple water pollutants. *Adv. Mater. Interfaces* **2020,** 2000664.

(25) Yap, P. L.; Nine, M. J.; Hassan, K.; Tung, T. T.; Tran, D. N. H.; Losic, D. Graphene-Based Sorbents for Multipollutants Removal in Water: A Review of Recent Progress. *Adv. Funct. Mater.* **2020,** 2007356.

(26) Anastas, P. T.; Warner, J. C. Principles of green chemistry. *Green chemistry: theory and practice* **1998,** 29-56.

APPENDICES

Appendix A: News article featured by NewsRx

Materials Research - Material Interfaces; Study Findings on Material Interfaces Are Outlined in Reports from University of Adelaide (All-in-one Bioinspired Multifunctional Graphene Biopolymer Foam for Simultaneous Removal of Multiple Water Pollutants)

Publication info: Journal of Technology ; Atlanta [Atlanta]01 Sep 2020: 3046.

ProQuest document link

FULL TEXT

2020 SEP 1 (VerticalNews) -- By a News Reporter-Staff News Editor at Journal of Technology -- Fresh data on Materials Research - Material Interfaces are presented in a new report. According to news originating from Adelaide, Australia, by VerticalNews correspondents, research stated, "Polluted waters are complex systems with many different co-existing contaminants that make their simultaneous removal a very challenging task. To address this problem, all-in-one ad/ab-sorbent with unique combination of interfacial properties and multiple surface chemistry is developed to simultaneously and efficiently remove several pollutants including heavy metals, dyes, oils, and organic solvents."

Funders for this research include ARC Research Hub for Graphene Enabled Industry Transformation, University of South Australia, South Australian State Government, Australian Federal Governments NCRIS scheme.

Our news journalists obtained a quote from the research from the University of Adelaide, "By mimicking the wetting micro-topology of a darkling beetle with a combined hydrophilic-hydrophobic surface, a new bioinspired adsorbent, graphene biopolymer foam (Alg-Fe3O4-rGO-4S) for removal of multiple water pollutants is engineered by combining alginate (Alg) and reduced graphene oxide (rGO) functionalized with tetrathiol that is also decorated with iron oxide nanoparticles (Fe3O4). This concept is first proved by single pollutant removal, showing adsorption capacity of 789.7 +/- 36 mg/g for methylene blue (MB), 107.0 +/- 2.1 mg/g for Hg (II), 73.5 +/- 0.7 mg/g for Cu (II), and rapid oil-water separation with high sorption capacity (11-18 g/g). A remarkable performance for simultaneous removal of their mixtures in milli-Q, river, and sea water is demonstrated with efficiency for MB (approximate to 90%), Cu (II) (>99.99%) and Hg (II) (100%) and rapid (approximate to 30 s) uptake of organic solvents and oils."

According to the news editors, the research concluded: "The obtained results indicate a valuable potential of proposed concept for simultaneous removal of co-existing water pollutants."

For more information on this research see: All-in-one Bioinspired Multifunctional Graphene Biopolymer Foam for Simultaneous Removal of Multiple Water Pollutants. *Advanced Materials Interfaces*, 2020;():. *Advanced Materials Interfaces* can be contacted at: Wiley, 111 River St, Hoboken 07030-5774, NJ, USA.

The news correspondents report that additional information may be obtained from Dusan Losic, University of Adelaide, School of Chemical Engineering and Advanced Materials, Adelaide, Sa 5005, Australia. Additional authors for this research include Pei Lay Yap, Kamrul Hassan, Farzaneh Farivar, Diana N. H. Tran, Negar Mansouri and Yow Loo Auyoong. and can be your direct source for a journal article and its citation.

Keywords for this news article include: Adelaide, Australia, Australia and New Zealand, Material Interfaces, Materials Research, University of Adelaide.

LLC

The citation for this news report is: NewsRx. Study Findings on Material Interfaces Are Outlined in Reports from University of Adelaide (All-in-one Bioinspired Multifunctional Graphene Biopolymer Foam for Simultaneous Removal of Multiple Water Pollutants). Journal of Technology. September 1, 2020; p 3046.

DETAILS

Subject:	Materials research; Pollutants; Graphene; Biopolymers
Location:	Australia Adelaide South Australia Australia
Company / organization:	Name: University of Adelaide; NAICS: 611310
Identifier / keyword:	Adelaide Australia Australia and New Zealand Material Interfaces Materials Research
Publication title:	Journal of Technology; Atlanta
First page:	3046
Publication year:	2020
Publication date:	Sep 1, 2020
Publisher:	NewsRx
Place of publication:	Atlanta
Country of publication:	United States, Atlanta
Publication subject:	Technology: Comprehensive Works
ISSN:	1944-1878
e-ISSN:	1944-1886
Source type:	Wire Feeds
Language of publication:	English
Document type:	News
ProQuest document ID:	2439462716
Document URL:	http://proxy.library.adelaide.edu.au/login?url=https://www.proquest.com/docview/2439462716?accountid=8203
Copyright:	Copyright 2020, NewsRx LLC
Last updated:	2020-09-02

Appendix B

Video links for 3 Minute Thesis (3MT)

Video Link 1 :

https://www.youtube.com/watch?v=TXgntAFBhJk&feature=youtu.be

Video Link 2 : https://www.adelaide.edu.au/3mt/finals

Video link for Visualize Your Thesis:

https://www.youtube.com/watch?v=kPWOKvDJhRk#action=share